Puget Sound Current Survey 2015–2017

Including the United States' Portions of the Greater Salish Sea

Silver Spring, Maryland
March 2021

noaa National Oceanic and Atmospheric Administration

U.S. DEPARTMENT OF COMMERCE
National Ocean Service
Center for Operational Oceanographic Products and Services

Center for Operational Oceanographic Products and Services
National Ocean Service
National Oceanic and Atmospheric Administration
U.S. Department of Commerce

The National Ocean Service (NOS) Center for Operational Oceanographic Products and Services (CO-OPS) provides the National infrastructure, science, and technical expertise to collect and distribute observations and predictions of water levels and currents to ensure safe, efficient and environmentally sound maritime commerce. The Center provides the set of water level and tidal current products required to support NOS' Strategic Plan mission requirements, and to assist in providing operational oceanographic data/products required by NOAA's other Strategic Plan themes. For example, CO-OPS provides data and products required by the National Weather Service to meet its flood and tsunami warning responsibilities. The Center manages the National Water Level Observation Network (NWLON), a national network of Physical Oceanographic Real-Time Systems (PORTS®) in major U. S. harbors, and the National Current Observation Program consisting of current surveys in near shore and coastal areas utilizing bottom mounted platforms, subsurface buoys, horizontal sensors and quick response real time buoys. The Center: establishes standards for the collection and processing of water level and current data; collects and documents user requirements, which serve as the foundation for all resulting program activities; designs new and/or improved oceanographic observing systems; designs software to improve CO-OPS' data processing capabilities; maintains and operates oceanographic observing systems; performs operational data analysis/quality control; and produces/disseminates oceanographic products.

NOAA Technical Report NOS CO-OPS 093

Puget Sound Current Survey 2015–2017

Including the United States' Portions of the Greater Salish Sea

Carl Kammerer
Greg Dusek
Lorraine Heilman
Katie Kirk
Christopher Paternostro

March 2021

U.S. DEPARTMENT OF COMMERCE
Gina M. Raimondo, Secretary

National Oceanic and Atmospheric Administration
Benjamin Friedman, Deputy Under Secretary for Operations, performing the duties of Under Secretary of Commerce for Oceans and Atmosphere and NOAA Administrator

National Ocean Service
Nicole LeBoeuf, Acting Assistant Administrator

Center for Operational Oceanographic Products and Services
Richard Edwing, Director

NOTICE

TABLE OF CONTENTS

LIST OF FIGURES

LIST OF TABLES

EXECUTIVE SUMMARY

The National Oceanic and Atmospheric Administration (NOAA) National Ocean Service (NOS) Center for Operational Oceanographic Products and Services (CO-OPS) works to promote safe navigation throughout the U.S. waterways. As part of this effort, the CO-OPS National Current Observation Program (NCOP) acquires, archives, and disseminates information on tidal currents in the coastal U.S., which is used to update the NOAA tidal current predictions. NCOP conducts internal assessments of locations in need of new tidal current predictions. Puget Sound and the greater Salish Sea were identified through this process. Tidal current data are collected at new locations to help increase spatial coverage in tidal current observations and predictions and also through revisits to historical stations to update the observations and predictions with increased quality and accuracy. The data products generated are utilized by NOAA and the user community to help ensure safe navigation, make informed coastal zone management decisions, and support the protection of life and property. Furthermore, data collected can be used to inform the development of new hydrodynamic models, or provide validation to existing ones.

This report summarizes the data collection and analysis completed by NCOP in the 2015–2017 Puget Sound Current Survey in Washington State. A total of 136 stations were installed for at least one lunar month between 2015 and 2017 (48 stations in 2015, 42 stations in 2016, and 46 stations in 2017). Currents were measured at each station with an acoustic Doppler current profiler (ADCP) moored with a configuration determined by factors such as station depth, seafloor composition, expected maritime activities, anticipated currents, and available inventory. Additional measurements of temperature, conductivity, and depth (CTD) were observed and recorded at select stations. Hydrophones were deployed at several stations in conjunction with researchers at the University of Washington. Concurrent with each deployment and recovery of an ADCP, a vertical CTD profile was taken to ascertain the physical properties of the seawater at the approximate location of each station.

Each ADCP was configured to collect data in 6-minute ensembles of averaged velocity observations. Of the 136 stations, 135 stations collected data of sufficient quality, including vertical current profiles (speed and direction), water temperature, pressure, and additional quality control variables. The one station without successful data collection was PUG1621 (Marrowstone Point, 3 miles NE of, Admiralty Bay), which had an internal memory card malfunction. The successful collection of high quality data at several stations was not without challenges including: a mooring released and surfaced early due to a cable crimp failure (PUG1703, San Juan Channel, south entrance); a bottom mount and ADCP tumbled and moved off-station due to high currents and was later found post-survey (PUG1701, Deception Pass [Narrows]); and a platform flipped upon deployment and did not record good data initially, but the equipment was re-deployed on a second leg in order to collect good data (PUG1725, Cherry Point, 1.8 nautical miles (nmi) southeast of). This study includes nine updated and/or new harmonic reference stations for the Tidal Current Tables: PUG1524 (The Narrows, North end –

midstream); PUG1539 (Dana Passage); PUG1624 (Point Wilson, 1.6 mi NE of); PUG1640 (Race Rocks, 4.5 mi S of); PUG1642 (Strait of Juan de Fuca Entrance); PUG1701 (Deception Pass [Narrows]); PUG1702 (Rosario Strait); PUG1703 (San Juan Channel, south entrance); PUG1708 (Lawrence Point, Orcas Island, 1.3 nmi NE of). Currents were analyzed for tidal constituents using harmonic analysis of the velocity time series data collected by the ADCP. Of the 135 stations analyzed, three did not yield predictions. Tidal current predictions for each station were made available online via the CO-OPS Tides and Currents website and the paper NOAA Tidal Current Tables. Updates for these stations were first published in the 2017, 2018, and 2019 Tidal Current Tables for the 2015, 2016, and 2017 survey years, respectively. Note that 2020 is the last year that the paper Tidal Current Tables will be published. After 2020, all predictions are available through the CO-OPS Tides and Currents website.

1. INTRODUCTION

The National Ocean Service (NOS) Center for Operational Oceanographic Products and Services (CO-OPS) manages the National Current Observation Program (NCOP). The program's main goal is to improve the quality and accuracy of tidal current predictions. Improving this information is a critical part of NOS' efforts toward promoting safe navigation in our nation's waterways. Mariners require accurate and dependable information on the movement of the waters in which they navigate. As increasingly larger ships utilize our ports and as seagoing commerce continues to increase, there is an increased risk to safe navigation in the nation's ports (NOAA, 2018). CO-OPS acquires, archives, and disseminates information on tides and tidal currents in U.S. ports and estuaries, a vital NOS function since the 1840s. The main sources of this information for the public are the CO-OPS Tides and Currents website (NOAA, 2019a) and the National Oceanic and Atmospheric Administration (NOAA) Tidal Current Tables (TCTs) (NOAA, 2019c), which were published annually as required by the Navigation and Safety Regulations section of the U.S. Code of Federal Regulations (33CFR§164.33) until 2020. NOAA discontinued the production of these tables due to changes in paper carriage requirements as set forth by the U. S. Coast Guard (2016) as well as the availability of the predictions digitally by NOAA. Both the collection and analysis of current observations as well as the dissemination of the data fall under the authority of the Navigation and Navigable Waters title of the U. S. Code (33USC§883a-b).

The flow dynamics of an estuary or tidal river can be modified by changes in natural factors, such as land motion and other morphologic changes, or through man-made alterations, such as the deepening of channels by dredging, harbor construction, bridge construction, the deposition of dredge materials, and the diversion of river flow. Changes in water flow and tidal dynamics can affect the accuracy of tidal current predictions; therefore, new data must be collected periodically to ensure that predictions remain reliable and to adjust them when necessary.

CO-OPS has developed expertise in deploying current profilers throughout the nation's coastal waters via the NCOP program. These data are used for a number of products. In addition to updating existing tidal current predictions (NOAA, 2019c) and the establishment of new tidal current prediction locations (Fanelli et al., 2014), data collected through this program are utilized by NOAA and the user community in the production and refinement of other products, such as the validation of hydrodynamic forecast systems (Lanerolle et al., 2011) and integration into commercial navigation software. These products are used to ensure safe navigation, make informed coastal zone management decisions, and protect life and property.

The data described in this report were collected by NCOP during a survey from 2015–2017. A total of 136 stations were occupied for at least one lunar month. Of the 136 stations, 135 produced time series of good quality data of sufficient length (generally >29 days) to perform harmonic analysis and generate tidal current predictions. Data collected contain 6-minute time series of vertical current profiles (speed and direction), water temperature, pressure, and additional quality control variables, such as echo intensity and correlation magnitude. The collected data were analyzed, and reports were generated detailing statistical and harmonic analyses to ensure high quality tidal current predictions. Although the analyses were done on all 135 stations that had data of sufficient quality, there were three stations (1525 [The Narrows, North End east side], 1633 [Point Partridge, 2.4 miles NW of], and 1716 [Waldron Island, 1.7 nmi west of]), where the currents were not rectilinear enough or predictable enough to generate tidal current predictions. All data and analysis reports presented herein are available on the Tides and Currents website (NOAA, 2019a) or by contacting CO-OPS User Services (NOAA, 2019b).

2. PROJECT DESCRIPTION

Puget Sound (PUG) and the surrounding estuarine areas of the Salish Sea were identified by internal assessments within CO-OPS as a high-priority location for an NCOP current observation project utilizing modern acoustic Doppler current profilers (ADCPs). An extensive current survey effort was put forth by NOAA NOS in the 1970s in which current measurements were made at over 200 station locations in the region. These measurements were made generally for at least 15 days and in most cases utilized moored Aanderaa current meters. However, the 1970s data were never used to update the predictions in the NOAA TCTs, also reflecting the need for an updated currents survey. The data used to create the predictions in the TCTs came from studies conducted during the 1940s–1960s with some observations as far back as the 1930s. These older data were collected over short durations (<10 days) and utilized radio current meters or captive drift poles (Cox et al., 1984).

Site locations were proposed based upon the internal needs and capabilities of NOAA and meetings with users including professional mariners, federal, state and local partners, as well as academia and researchers. They were finalized based on oceanographic needs, engineering restrictions, and criteria set forth by the International Hydrographic Organization (IHO S-44 §4.5). Figure 2-1 shows a graphic of the stations in the San Juan Islands during the third year of the survey. As an example of the type of information used for site selection, this map is overlaid with automatic identification system or AIS ship tracks showing that ship track density is a key determination for selecting stations.

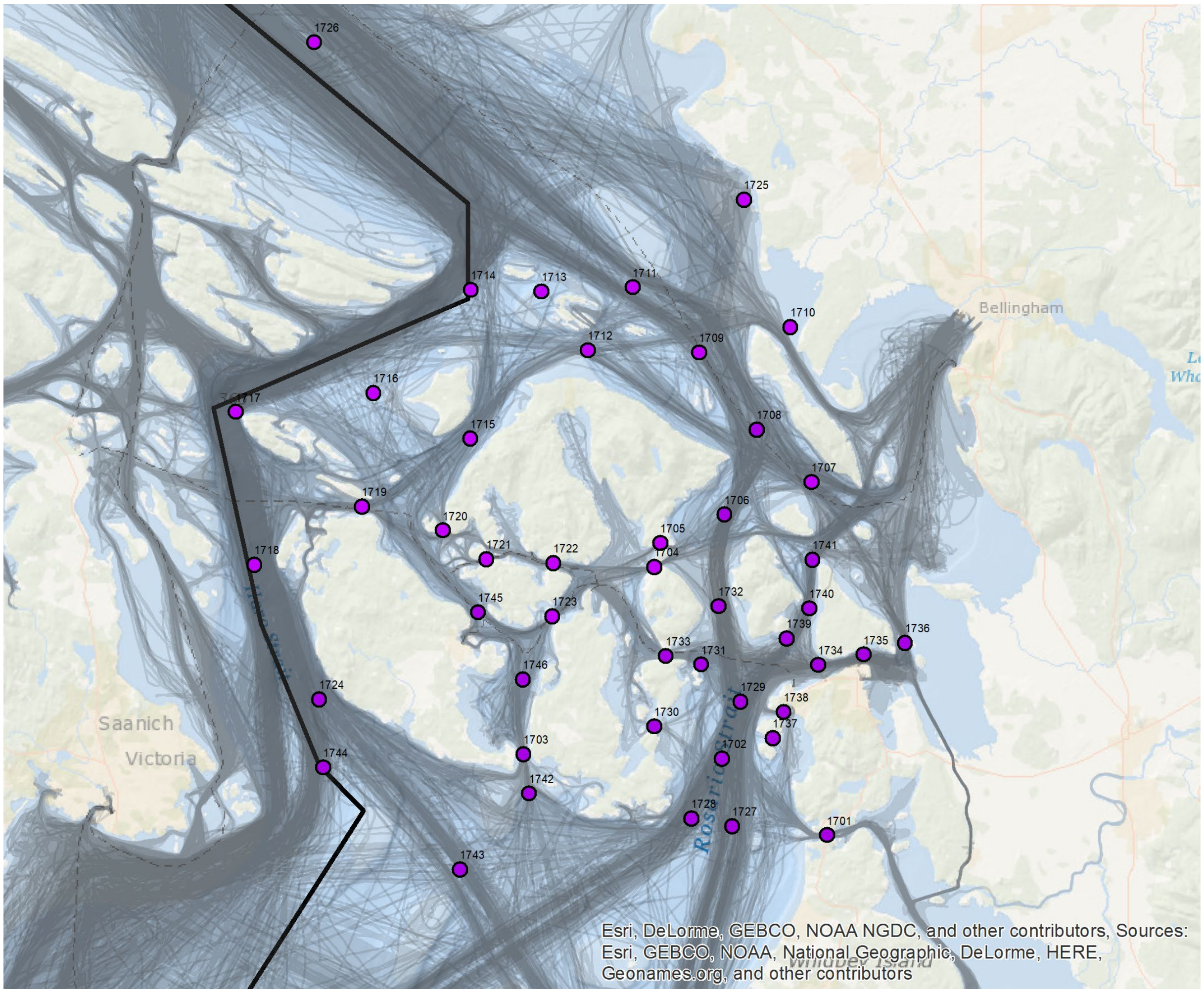

Figure 2-1. Survey stations and ship tracks. Dark black line is the border between Canada and the U.S.

From 2010 to 2013, a series of reconnaissance cruises were conducted to gather information about the physical characteristics of proposed sites. These reconnaissance cruises provided the necessary information for exact locations, platform engineering, and instrument frequencies for the proposed stations. All proposed sites were visited to gather data about their physical characteristics such as depth, bottom type, and vertical profiles of water temperature and salinity. This information was then used to plan the platform and sensor configurations for each current observation station. During reconnaissance operations, each site was visited using a vessel equipped with a fathometer to determine the depth of the site, a CTD sensor to determine salinity and water temperature, and a Ponar-style bottom sampler to determine the nature of the seabed at the site (e.g., mud, silt, sand). Based upon the reconnaissance, 136 deployment locations were identified and, during the summers of 2015, 2016, and 2017, were occupied using methods described in section 3. This technical report focuses on the results of these current profiler deployments.

2.1. Geographic scope

Puget Sound and the greater Salish Sea are an extensive estuarine system encompassing an area of over 12,000 square kilometers (km^2) (Lavelle et al., 1988; Thomson, 1994), outflowing into the Pacific Ocean and bounded by Washington State, British Columbia, and Vancouver Island (Figure 2-2). The Salish Sea is a relatively new geographic name and primarily consists of three basins (Puget Sound, the Strait of Georgia, and the Strait of Juan de Fuca), for which similar physical forcing mechanisms result in distinct and often complex circulation regimes. The complex estuarine circulation of the Salish Sea as well as the system's importance to commerce and navigation in the Pacific Northwest has resulted in a significant amount of scientific research investigating the region's circulation and physical oceanography. This research includes both observations (Ebbesmeyer and Barnes, 1980; Ebbesmeyer et al., 1984; Parker, 1977; Thomson et al., 2007; etc.) and circulation modeling (Foreman et al., 1995; Khangaonkar et al., 2011; Sutherland et al., 2011; etc.), which combine to provide information essential to choosing optimal ADCP deployment locations for the current survey project.

Current measurements were collected throughout the United States portion of the Salish Sea (Figure 2-3 and Table A-1 in the appendix) from the entrance of the Strait of Juan de Fuca and Strait of Georgia to the north, south through the Tacoma Narrows, to the numerous inlets, passages, and embayments of the southern Puget Sound. Additionally, the tidal currents in the waters of the San Juan Islands were extensively measured, as well as the waters of Puget Sound and Admiralty Inlet.

Figure 2-2. The Puget Sound Estuarine System with individual basins or regions shaded. Shown are the Strait of Juan de Fuca (white), the Strait of Georgia (green), the San Juan Islands (orange), and Puget Sound (red). These areas comprise the Salish Sea.

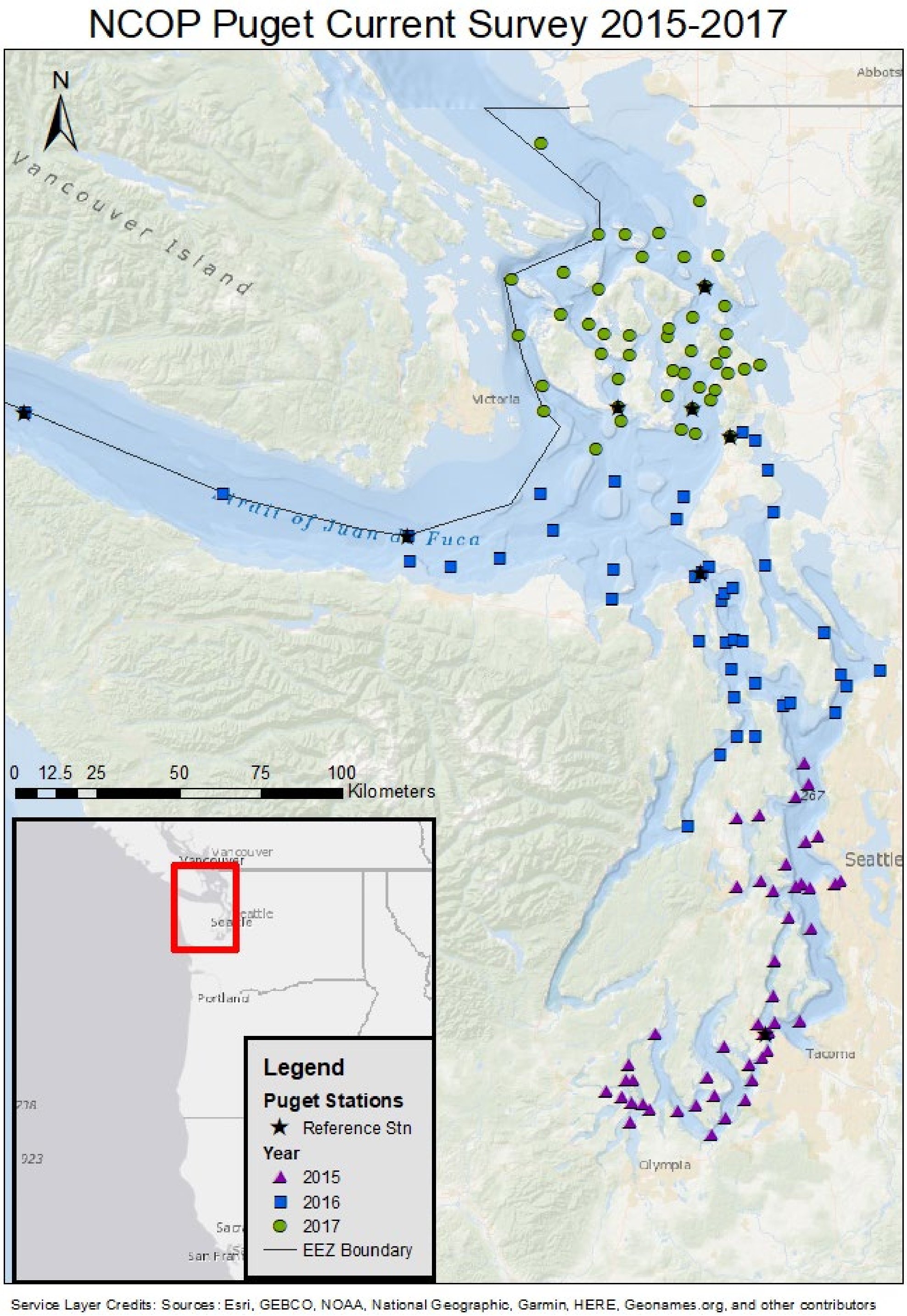

Figure 2-3. All stations surveyed. Reference stations are denoted as a star.

3. METHODS

3.1. Description of instrumentation and platforms

On-water operations were primarily conducted on the Research Vessel (R/V) Harmony, a 94-foot converted U.S. Coast Guard licensed fishing vessel (Figure 3-1) operated under contract by NOAA. These operations consisted of deploying a calibrated ADCP in an appropriate platform at each station location and recovering it after the planned station occupation period (Table A-1). For each station deployment and recovery, the water depth from the vessel's fathometer was recorded, and a CTD vertical profile was taken using a YSI CastAway®-CTD to ascertain the physical properties of the seawater at the approximate location of each station. All station metadata were recorded on station log sheets. The internal ADCP compass for each station was calibrated after the batteries were installed and before deployment.

Figure 3-1. The R/V Harmony in Friday Harbor, Washington during the 2017 deployment.

Currents were measured at each station using a moored ADCP with a platform configuration determined by factors such as station depth, seafloor composition, expected maritime activities, anticipated currents, and available instrument and platform inventory. All stations were equipped with one of the following: Teledyne RD Instruments (TRDI) Workhorse Sentinel with frequencies of 300 kilohertz (kHz), 600 kHz, or 1200 kHz or a TRDI Long Ranger (75 kHz). The maximum distance of an ADCP profile is a function of the instrument frequency, with lower frequency instruments capable of longer profiles. The instrument frequency for each station was therefore determined primarily by anticipated platform depth below the surface at mean higher high water (MHHW) plus an added range buffer to account for uncertainties in depth and potential significant events (Table B-1).

At each station, the ADCP was mounted in one of three types of bottom-mounted platform configurations, or a subsurface mooring, such as a SUBS or a Deep Water mooring (Table B-1).

3.2. Bottom mounts

Bottom mounts are designed to rest on the seafloor and provide a stable platform for an upward-facing ADCP during station occupation. All bottom-mounted platforms were positioned on the seafloor with no surface presence and were recovered by activating an acoustic release. In the event that the acoustic release failed to work properly, a secondary means of recovery (such as dragging or the use of divers) was employed. Bottom-mount platform configurations used during this project were either manufactured by Mooring Systems Inc. (MSI) (miniaturized-TRBM (MTRBM), and ES-2) or by DeepWater® Buoyancy (previously Flotation Technologies) (TRBM). Table 3-1 provides general specifications, as well as deployment and recovery methods, for each platform.

Table 3-1. Platform configurations

Platform	Specifications	Deployment and Recovery Method	Picture of Platform
MTRBM	Base: 2.5 cm fiberglass grate Shell: Fiberglass or urethane cover with Length: 178 cm Width: 122 cm Height: 48 cm Weight in water (without ballast): 23 kg Weight in air: 60 kg	Platform is lowered to place and released. Recovery is by acoustically releasing a float to the surface with a line tethered to the base.	
ES-2	224 × 178 × 84 (in centimeters) Weight in air: 363 kg	Lowered to the bottom. Acoustically released pop-up buoy to the surface. Entire platform is pulled from bottom.	
TRBM	185 × 178 × 51 (in centimeters) Weight in water: 109 kg Weight in air: 454 kg Float buoyancy: 91 kg	Platform is lowered to place and released with a slip line. A ground line is attached between the platform and a small anchor. Recovery is performed by activating an acoustic release. If the release fails to operate as intended, a backup recovery via the ground line is performed by dragging a grapnel to snag the line.	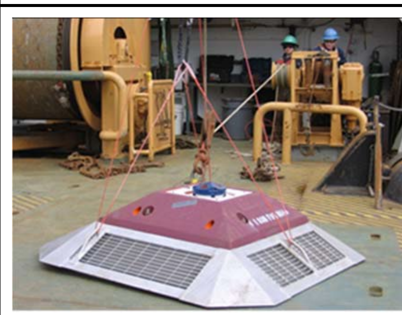

3.3. SUBS

The taut-line mooring systems are comprised of a model A2 Streamlined Underwater Buoyancy System (SUBS) flotation unit manufactured by Open Seas Instrumentation, Inc., two (2) EdgeTech acoustic releases (typically either a Coastal Acoustic Release Transponder [CART] model or a Push Off Release Transponder [PORT]) in a tandem configuration, and railroad wheel(s) for an anchor and related hardware. For this report, the term SUBS may refer to both the buoy and entire mooring system (Figure 3-2). The ADCP is held in the SUBS A2 buoy unit by a modified bucket and stainless steel arm assembly. The name A2 denotes that the ADCP is held in the buoy unit and the unit contains two flotation balls. CO-OPS typically fills voids in the A2 unit with foam to mitigate loss of buoyancy due to sedimentation. If more flotation is needed for deeper stations with faster currents, additional SUBS buoys (B3) are used below the A2 in the mooring. A design drawing of a SUBS showing A2 SUBS and additional B3 buoyancy units is found in appendix D. While deployed, the railroad wheel anchor rests on the seafloor, and the SUBS points into the current with the ADCP facing upward, collecting data vertically through the water column.

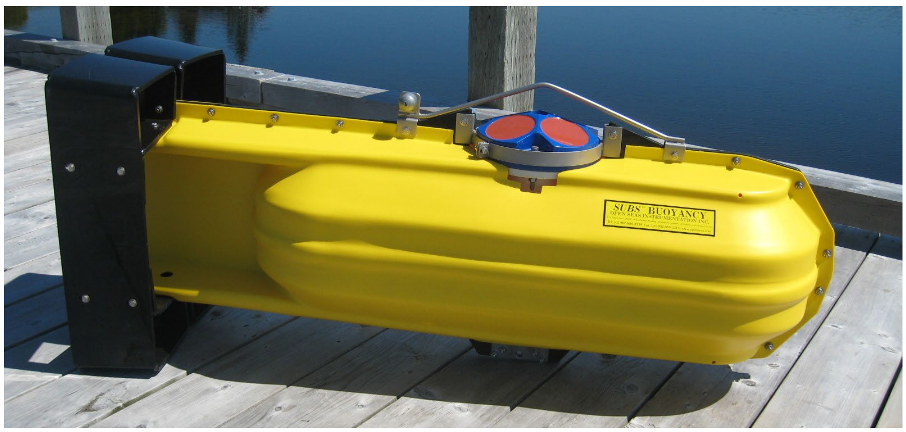

Figure 3-2. A2 SUBS

3.4. Deep water moorings

The deep water, taut-line mooring systems (Figure 3-3) are comprised of a subsurface spherical buoy made of DeepTec® syntactic foam manufactured by DeepWater Buoyancy, an EdgeTech acoustic release (typically model 8242XS, rated for deeper water), railroad wheel(s) for an anchor, and related hardware. Two different buoy diameters were used (101 centimeter [cm] [DW40] and 124 cm [DW49]). The ADCP is held within the buoy by the stainless steel cage and is upward facing so it collects data vertically through the water column during deployment. Deep water moorings are typically used in deep stations that need a larger range ADCP (typically TRDI 75 kHz) to capture data at the surface. Design drawings of deep water moorings are found in appendix D.

Figure 3-3. DeepWater Buoyancy spherical ADCP buoy.

3.5. ADCP setup and data collection

ADCPs compute water velocity by sending out a series of acoustic pulses, or pings, and measuring each acoustic ping's return signal for Doppler shift. Unlike single-point current meters, ADCPs are generally configured to measure profiles of the water column. Profiles consist of a number of discrete 'bins' of data where all the acoustic returns from single pings are sorted and collected (binned) by return time and converted into a distance from the instrument transducer by using the speed of sound in water to convert the two-way travel time into distance. Bins therefore represent the spatially averaged subdivisions along the profile. Optimal bin size is a compromise between higher spatial resolution (smaller bins) and lower standard deviation of the velocity ensemble (larger bins mean more ping returns in the spatial average). Bin size, like profile distance, is also a function of ADCP frequency. Higher frequency instruments can measure smaller bins than low frequency instruments with the same standard variation; however, lower frequency instruments can measure longer (deeper) profiles.

Velocity profiles can be collected either vertically (upward and downward facing ADCPs) or horizontally (side-looking ADCPs). Because the ADCP is measuring either a three-dimensional (bottom and ATON platforms) or two-dimensional (side-looking) flow field, the acoustic transducer heads are set at an angle to instrument measurement profile. For the upward-facing ADCPs used in this survey, the angle is either 20 degrees or 25 degrees. For three-dimensional flow measurements, a minimum of three acoustic transducers are necessary. The Doppler-shifted velocities along each beam can then be transformed mathematically into any orthogonal coordinate system, such as an east-north-up orientation (with the help of a compass).

Each ADCP was configured to collect profiles of data in 6-minute averages (called ensembles) of acoustic pulses (pings). The pings per ensemble (the number of transmitted acoustic pulses whose returns as described above are averaged in time to form a single velocity measurement for each bin) should minimize the theoretical standard deviation of expected velocity within an ensemble with respect to the engineering constraints of the system. This was determined using *PlanADCP,* software, which calculates the ensemble standard deviation, battery usage, and memory usage for the anticipated duration of the deployment for a specified number of pings per ensemble, number of bins, and bin size. All these factors affect battery life.

The optimal number of pings is a compromise between reducing the ensemble standard deviation and choosing an appropriate bin size and number of bins to ensure sufficient battery life and data storage for the expected conditions at each station. TRDI Workhorse are self-contained ADCPs with internal data storage and battery packs. For this project, stations were configured to minimize standard deviation by maximizing pings per ensemble while still ensuring sufficient battery-life to complete the planned deployment duration.

There are some additional constraints on velocity profiles from ADCPs. Because of the angled beams, a portion of the water column near the water surface (or bottom) will be lost to sidelobe interference, (approximately 6 percent of the profile depth for a 20-degree beam angle). Transducer ringing, the result of the noise of the transmit pulse on the co-located transducer and receiver, leads to the loss of part of the profile nearest the ADCP head. Blanking distance accounts for this and varies as a function of ADCP frequency and transducer properties. The manufacturer's recommended default settings for blanking distance on the TRDI Workhorse were used: 44 cm for 1200 kHz, 88 cm for 600 kHz, 176 cm for 300 kHz, and 704 cm for 75 kHz.

In bottom-mounted platforms, the ADCPs have an upward orientation; thus, bin 1 is the bin closest to the ADCP near the seafloor, and the profile reaches to, or nearly to, the surface. This also applies for the ADCPs mounted in SUBS and DeepWater Buoyancy moorings.

The following ancillary measurements were collected and used as data quality assurance parameters: water temperature and pressure (depth) collected at the sensor head, instrument tilt and orientation, and beam echo and correlation magnitude for each of the four separate transducers at each depth bin of the water column.

ADCPs were calibrated and tested for proper operation using built-in internal testing algorithms. Upon completion of these procedures, a unique configuration file was uploaded to each instrument based upon settings derived from the manufacturers' software, in this case *PlanADCP.* A unique, five-character deployment name and the time to start pinging were also programmed. For all instruments that were redeployed for the second half of the survey in a given year, an examination of the ADCP's performance was conducted, and a setup file was uploaded based upon new configuration settings for the new location. Instruments were recalibrated between deployments after the battery packs were changed.

3.6. Description of data processing and quality control

The sampling rate for the ADCP data was ten times per hour (centered every 6 minutes from the top of the hour through 54 minutes past the hour). Each sample was an average of up to 360 evenly-timed pings based on the ADCP setup and frequency. Even though the shortest tidal constituent period is about 2 hours, 6-minute samples are frequent enough to enable a high-resolution estimation of the maximum and minimum tidal currents and the ability to capture short duration non-tidal events. This rate also provides a statistically sound time series in which erroneous records are less likely to influence the longer series.

Quality control measures were used to mark each record as bad, good, or questionable based on best practices implemented by CO-OPS (Paternostro et al., 2005) and based on the community-accepted QARTOD (Quality Assurance/Quality Control of Real-Time Oceanographic Data) standards and recommendations (U.S. Integrated Ocean Observing System, 2019; Cothran, 2006). Quality control measures consist of boundary threshold checks for speed, tilt (pitch and roll), echo amplitude, correlation magnitude, and rate of change checks for speed, pitch, roll, and heading. An automated algorithm flagged the records that failed any of these thresholds. Questionable data were reviewed by an experienced analyst and marked as either bad or good. Only good data are disseminated to the public and used for harmonic analysis.

The principal flow direction is calculated by maximizing the direction of variance. This calculation enables an orthogonal transformation from an east-north coordinate system to major and minor flow direction axes (generally along- and cross-channel, respectively). Representing the currents in the major and minor axes components is especially beneficial in coastal and estuarine areas which exhibit a rectilinear reversing flow rather than a rotary flow. In these cases, a significant majority of energy is along the major axis, and we can effectively represent the tidal currents with a single variable (major axis current speed).

All ADCP data collected were analyzed to separate the harmonic tidal part of the signal from the residual or non-tidal flow (Parker, 2007). Data were extracted from the binary instrument output into columnar ASCII data and then were further processed by NOAA's harmonic analysis routines (Zervas, 1999). Harmonic analyses were then performed upon the current velocity time series in the major and minor flow directions.

The preferred analysis method for tidal current data is an optimization technique called Least Squares Harmonic Analysis (LSQHA) (Parker, 2007). The least squares technique allows for the presence of data gaps and can be used on time series of varying lengths. Amplitudes and phases of a given set of tidal constituents are solved for by using this method. The frequencies and number of tidal constituents for each station are determined by the length of the time series. The least squares method was used to calculate harmonic constituents at all of the Puget Sound stations that had good data. We typically collect at least 33 days of data to ensure that most tidal energy can be adequately resolved by the least squares analysis. Despite some deployment challenges, we used least squares analysis for data collected at nearly all stations.

Predictions provided online by CO-OPS are generated directly from harmonic constituents to meet carriage requirements. However, due to the previous legal requirement to publish paper TCTs and the need to limit the physical size of these publications, a ‘reference’ and ‘subordinate’ relationship was created. Daily-predicted tidal currents were provided by NOAA every year for select stations in Table 1 of the TCTs. Stations listed in TCT Table 1 were considered reference stations. They were selected for navigational significance due to geographic location, heavy traffic, hazardous locations, strong currents, or a combination of these factors. For this project, nine stations were selected as reference stations and were added to Table 1 of the TCTs (PUG1524 [The Narrows, North end – midstream], PUG1539 [Dana Passage)], PUG1624 [Point Wilson, 1.6 miles NE of], PUG1640 [Race Rocks, 4.5 miles S of], PUG1642 [Strait of Juan de Fuca Entrance], PUG1701 [Deception Pass (Narrows], PUG1702 [Rosario Strait], PUG1703 [San Juan Channel, south entrance], and PUG1708 [Strait of Juan de Fuca Entrance]). Remaining stations from this project were listed in Table 2 of the TCTs. These ‘subordinate’ stations list average timing and speed ratio offsets from one of the designated reference stations located in Table 1 of the TCTs at each of the four phases of the tidal current (slack before ebb [SBE], maximum ebb [MEC], slack before flood [SBF], and maximum flood [MFC]). The time offset from a reference station to a subordinate is calculated using the Greenwich Interval (GI), the mean time interval between the moon passing over the prime meridian and each phase of the tidal current at a station location. This reference-subordinate relationship exists online at legacy stations, where full harmonic constituents are not available. One station (PUG1716 [Waldron Island, 1.7 nmi west of]) from this study is listed online as a subordinate station due to irregular harmonic analysis results for the time series. Four stations were found to have weak and variable currents. These stations are PUG1504 (Entrance to Ballard Locks), PUG1505 (Entrance to Eagle Harbor), PUG1506 (Harbor Island East), and PUG1613 (Everett). Two stations were excluded from online predictions due to the inability to fully analyze them using traditional harmonic analysis: PUG1525 [The Narrows, North End east side]) was excluded due to a strong ebb dominance, and PUG1633 [Point Partridge, 2.4 miles NW of]) was excluded because of strong flood dominance.

3.7. CTDs and hydrophones

CTD sensors manufactured by Sea-Bird Scientific (model SBE 37 MicroCAT) were deployed below the ADCP on the taut-line mooring at the following stations: PUG1512 (Restoration Point), PUG1518 (Blake Island, S of), PUG1527 (The Narrows, 0.3 miles North of Bridge), PUG1532 (Steilacoom, 0.8 miles North of), PUG1534 (Nisqually Reach, 0.5 miles South of Lyle Point), PUG1539 (Dana Passage), PUG1604 (Port Gamble Bay Entrance), PUG1624 (Point Wilson, 1.6 miles NE of), PUG1625 (Point Wilson, 2.7 miles NE of), PUG1639 (Angeles Pt., 2 miles NNE of), PUG1640 (Race Rocks, 4.5 miles S of), PUG1716 (Waldron Island, 1.7 nmi west of), PUG1724 (South Haro Strait, south of Lime Kiln Light), PUG1726 (Strait of Georgia, 4.5 nmi SW of Point Roberts), PUG1727 (Point Colville, 3.0 nmi east of (Lawson Reef, 1 nmi NW of)), and PUG1746 (Pear Point, east of). PUG1625 (Point Wilson, 2.7 miles NE of) also measured dissolved oxygen using an instrument supplied by the Washington State Department of

Ecology along with two Sea-Bird CTDs. The University of Washington deployed hydrophones at stations PUG1531 (Gibson Point, 0.8 mile East of) and PUG1540 (Budd Inlet Entrance) through a partnership with NCOP.

4. PHYSICAL OCEANOGRAPHIC OVERVIEW OF THE REGION

The three basins of the Salish Sea system are all dominated by estuarine circulation—a net outflow of fresher water at the surface and a net inflow of saltier water at depth (Thomson, 1994). The nature of estuarine flow in a fjord-like estuary is dictated by a number of factors including freshwater input (e.g., river inflow, run-off, and rainfall), the sill locations and depths, and wind forcing (Thomson, 1994; Dyer, 1997). In addition to the predominant estuarine circulation, according to Thomson (1994) there are three additional forcing mechanisms to consider: tidal forcing, wind forcing, and coastal ocean forcing. All four forcing mechanisms will be discussed for each basin in greater detail below.

4.1. Puget Sound

The Puget Sound region of the Salish Sea (Figures 2-2, 2-3) is a partially mixed estuary with predominantly two-layer estuarine flow driven by freshwater outflow (for which the Skagit River accounts for about 60 percent) and inflow of more saline water over the Admiralty Inlet sill zone at the mouth (Barnes and Ebbesmeyer, 1978; Ebbesmeyer and Barnes, 1980; Thomson, 1994). The depth of no motion (i.e., the depth where the seaward surface flow transitions to a landward flow at depth) is about 50 meters (m) in the Main Basin, with bulk residence time of the lower layer water on the order of 3 weeks; however, short-term discharge can remain in the basin for much longer due to re-circulation of mixed waters (Ebbesmeyer and Barnes, 1980). Seasonal variations in estuarine flow will occur due to changes in freshwater inputs, winds, and stratification.

Mixing is predominantly driven by tides and occurs almost entirely at the sill zones where there are high velocity tidal currents (e.g., in excess of 2 meters per second (m/s) at Admiralty Inlet). Tidal currents are mixed, mainly semidiurnal, with a majority of energy resulting from the M_2 constituent. Wind-driven circulation is significant despite accounting for only a small portion of kinetic energy (dissipation of energy by wind over the entire basin is approximately 1 percent of that by tidal currents at Admiralty Inlet) (Ebbesmeyer and Barnes, 1980). Wind forcing accounts for about 50 percent of non-tidal residual flow (Thomson, 1994) and can significantly alter the depth of no motion; it indirectly contributes to mixing through increased circulation of surface waters (Cannon, 1983). Due to the distance from the open ocean, coastal ocean forcing is less significant although not unimportant to overall circulation. Reversals in flow in the Strait of Juan de Fuca resulting from coastal ocean forcing (detailed below) can contribute to deep water intrusive events at Admiralty Inlet, which occur with greater frequency in the winter months (approximately every 2 weeks; Cannon et al., 1990).

4.2. Strait of Georgia – San Juan Islands

The Strait of Georgia is a partially mixed estuary where exchange with oceanic waters occurs predominantly through the San Juan Islands in the southern strait. The San Juan Islands contain a complex series of channels and passages, which result in complex circulation dominated by tidal forcing. Similar to Puget Sound, two-layer estuarine flow characterizes the mean circulation of the basin, although the San Juan Islands is a region of complex exchange and mixing. The three most significant channels in the San Juan Islands are Haro Strait, Rosario Strait, and Middle Passage (Figures 2-2, 2-3). Most exchange and deep water inflow occurs through Haro Strait, as it is the widest (about 10 km) and deepest (up to 350 m deep) of the three channels and also has the deepest sill depth (about 90 m) (Pawlowicz, 2002). Rosario Strait and Middle Passage are assumed to be minor exchange pathways when compared to Haro Strait (Pawlowicz, 2002).

Estuarine flow in the San Juan Islands is driven by freshwater outflow, predominantly from the Fraser River north of the islands in the Strait of Georgia (LeBlond et al., 1983; Masson, 2006). Similar to Puget Sound, the estuarine circulation demonstrates seasonality. River inflow can fluctuate from 1,000 m^3/s in the winter to more than 10,000 m^3/s in late spring (Thomson, 1994). Additionally, wind forcing and coastal ocean effects from the Strait of Juan de Fuca (detailed below) vary significantly by season and can alter circulation as well as intermediate and deep water replacement (Thomson, 1994; Masson, 2006).

Tidal hydrodynamics in the San Juan Islands region are extremely complex. Tidal currents are often strong (>2 m/s) and highly rectilinear in the narrow passages in and around the San Juan Islands (Parker, 1977). These strong tidal currents induce much of the mixing that occurs around sill regions. The area is generally mixed, mainly semidiurnal, and thus the semidiurnal constituents usually dominate. However, there are some locations (e.g., in Rosario Strait) where the K_1 (diurnal) constituent is nearly as great as the M_2 (Parker, 1977). Further, the tidal current ellipses (which visualize the tidal energy along the semi-major and semi-minor axes of flow) for each constituent can vary dramatically over short distances, resulting in opposing flow and strong tidal rips or convergence zones (Parker 1977).

4.3. Strait of Juan de Fuca

The Strait of Juan de Fuca is a weakly stratified, partially to well-mixed estuary with considerable direct influence from the coastal Pacific Ocean. The western part of the estuary is predominantly driven by oceanic processes from the continental shelf, while the eastern Juan de Fuca Strait exhibits intense tidal motions from its intersection with the other two basins (Thomson, 1994). There are two modes of circulation in the Strait of Juan de Fuca: 1) typical estuarine flow characterized by outflow at the surface (greater than about 60 m) and inflow at depth and 2) a transient regime characterized by flow reversals at the surface, which intensify at the southern boundary (Thomson et al., 2007). Estuarine flow is much more common in the summer months (approximately 90 percent of the time), while in winter the balance between the two modes is fairly even (Thomson et al., 2007). Like the San Juan Islands, estuarine flow is driven predominantly by freshwater input (approximately 80 percent) from the Fraser River (Cannon, 1978) and is modulated fortnightly due to tidal mixing effects (i.e., strongest during neap tides and weakest during spring tides) (Thomson et al., 2007). The flow reversals from the transient regime can be about 1 m/s in the southern Strait of Juan de Fuca and are driven by landward Ekman transport from southerly winds on the continental shelf (Cannon, 1978; Holbrook et al., 1980; Thomson et al., 2007). Although most intense in the eastern strait, strong flow reversals can influence the western strait (Holbrook et al., 1983), and can even influence flow into Puget Sound and the San Juan Islands (Masson, 2002; 2006).

Winds can also have a direct influence on surface flow in the Strait of Juan de Fuca. Similar to much of the Puget Sound System, winds are topographically constrained in the Strait of Juan de Fuca and thus often blow along-strait, typically seaward in the winter and landward in the summer (Cannon, 1978). Winds can be strong enough to influence both surface flow and the depth of no motion (Cannon, 1978). Perhaps the most significant wind forcing for the purpose of a tidal current study is the land-sea breeze diurnal cycle. In the summer months a maximum westerly sea breeze was observed around 6:00 PM local time (Cannon, 1978), whose speed can exceed 15–20 m/s (Thomson et al., 2007). This could result in surface flow on the order of 0.5 m/s, which will occur on a diurnal frequency similar to the K_1 constituent (Parker, 1977).

5. DATA ACQUIRED

Data were acquired at 135 of 136 stations occupied during the summers of 2015, 2016, and 2017. The lack of good data at PUG1621 (Marrowstone Point, 3 miles NE of, Admiralty Bay) was due to a data card failure and is not discussed in the report. The tables in appendices A and B describe station data and metadata used in the analysis. Additionally, all stations have CTD data from vertical profile casts taken at deployment and recovery. On select stations, a CTD was attached near the bottom of the mooring chain, and a time series was collected throughout the station's deployment. CTD data for these stations are available by contacting CO-OPS' User Services at co-ops.userservices@noaa.gov.

The estimated depth of the current profiler platform and the measurement bin depths are given in meters relative to an approximation of mean lower low water (MLLW). This MLLW depth is calculated statistically from the known height of the platform above the bottom in combination with the time series from the ADCP's pressure sensor. Error in the MLLW calculated at a given current station is the result of both the length of time of observations and uncertainties in the observed station depth. Station depth uncertainty is affected by any pressure sensor errors, such as drift and offset errors, and platform instability, such as vertical excursions for taut-line moorings. MLLW calculations from a tide gage with time series of 30–90 days have, on average, between 0.4 m and 0.3 m of accuracy, (Swanson, 1974). Calculated depth is therefore a best approximation. This MLLW approximation can be compared to the station depth, which is logged using the ship's fathometer during deployment and recovery and entered into the database. In cases where the pressure sensor malfunctioned (determined by this comparison), the station depth measured at deployment with the ship's fathometer was used. There were 13 stations with unusable pressure sensors (denoted in Appendix B with a dagger symbol (†)).

Stations in Table A-1 of the appendix are listed with position, depth as recorded at deployment, and station occupation start and end dates. The stations in bold were selected as reference stations. These stations are: PUG1524 (The Narrows, North end - midstream), PUG1539 (Dana Passage), PUG1624 (Point Wilson, 1.6 miles NE of), PUG1640 (Point Wilson, 1.6 miles NE of), PUG1642 (Point Wilson, 1.6 miles NE of), PUG1701 (Deception Pass (Narrows)), PUG1702 (Rosario Strait), PUG1703 (San Juan Channel, south entrance), and PUG1708 (Lawrence Point, Orcas Island, 1.3 nmi NE of). As discussed earlier, station PUG1621 (Marrowstone Point, 3 miles NE of, Admiralty Bay) was occupied but, due to a hardware malfunction, did not record data and will not be discussed further in this report.

6. STATION RESULTS

A brief, quantitative description of a subset of survey stations is provided in this section. These stations include many of the newly established reference stations for the region and those that exhibit characteristics of different flow regimes. A map of the stations described in this section is shown in figure 6-0.

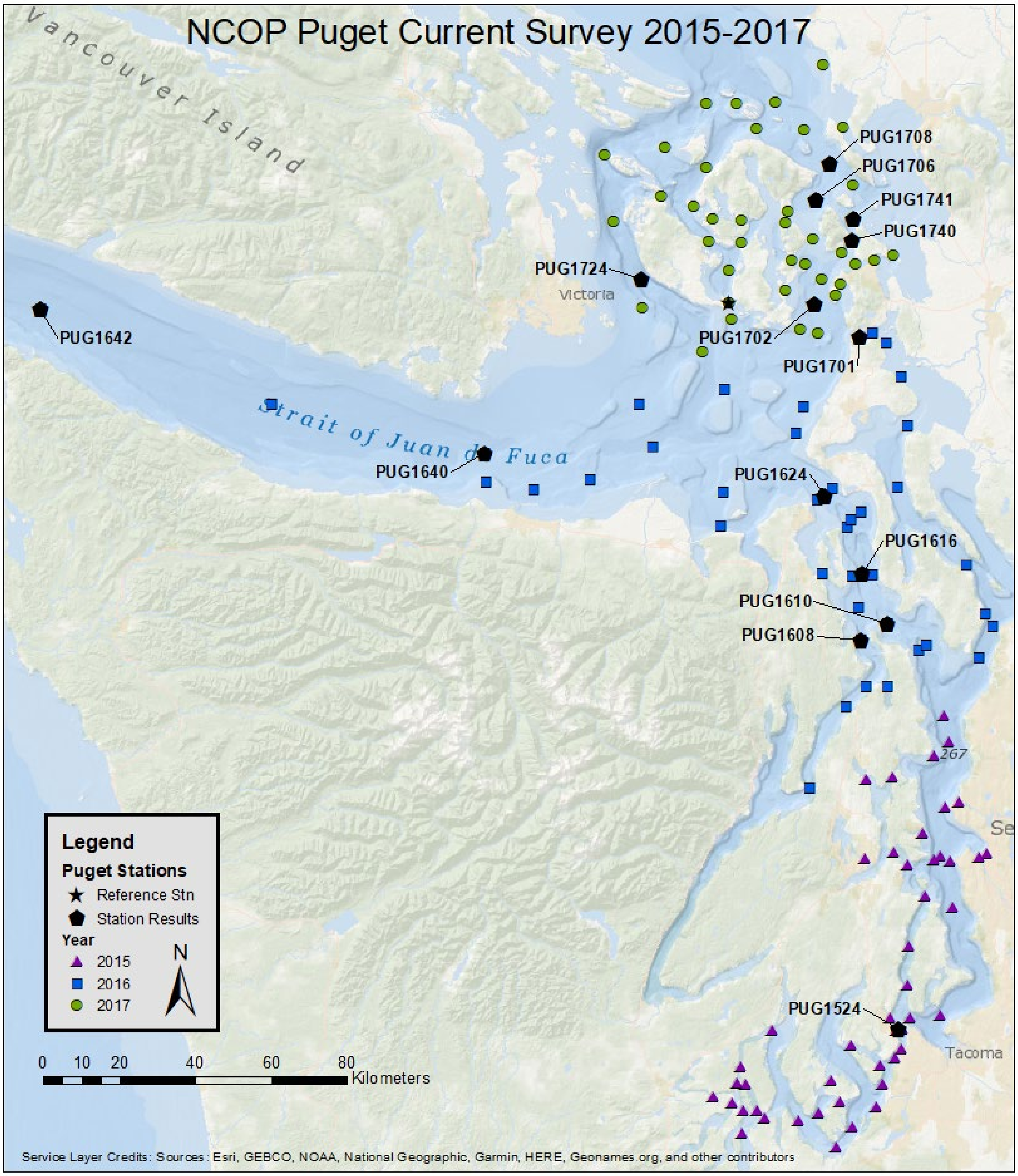

Figure 6-0. Map of all stations. Stations labeled are highlighted in this section.

For each station in this section, a description of the mean maximum flood current (MFC) and mean maximum ebb current (MEC) is given for the station's near-surface depth bin represented in the TCT. For some stations, up to two additional depth bins are available in the TCT. For all stations, all quality-controlled depth bins that passed standard metrics are available through the Tides and Currents website (NOAA, 2019a). For all deep water, SUBS, and bottom-mounted ADCPs, bin 1 refers to the deepest measurement, and the bin number increases as you approach the water surface. The principal flood direction is the predominant axis of flow as described in section 3. Directions are provided in degrees from true north. The variance along this axis is provided to give an indication of how confined the flow is along the axis; a high percentage variance implies a rectilinear flow. Fourteen stations are described in this section. These stations were selected based on spatial representation and/or scientific interest. The results presented below are a small subset of the full analyses conducted on the data sets. For each of the 14 stations described, there are five figures that include the following:

- North versus east velocity component scatter plot at the near-surface depth bin including data from the entire time series.
- A velocity time series sample at the near-surface depth bin separated into two plots. The upper plot shows a comparison of observed (green dots) major-axis velocity and the calculated (red line) tidal predicted velocity; the lower plot shows the residual flow (the difference between observed and predicted velocity).
- A vertical profile of the mean velocity along the major (red '×') and minor (blue '+') axis of the water column. This represents the approximate mean residual (non-tidal) circulation throughout the water column. The surface level is estimated (shown as a blue wavy line).
- A vertical profile plot showing the timing and speed of MFC throughout the water column.
- A vertical profile plot showing the timing and speed of the MEC throughout the water column.

6.1. PUG1524 - The Narrows, north end - midstream (reference station)

This station was deployed for 106 days (May 29, 2015–September 12, 2015) in 52.7 m (173.0 ft) of water. A TRDI Workhorse 300 kHz ADCP mounted in a single SUBS collected 18, 2 m bins of data, 16 of which met quality control criteria for full analysis. Bins 1, 9, and 16 are published in the TCTs, representing approximate depths of 42.4 m, 26.4 m, and 12.4 m (139.2 ft, 86.7 ft, and 40.7 ft) below MLLW, respectively. Information from bin 16 (12.4 m [40.7 ft] below MLLW) serves as a new reference station.

The Narrows is an 8-km-long strait near Tacoma, Washington that connects the south basin of Puget Sound to the larger northern sound. Observed currents are rectilinear and fairly strong. A small dogleg seen in Figure 6-1 implies bathymetric steering differences between flood and ebb tide. This station is very tidal, which is indicated by the total energy accounted for, as seen in Figure 6-2. Dietrich ratios fall between 0.4 and 0.5 for all bins, indicating that this station is mixed, but mainly semidiurnal. LSQHA resolved 29 constituents and accounted for 96–98 percent of the total energy in the velocity data. Mean MFC and MEC currents range between 144 cm/s and 164 cm/s (2.8 knots (kn) and 3.1 kn), and their timing does not vary much with depth.

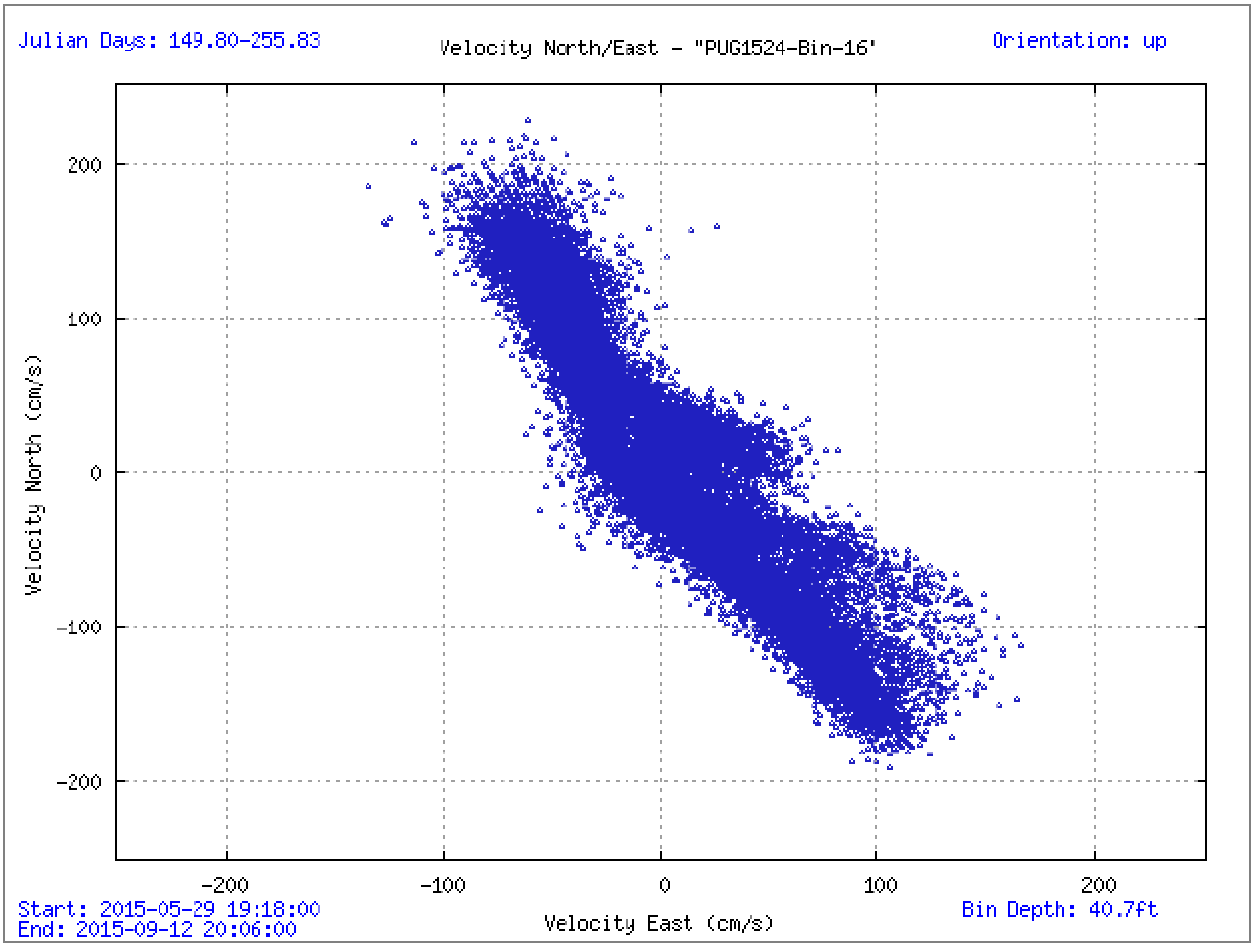

Figure 6-1. Scatter plot of north-versus-east velocity for station PUG1524 at the near-surface bin, bin 16 at 12.4 m below MLLW.

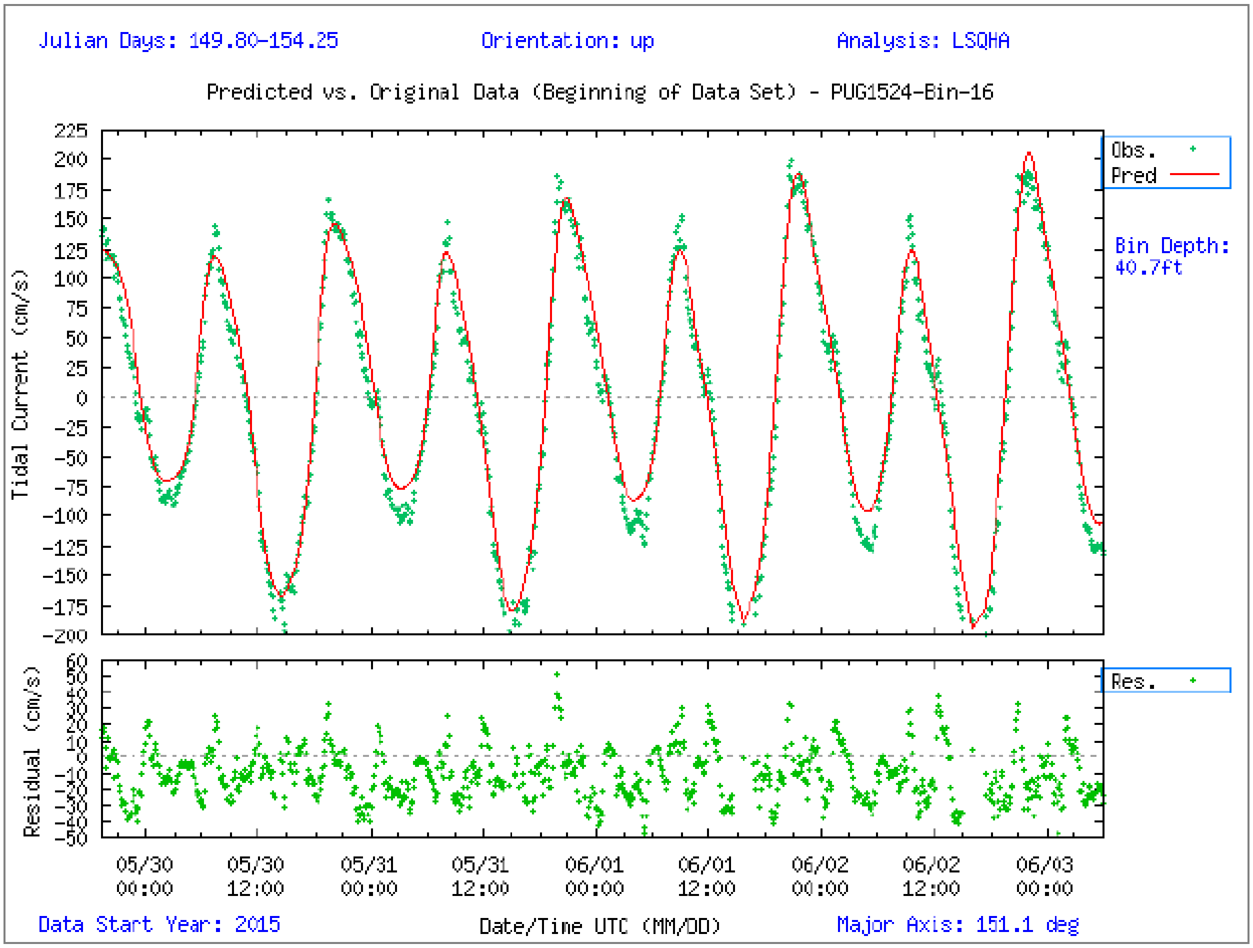

Figure 6-2. Comparison of observed major axis velocity data (green points) to predicted tidal velocity along the major axis for station PUG1524. The lower figure shows the non-tidal residual, the difference between the predicted and observed velocity from the upper panel.

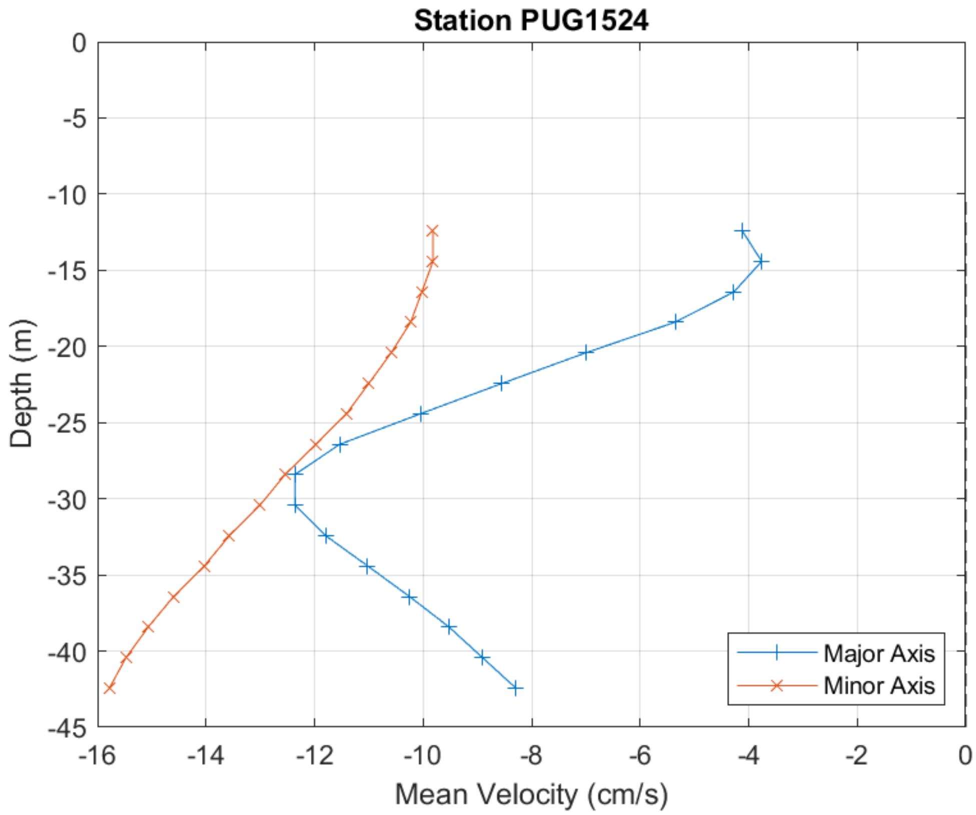

Figure 6-3. PUG1524 mean velocity profile by depth. Only depths that passed quality control criteria are shown. This station was configured to collect 2.0 m bins.

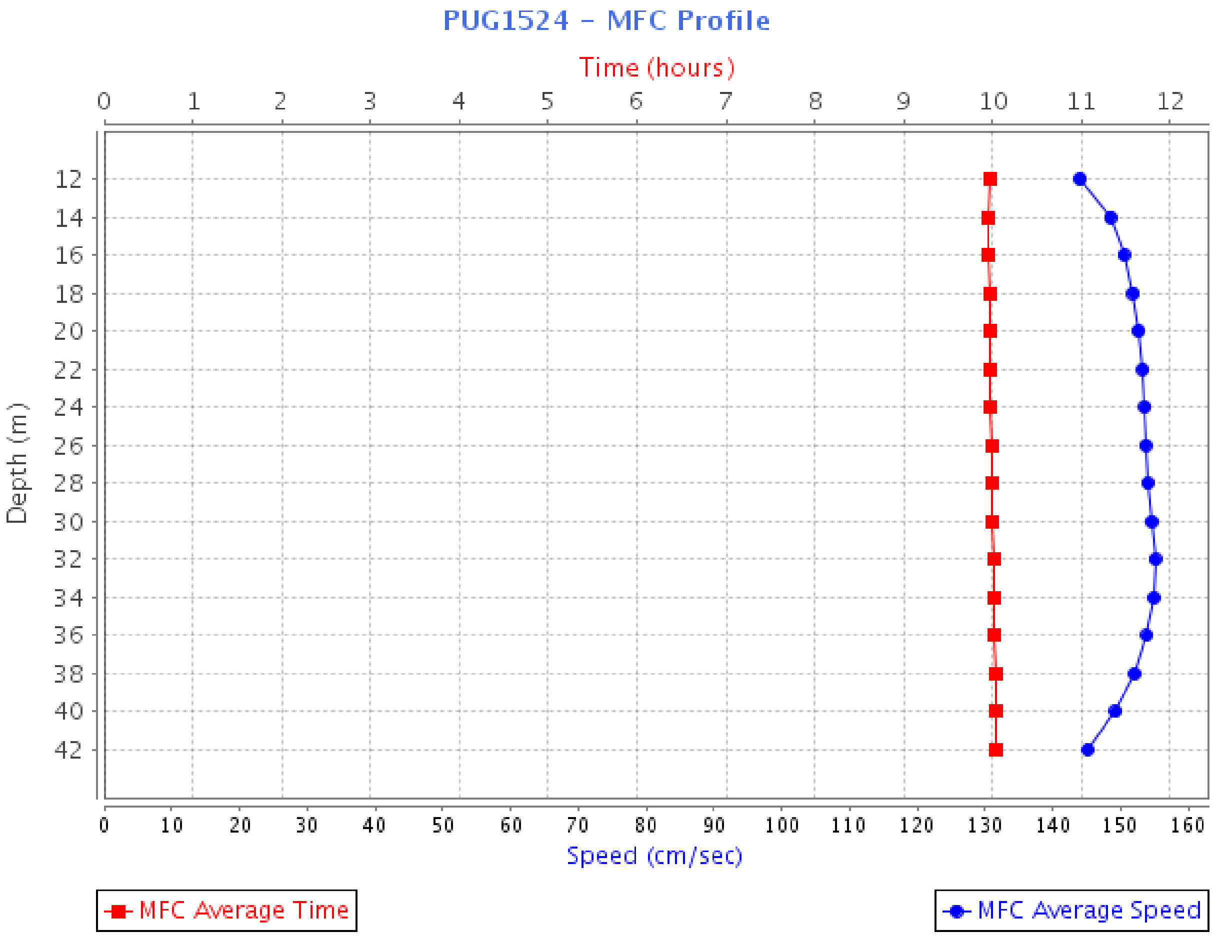

Figure 6-4. PUG1524 MFC timing (GI - in red squares) and speed (blue circles) by depth bin. Bin 1 is the deepest bin observed at approximately 42.5 m below MLLW, and the top-most good bin is bin 16 (12.4 m below MLLW).

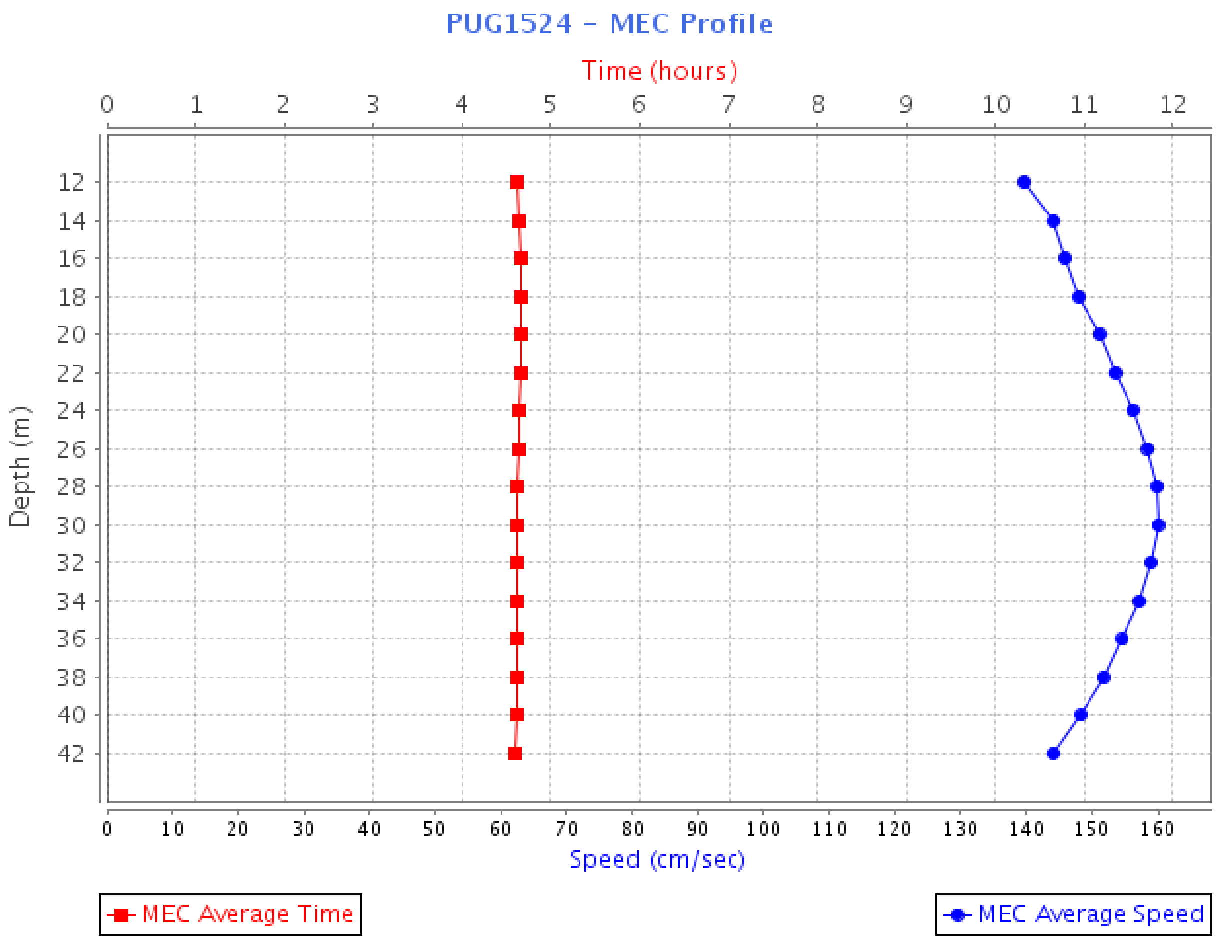

Figure 6-5. PUG1524 MEC timing (GI – red squares) and speed (blue circles) by depth bin. Bin 1 is the deepest bin observed at approximately 42.5 m below MLLW, and the top-most good bin is bin 16 (12.4 m below MLLW).

6.2. PUG1608 - Hood Canal Entrance

Hood Canal Entrance was deployed for 128 days (April 20, 2016–August 26, 2016) in 91.9 m (301.4 ft) of water. A TRDI Workhorse Sentinel 300 kHz ADCP mounted on a SUBS, 10 m above the bottom collected 39, 2 m bins of data, 36 of which met quality control criteria for full analysis. Bins 1, 28, and 35 representing depths of 77.7 m, 23.7 m, and 9.7 m (255.0 ft, 77.8 ft, and 31.9 ft) below MLLW, respectively are published in the TCTs. Information from bin 35 (9.7 m [31.9 ft]) is used in the time series plots below.

Station PUG1608, Hood Canal Entrance, lies on the southwest side of Foulweather Bluff, about 2.5 nmi SW of station PUG1610 (Foulweather Bluff, 1.9 miles NE of) and was deployed to determine the flow in and out of Hood Canal. However, due to the limited length of Hood Canal, the flow at this station is significantly different from PUG1610. Tidal signal strength is about half that of PUG1610. Currents are mixed semidiurnal and rectilinear with faster floods than ebbs throughout the water column. The max MFC was 0.96 kn in bins 27 and 28 (84.4 ft and 77.8 ft, respectively) and the fastest MEC was 41.2 cm/s (0.80 kn) in bin 35.

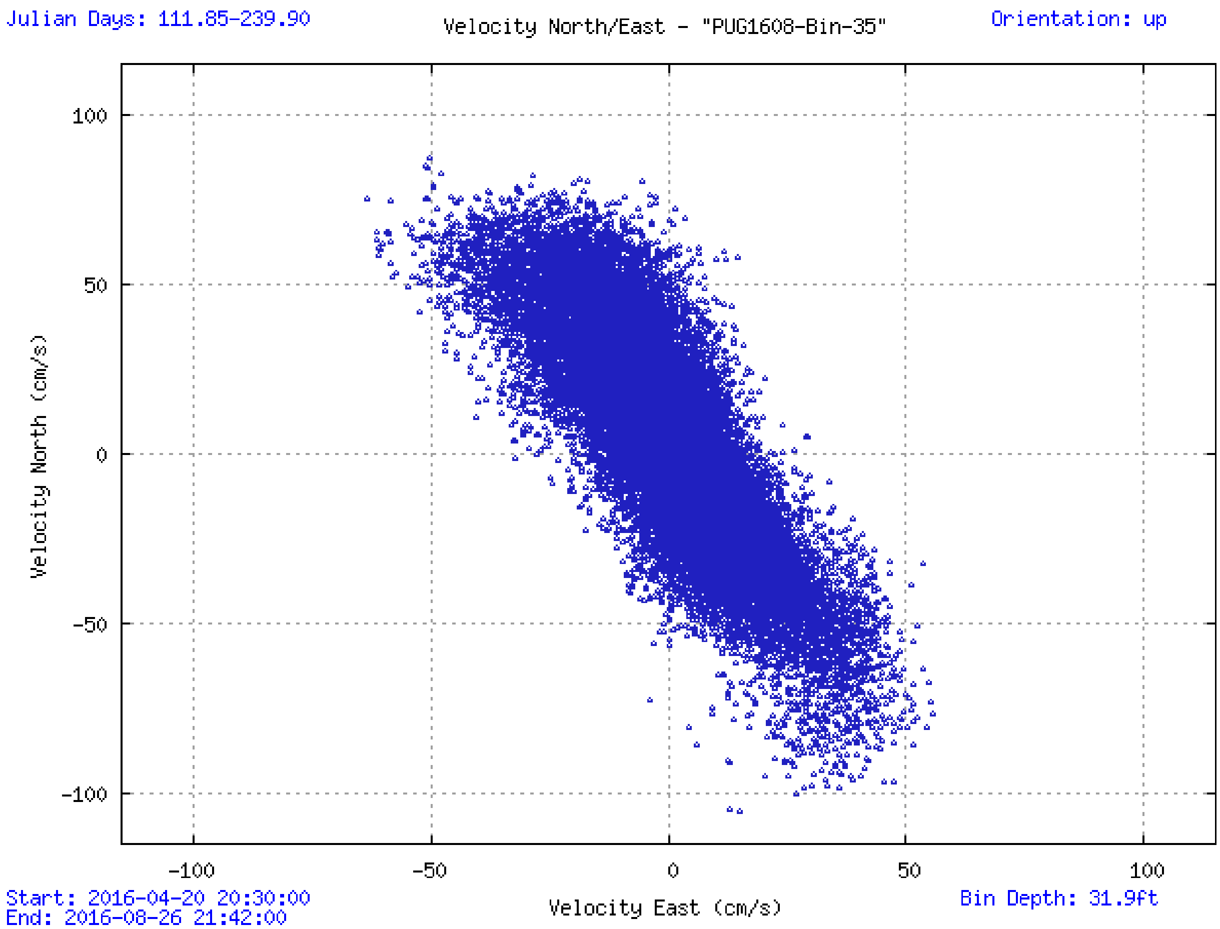

Figure 6-6. Scatter plot of north-versus-east velocity for station PUG1608 at the near-surface bin, bin 35 at 9.7 m below MLLW.

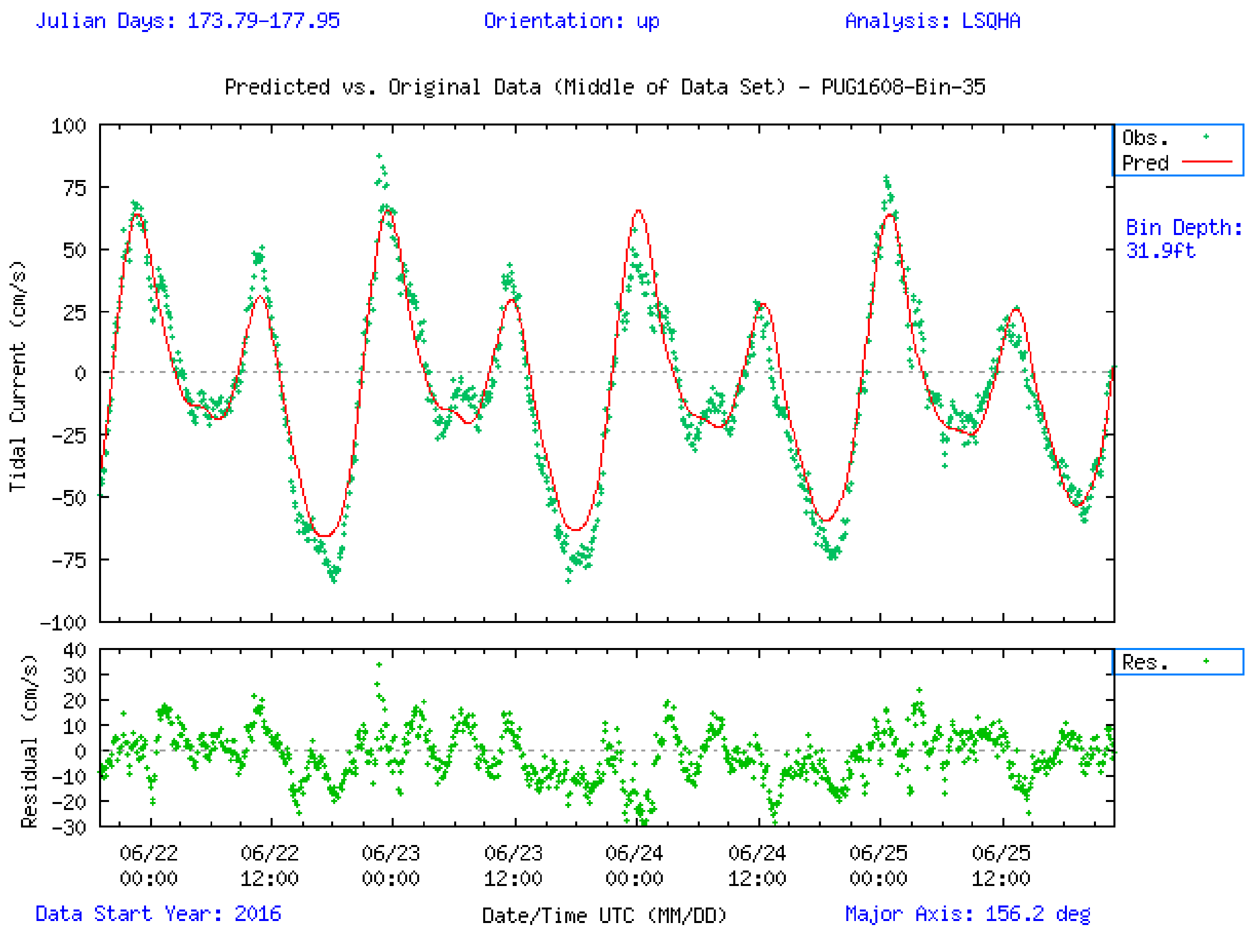

Figure 6-7. Comparison of observed major axis velocity data (green points) to predicted tidal velocity along the major axis for station PUG1608. The lower figure shows the non-tidal residual, the difference between the predicted and observed velocity from the upper panel.

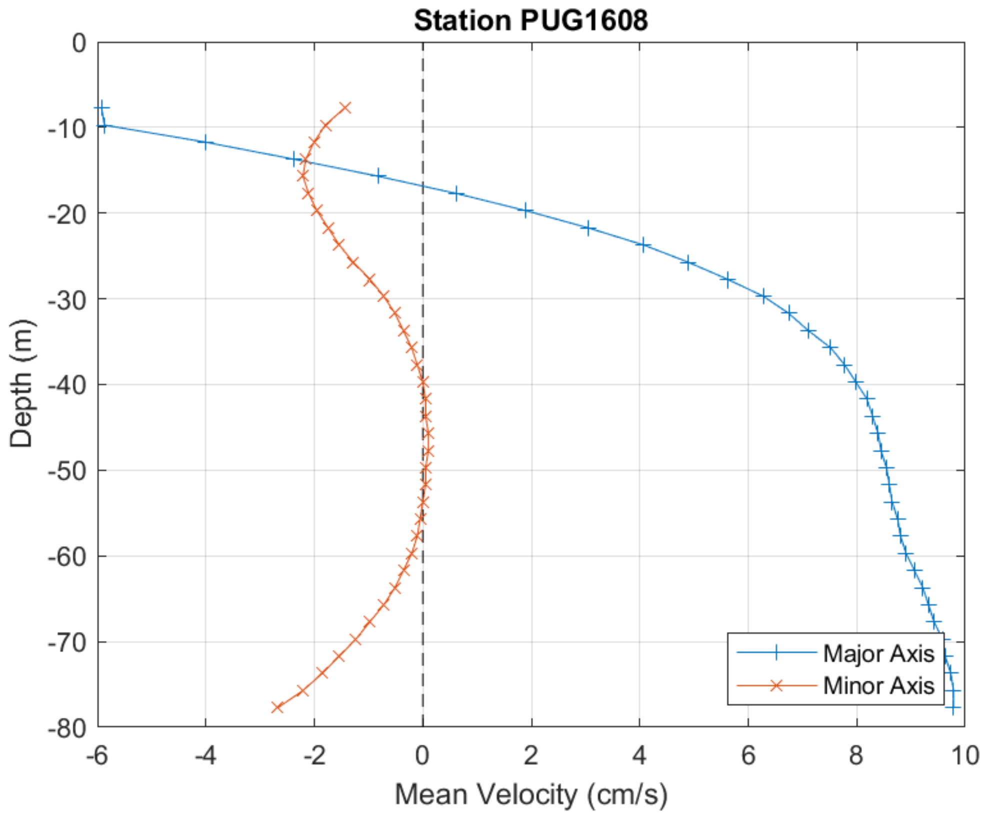

Figure 6-8. PUG1608 mean velocity profile by depth. Only depths that passed quality control criteria are shown. This station was configured to collect 2.0 m bins.

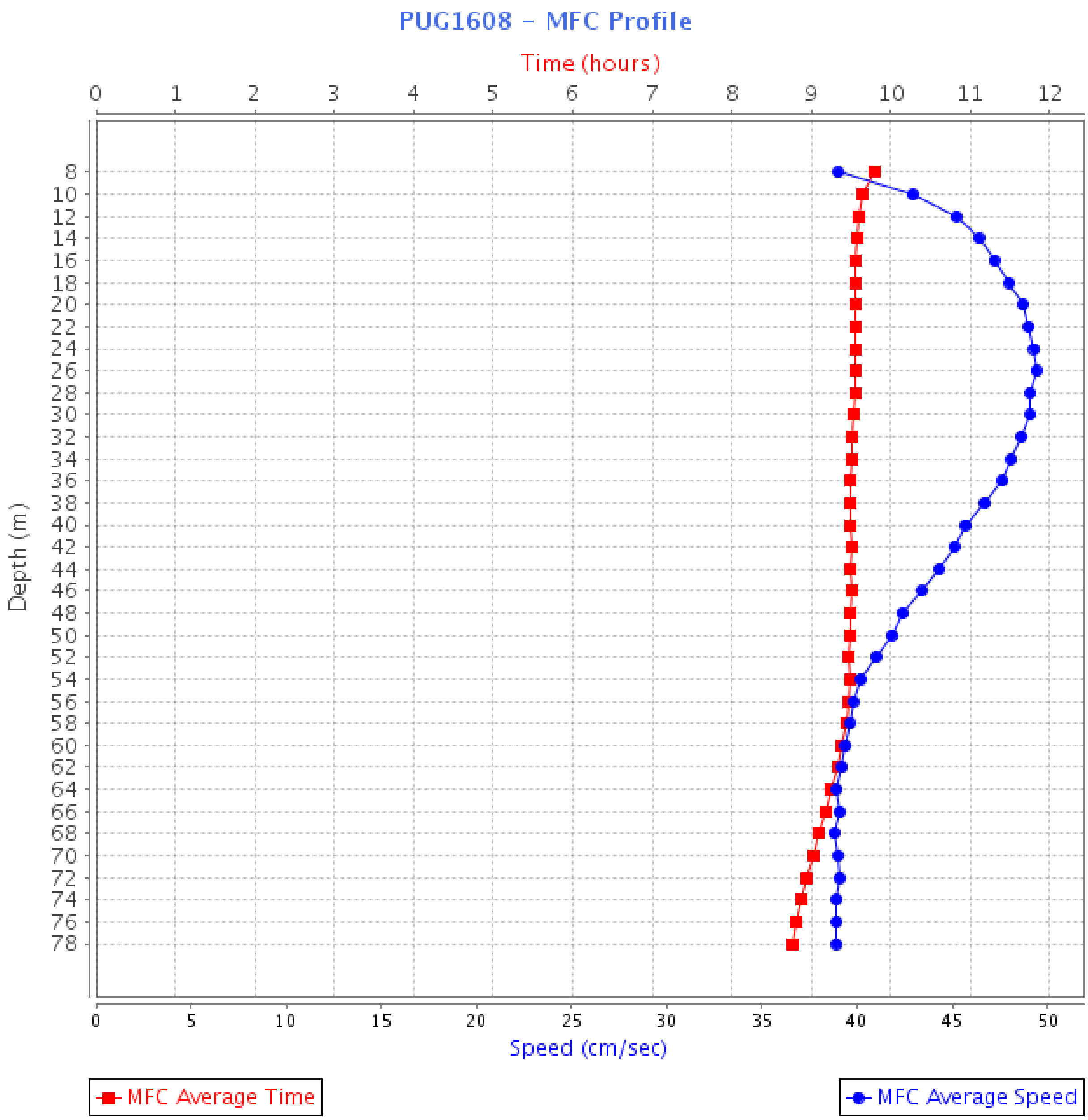

Figure 6-9. PUG1608 MFC timing (GI - in red squares) and speed (blue circles) by depth bin. Bin 1 is the deepest bin observed at approximately 77.7 m below MLLW, and the top-most good bin is bin 36 (7.7 m below MLLW).

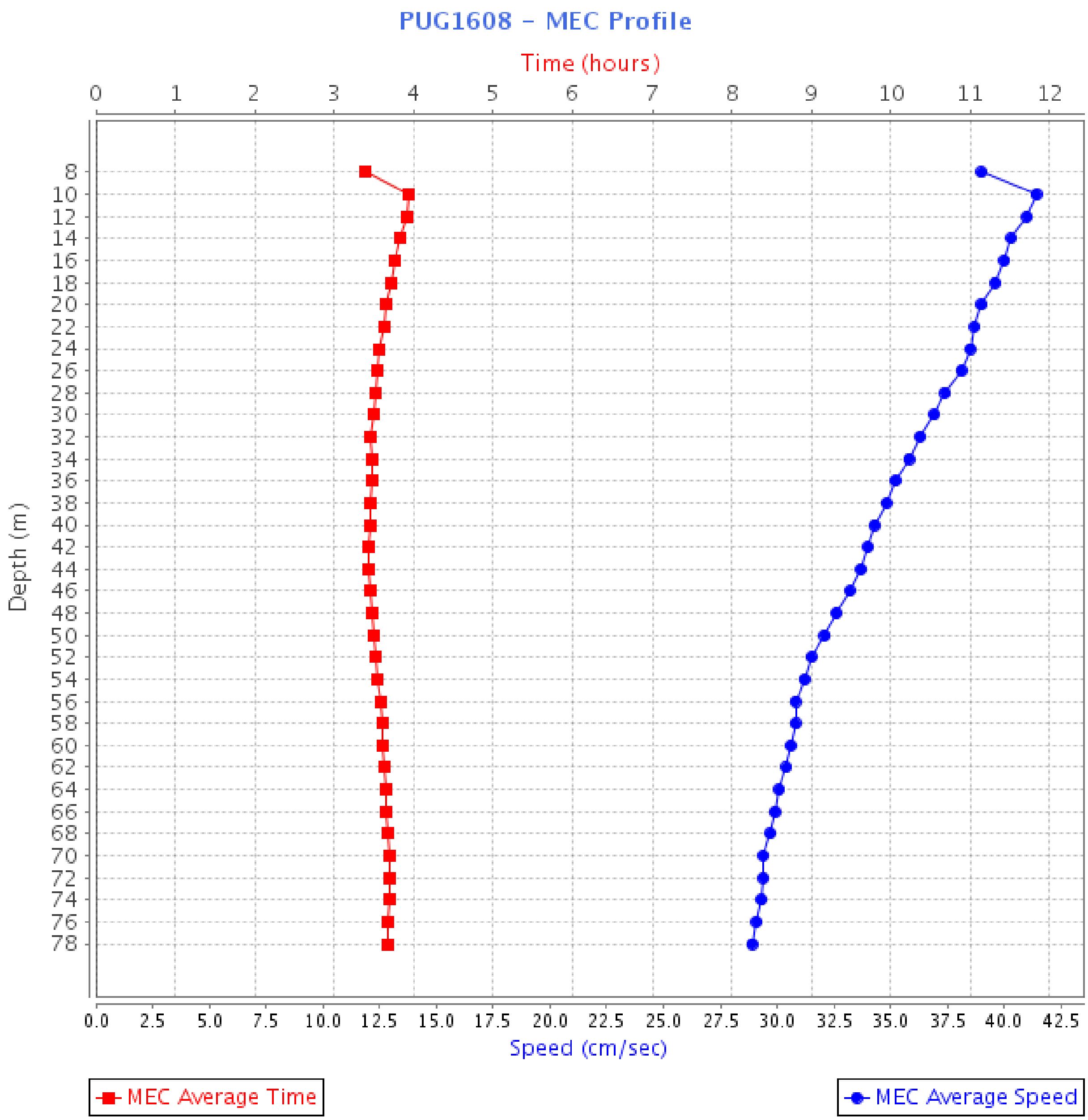

Figure 6-10. PUG1608 MEC timing (GI – red squares) and speed (blue circles) by depth bin. Bin 1 is the deepest bin observed at approximately 77.7 m below MLLW, and the top-most good bin is bin 36 (7.7 m below MLLW).

6.3. PUG1610 - Foulweather Bluff, 1.9 miles NE of

Foulweather Bluff was deployed for 128 days (April 20, 2016–August 26, 2016) in 107.3 m (351.8 ft) of water. A TRDI Workhorse 300 kHz ADCP mounted in a double SUBS collected 36, 2 m bins of data, 33 of which met quality control criteria for full analysis. Bins 17, 32, and 33 are published in the TCTs, representing approximate depths of 38.1 m , 8.1 m, and 6.1 m (124.9 ft, 26.5 ft, and 19.9 ft) MLLW, respectively, and supersede a historical station that was based on 4 days of data collected on June 17–21, 1963 in the TCTs. The tidal signal is very strong as shown by the harmonic analysis (LSQHA-29), which solved 94–98 percent of the total current energy. The currents are mostly rectilinear with the exception of the slight dogleg observed in the upper bins closer to the surface. Tides at this station are mixed, mainly semidiurnal with a Dietrich ratio of 0.48 in bin 32. MFC speeds range between 82 cm/s and 97 cm/s (1.59 kn and 1.88 kn), MEC speeds ranged between 80 cm/s and 111 cm/s (1.56 kn and 2.16 kn). This station is located near a bend in the shipping channel, most likely accounting for the dogleg seen in the velocity direction. Current directions are close to the orientation of this channel. The non-tidal residual current shows a traditional, two-way estuarine circulation pattern. Strong non-tidal flow in the minor axis direction is evidence of the irregular flood and ebb axes relative to each other.

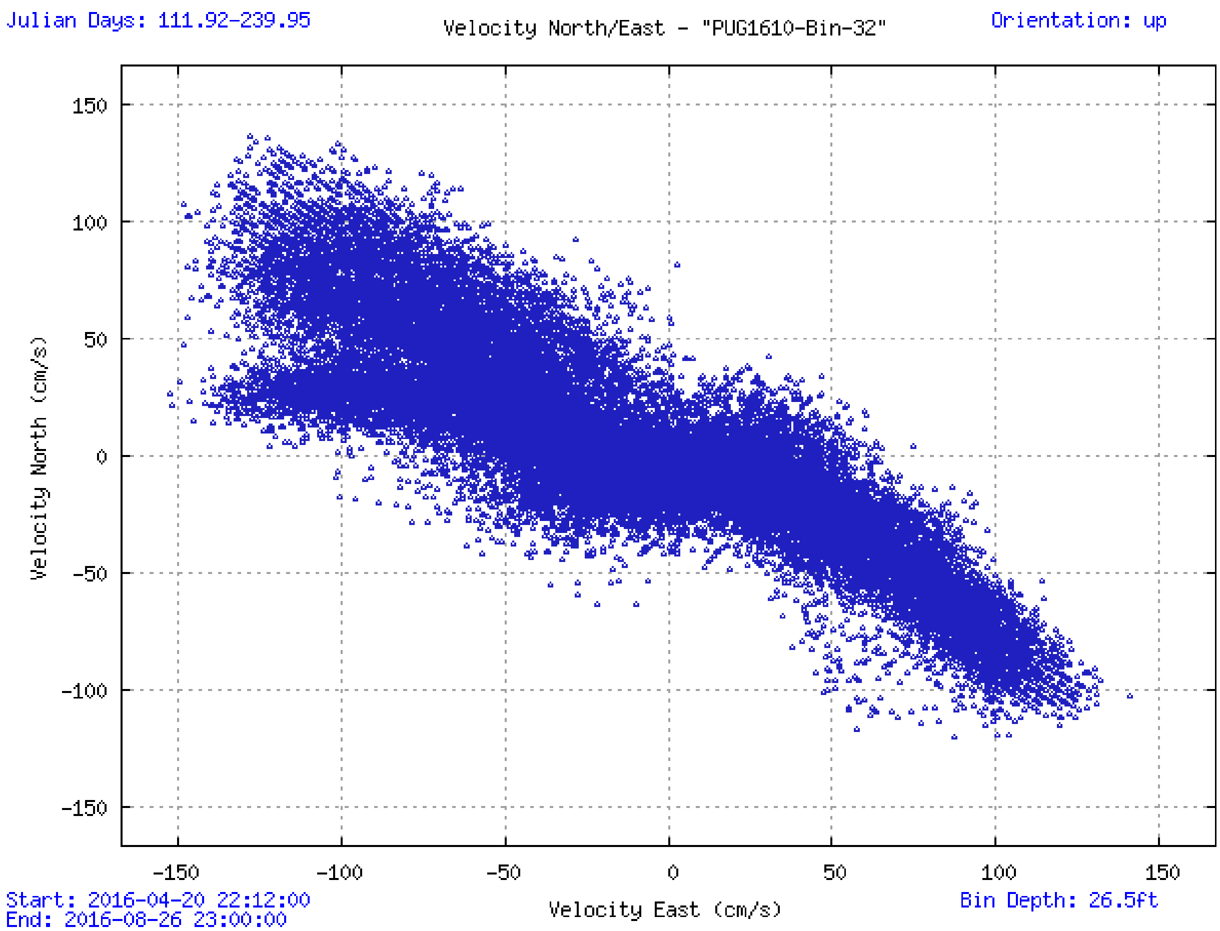

Figure 6-11. Scatter plot of north-versus-east velocity for station PUG1610 at the near-surface bin, bin 32 at 8.1 m below MLLW.

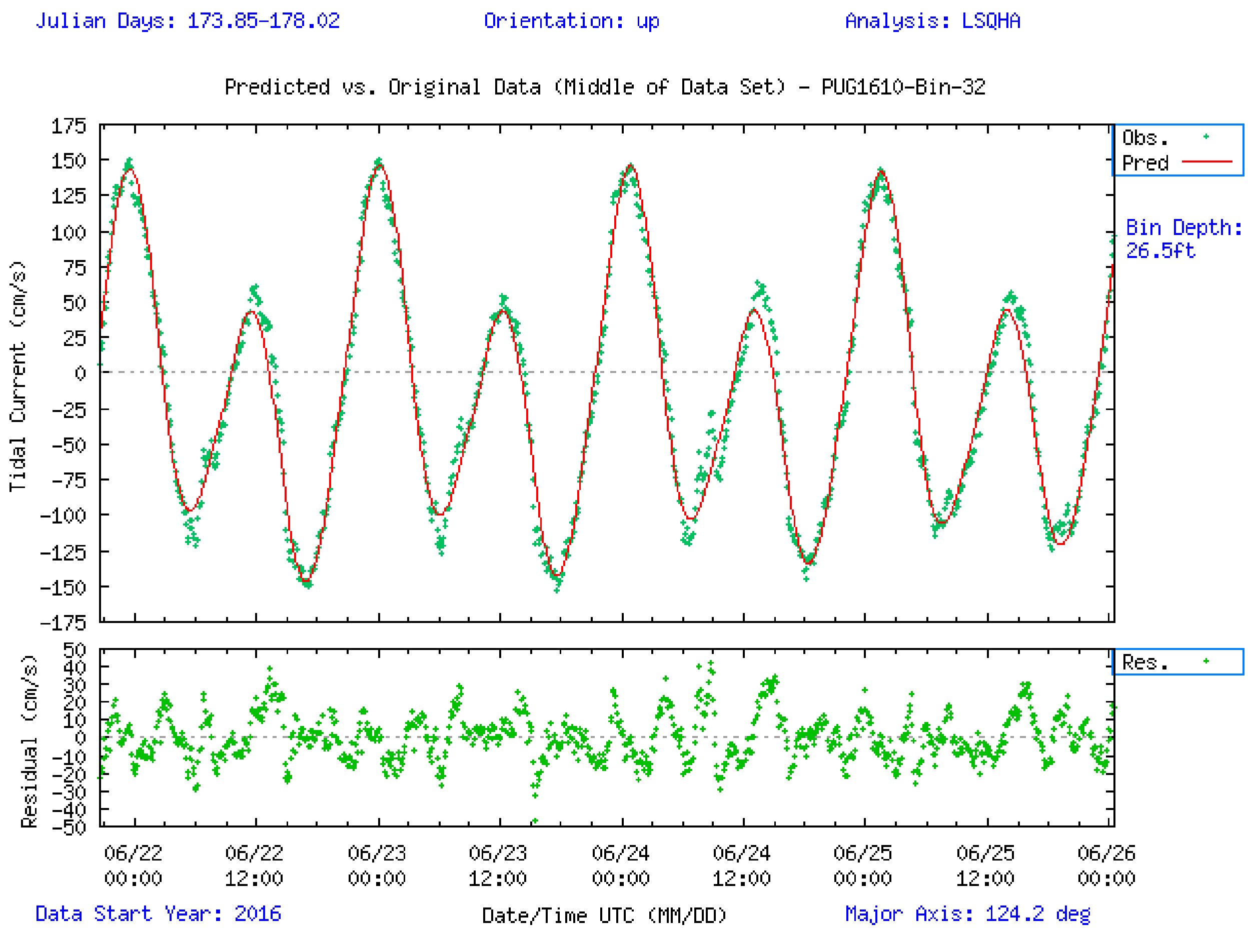

Figure 6-12. Comparison of observed major axis velocity data (green points) to predicted tidal velocity along the major axis for station PUG1610. The lower figure shows the non-tidal residual, the difference between the predicted and observed velocity from the upper panel.

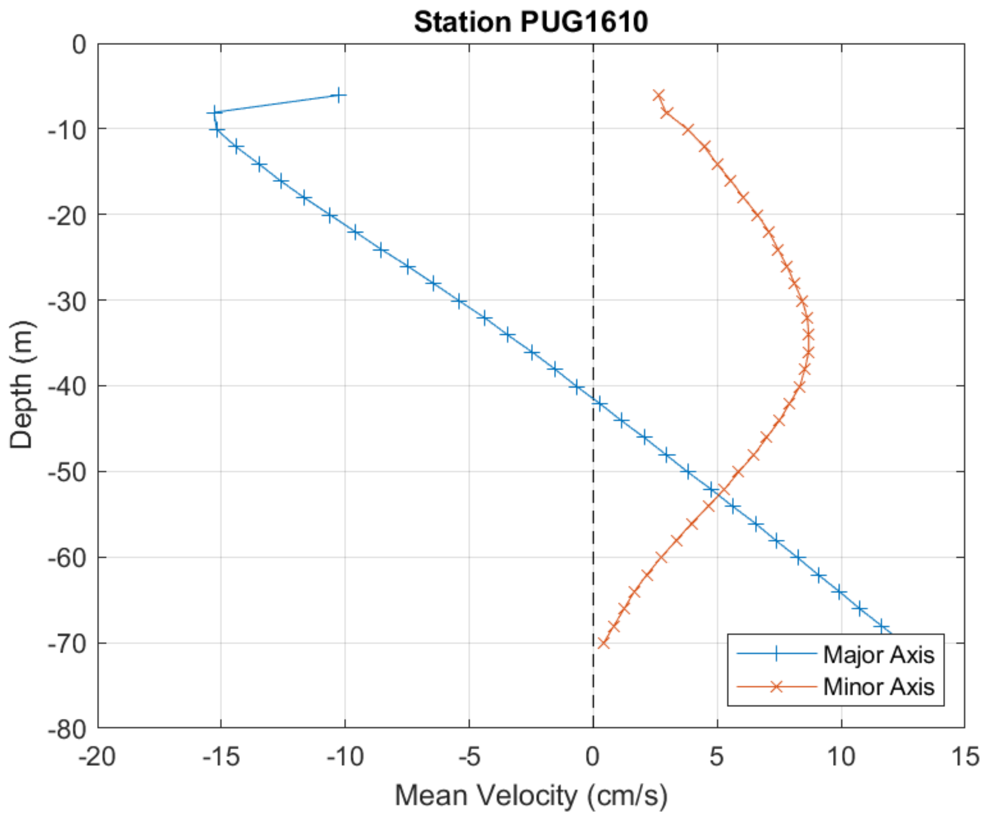

Figure 6-13. PUG1610 mean velocity profile by depth. Only depths that passed quality control criteria are shown. This station was configured to collect 2.0 m bins.

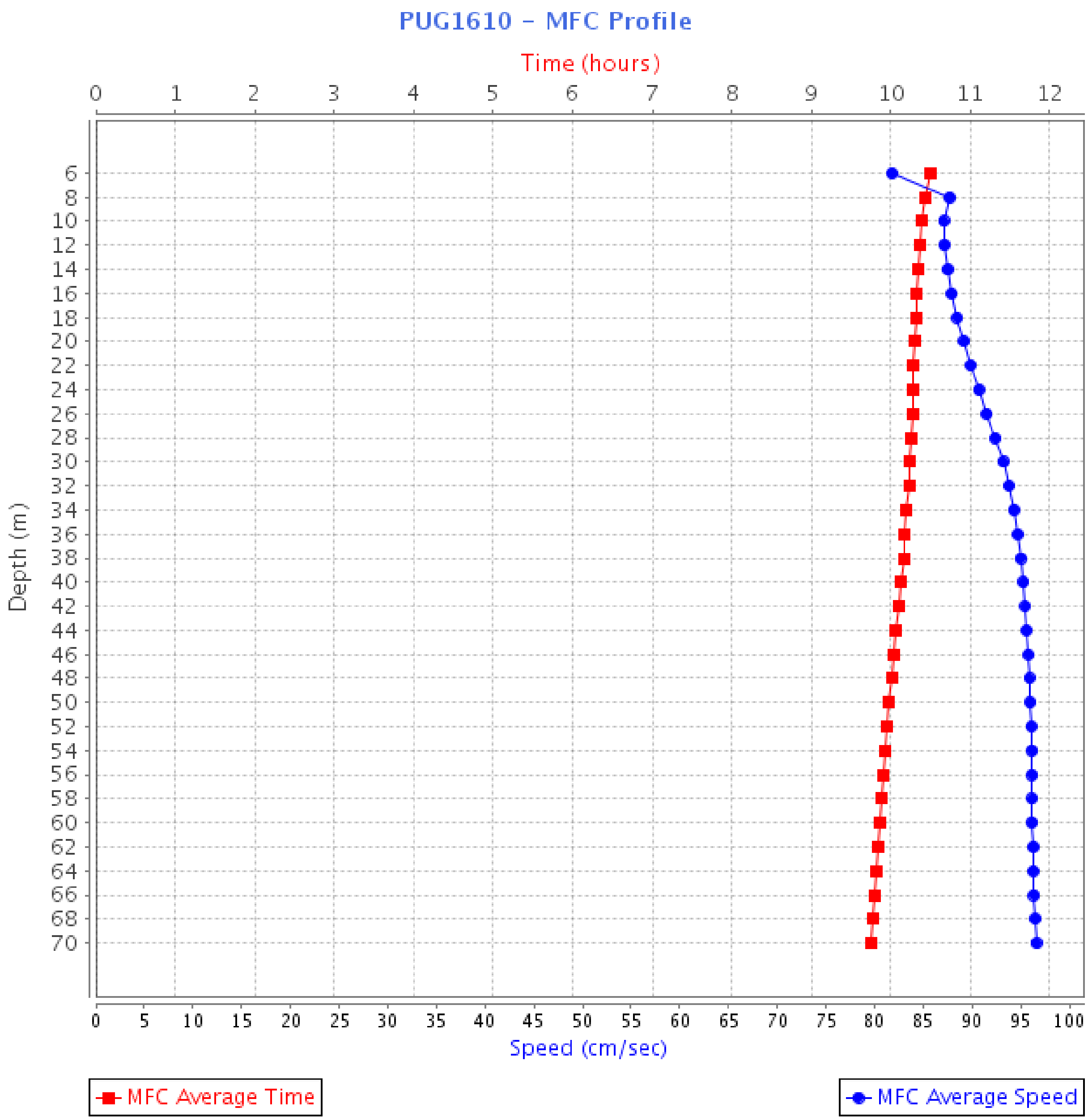

Figure 6-14. PUG1610 MFC timing (GI - in red squares) and speed (blue circles) by depth bin. Bin 1 is the deepest bin observed at approximately 70 m below MLLW, and the top-most good bin is bin 33 (6.1 m below MLLW).

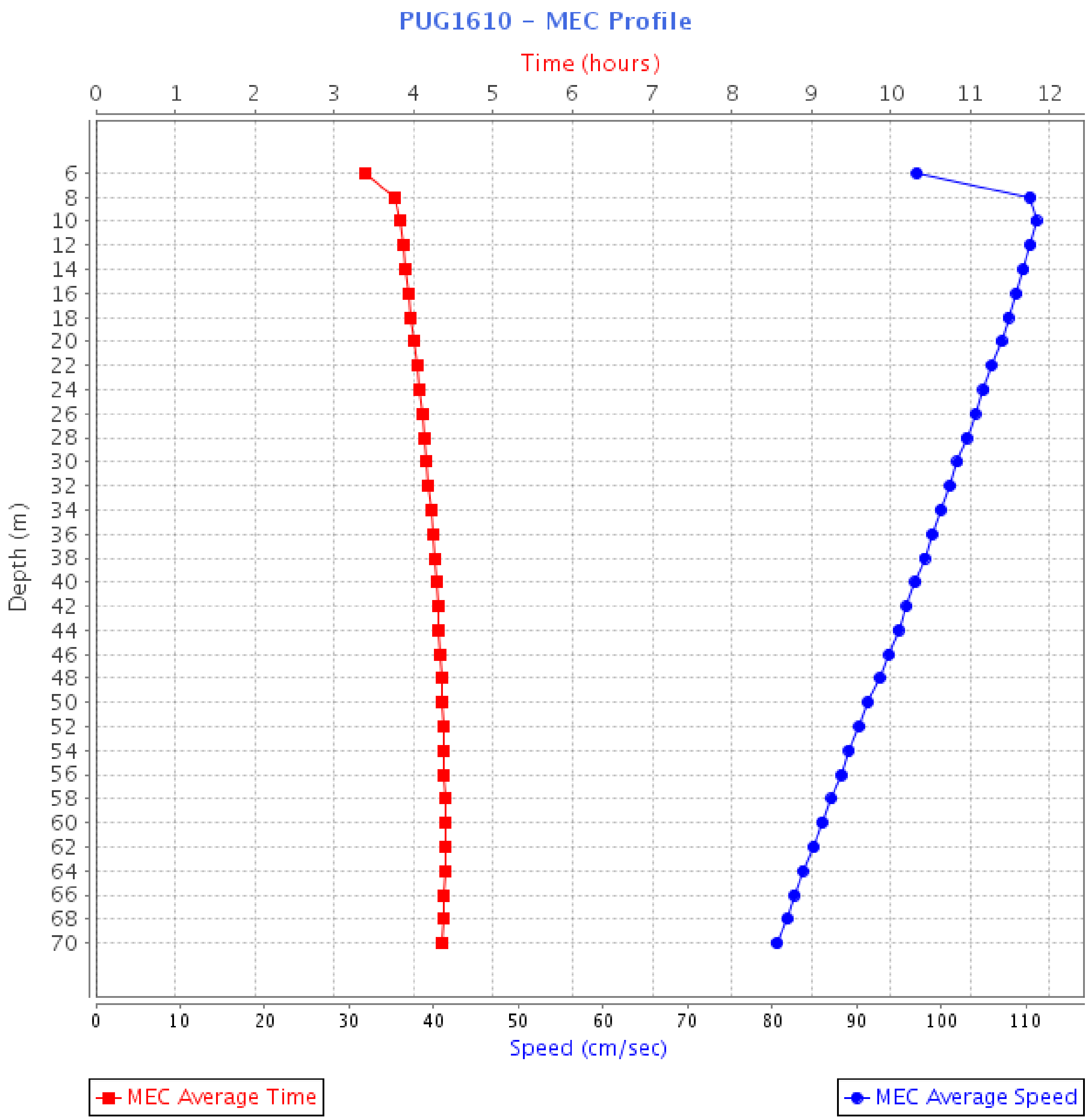

Figure 6-15. PUG1610 MEC timing (GI – red squares) and speed (blue circles) by depth bin. Bin 1 is the deepest bin observed at approximately 70 m below MLLW, and the top-most good bin is bin 33 (6.1 m below MLLW).

6.4. PUG1616 - Admiralty Inlet (off Bush Point)

This station was deployed for 121 days (April 20, 2016–August 19, 2016) in 106.3 m (347.9 ft) of water. A TRDI Workhorse 300 kHz ADCP mounted in a double SUBS collected 35, 2 m bins of data, 32 of which met quality control criteria for full analysis. Bins 6, 25, and 31 were published as a NOAA currents prediction, representing approximate depths of 58.9 m, 20.9 m, and 8.9 m (193.1 ft, 68.4 ft, and 29.0 ft) MLLW, respectively.

This station in Admiralty Inlet is at the center of a major thoroughfare of shipping for Seattle and Tacoma. Currents are rectilinear and fairly strong with a small dogleg, which is consistent with the orientation of the underlying bathymetry. This station is very tidal, which is seen in the harmonic analysis where 29 constituents are resolved, accounting for 95–98 percent of the total current energy. The Dietrich ratio falls between 0.5 and 0.6 for all bins; therefore, this station is mixed, mainly semidiurnal. The mean MFC and MEC currents (130 cm/s and 110 cm/s, respectively) are somewhat slower than the observed velocity maximums (around 200 cm/s) due to the mixed tidal regime. This effect is observed at many stations in this region.

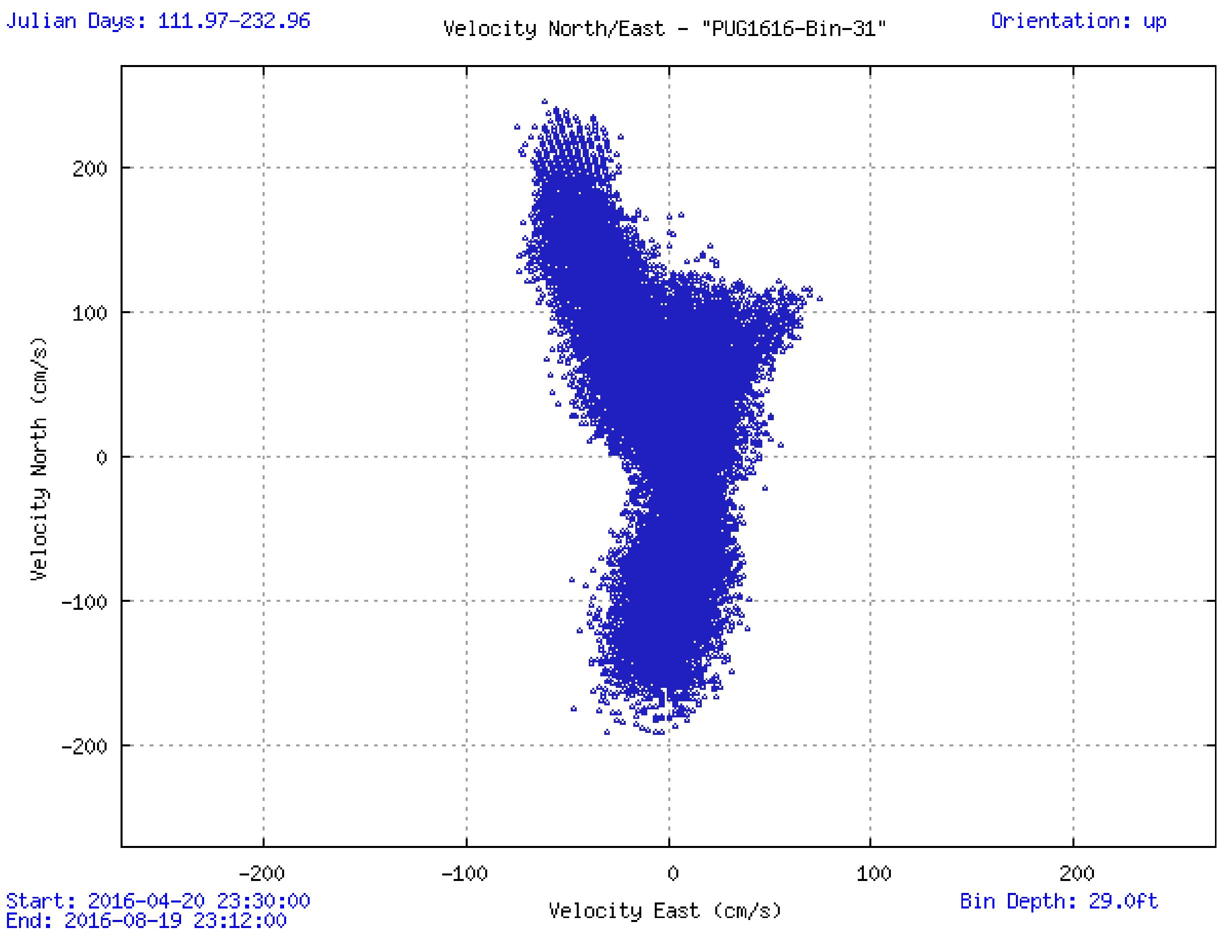

Figure 6-16. Scatter plot of north-versus-east velocity for station PUG1616 at the near-surface bin, bin 31 at 8.9 m below MLLW.

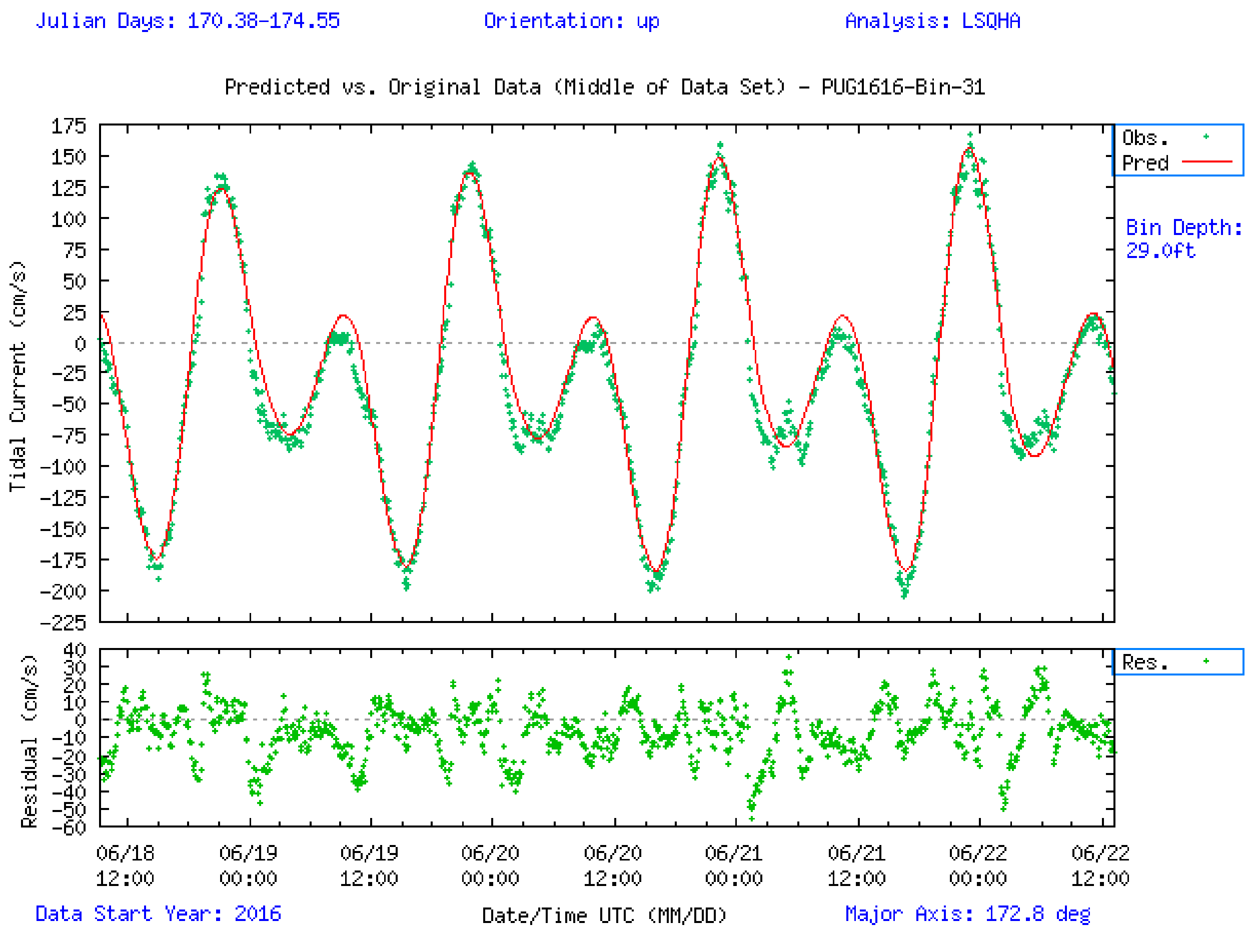

Figure 6-17. Comparison of observed major axis velocity data (green points) to predicted tidal velocity along the major axis for station PUG1616. The lower figure shows the non-tidal residual, the difference between the predicted and observed velocity from the upper panel.

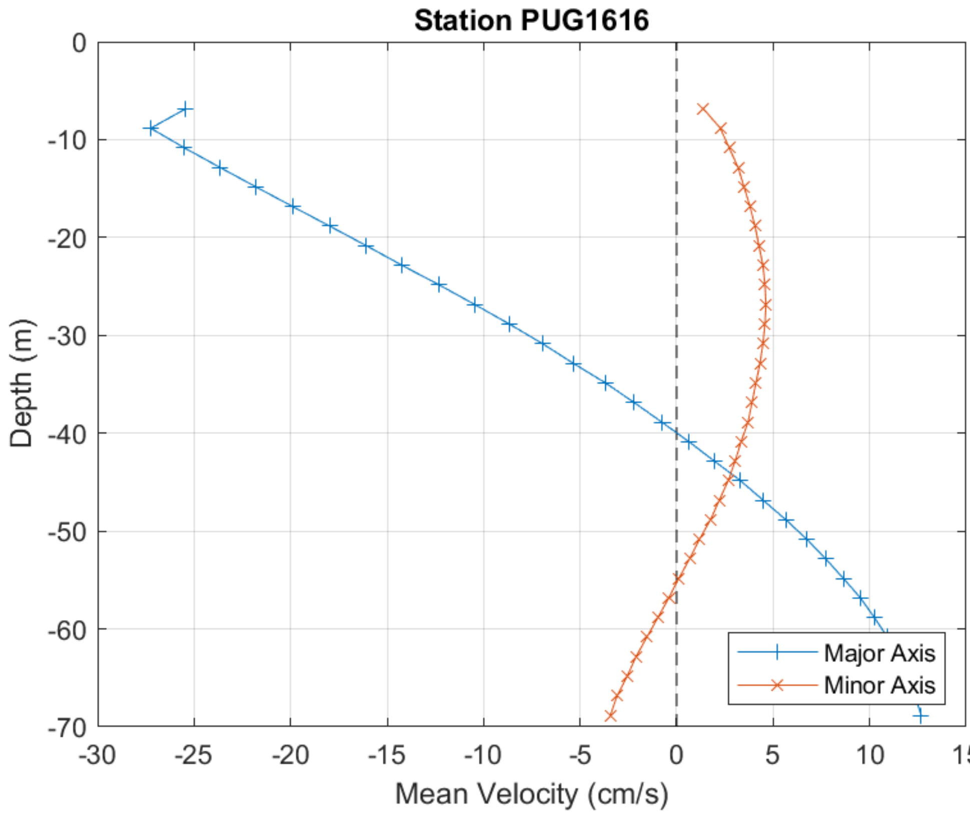

Figure 6-18. PUG1616 mean velocity profile by depth. Only depths that passed quality control criteria are shown. This station was configured to collect 2.0 m bins.

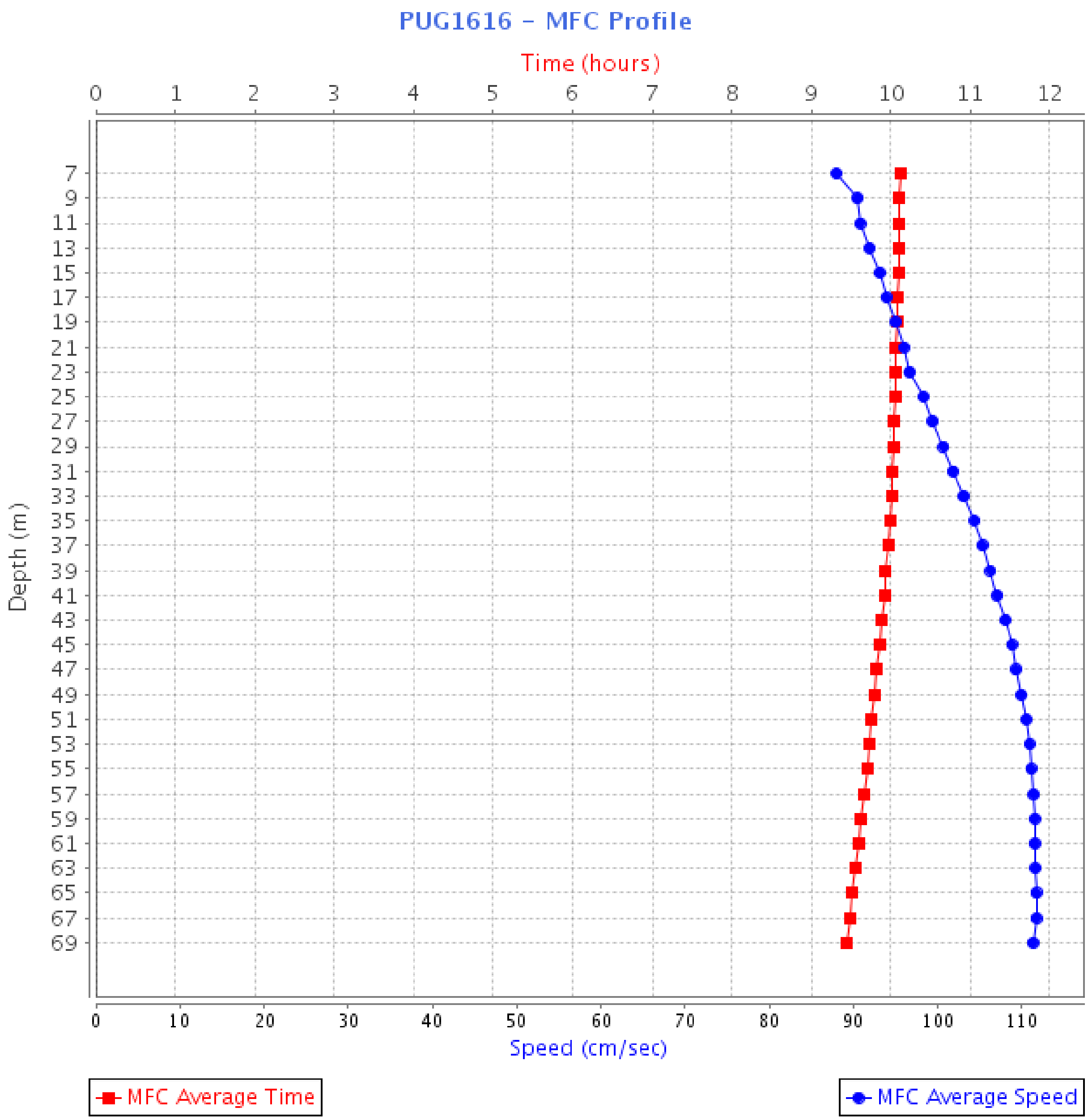

Figure 6-19. PUG1616 MFC timing (GI - in red squares) and speed (blue circles) by depth bin. Bin 1 is the deepest bin observed at approximately 70 m below MLLW, and the top-most good bin is bin 32 (6.9 m below MLLW).

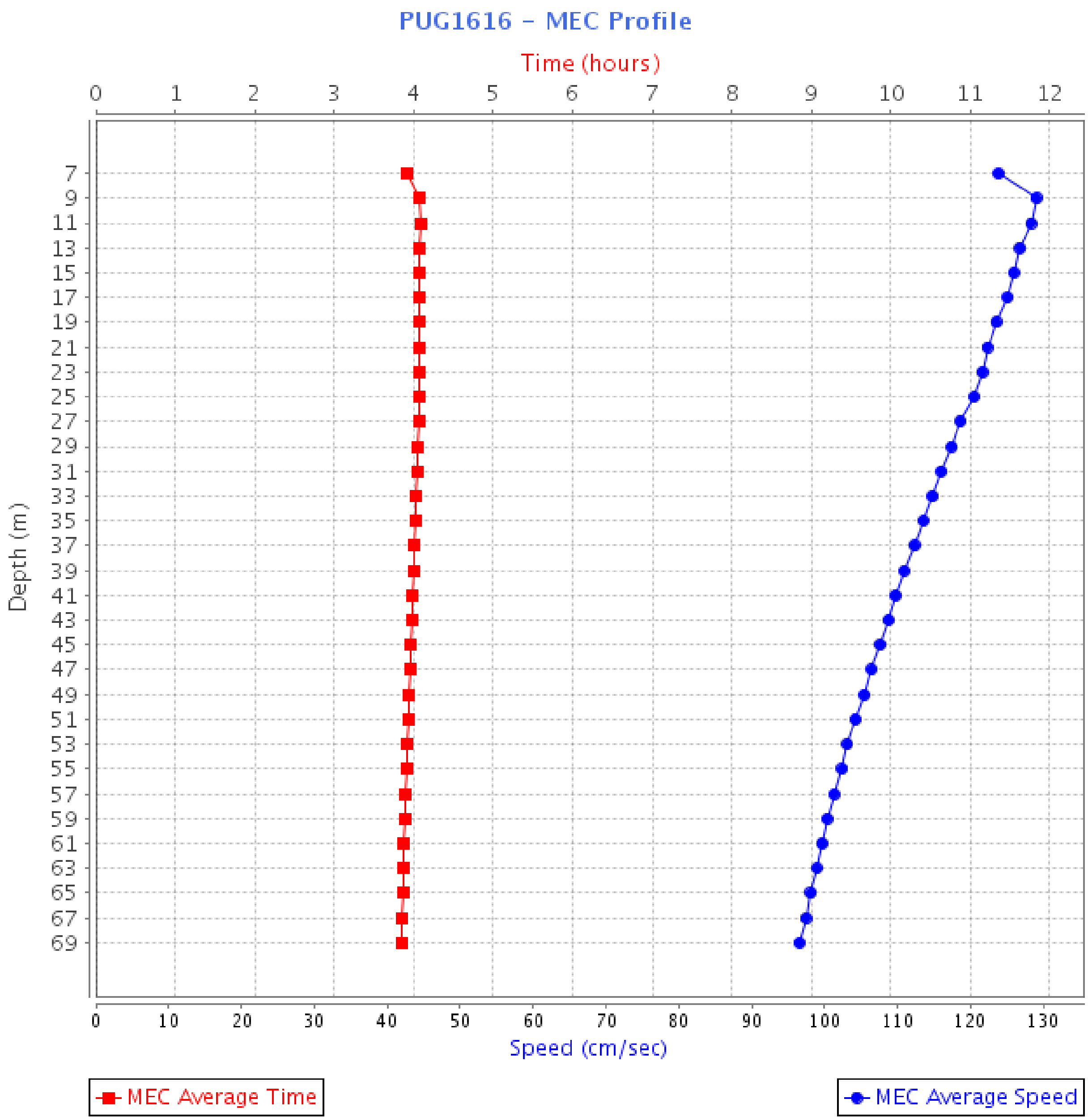

Figure 6-20. PUG1616 MEC timing (GI – red squares) and speed (blue circles) by depth bin. Bin 1 is the deepest bin observed at approximately 70 m below MLLW, and the top-most good bin is bin 32 (6.9 m below MLLW).

6.5. PUG1624 - Point Wilson, 1.6 miles NE of

This station was deployed for 117 days (April 26, 2016–August 21, 2016) in 66.5 m (218.1 ft) of water. A TRDI Workhorse 300 kHz ADCP mounted in a single SUBS collected 53, 1 m bins of data, 49 of which met quality control criteria for full analysis. Bins 1 (52.4 m [171.8 ft]), 27 (26.4 m [86.5 ft]), and 47 (6.4 m [21 ft]) are published in the TCTs. Bin 47 is a new reference station for the entrance to Puget Sound from the Strait of Juan de Fuca and the San Juan Islands.

Point Wilson marks the largest and busiest entrance to Puget Sound from the Strait of Juan de Fuca, while providing northbound access to the Strait of Juan de Fuca, the San Juan Islands, and the Inside Passage.

Currents are rectilinear with strong, mixed semidiurnal tidal forcing. LSQHA resolved 29 constituents and accounted for 97–99 percent of the total current energy. Currents move quickly through this opening with maximum ebb and flood speeds of upwards of 185 cm/s and 150 cm/s (3.6 kn and 2.9 kn), respectively. The mean velocity profile plot shows a characteristic estuarine circulation with net inflow at the bottom and net outflow near the surface and a bathymetrically driven net flow westward toward Point Wilson.

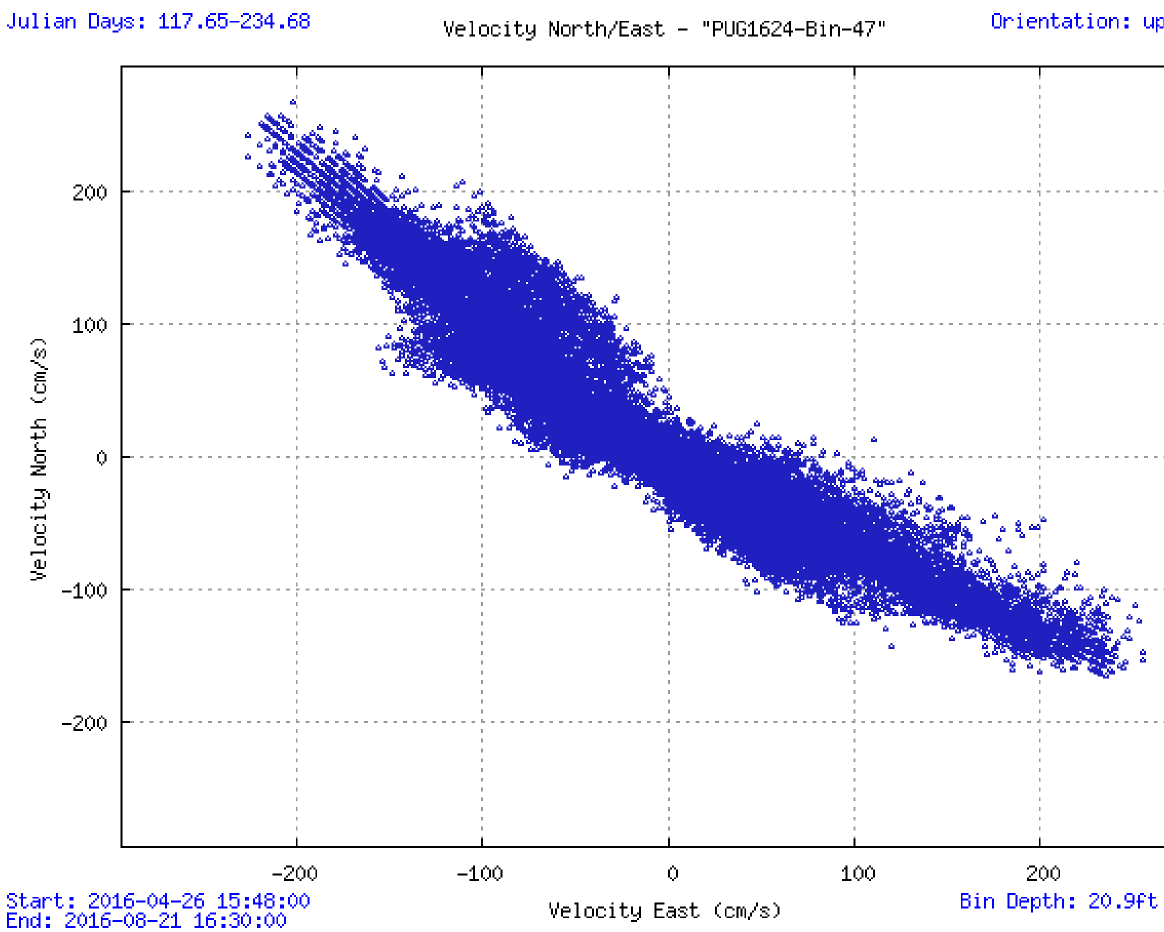

Figure 6-21. Scatter plot of north-versus-east velocity for station PUG1624 at the near-surface bin, bin 47 at 6.4 m below MLLW.

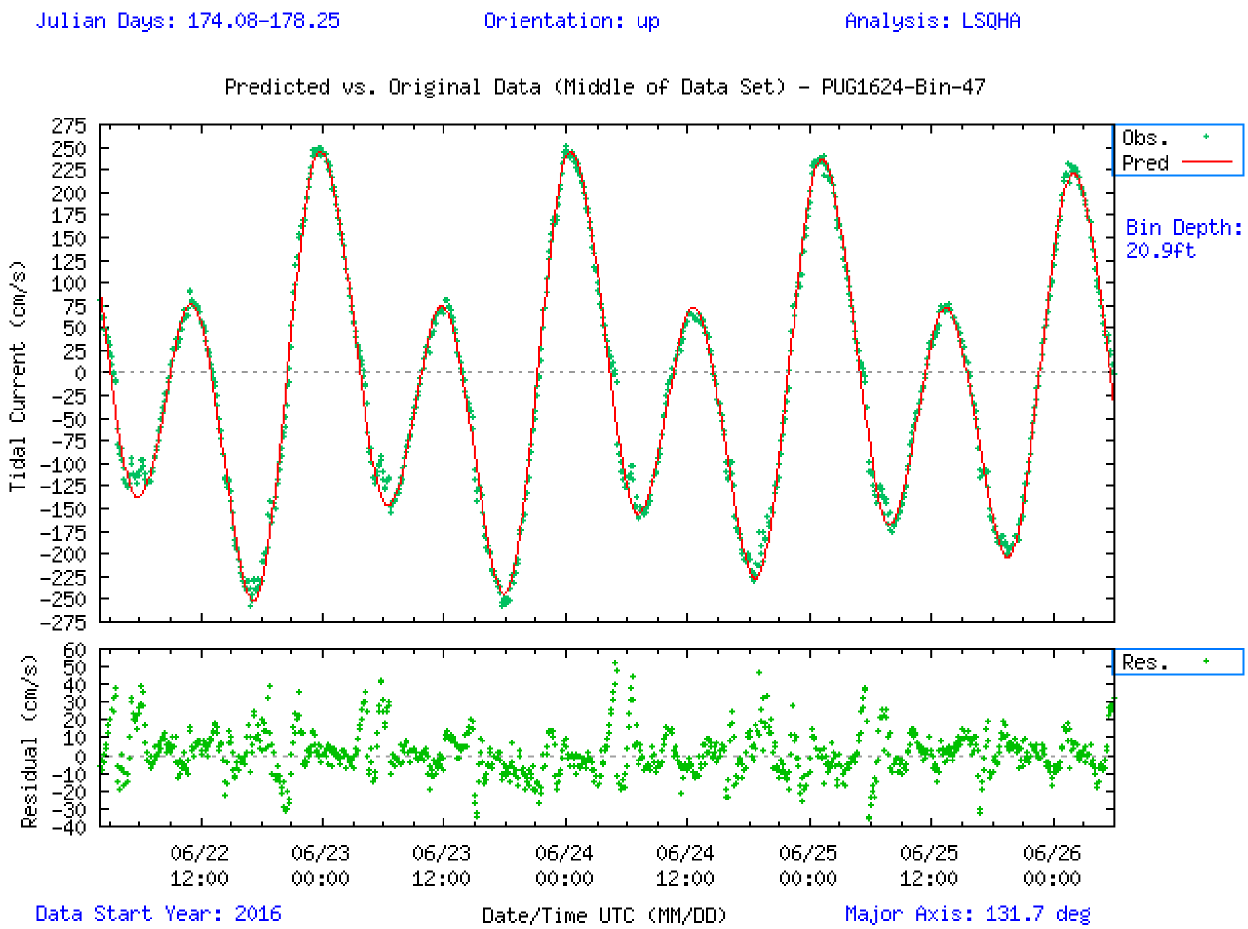

Figure 6-22. Comparison of observed major axis velocity data (green points) to predicted tidal velocity along the major axis for station PUG1624. The lower figure shows the non-tidal residual, the difference between the predicted and observed velocity from the upper panel.

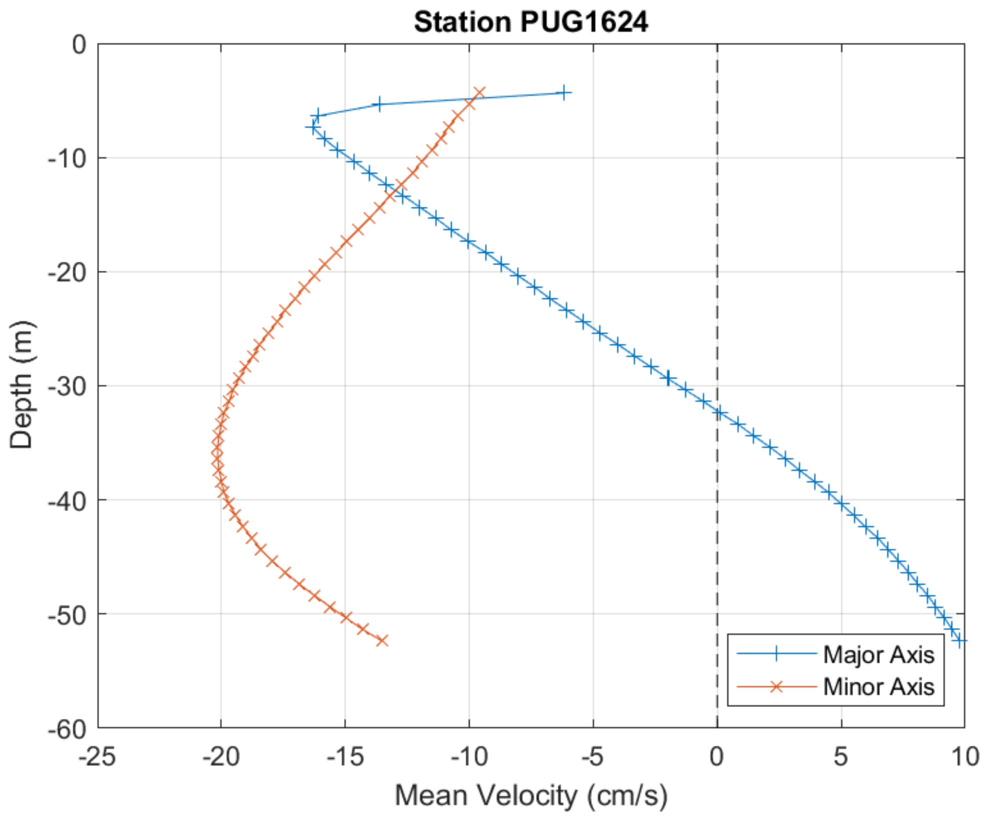

Figure 6-23. PUG1624 mean velocity profile by depth. Only depths that passed quality control criteria are shown. This station was configured to collect 2.0 m bins.

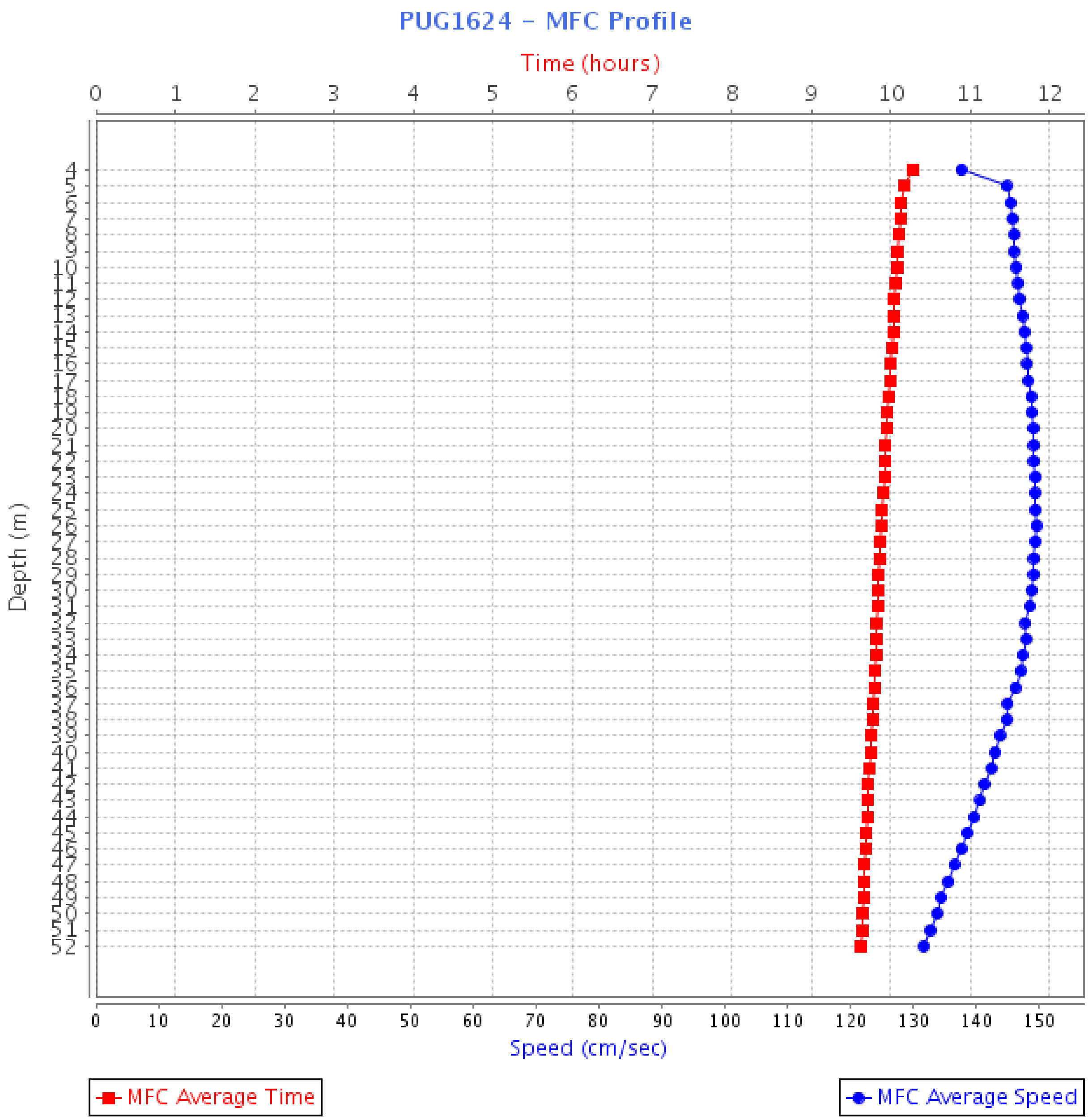

Figure 6-24. PUG1624 MFC timing (GI – red squares) and speed (blue circles) by depth bin. Bin 1 is the deepest bin observed at approximately 52.4 m below MLLW, and the top-most good bin is bin 49 (4.4 m below MLLW).

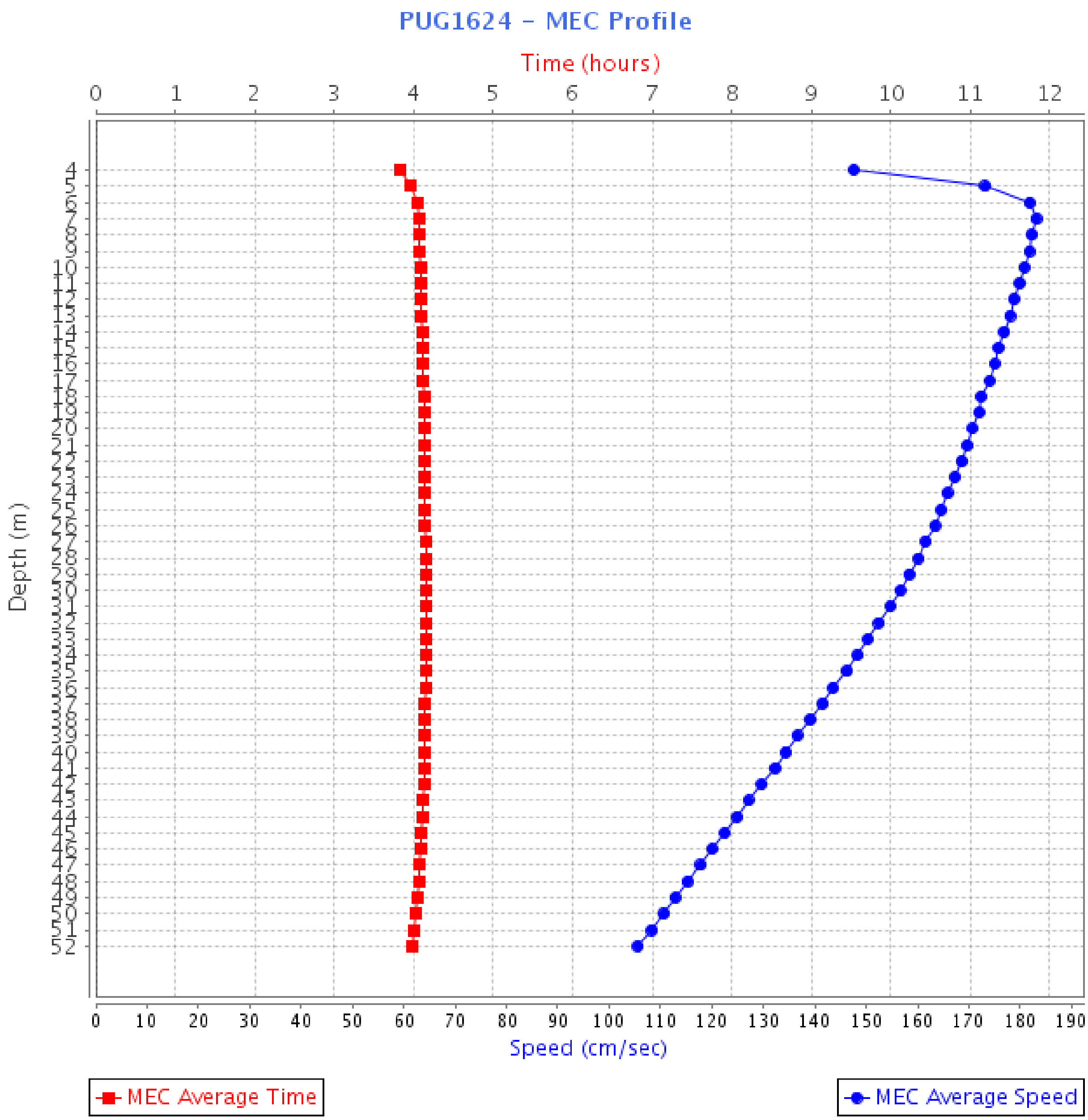

Figure 6-25. PUG1624 MEC timing (GI – red squares) and speed (blue circles) by depth bin. Bin 1 is the deepest bin observed at approximately 52.4 m below MLLW, and the top-most good bin is bin 49 (4.4 m below MLLW).

6.6. PUG1640 - Race Rocks, 4.5 miles S of

This station was deployed for 123 days (April 23, 2016–August 24, 2016) in 149.3 m (489.7 ft) of water. A TRDI Workhorse 300 kHz ADCP mounted in a deep water mooring collected 21, 6 m bins of data, 18 of which met quality control criteria for full analysis. Bins 1 (120.2 m [394.4 ft]), 9 (72.2 m [236.9 ft]), and 18 (18.2 m [59.7 ft]) are published in the TCTs. The nearest surface good bin measured (bin 18) is a new reference station in the TCTs for the eastern end of the Strait of Juan de Fuca.

This station at Race Rocks is at the eastern end of the Strait of Juan de Fuca, providing a point to understand the flow through the strait when compared with station PUG1642 (Point Wilson) at the western end of the strait. Currents at this location are rectilinear, following the east-west channel orientation. Currents are mixed, mainly semidiurnal. LSQHA with 29 constituents solved 95–97 percent of total current energy, making this location very tidal. Permanent current along the major axis exhibits behavior similar to station PUG1642 with net inward flow at depth and net outflow in the upper layers. Mean MEC range is between 67 cm/s and 103 cm/s (1.3 kn and 2.0 kn), the strongest being in the upper good bins 15–18. Mean MFC ranges from 51 cm/s to 93 cm/s (1.0 kn to 1.8 kn) and is the strongest in bins 4–9.

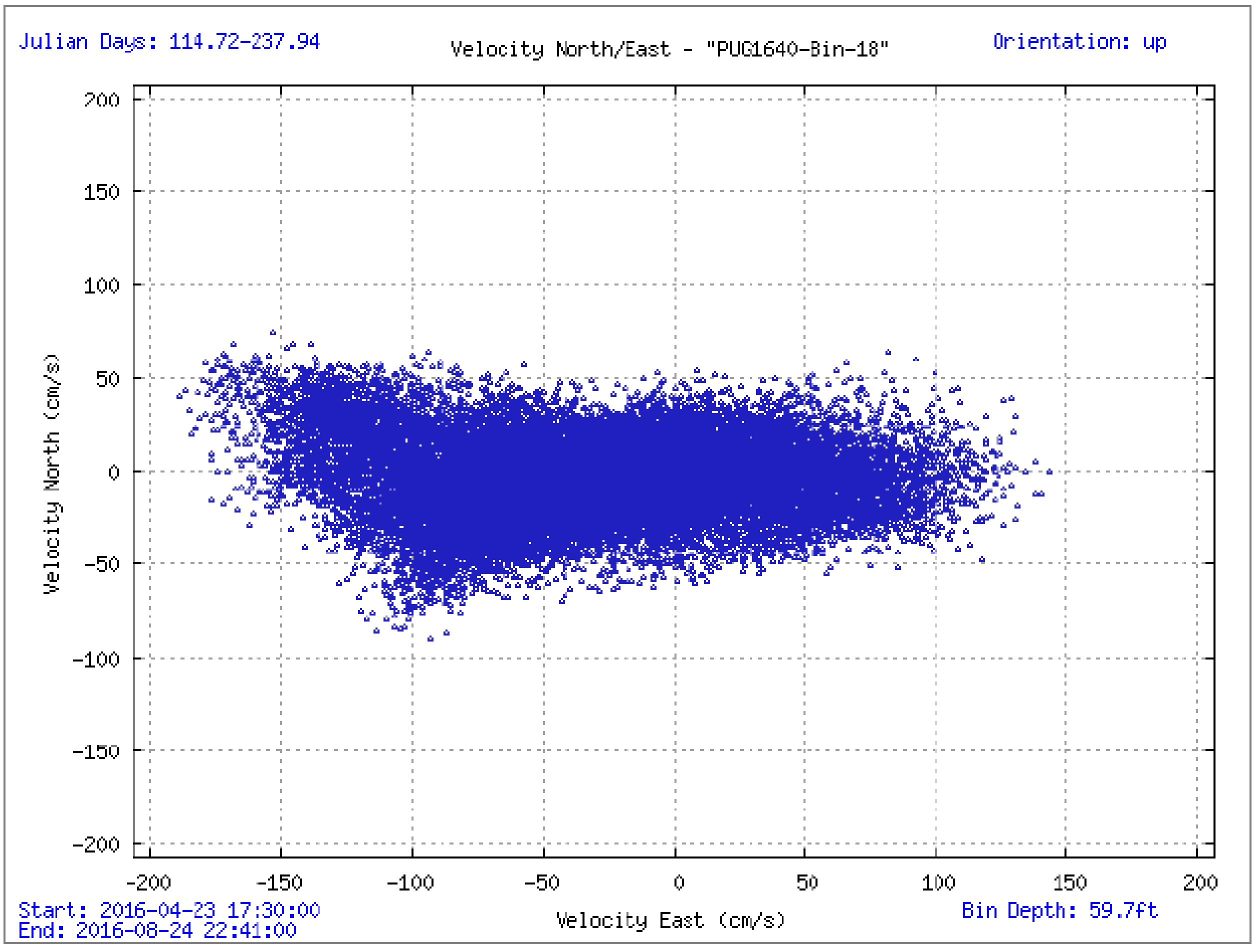

Figure 6-26. Scatter plot of north-versus-east velocity for station PUG1640 at the near-surface bin, bin 18 at 18.2 m below MLLW.

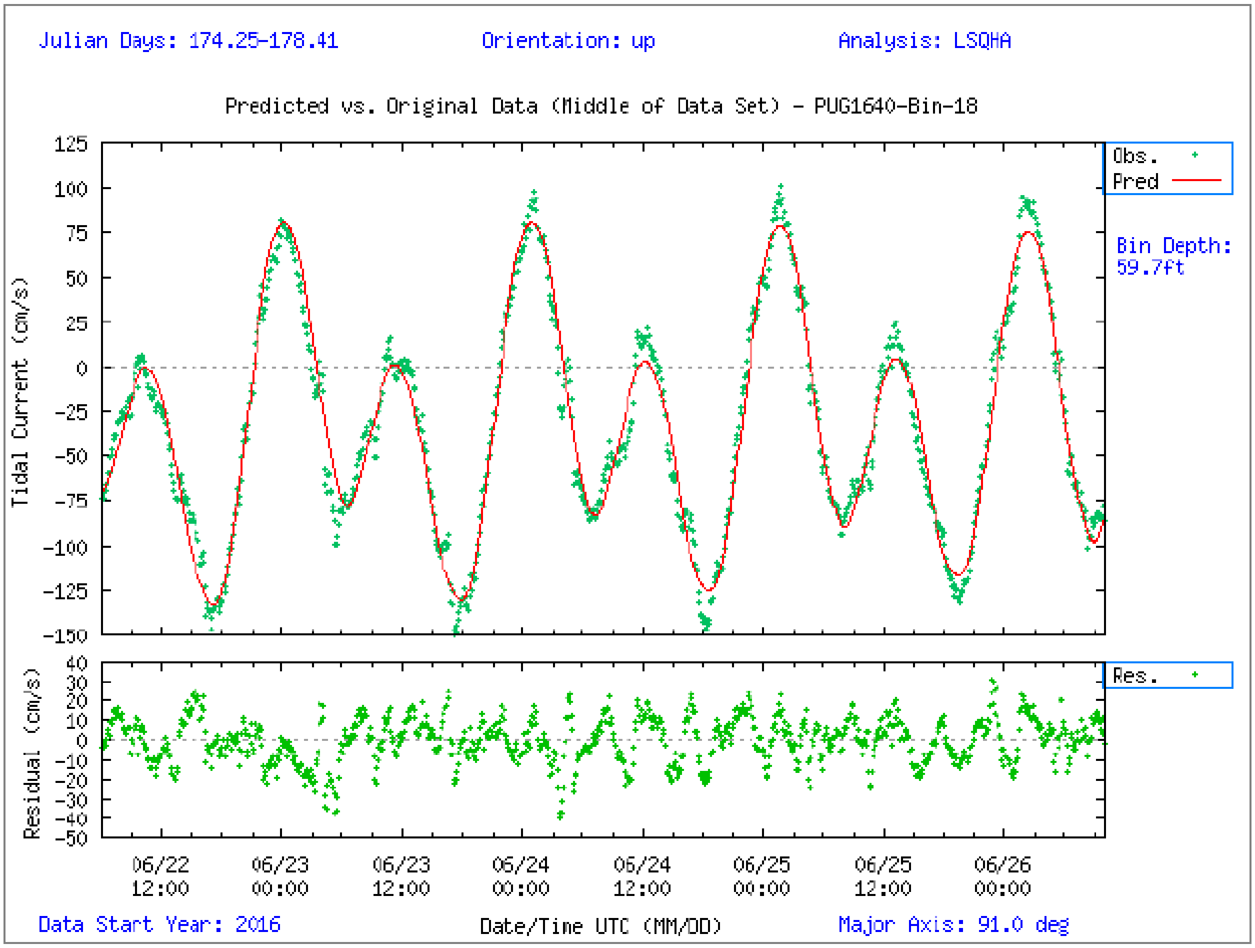

Figure 6-27. Comparison of observed major axis velocity data (green points) to predicted tidal velocity along the major axis for station PUG1640. The lower figure shows the non-tidal residual, the difference between the predicted and observed velocity from the upper panel.

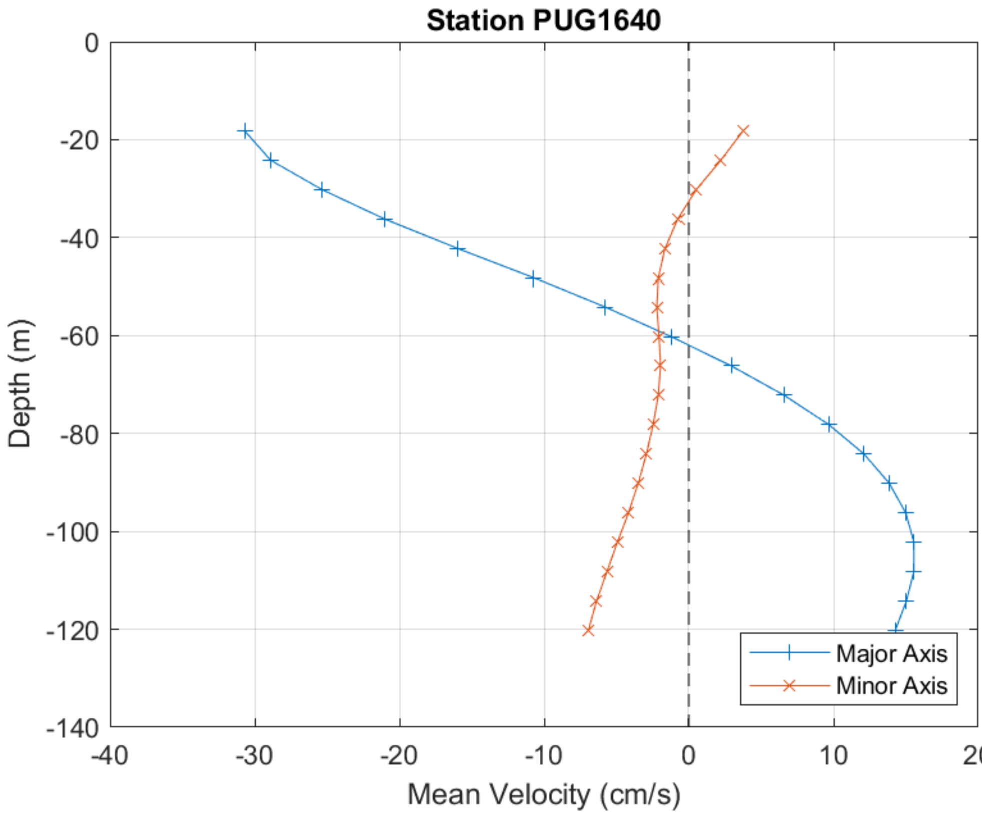

Figure 6-28. PUG1640 mean velocity profile by depth. Only depths that passed quality control criteria are shown. This station was configured to collect 6.0 m bins.

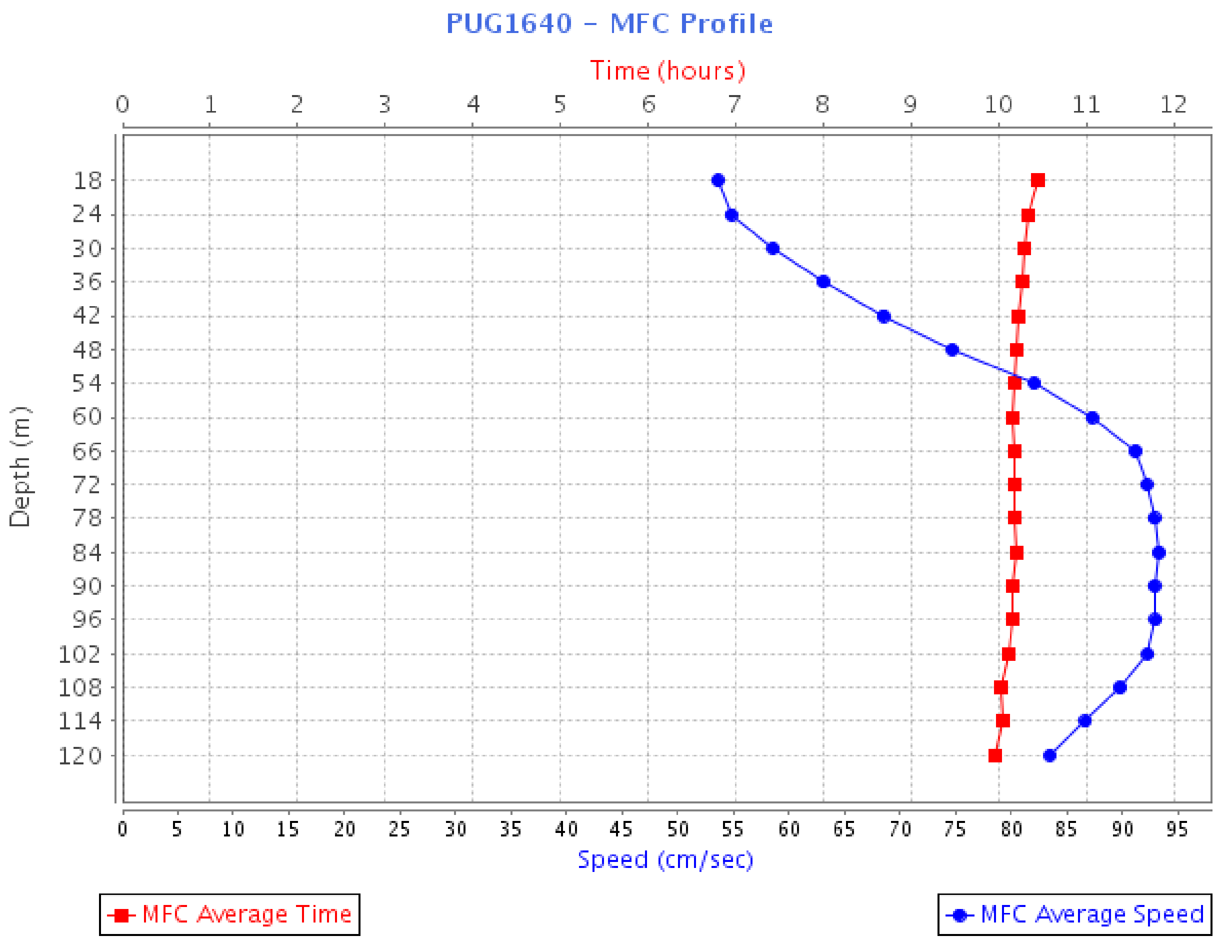

Figure 6-29. PUG1640 MFC timing (GI – red squares) and speed (blue circles) timing (GI – red squares) and speed (blue circles) by depth bin. Bin 1 is the deepest bin observed at approximately 52.4 m below MLLW, and the top-most good bin is bin 18 (18.2 m below MLLW).

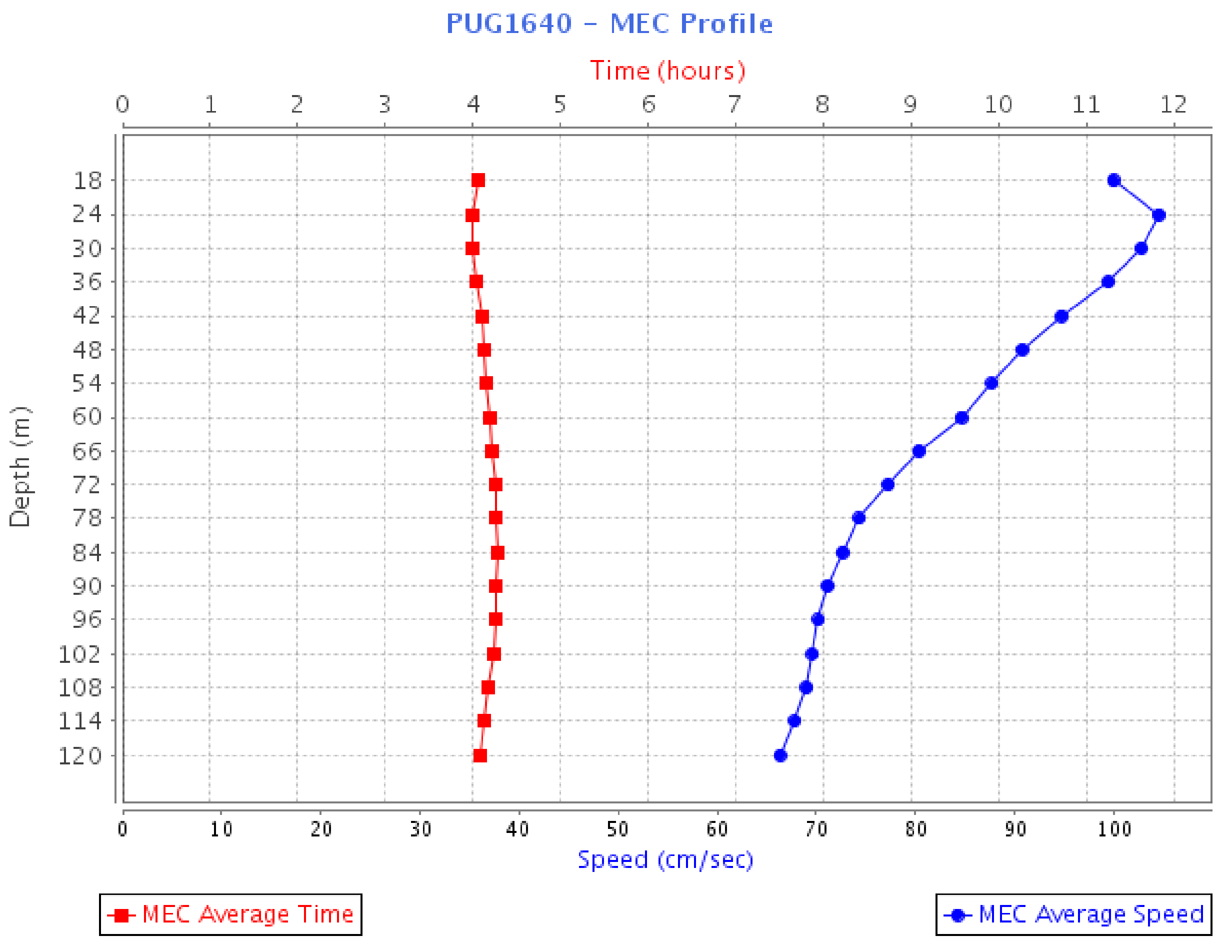

Figure 6-30. PUG1640 MEC timing (GI – red squares) and speed (blue circles) by depth bin. Bin 1 is the deepest bin observed at approximately 120 m below MLLW, and the top-most good bin is bin 18 (18.2 m below MLLW).

6.7. PUG1642 – Strait of Juan de Fuca Entrance

This station was deployed for 123 days (April 22, 2016–August 24, 2016) in 251.0 m (823.3 ft) of water. A TRDI Workhorse 75 kHz ADCP mounted in a deep water mooring collected 56, 4 m bins of data, 50 of which met quality control criteria for full analysis. Bins 22 (139.0 m [456.1 ft]), 49 (31.0 m [101.8 ft]), and 50 (27.0 m [88.6 ft]) are published in the TCTs. Bin 50 is a new reference station for the entrance of the Strait of Juan de Fuca at its opening to the Pacific Ocean.

The Strait of Juan de Fuca is an important passage between Vancouver Island and Washington State as it is the primary pathway for exchange between the Salish Sea and the Pacific Ocean. It is the seaward terminus for the Puget Sound and, along with the Strait of Georgia, provides access to the San Juan Islands. Currents are rectilinear with tides that are mixed-semidiurnal. LSQHA resolved 29 constituents and accounted for 84–97 percent of the total current energy. Tidal currents move at mean ebb and flood speeds between 31 cm/s and 77 cm/s (0.6 kn and 1.5 kn), respectively. The mean velocity profile plot (Figure 6-34) shows there is a slow net inflow of ocean water occurring below 70 m (bin 39 [230 ft]) and a faster net outflow above 70 m.

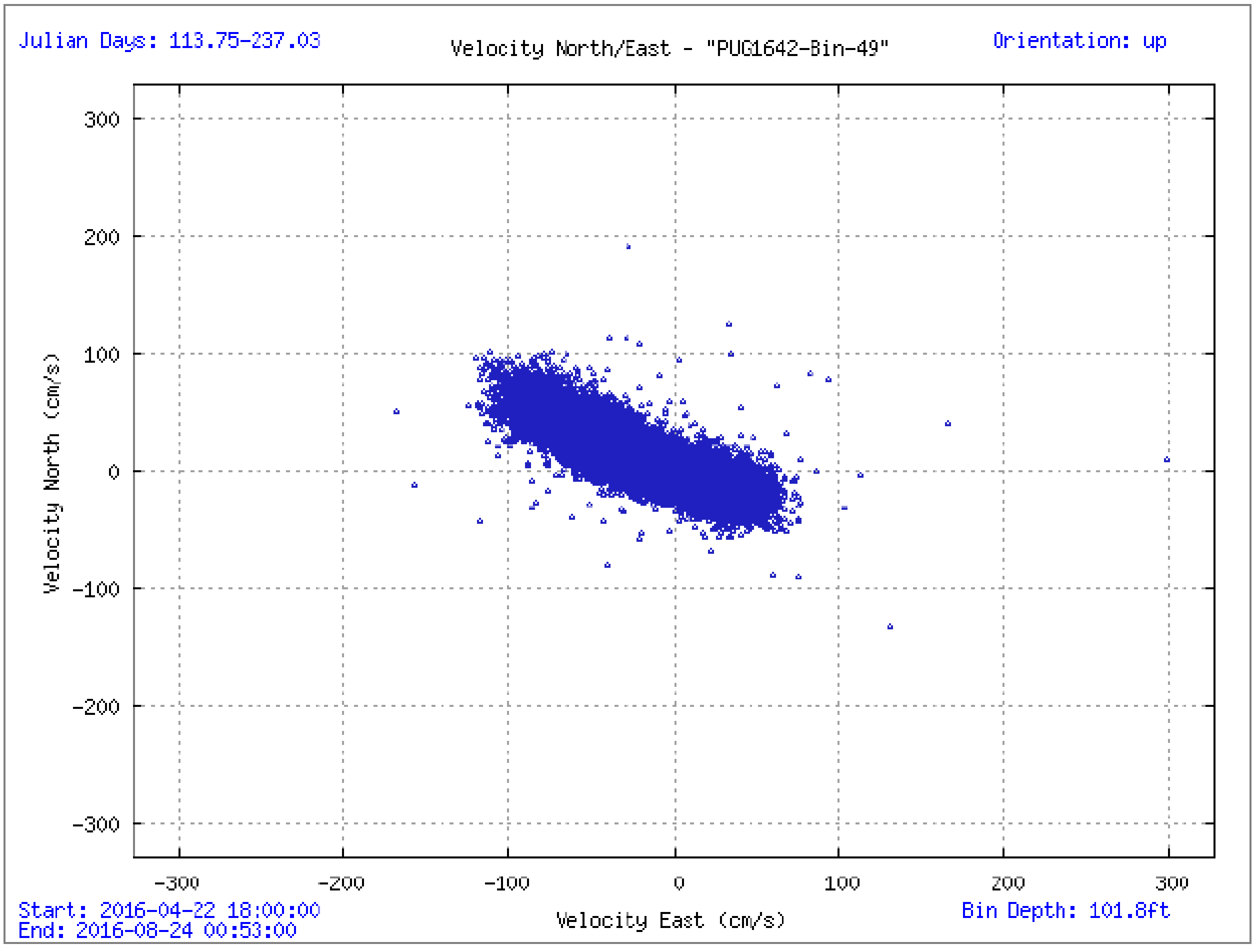

Figure 6-31. Scatter plot of north-versus-east velocity for station PUG1642 at the near-surface bin, bin 49 at 31 m below MLLW. Bin 49, although not the uppermost good bin (50) was selected as it was more indicative of the currents in this location.

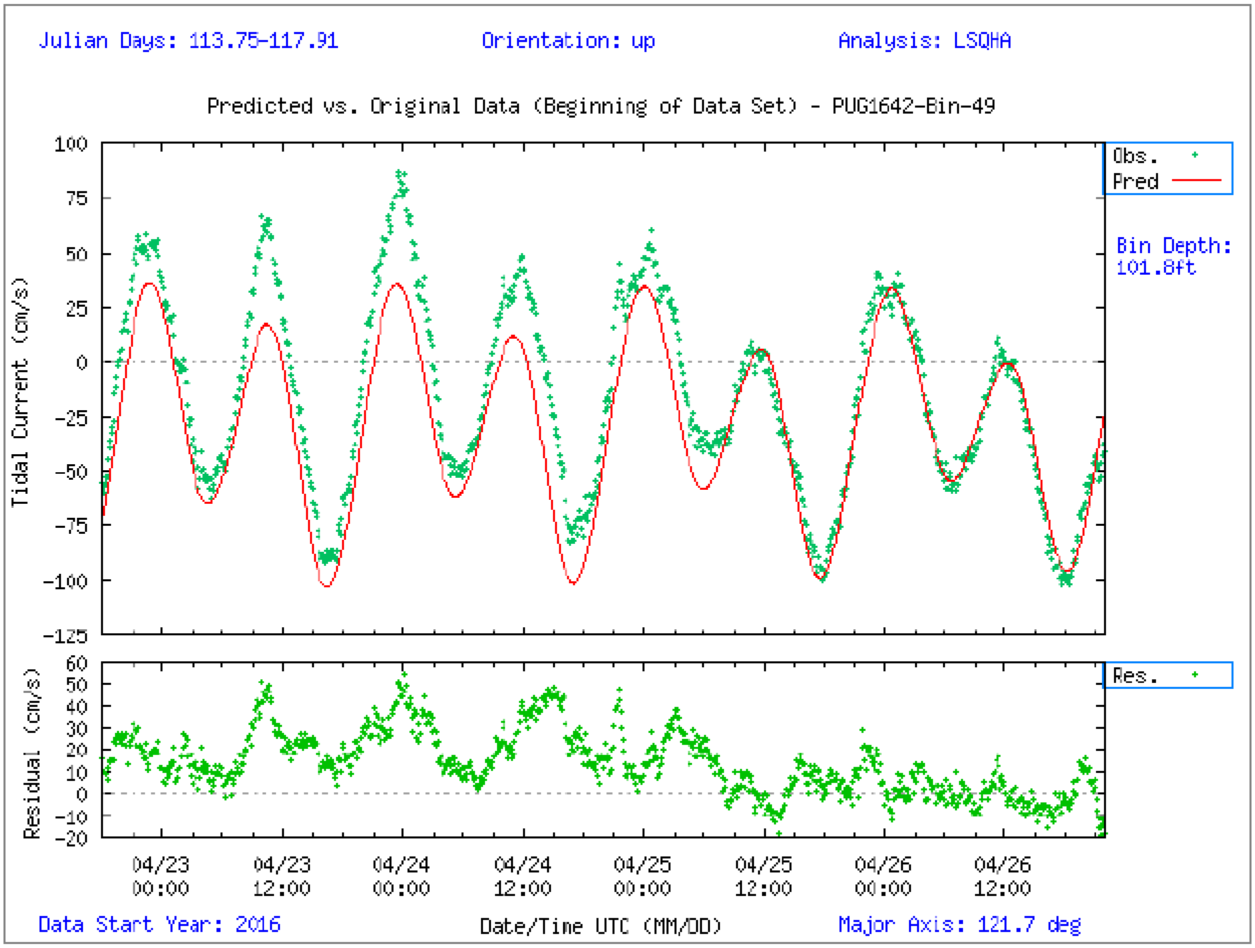

Figure 6-32. Comparison of observed major axis velocity data (green points) to predicted tidal velocity along the major axis for station PUG1642. The lower figure shows the non-tidal residual, the difference between the predicted and observed velocity from the upper panel. This example comparison shows data near spring tides when the difference is smallest between the stronger and weaker of the daily semidiurnal flood and ebb tides.

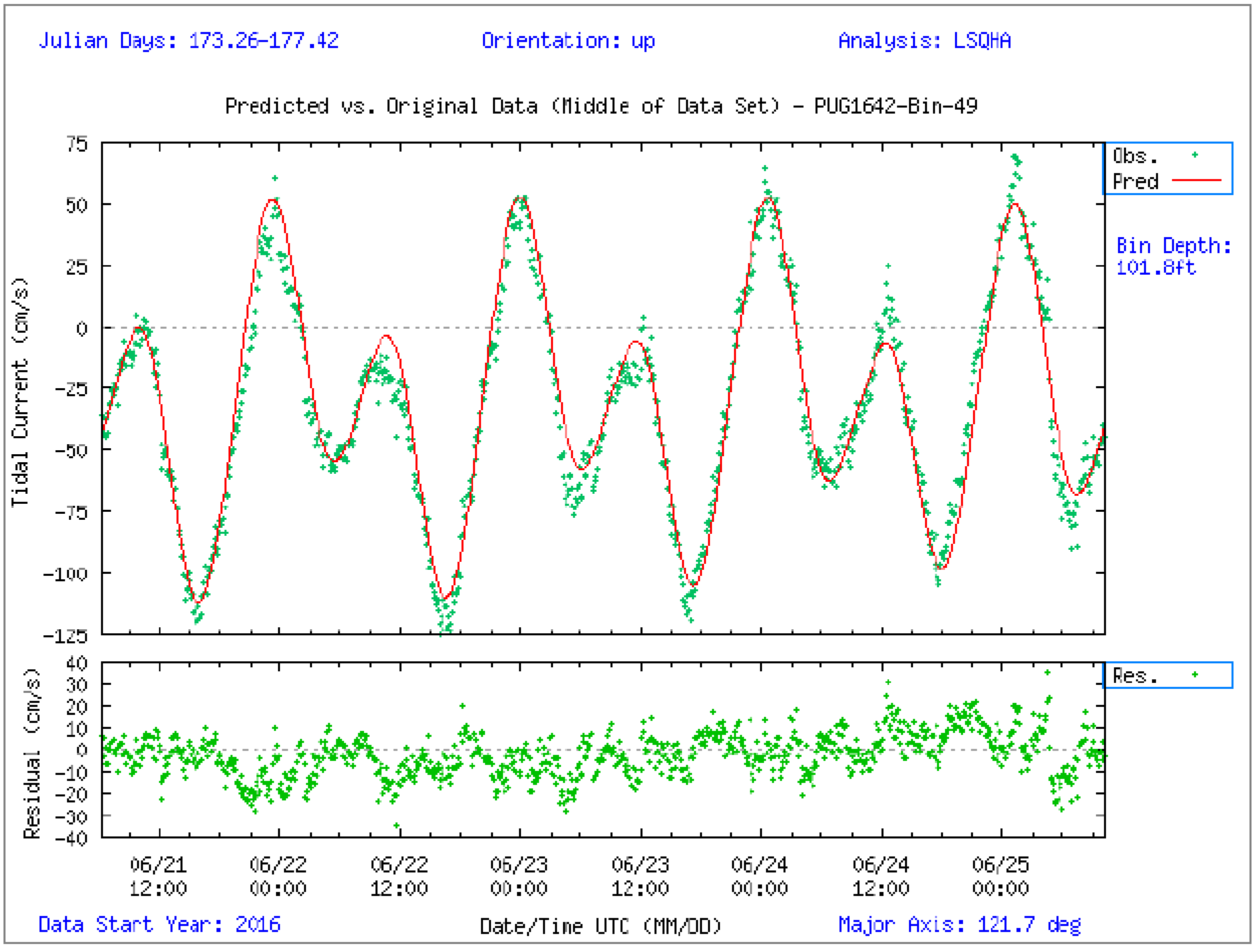

Figure 6-33. Comparison of observed major axis velocity data (green points) to predicted tidal velocity along the major axis for station PUG1642. The lower figure shows the non-tidal residual, the difference between the predicted and observed velocity from the upper panel. This example comparison shows data near neap tides when the difference is greatest between the stronger and weaker of the daily semidiurnal flood and ebb tides.

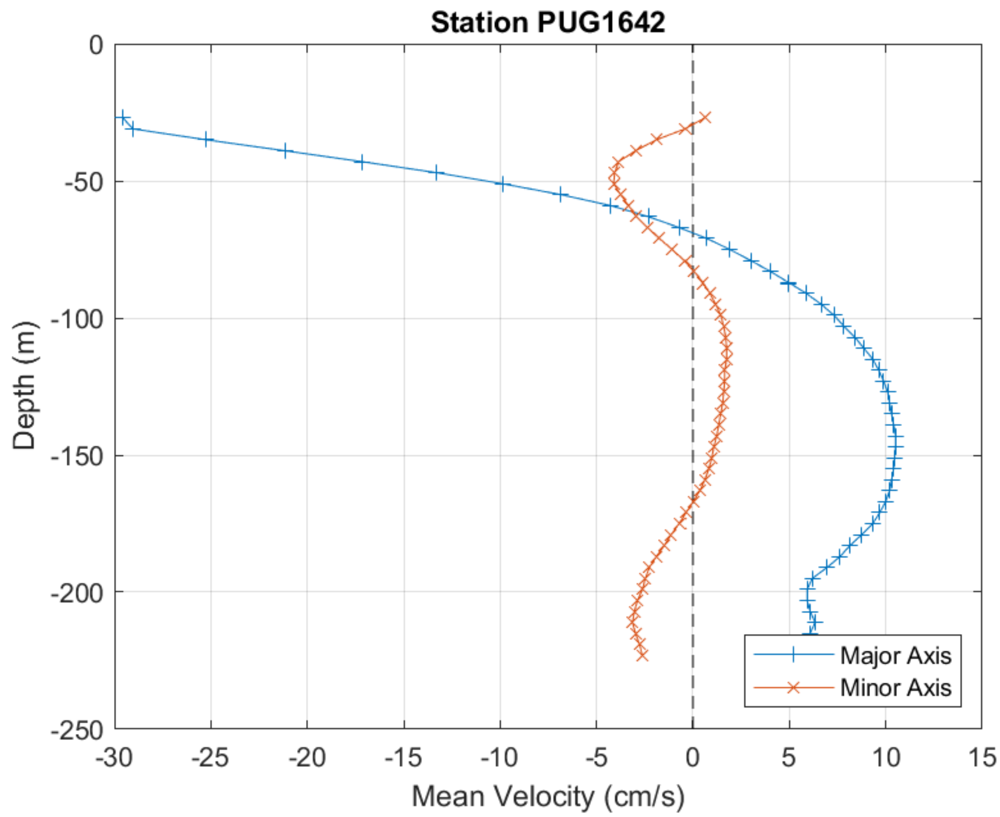

Figure 6-34. PUG1642 mean velocity profile by depth. Only depths that passed quality control criteria are shown. This station was configured to collect 4.0 m bins.

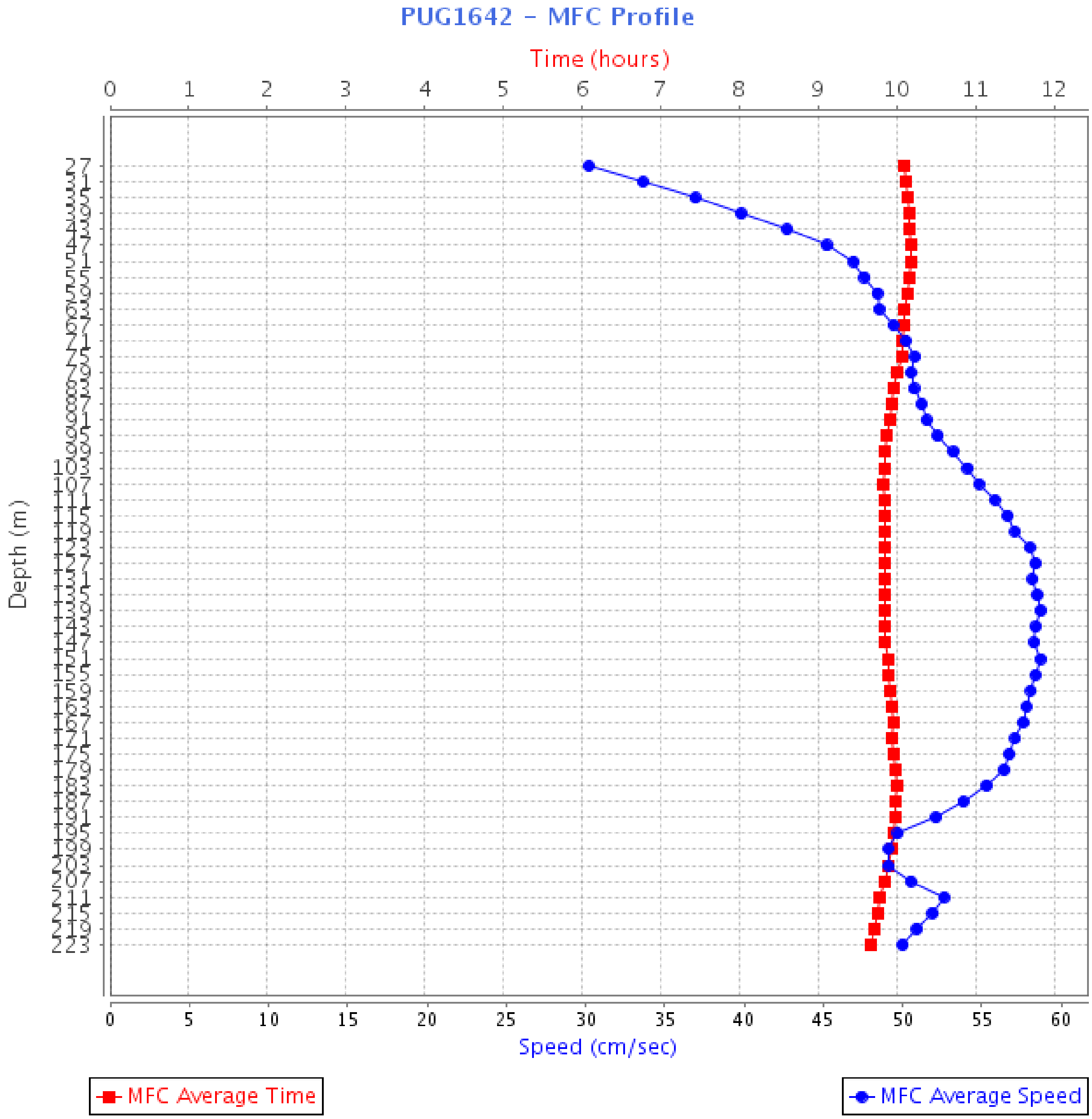

Figure 6-35. PUG1642 MFC timing (GI – in red squares) and speed (blue circles) by depth bin. Bin 1 is the deepest bin observed at approximately 223.0 m below MLLW, and the top-most good bin is bin 50 (27.0 m below MLLW).

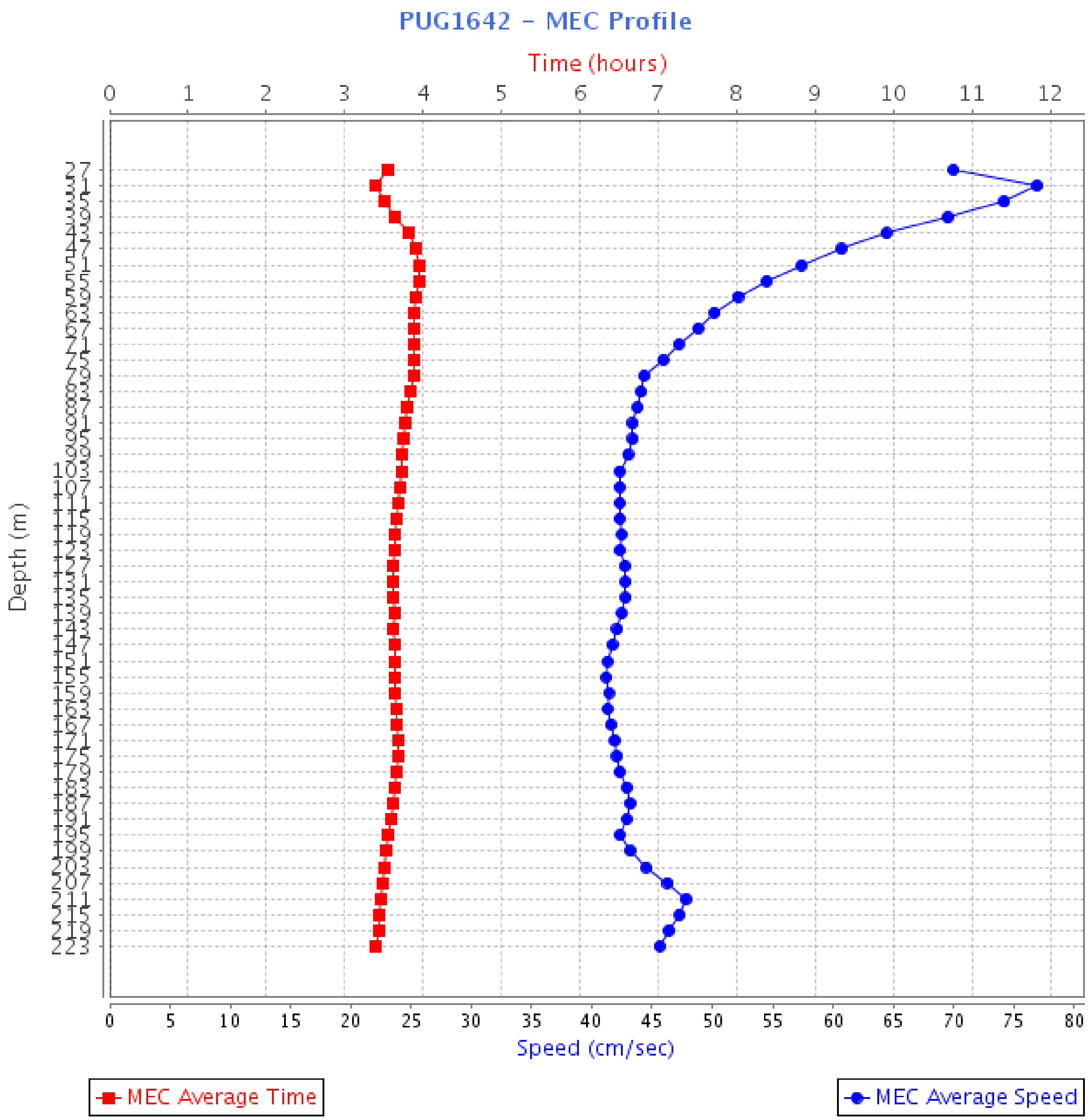

Figure 6-36. PUG1642 MEC timing (GI – red squares) and speed (blue circles) by depth bin. Bin 1 is the deepest bin observed at approximately 223.0 m below MLLW, and the top-most good bin is bin 50 (27.0 m below MLLW).

6.8. PUG1701 – Deception Pass (Narrows)

Station PUG1701 was deployed for 141 days (April 20, 2017–September 8, 2017) in the Deception Pass (Narrows), a hydraulic strait with the fastest water velocities in the Salish Sea. Due to the extreme difficulty of placing a mooring in this region, the bottom mount remained stable for only 31 days of the deployment (April 26, 2017–May 27, 2017) before the mooring moved significantly, which could be seen in the pressure, heading, pitch, and roll signals. Therefore, much of the collected data could not be used in the analysis. The 31 days of stable data provided a long enough time series for harmonic analysis. A TRDI Workhorse 600 kHz ADCP mounted in a TRBM was deployed in 40.0 m (131.2 ft) of water and collected 38, 1 m bins of data, 34 of which met quality control criteria for full analysis. Bins 3, 24, and 34 are published in the TCTs, representing approximate depths of 35.4 m, 14.4 m, and 4.4 m (116.0 ft, 47.1 ft, and 14.3 ft) MLLW, respectively. The analysis from bin 34 serves as a new reference station for the TCTs.

With currents that exceed 400 cm/s (7.8 kn), Deception Pass (Narrows) is a difficult passage to navigate. It is the northernmost entrance into Puget Sound from the Strait of Juan de Fuca. At just 0.4 km (0.22 nautical mile (nmi) wide, there is substantial flow through this narrow and relatively shallow passage. The tidal signal is very strong, with harmonic analysis LSQHA resolving more than 98 percent of the total current energy. The currents are strongly rectilinear with a permanent residual westward flow at all levels of the water column. Velocities are extremely close to the previously measured historical data, but timing differs by up to 20 minutes—most likely due to the difference in previous hydraulic calculations versus the new analysis, which uses LSQHA. Predicted maximum flood and ebb both occur later than the historical predictions, but slack occurs earlier. This information has been updated in the TCTs.

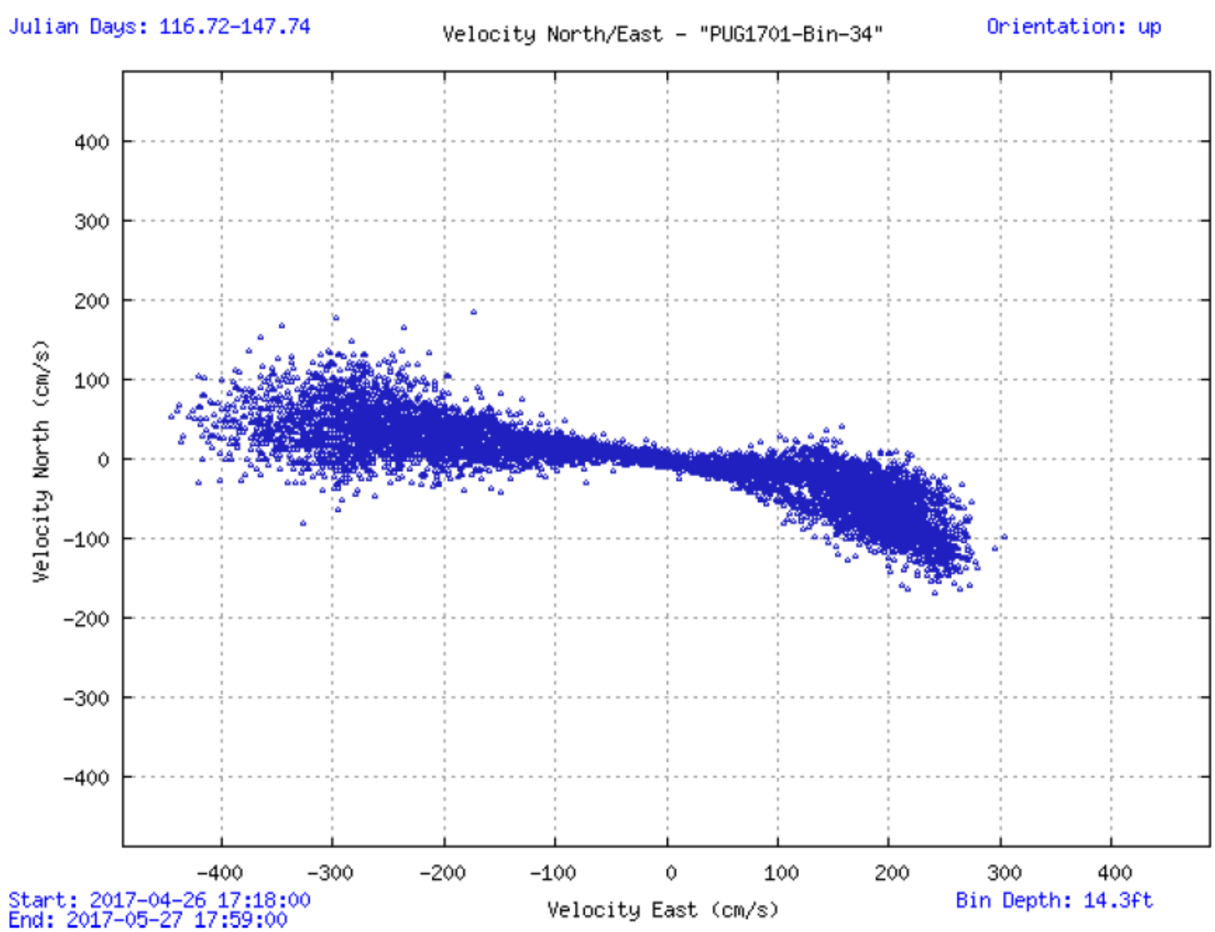

Figure 6-37. Scatter plot of north-versus-east velocity for station PUG1701 at the near-surface bin, bin 34 at 4.4 m below MLLW.

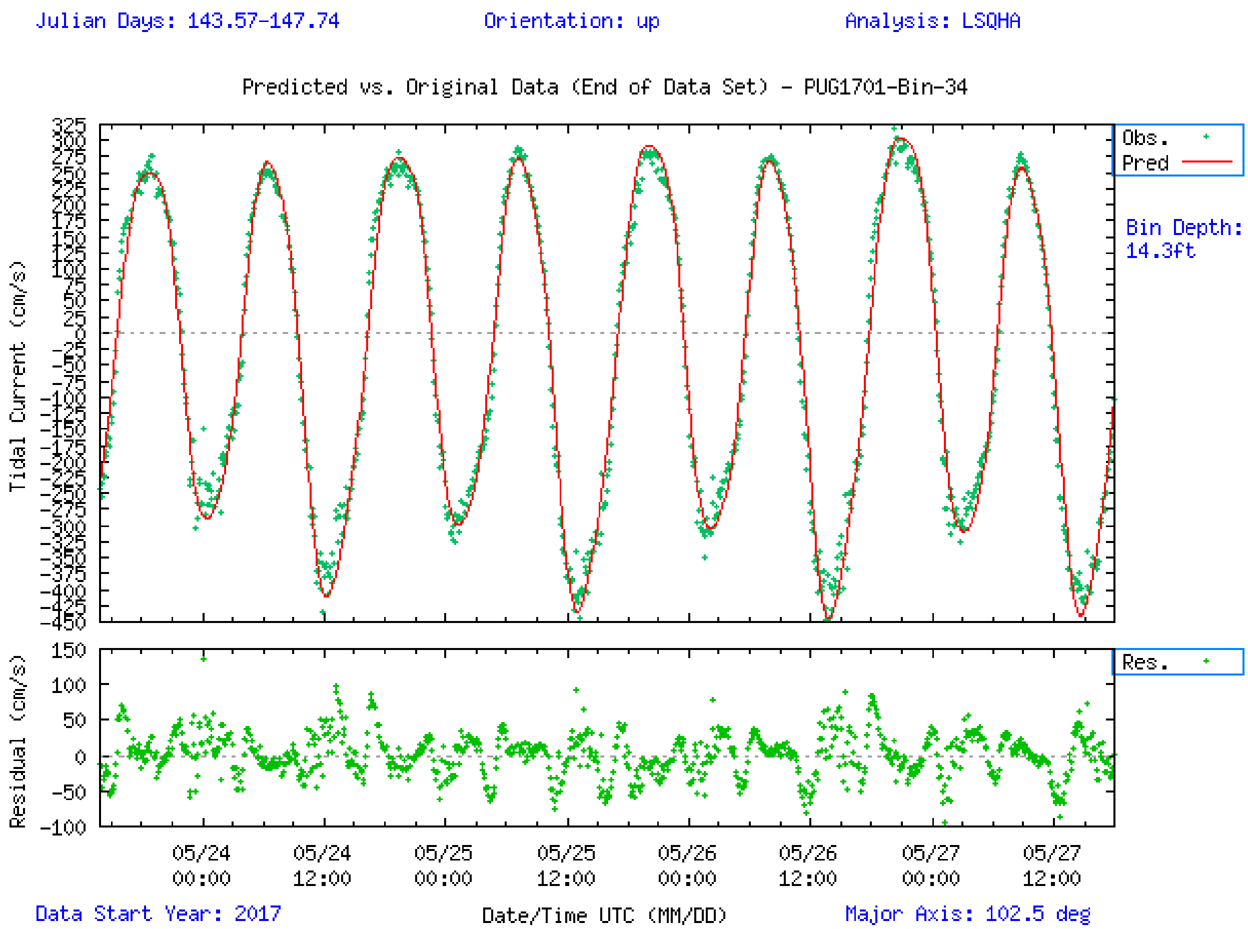

Figure 6-38. Comparison of observed major axis velocity data (green points) to predicted tidal velocity along the major axis for station PUG1701. The lower figure shows the non-tidal residual, the difference between the predicted and observed velocity from the upper panel.

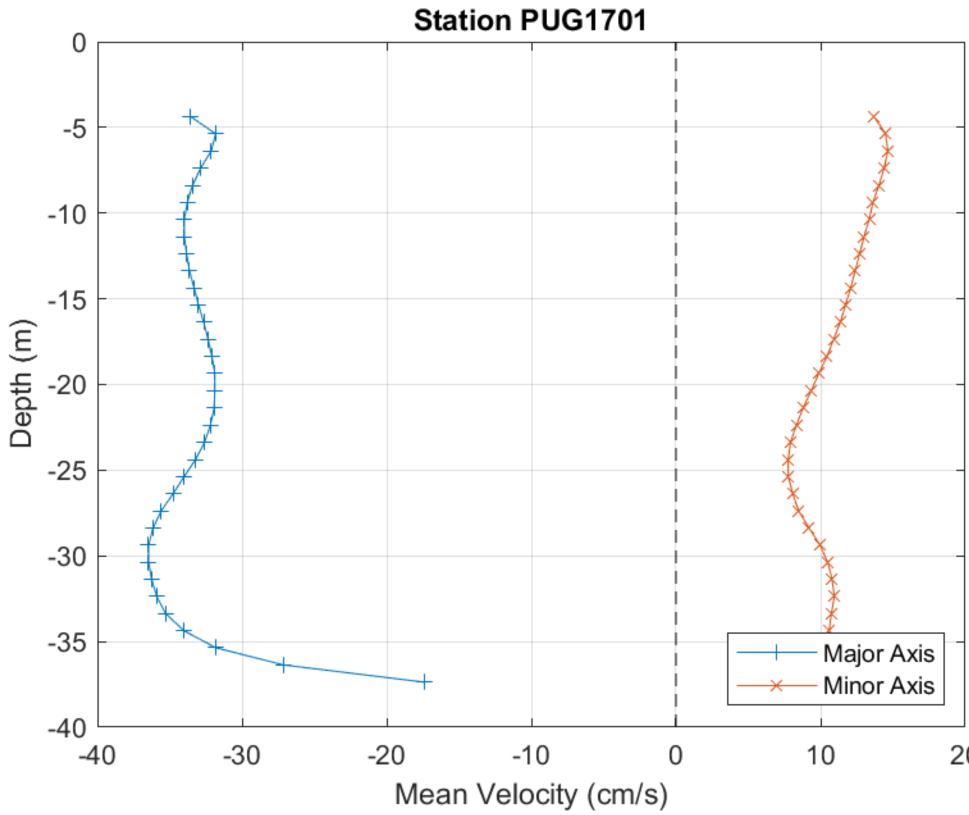

Figure 6-39. PUG1701 mean velocity profile by depth. Only depths that passed quality control criteria are shown. This station was configured to collect 1.0 m bins.

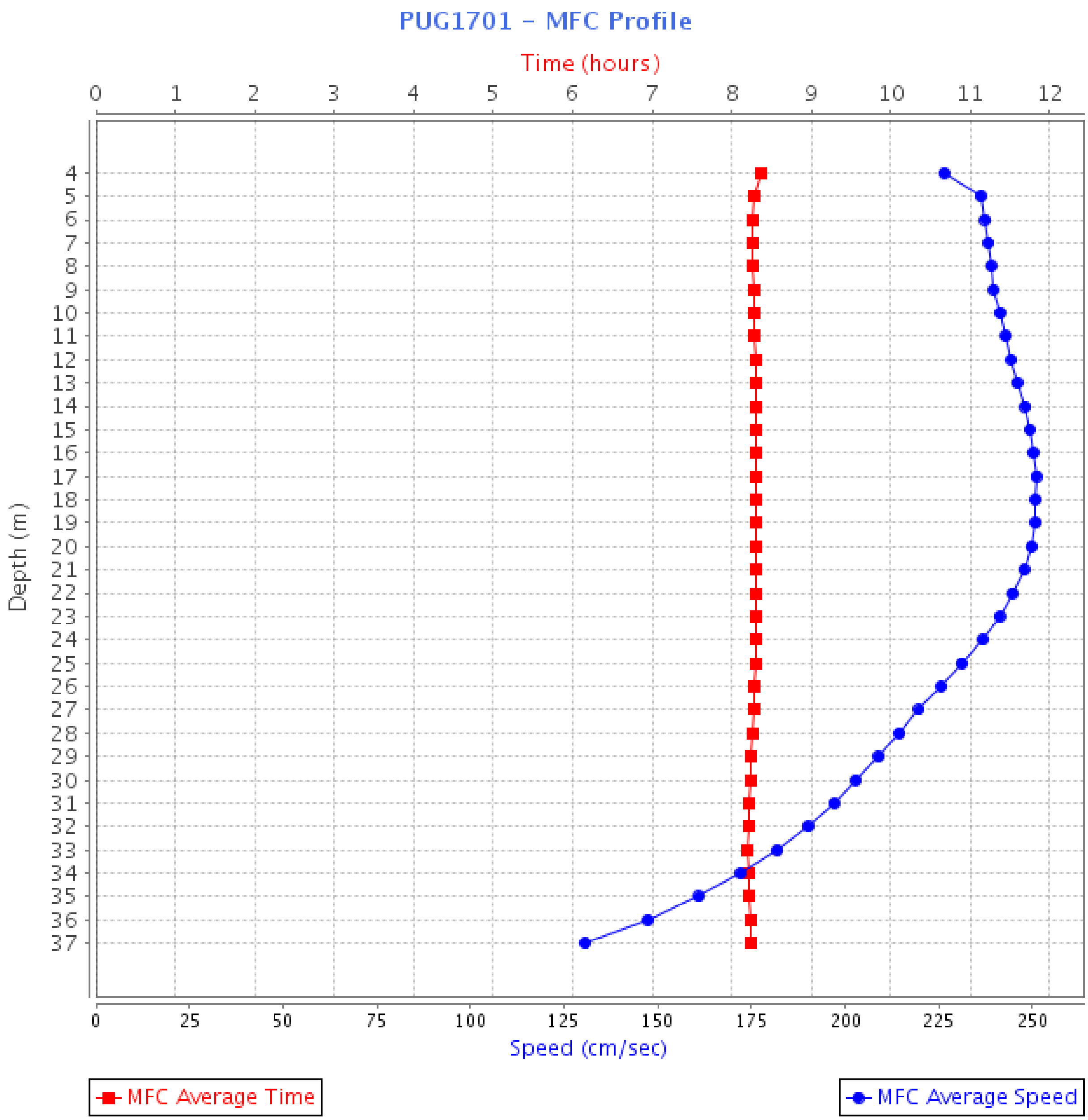

Figure 6-40. PUG1701 MFC timing (GI – red squares) and speed (blue circles) by depth bin. Bin 1 is the deepest bin observed at approximately 37.4 m below MLLW, and the top-most good bin is bin 34 (4.4 m below MLLW).

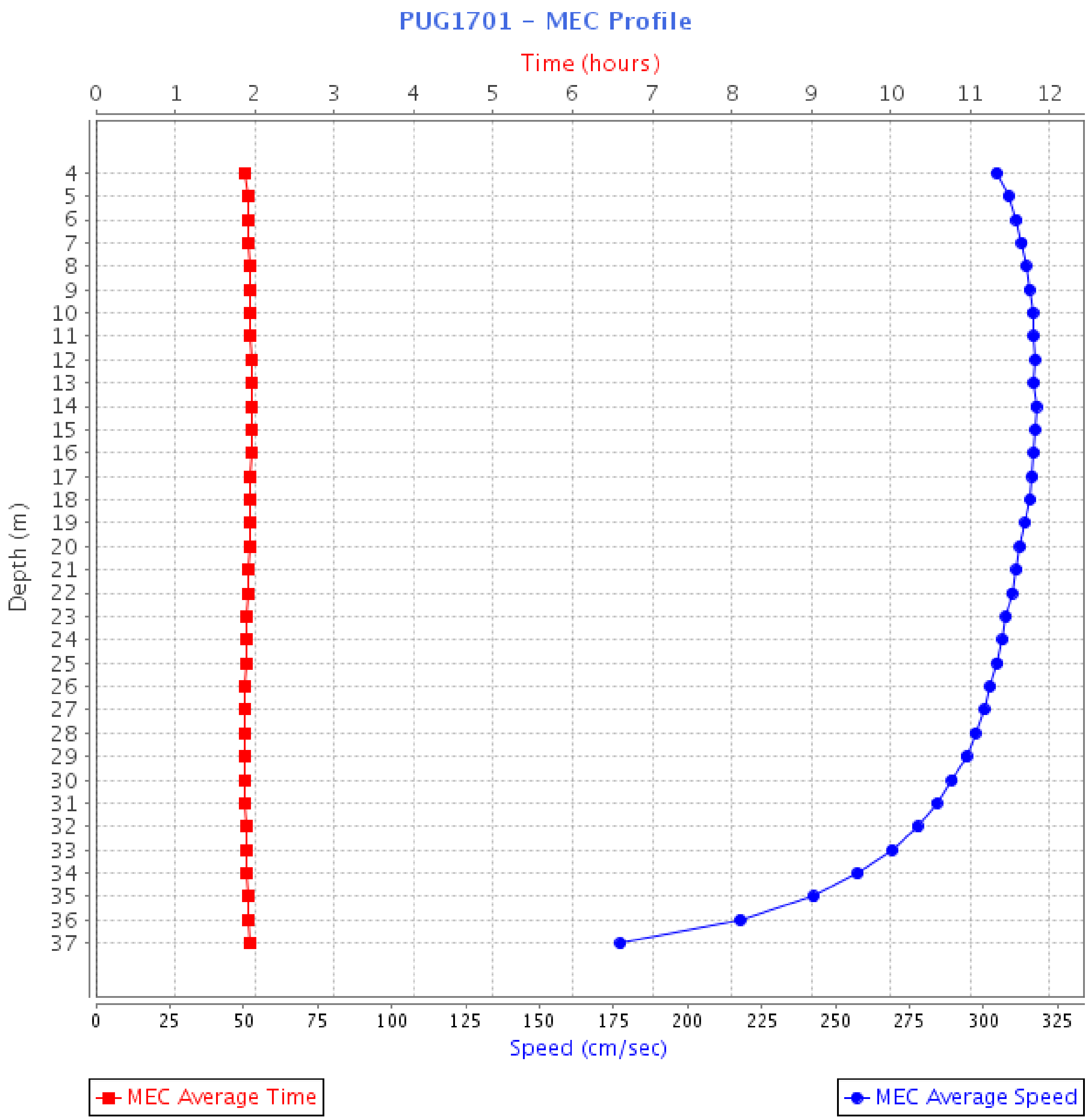

Figure 6-41. PUG1701 MEC timing (GI – red squares) and speed (blue circles) by depth bin. Bin 1 is the deepest bin observed at approximately 37.4 m below MLLW, and the top-most good bin is bin 34 (4.4 m below MLLW).

6.9. PUG1702 – Rosario Strait

Station PUG1702 at Rosario Strait was deployed for 125 days (April 20, 2017–August 23, 2017) in 72.0 m (236.2 ft) of water. A 300 kHz TRDI Workhorse ADCP mounted in a SUBS collected 20, 3 m bins of data, 16 of which met quality control criteria for full analysis. Bins 9, 13, and 16 are published in the TCTs, representing approximate depths of 35.3 m, 23.3 m, and 14.3 m (115.7 ft, 76.3 ft, and 46.8 ft) MLLW, respectively. Information from bin 16 serves as a new reference station.

Rosario Strait is the easternmost deep water shipping channel in the Salish Sea It is a major passage separating the San Juan Islands and Washington State and used by vessels bound for British Columbia or Alaska, as well as oil refineries at nearby Cherry Point. According to the U.S. Coast Pilot 7 (2019), the currents in Rosario Strait are strong, with heavy tide rips and swirls found off Black Rock, Obstruction Pass, Peapod Rocks and Lawrence Point. The tides at this station are mixed, mostly semidiurnal with Dietrich ratios between 0.98 and 1.18. Currents are rectilinear with major axis variance between 92–99 percent, capturing between 95–98 percent of the total current energy. MEC are at bin 16 at 2.3 kn and MFC at bin 13 at 1.8 kn. Maximum speeds approach 300 cm/s in bin 16.

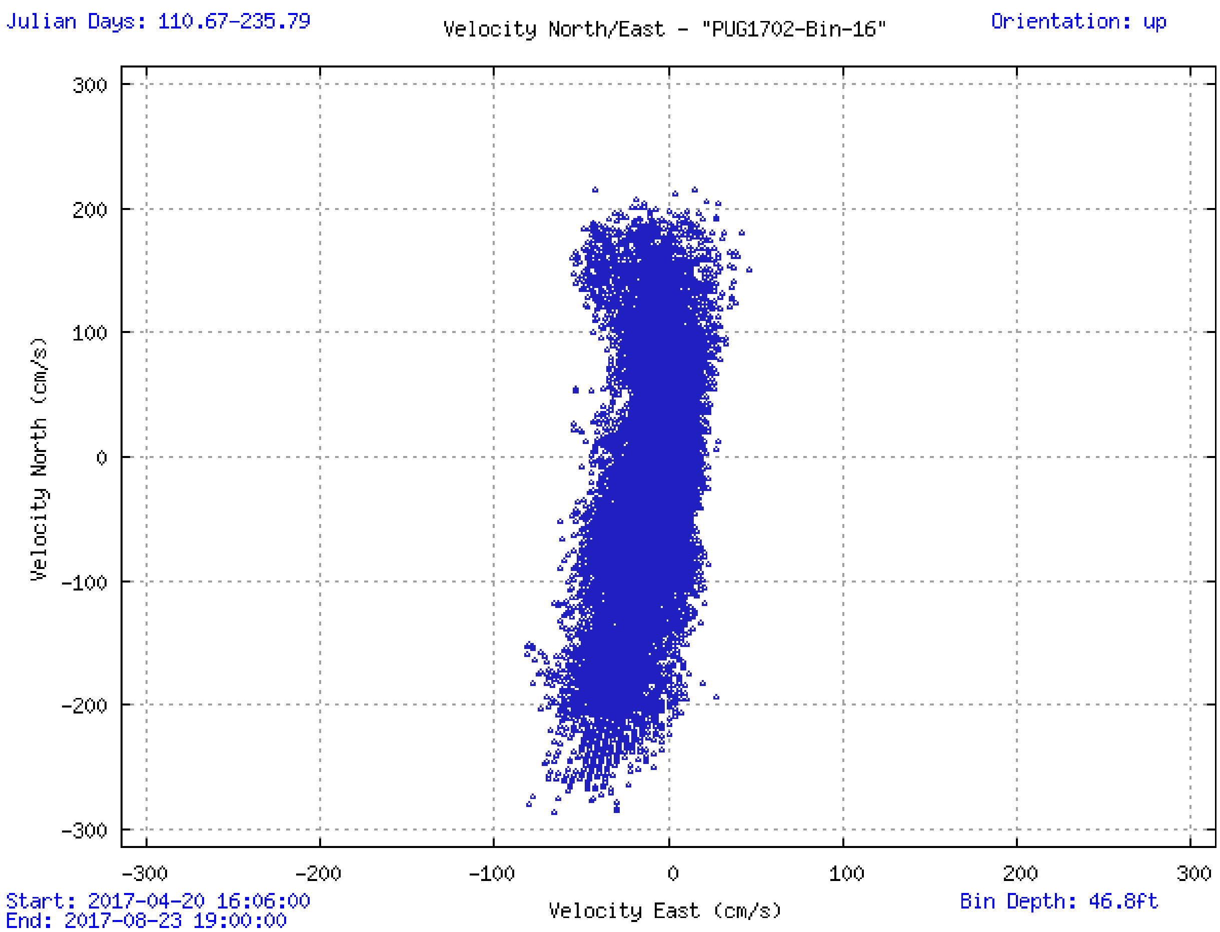

Figure 6-42. Scatter plot of north-versus-east velocity for station PUG1702 at the near-surface bin, bin 16 at 14.3 m below MLLW

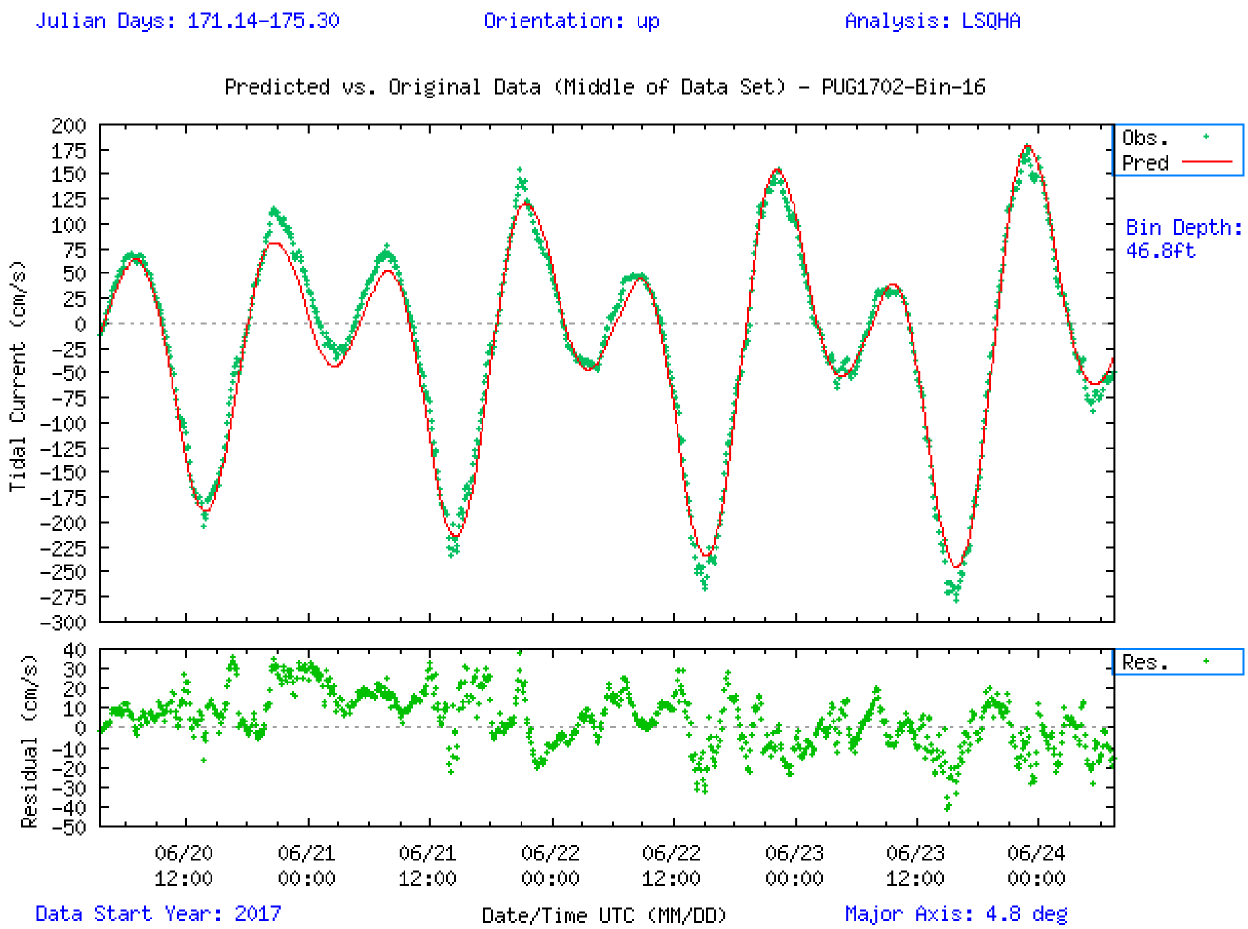

Figure 6-43. Comparison of observed major axis velocity data (green points) to predicted tidal velocity along the major axis for station PUG1702. The lower figure shows the non-tidal residual, the difference between the predicted and observed velocity from the upper panel.

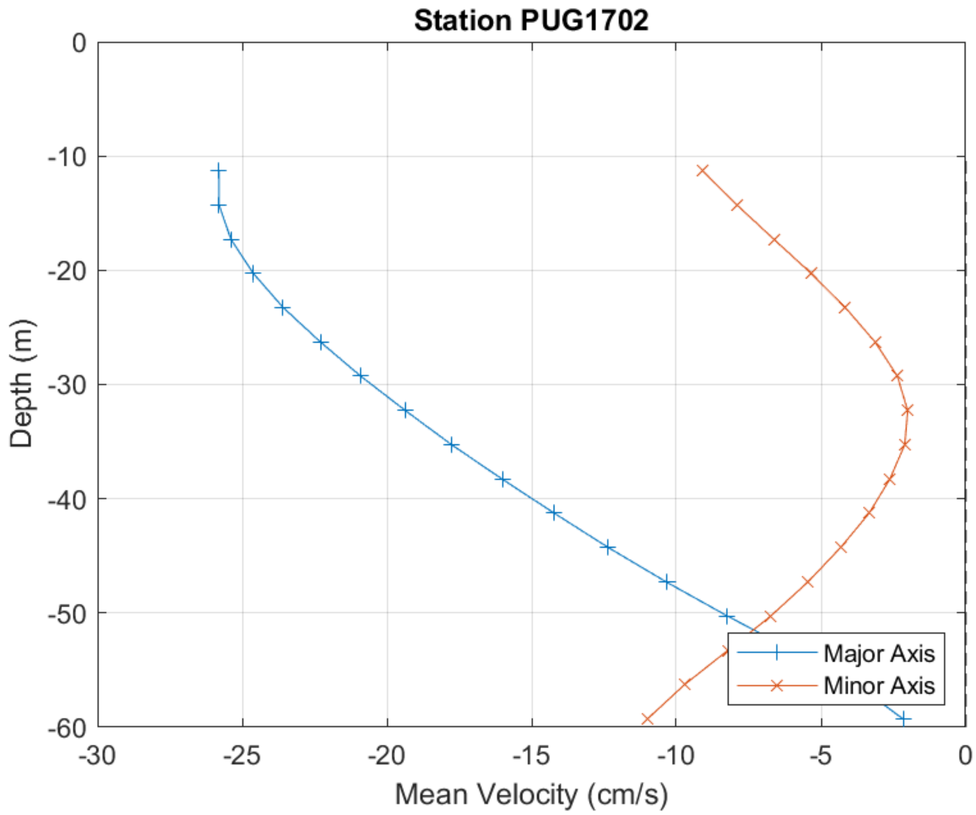

Figure 6-44. PUG1702 mean velocity profile by depth. Only depths that passed quality control criteria are shown. This station was configured to collect 3.0 m bins.

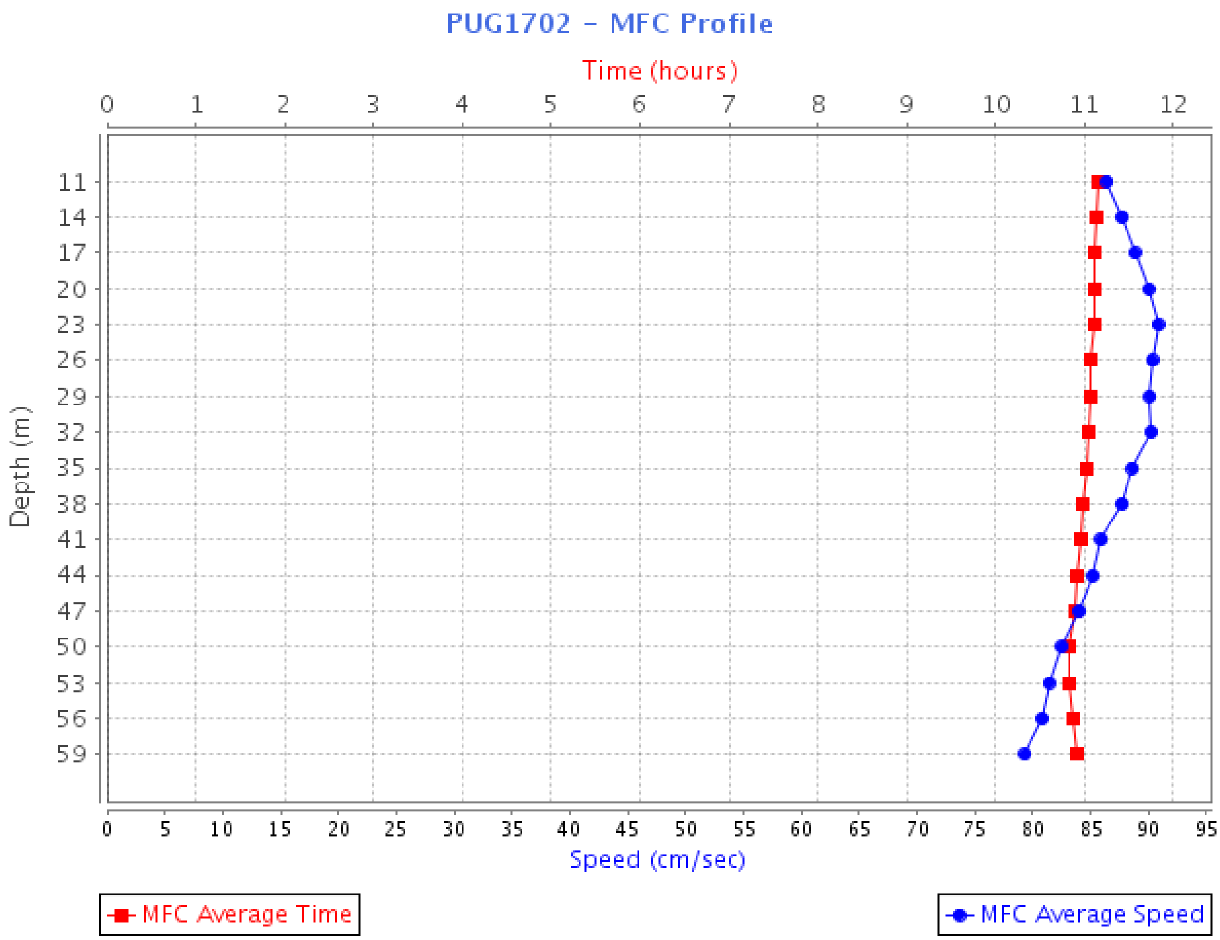

Figure 6-45. PUG1702 MFC timing (GI – red squares) and speed (blue circles) by depth bin. Bin 1 is the deepest bin observed at approximately 59.3 m below MLLW, and the top-most good bin is bin 17 (11.3 m below MLLW).

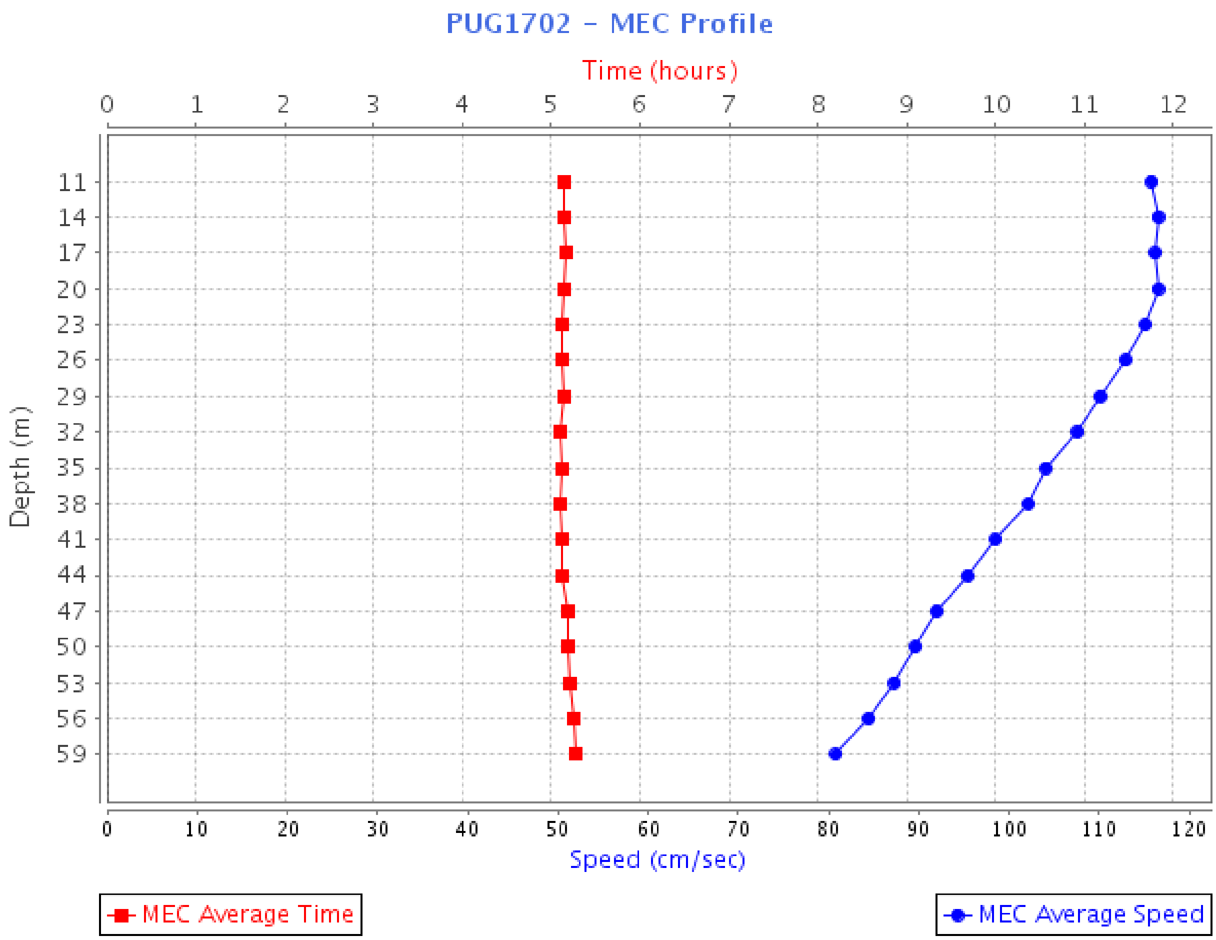

Figure 6-46. PUG1702 MEC timing (GI – red squares) and speed (blue circles) by depth bin. Bin 1 is the deepest bin observed at approximately 59.3 m below MLLW, and the top-most good bin is bin 17 (11.3 m below MLLW).

6.10. PUG1706 – Peapod Rocks Light, 1.2 nautical miles south of

Peapod Rocks Light, 1.2 nmi south of, was deployed for 128 days (April 19, 2017–August 25, 2017) in 65.6 m (215.2 ft) of water. A 300 kHz TRDI ADCP mounted in a SUBS collected 13, 4 m bins of data, 11 of which met quality control criteria for full analysis. Bins 1, 8, and 11 are published in the TCTs, representing approximate depths of 35.3 m, 23.3 m, and 14.3 m (115.7 ft, 76.3 ft, and 46.8 ft) MLLW, respectively

Peapod Rocks Light is toward the northern end of Rosario Strait. Currents at this station are fast, exceeding 200 cm/s (3.9 kn) at times. The tides at this station are mixed, mainly semidiurnal with slightly stronger mean floods than ebbs in the upper water column and stronger ebbs in the lower water column. Currents are rectilinear, capturing between 95-97 percent of the total energy.

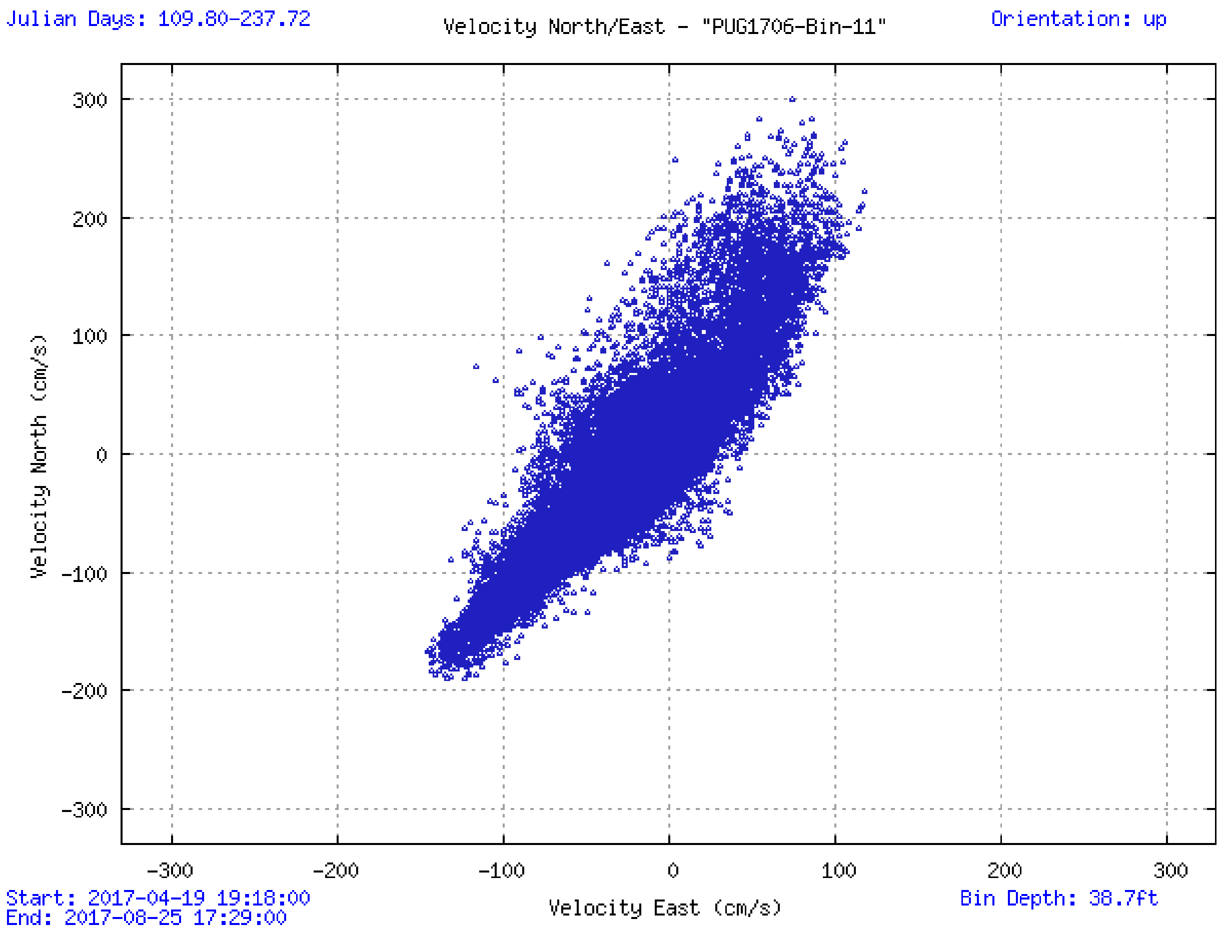

Figure 6-47. Scatter plot of north-versus-east velocity for station PUG1706 at the near-surface bin, bin 11 at 14.3 m below MLLW.

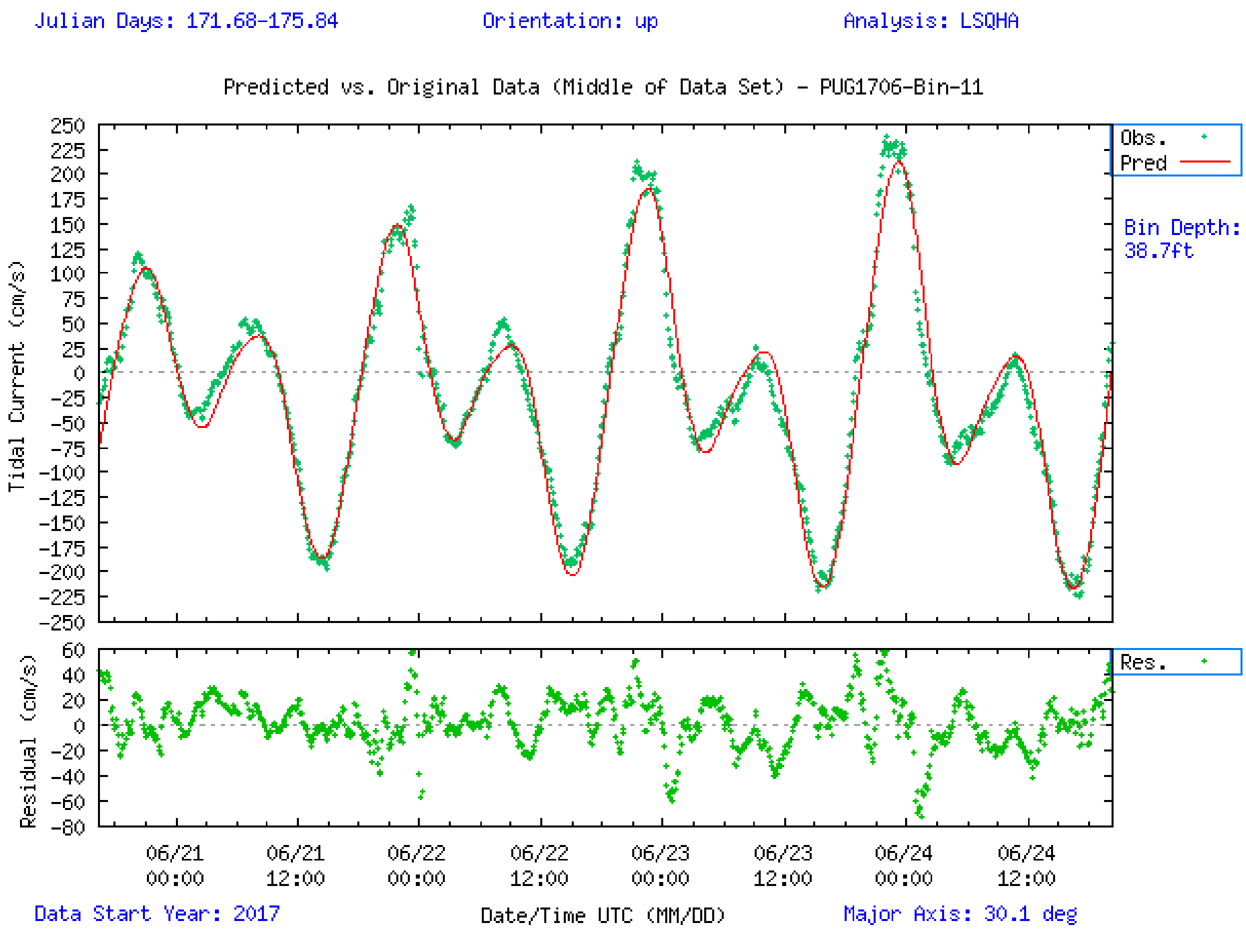

Figure 6-48. Comparison of observed major axis velocity data (green points) to predicted tidal velocity along the major axis for station PUG1706. The lower figure shows the non-tidal residual, the difference between the predicted and observed velocity from the upper panel.

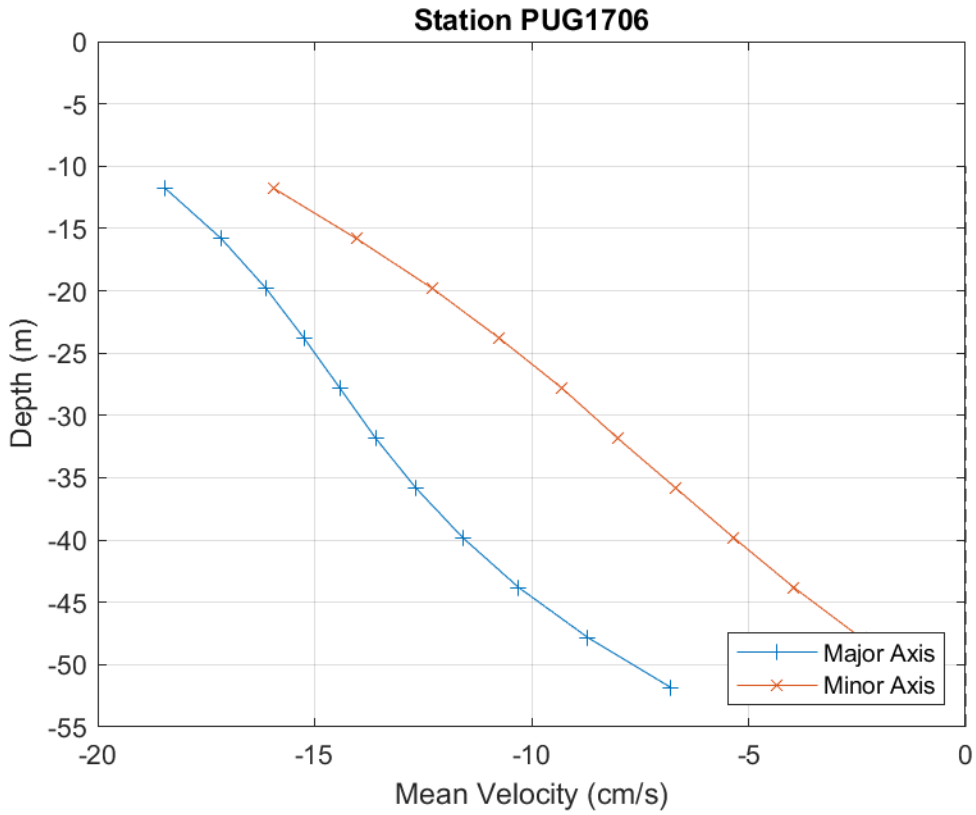

Figure 6-49. PUG1706 mean velocity profile by depth. Only depths that passed quality control criteria are shown. This station was configured to collect 4.0 m bins.

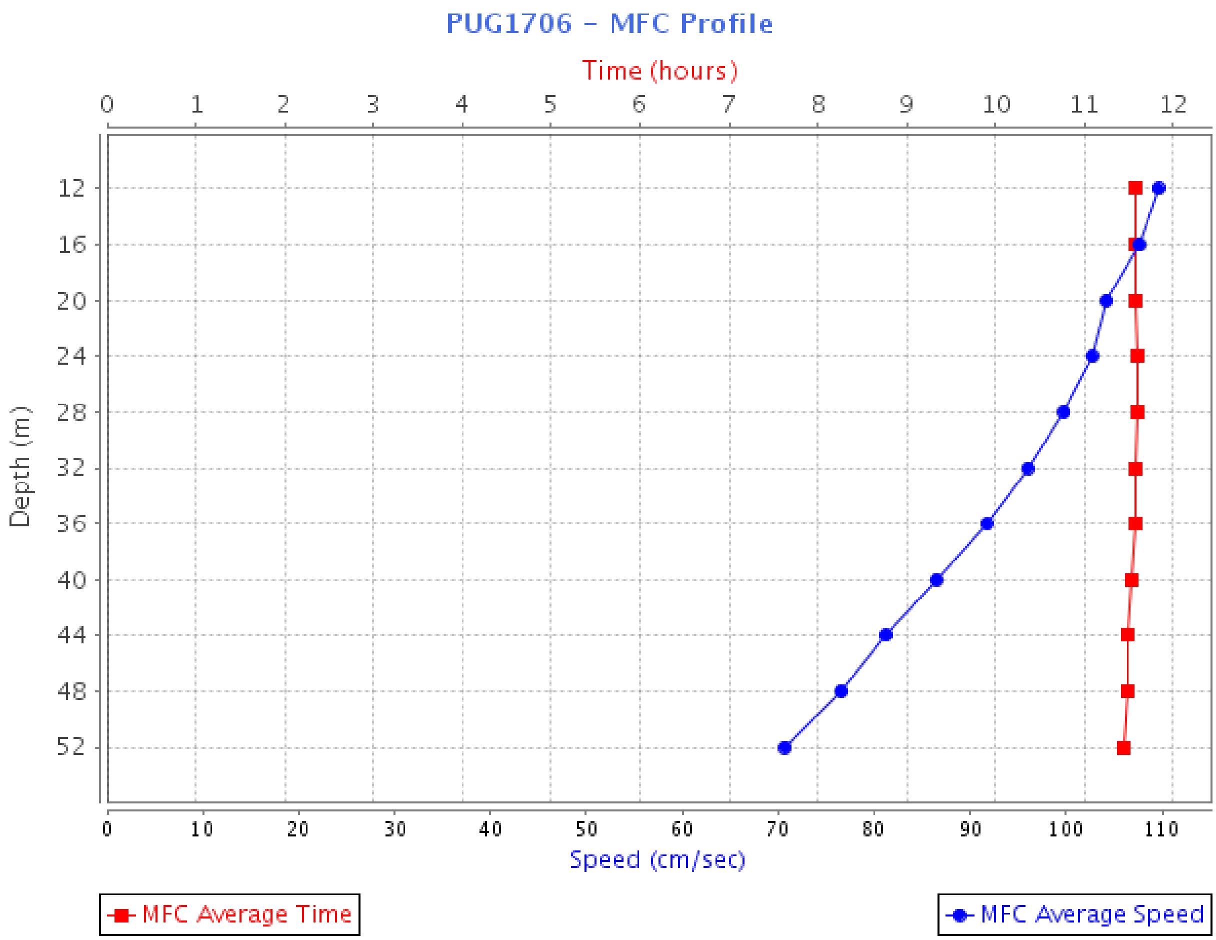

Figure 6-50. PUG1706 MFC timing (GI - in red squares) and speed (blue circles) by depth bin. Bin 1 is the deepest bin observed at approximately 51.8 m below MLLW, and the top-most good bin is bin 11 (11.8 m below MLLW).

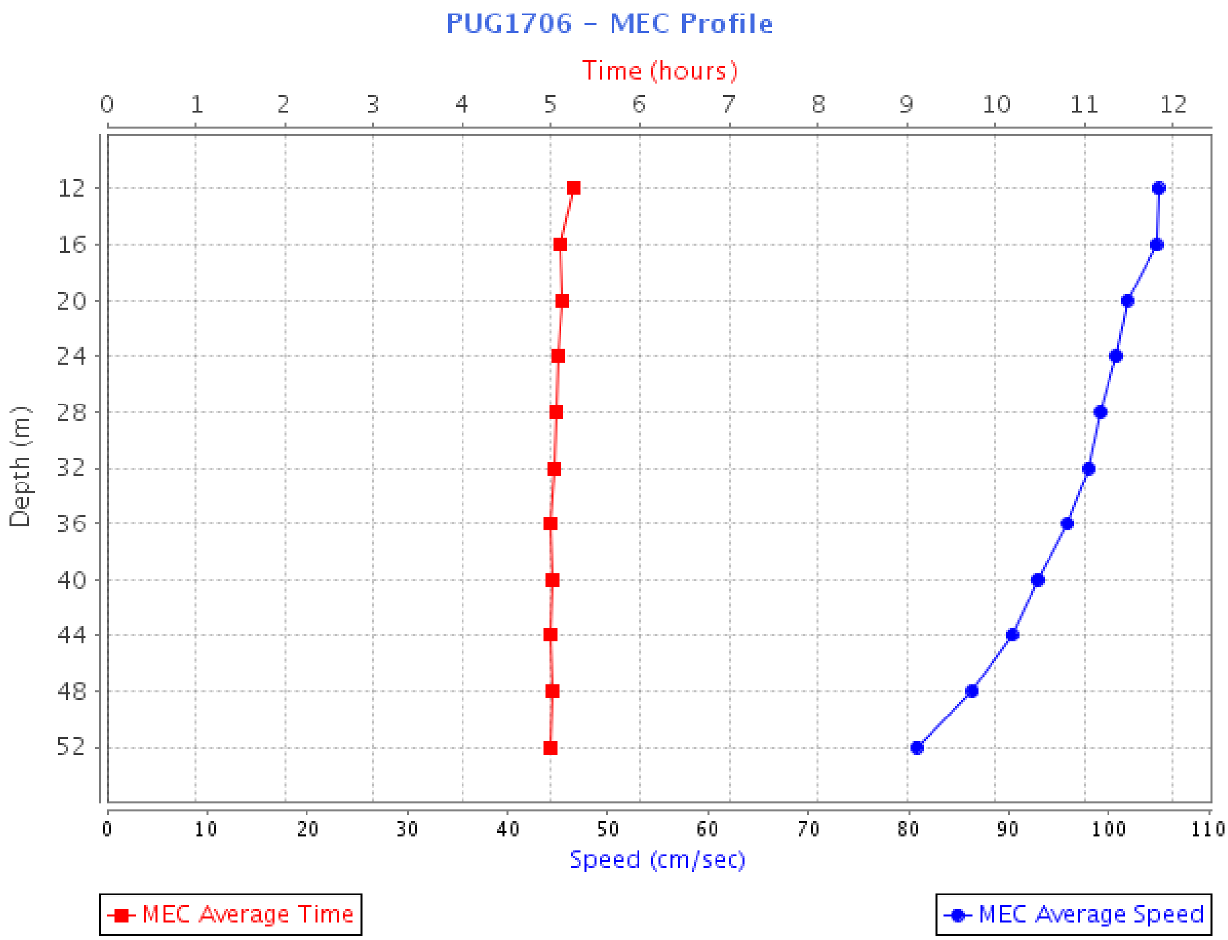

Figure 6-51. PUG1706 MEC timing (GI - red) and speed (blue) by depth bin. Bin 1 is the deepest bin observed at approximately 51.8 m below MLLW, and the top-most good bin is bin 11 (11.8 m below MLLW).

6.11. PUG1708 - Lawrence Point, Orcas Island, 1.3 nautical miles NE of

Lawrence Point, Orcas Island, 1.3 nmi NE of, was deployed for 123 days (April 24, 2017–August 25, 2017) in 86.6 m (284.0 ft) of water. This station consists of a 300 kHz TRDI Workhorse Sentinel ADCP mounted in a single SUBS with a 9.2 m taut-line mooring with a Sea-Bird SBE 37 CTD. The ADCP collected 18, 4 m bins of data, 17 of which met quality control criteria for full analysis. Bins 10, 14, and 16 are published in the TCTs, representing approximate depths of 35.2 m, 19.2 m, and 11.2 m (115.4 ft, 62.9 ft, and 36.7 ft) MLLW, respectively. Information from bin 16 serves as a new reference station.

The mixed, mainly semidiurnal currents are fairly rectilinear following the channel orientation. The floods are faster than ebbs throughout the water column with the mean MFC reaching up to 82 cm/s (1.6 kn). Harmonic analysis LSQHA solved up to 96 percent of the total current energy.

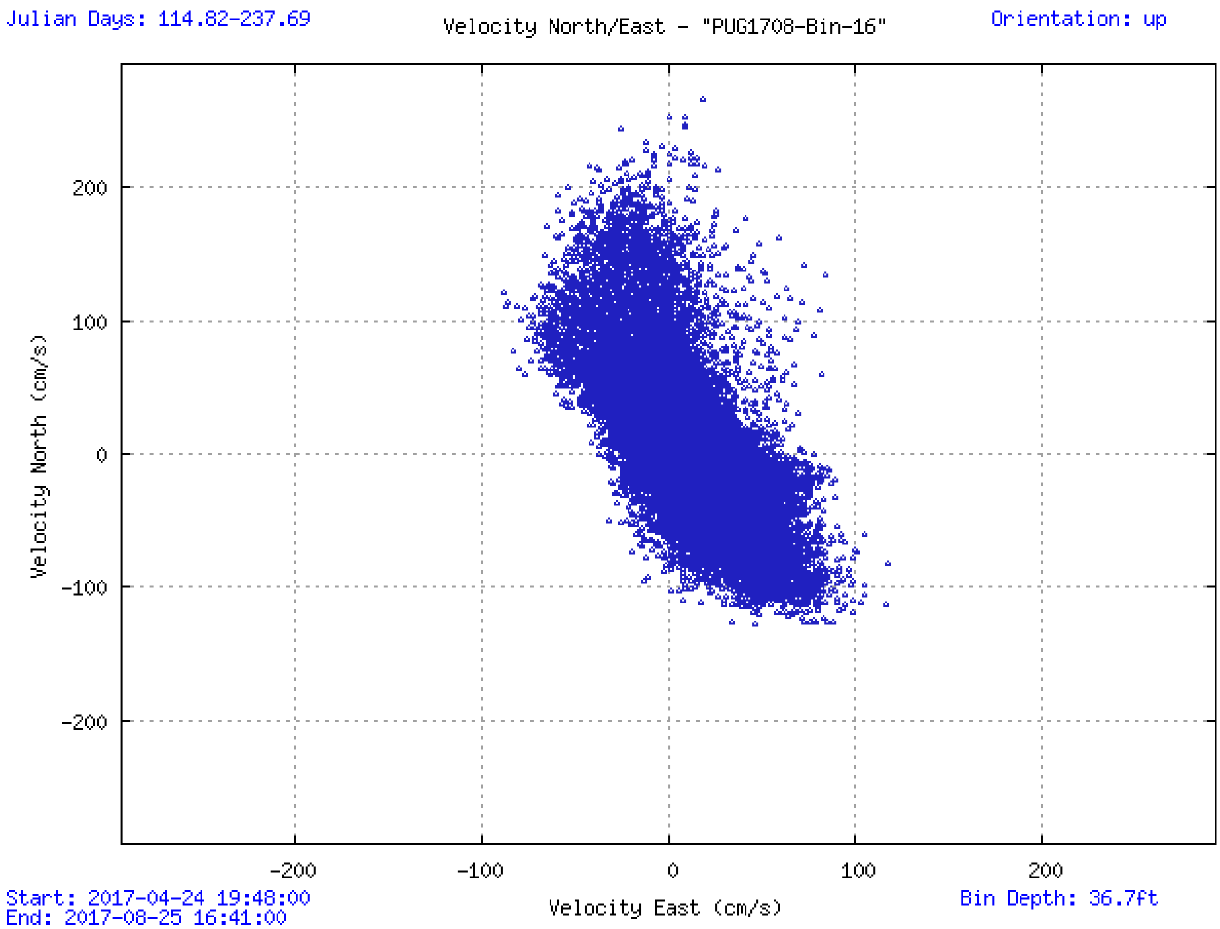

Figure 6-52. Scatter plot of north-versus-east velocity for station PUG1708 at the near-surface bin, bin 16 at 11.2 m below MLLW.

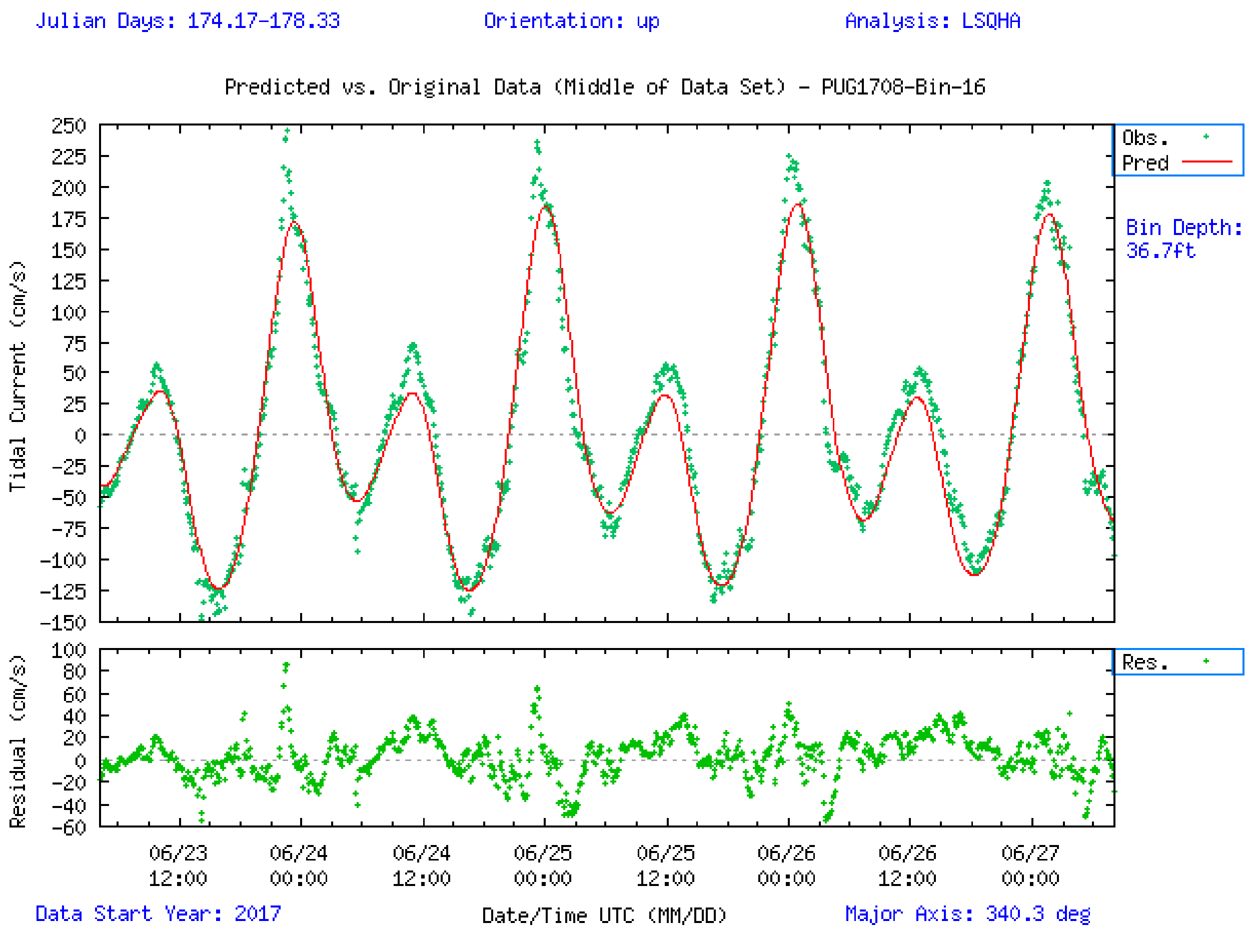

Figure 6-53. Comparison of observed major axis velocity data (green points) to predicted tidal velocity along the major axis for station PUG1708. The lower figure shows the non-tidal residual, the difference between the predicted and observed velocity from the upper panel.

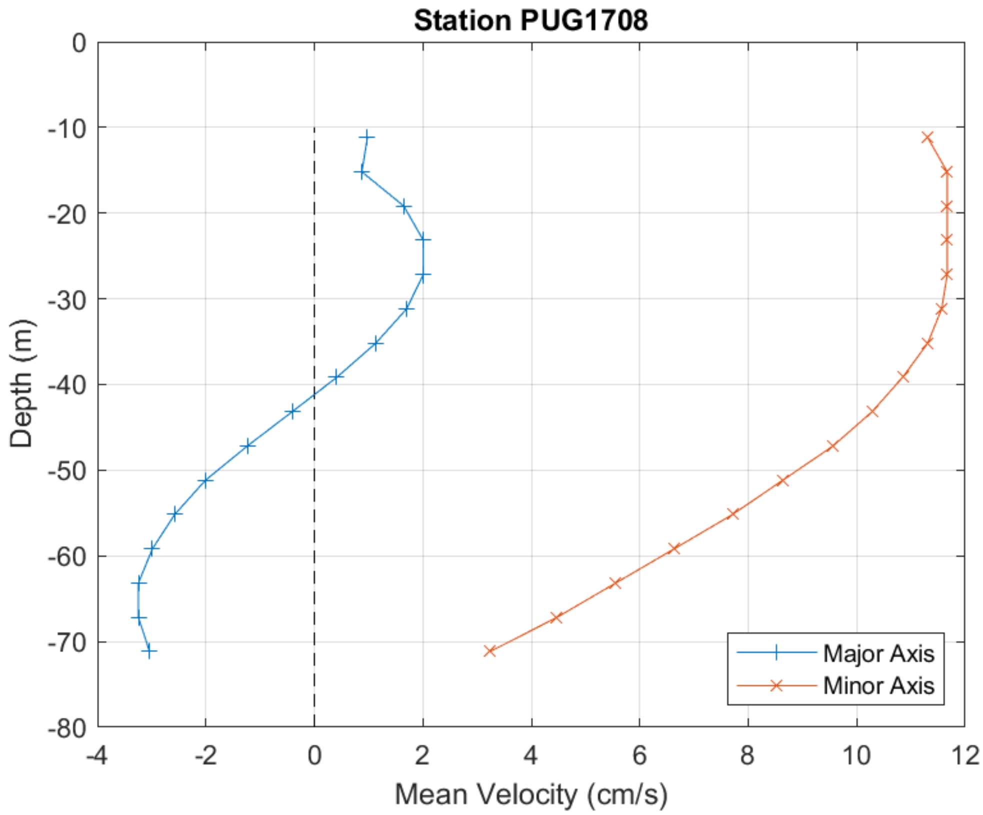

Figure 6-54. PUG1708 mean velocity profile by depth. Only depths that passed quality control criteria are shown. This station was configured to collect 4.0 m bins.

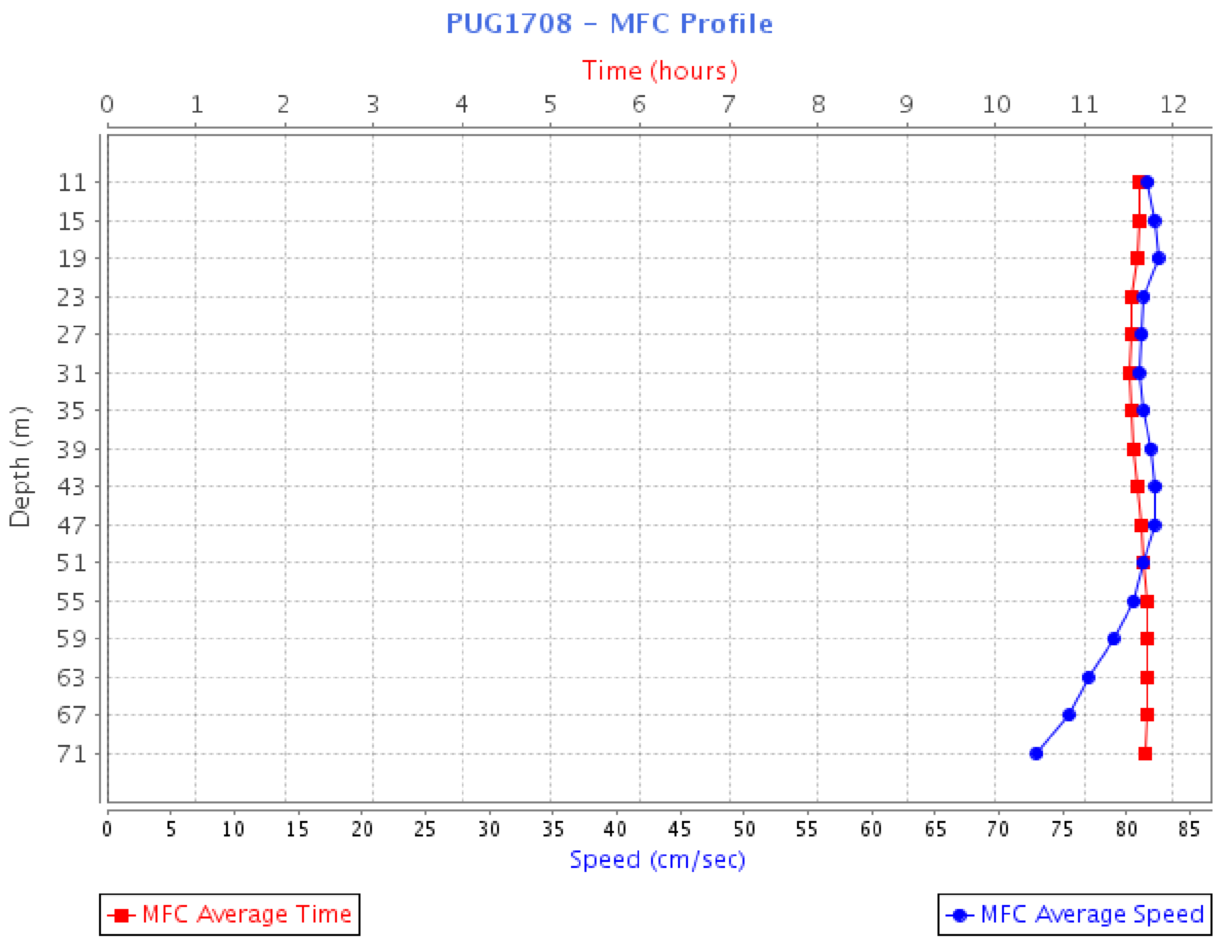

Figure 6-55. PUG1708 MFC timing (GI - red squares) and speed (blue circles) by depth bin. Bin 1 is the deepest bin observed at approximately 71.2 m below MLLW, and the top-most good bin is bin 16 (11.2 m below MLLW).

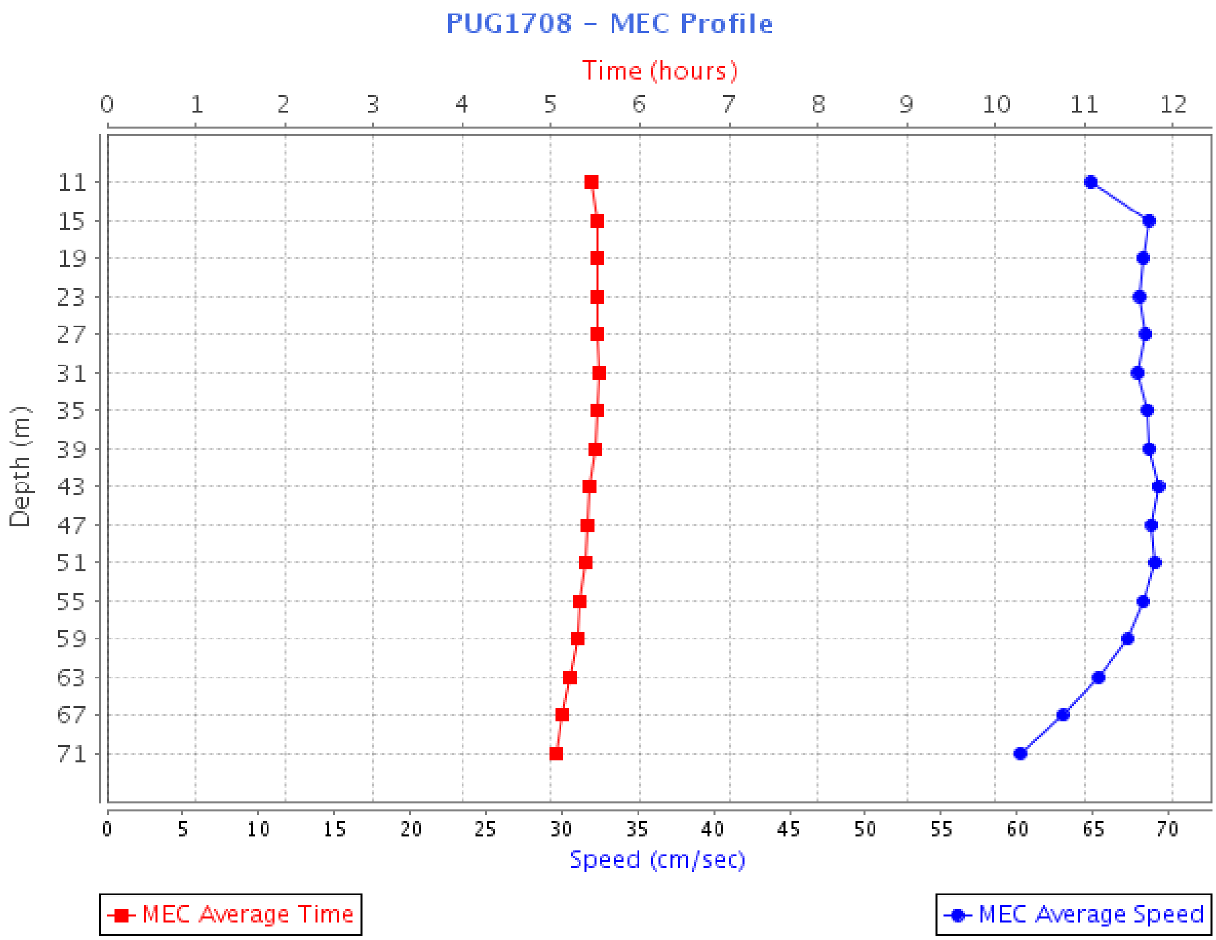

Figure 6-56. PUG1708 MEC timing (GI – red squares) and speed (blue circles) by depth bin. Bin 1 is the deepest bin observed at approximately 71.2 m below MLLW, and the top-most good bin is bin 16 (11.2 m below MLLW).

6.12. PUG1724 - South Haro Strait, south of Lime Kiln Light

South Haro Strait, south of Lime Kiln Light, was deployed for 123 days (April 20, 2017–August 28, 2017) in 308 m (1010.5 ft) of water. A TRDI WorkHorse ADCP 75 kHZ set in a DW49 mooring with 13 m chain collected 35, 8 m bins of data, 31 of which met quality control criteria for full analysis. Bins 20, 25, and 31 are published in the TCTs representing approximate depths of 120.6 m, 80.6 m, and 32.6 m (395.6 ft, 264.3 ft, and 106.9 ft) MLLW, respectively.

Haro Strait is the westernmost shipping channel that connects the Strait of Georgia to the Strait of Juan de Fuca. It straddles the border between the U.S. and Canada and is the major shipping passage to the Port of Vancouver. Harmonic analysis was run on 29 constituents accounting for 92 percent of tidal energy. While Dietrich ratios (1.17–2.73) suggest two tide types, this station is mixed, mainly semidiurnal. Deeper bins have a moderate permanent flow in the flood direction, possibly causing it to be more mixed-diurnal.

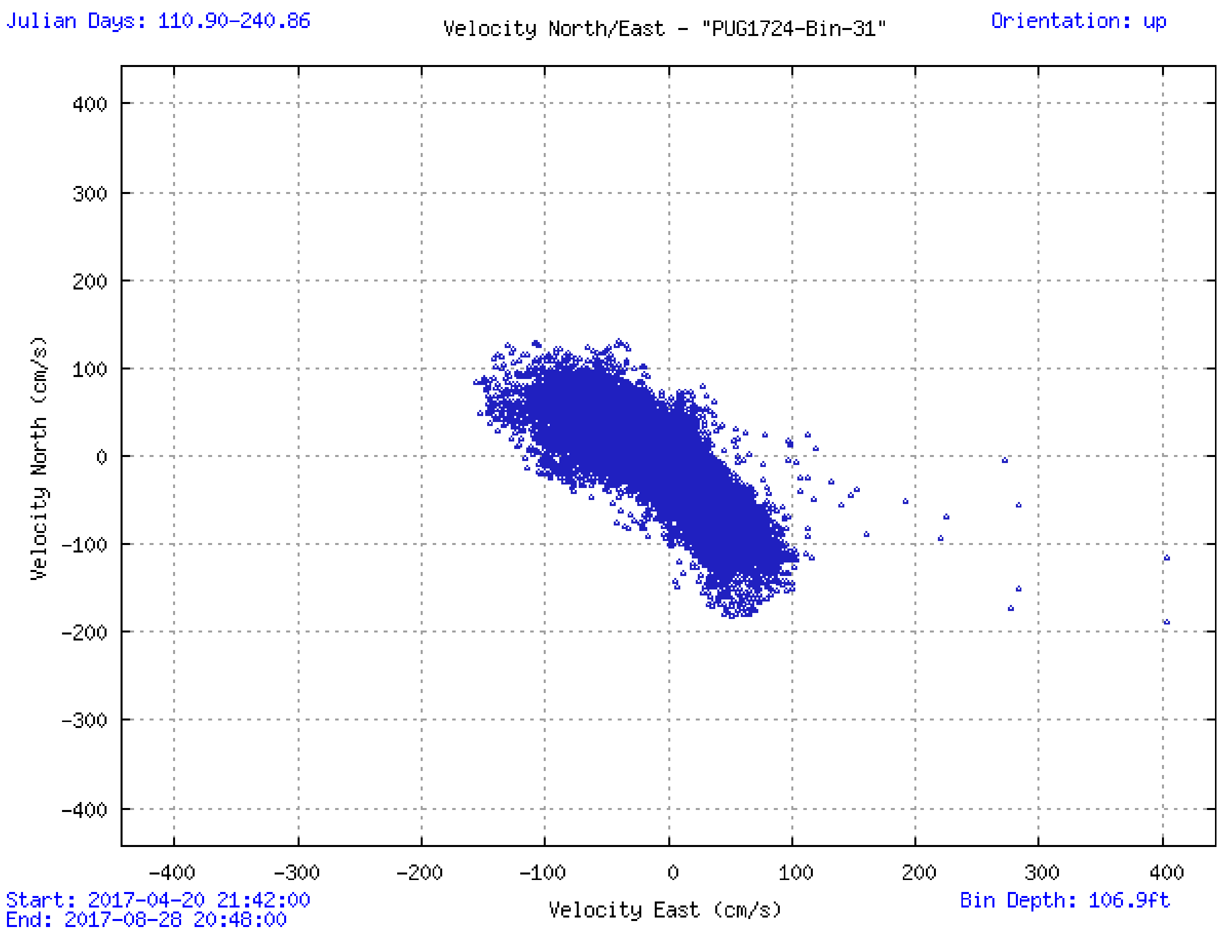

Figure 6-57. Scatter plot of north-versus-east velocity for station PUG1724 at the near-surface bin, bin 31 at 32.6 m below MLLW.

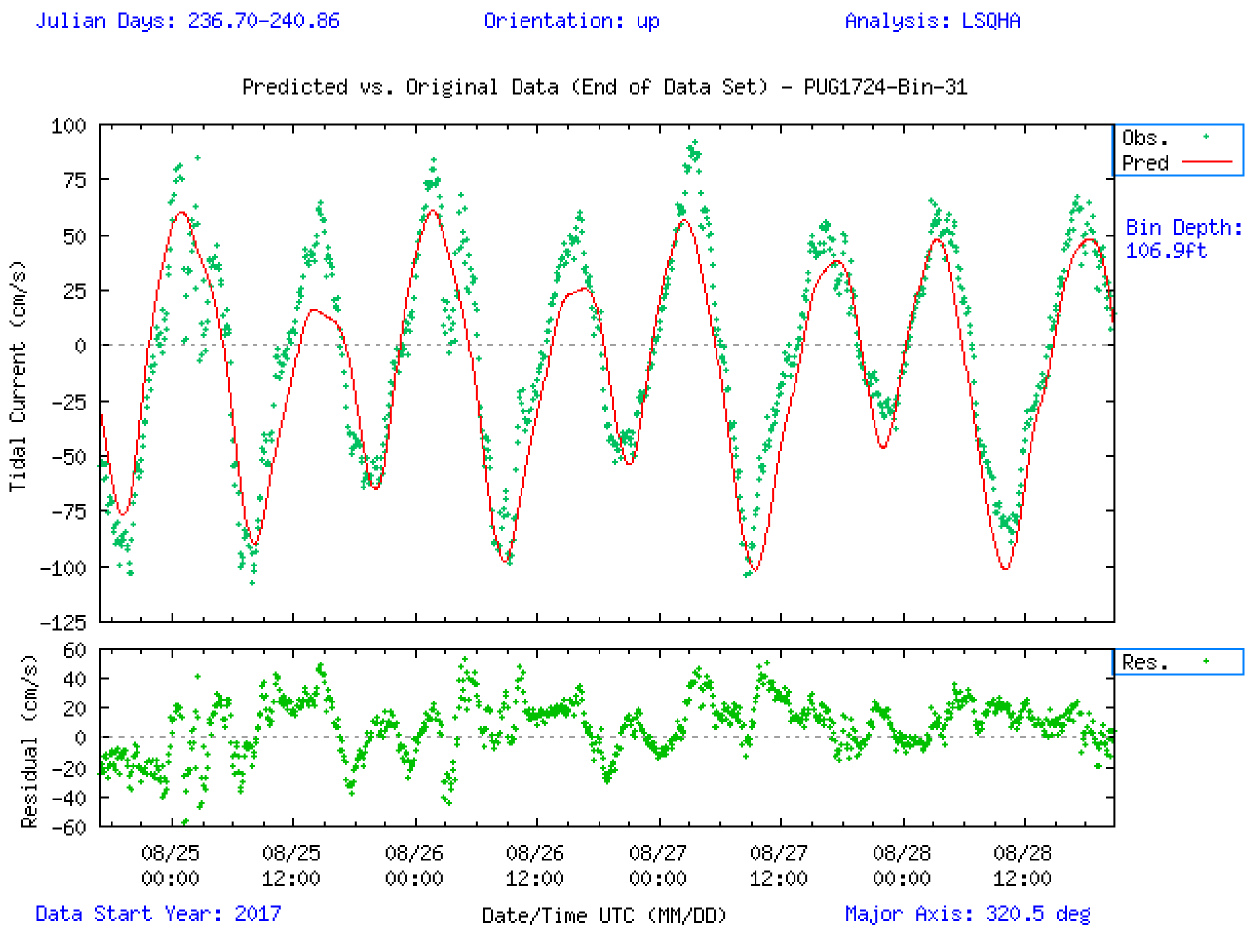

Figure 6-58. Comparison of observed major axis velocity data (green points) to predicted tidal velocity along the major axis for station PUG1724. The lower figure shows the non-tidal residual, the difference between the predicted and observed velocity from the upper panel.

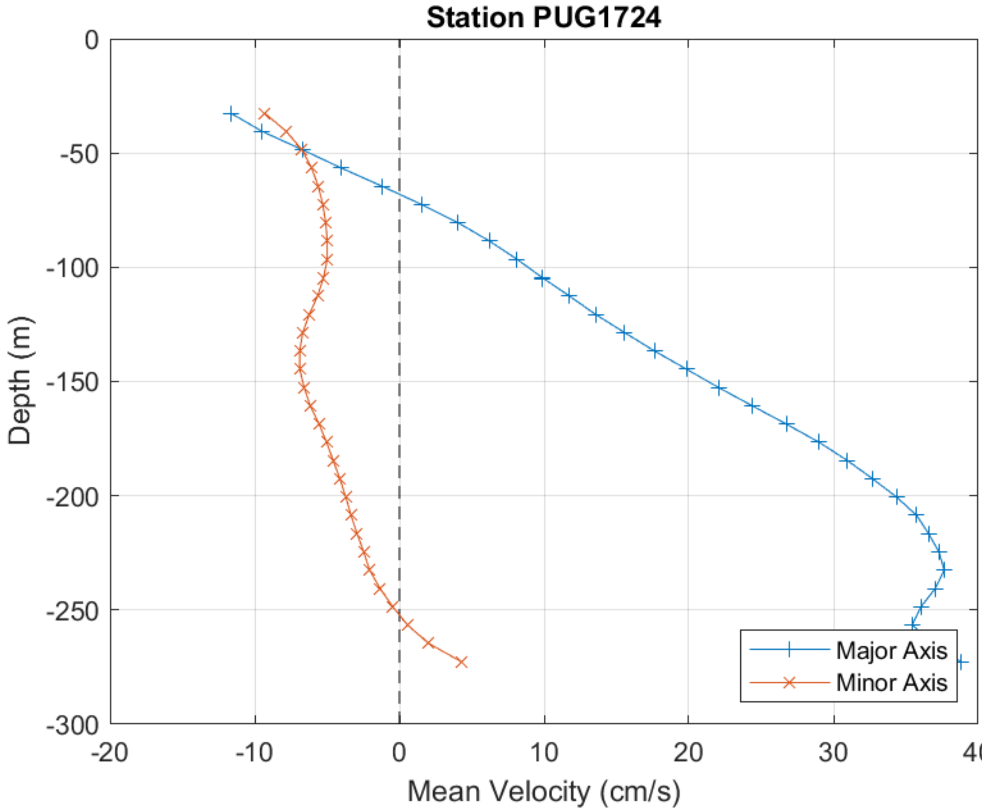

Figure 6-59. PUG1724 mean velocity profile by depth. Only depths that passed quality control criteria are shown. This station was configured to collect 8.0 m bins.

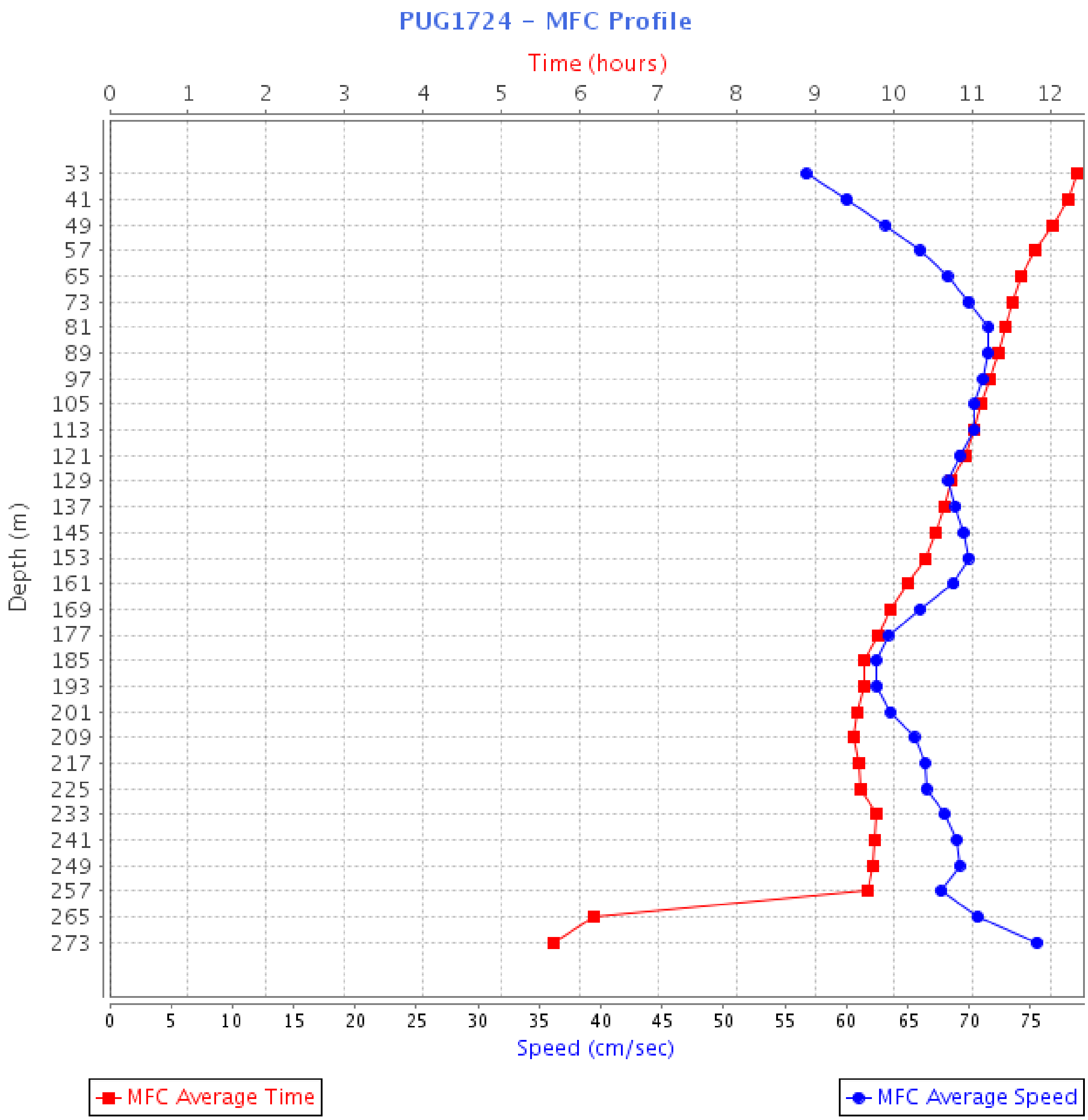

Figure 6-60. PUG1724 MFC timing (GI - red squares) and speed (blue circles) by depth bin. Bin 1 is the deepest bin observed at approximately 272.6 m below MLLW, and the top-most good bin is bin 31 (32.6 m below MLLW). The significantly earlier arrival of MFC at depth is due to a change in tide type from mixed, mainly semidiurnal to mixed mainly diurnal. The algorithm used to calculate GI does not calculate diurnal tides properly, therefore the values for the two deepest cells (265 m and 273 m) should be disregarded.

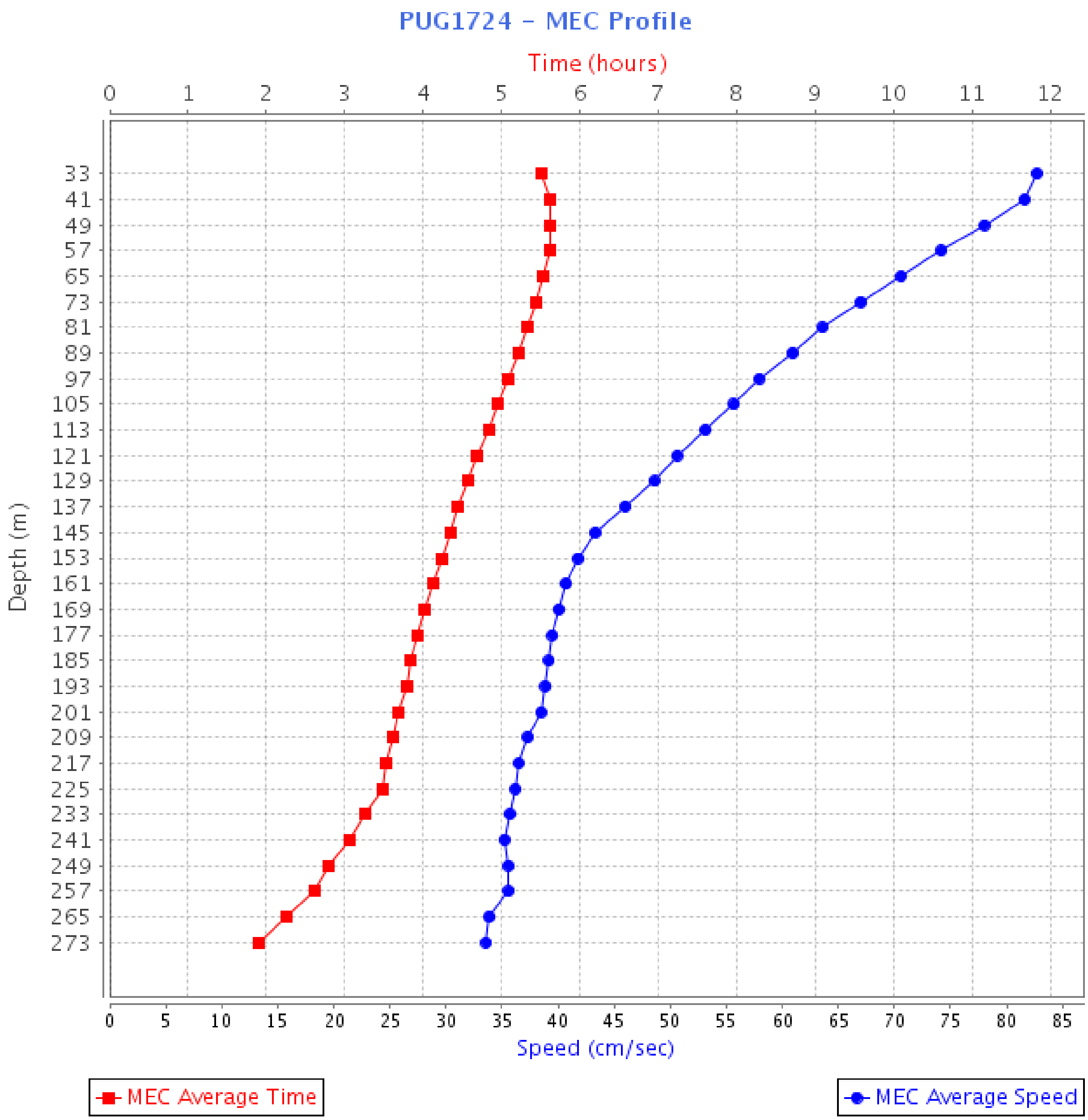

Figure 6-61. PUG1724 MEC timing (GI – red squares) and speed (blue circles) by depth bin. Bin 1 is the deepest bin observed at approximately 272.6 m below MLLW, and the top-most good bin is bin 31 (32.6 m below MLLW).

6.13. PUG1740 - Bellingham Channel, off Cypress Head Light

Bellingham Channel, off Cypress Head Light, was deployed for 61 days (June 23, 2017–August 24, 2017) in 74.1 m (243.2 ft) of water. A TRDI WorkHorse Sentinel 300 kHz ADCP mounted in a SUBS collected 22, 3 m bins of data, 20 of which met quality control criteria for full analysis. Bins 10, 17, and 19 are published in the TCTs, representing approximate depths of 36.3 m, 15.3 m, and 9.3 m (119.2 ft, 50.3 ft, and 30.6 ft) MLLW, respectively

Bellingham Channel is the most direct route to Bellingham Bay from Anacortes, and the tidal currents have considerable velocity (NOAA, 2019d). Harmonic analysis LSQHA solved 92–99 percent of the total current energy. The currents are rectilinear—mixed, mainly semidiurnal with stronger ebbs than floods. MFC reach their maximum in bin 17 (127.6 cm/s [2.5 kn]), and MEC are the strongest in bin 18 (152.8 cm/s [3.0 kn]). Significant permanent current along the major axis amplifies the ebb direction and increases from bottom to top (Figure 6-64). Compared to historical data, speeds are much stronger for both floods and ebbs.

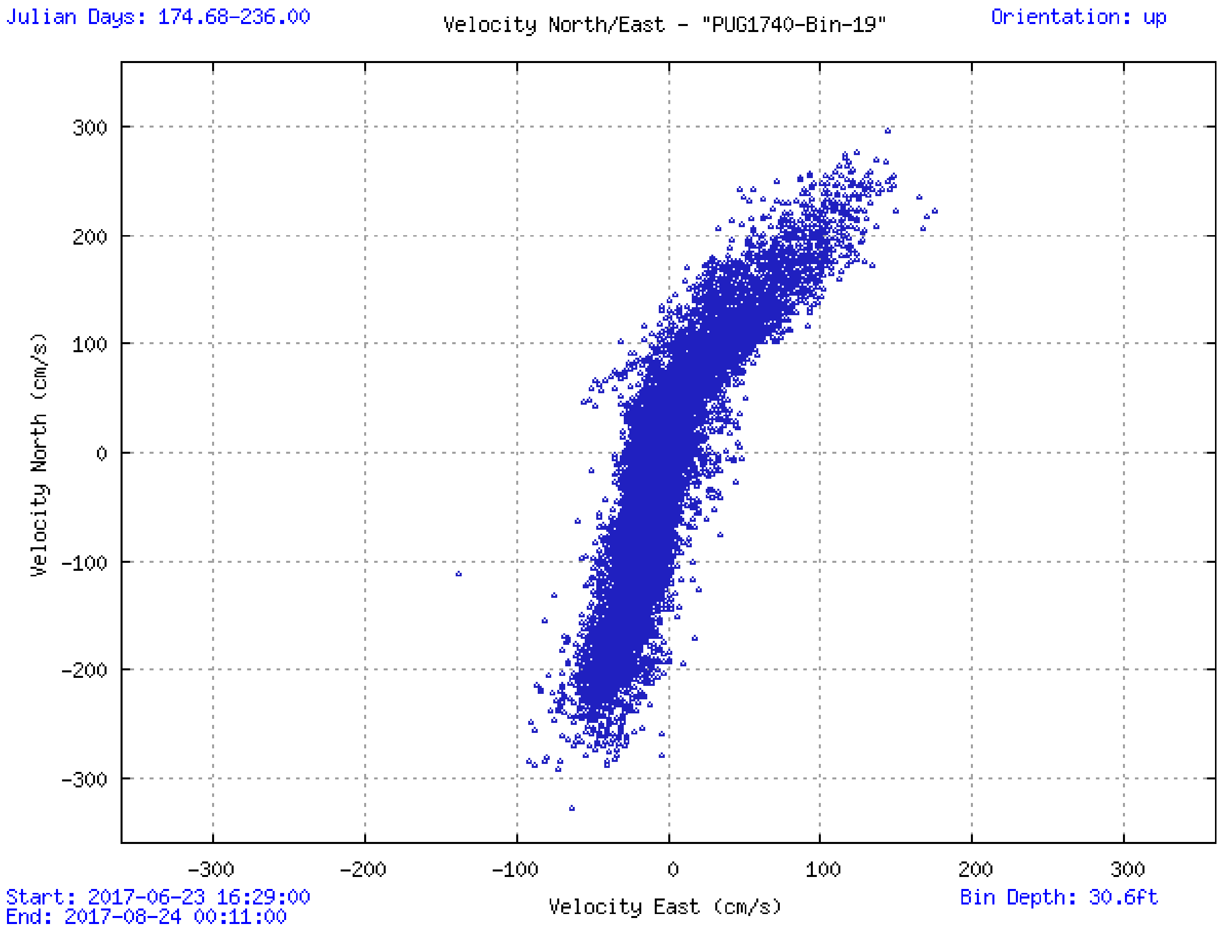

Figure 6-62. Scatter plot of north-versus-east velocity for station PUG1740 at the near-surface bin, bin 19 at 9.3 m below MLLW.

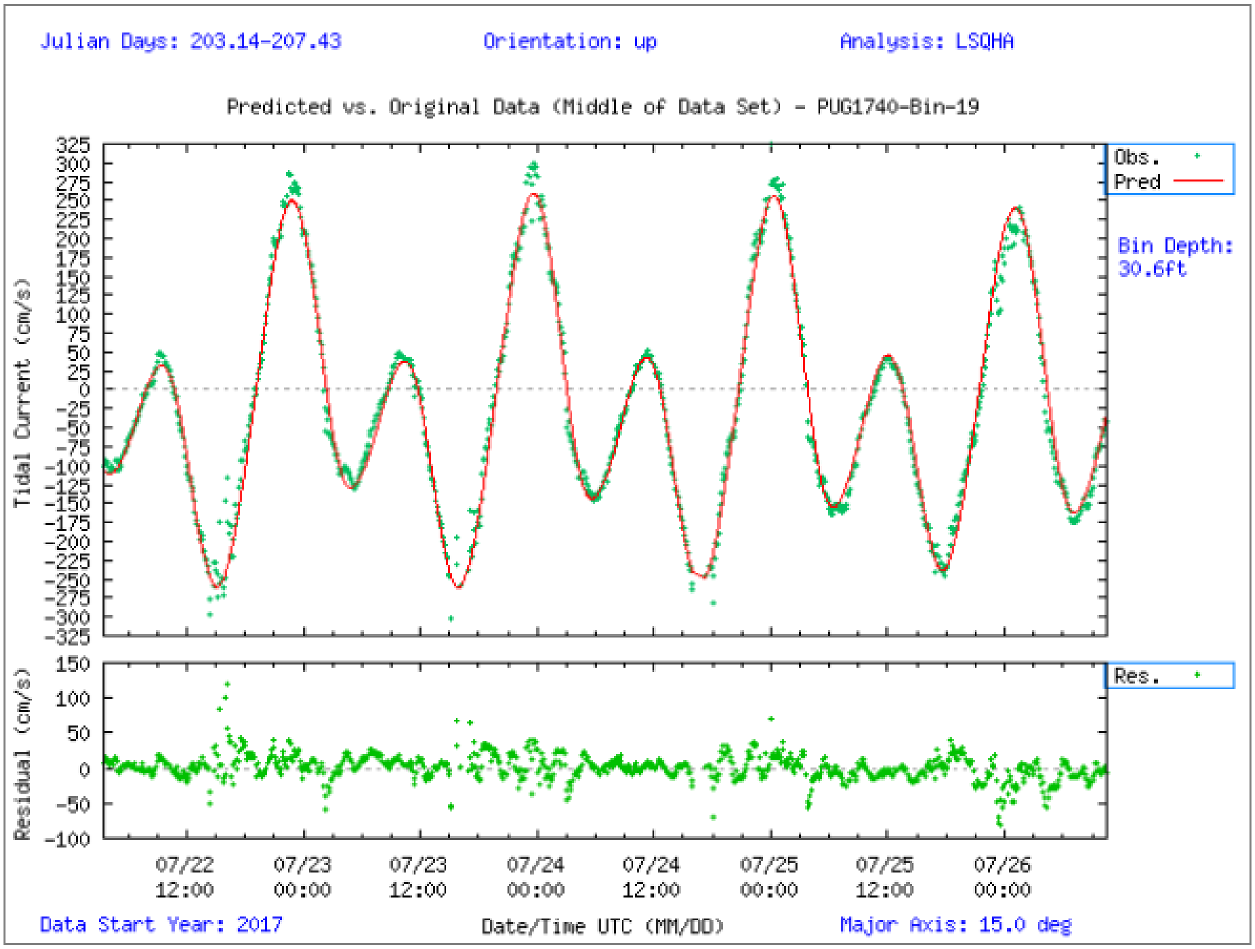

Figure 6-63. Comparison of observed major axis velocity data (green points) to predicted tidal velocity along the major axis for station PUG1740. The lower figure shows the non-tidal residual, the difference between the predicted and observed velocity from the upper panel.

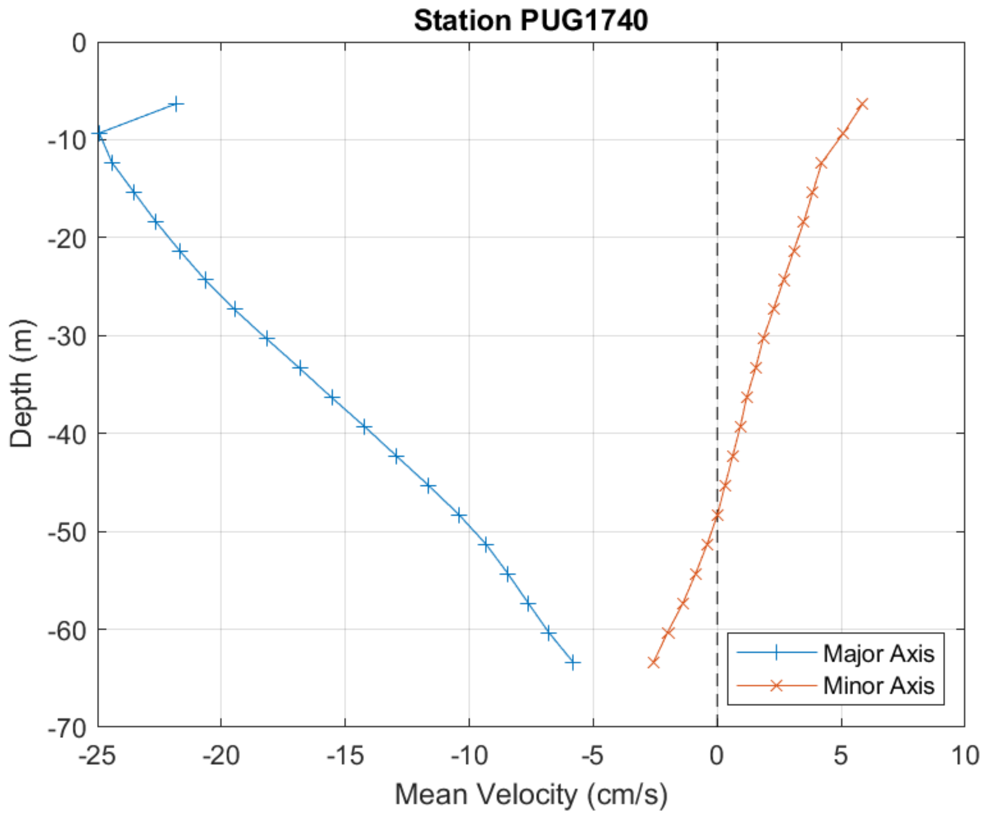

Figure 6-64. PUG1740 mean velocity profile by depth. Only depths that passed quality control criteria are shown. This station was configured to collect 3.0 m bins.

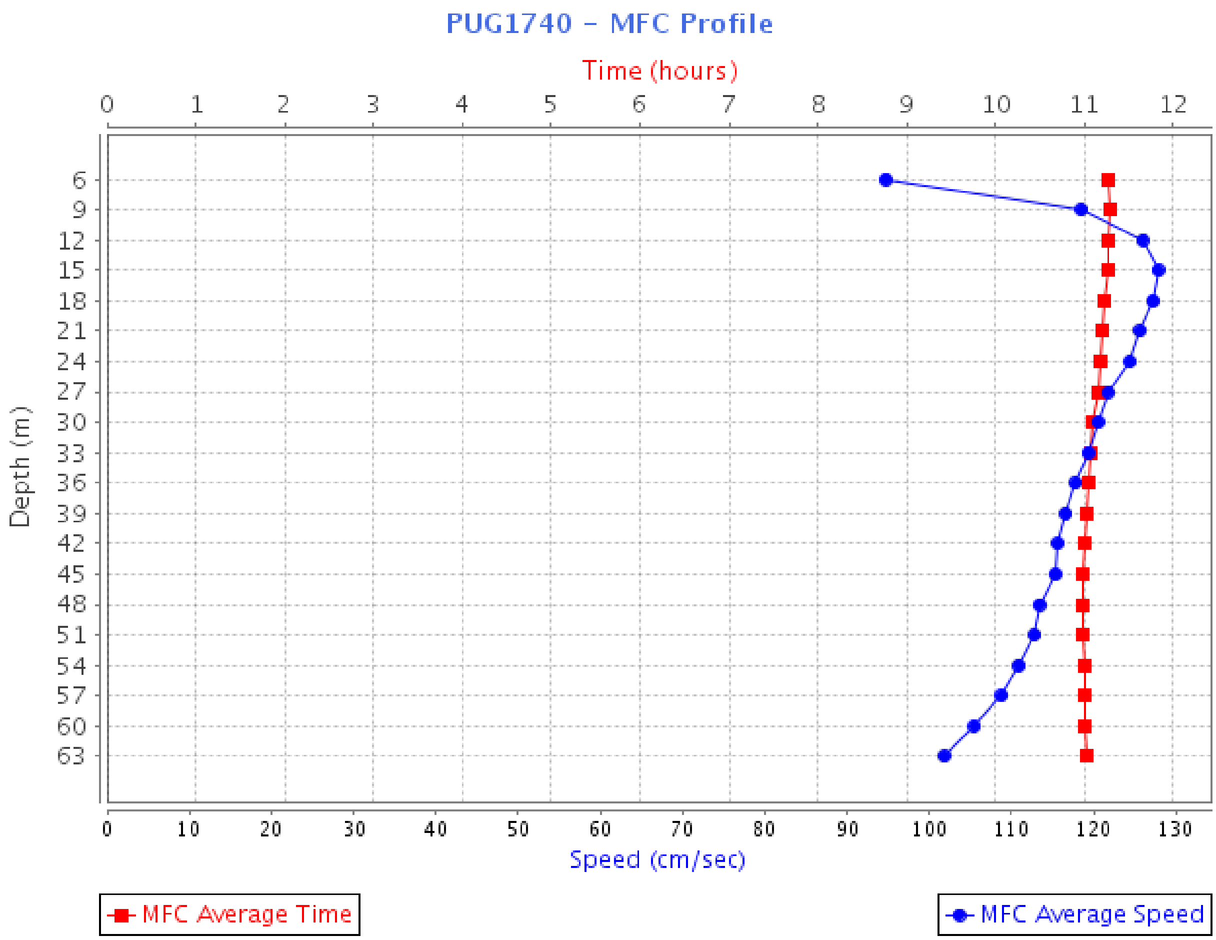

Figure 6-65. PUG1740 MFC timing (GI - red squares) and speed (blue circles) by depth bin. Bin 1 is the deepest bin observed at approximately 63.3 m below MLLW, and the top-most good bin is bin 20 (6.3 m below MLLW).

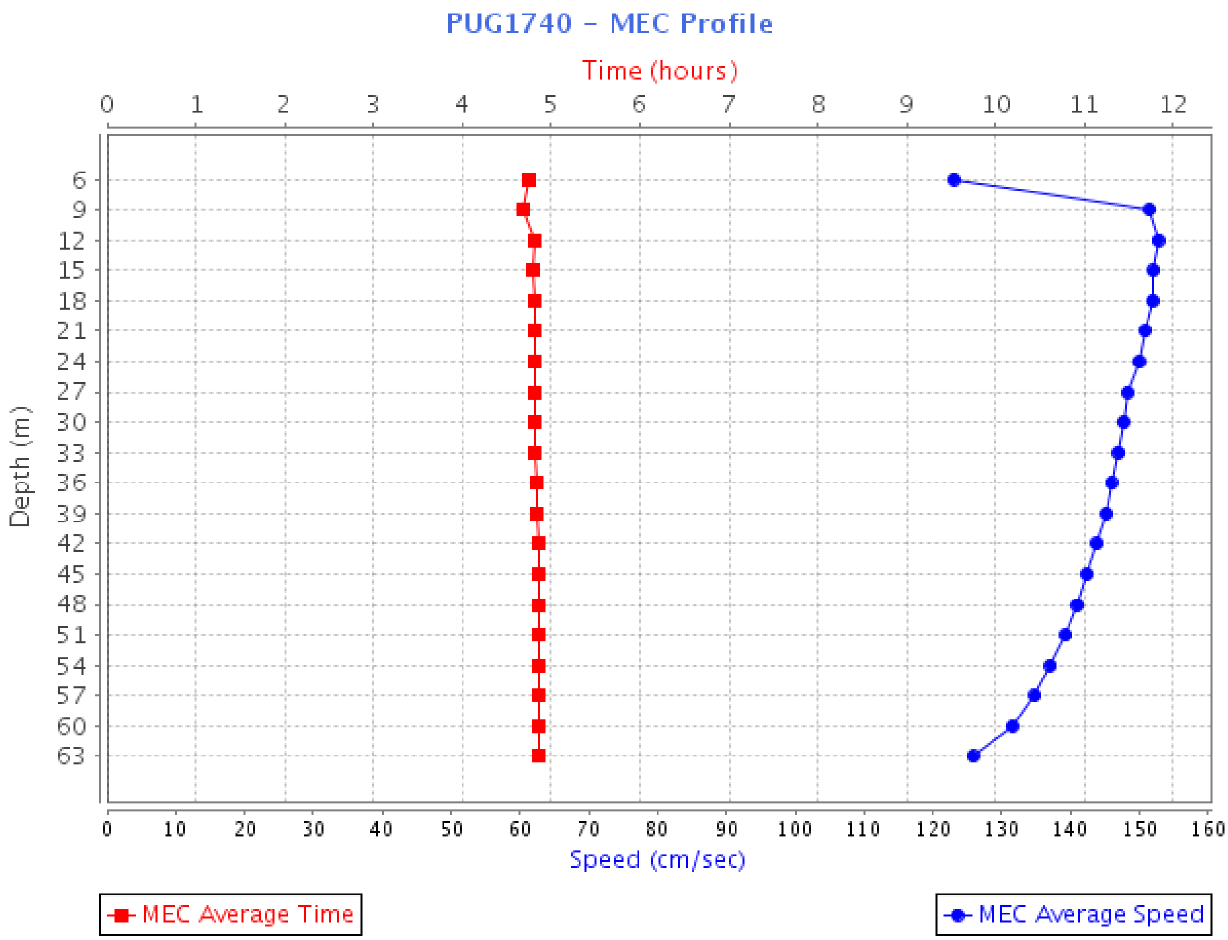

Figure 6-66. PUG1740 MEC timing (GI - red squares) and speed (blue circles) by depth bin. Bin 1 is the deepest bin observed at approximately 63.3 m below MLLW, and the top-most good bin is bin 20 (6.3 m below MLLW).

6.14. PUG1741 - Bellingham Channel North

Bellingham Channel North was deployed for 64 days (June 22, 2017–August 24, 2017) in 70.0 m (229.7 ft) of water. A TRDI Workhorse Sentinel 300 kHz ADCP mounted in a single SUBS collected 31, 2 m bins of data, 28 of which met quality control criteria for full analysis. Bins 5, 24, and 27 are published in the TCTs, representing approximate depths of 52.2 m, 14.2 m, and 8.2 m (171.2 ft, 46.5 ft, and 26.8 ft) MLLW, respectively.

Currents are mixed, mainly semidiurnal with dominant ebbs, which can be seen in the mean velocity profile (Figure 6-69). The mean MFC ranges from 1.5 kn to 1.9 kn, with stronger floods at the surface. The mean MEC ranges from 98.3 cm/s to 125.5 cm/s (1.9 kn to 2.4 kn) with the stronger ebbs at depth. The currents are rectilinear and show the reversing direction on the ebb flow; however, there is some cross-flow at the surface due to the influence of islands and convergence of waterways. Harmonic analysis solved for 90–96 percent of the total current energy.

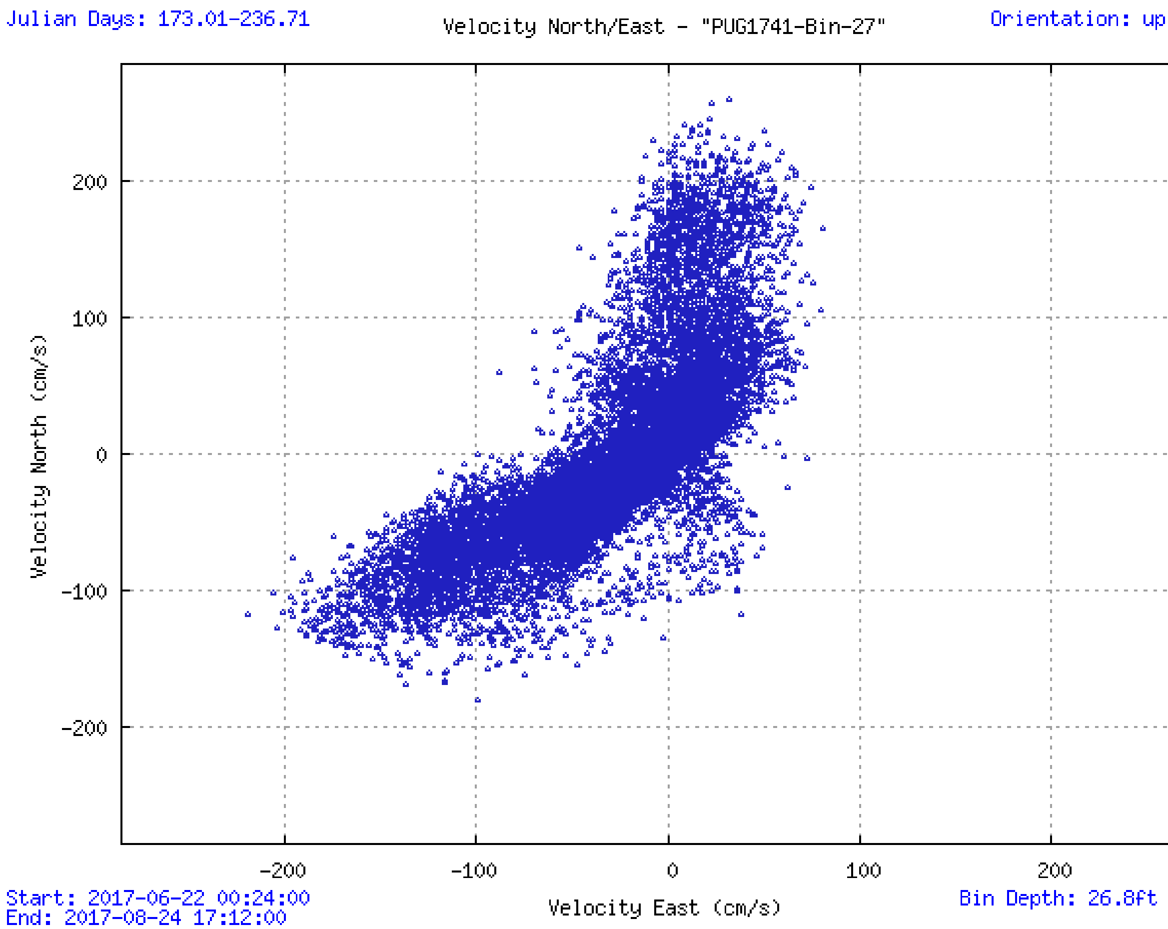

Figure 6-67. Scatter plot of north-versus-east velocity for station PUG1741 at the near-surface bin, bin 27 at 8.2 m below MLLW.

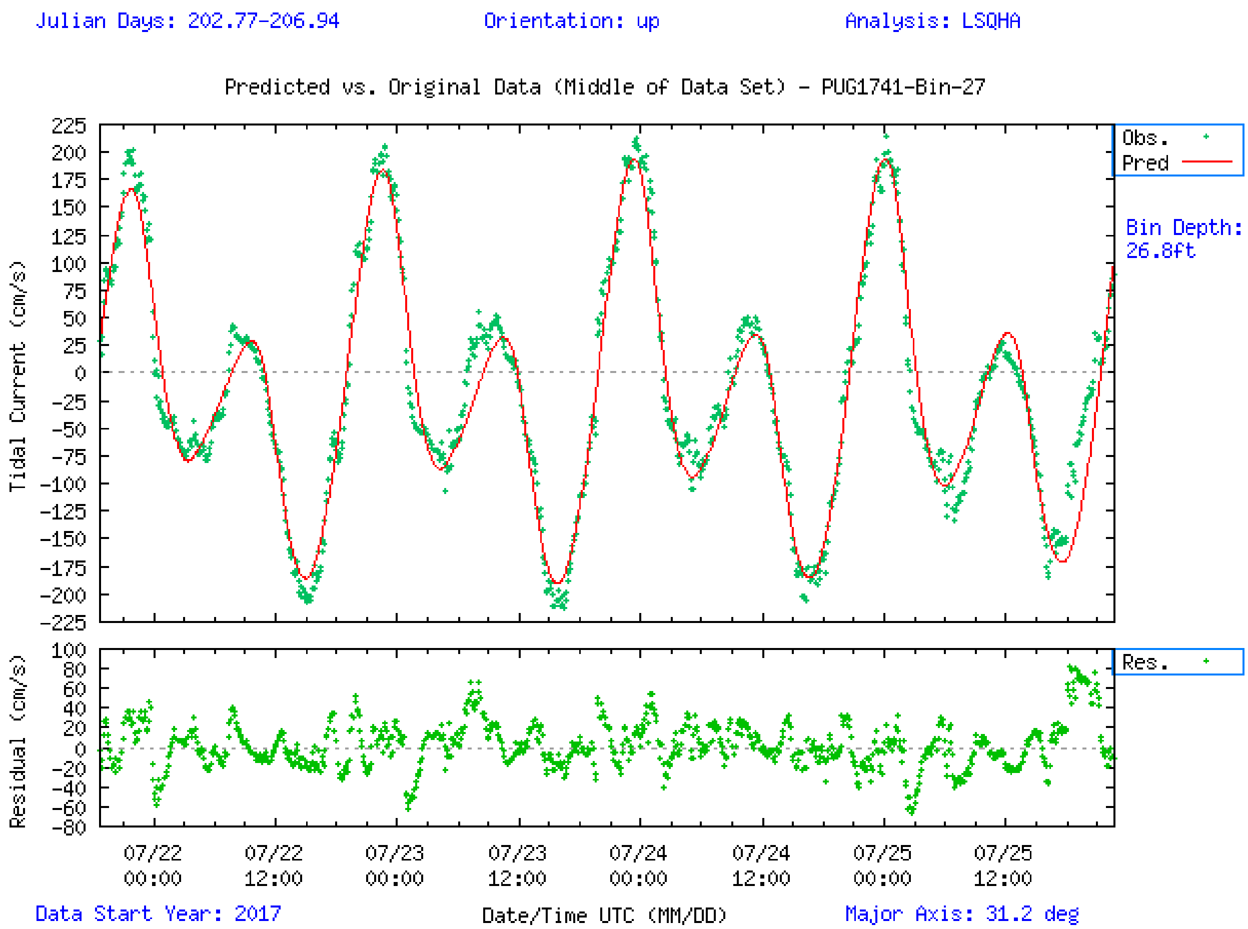

Figure 6-68. Comparison of observed major axis velocity data (green points) to predicted tidal velocity along the major axis for station PUG1741. The lower figure shows the non-tidal residual, the difference between the predicted and observed velocity from the upper panel.

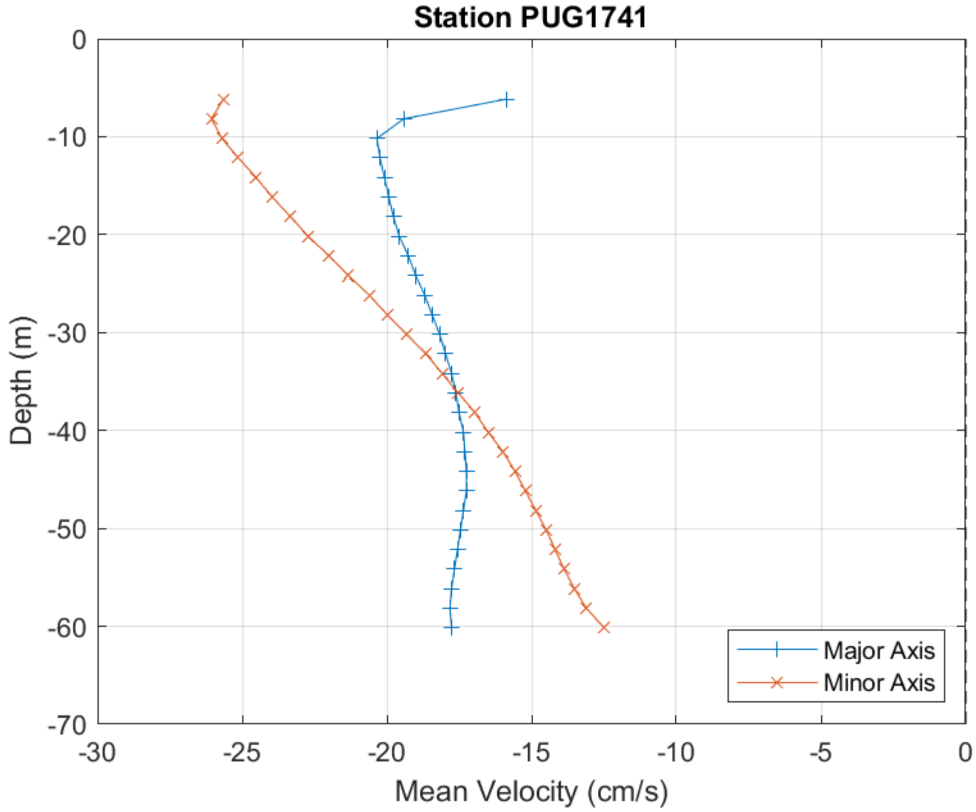

Figure 6-69. PUG1741 mean velocity profile by depth. Only depths that passed quality control criteria are shown. This station was configured to collect 2.0 m bins.

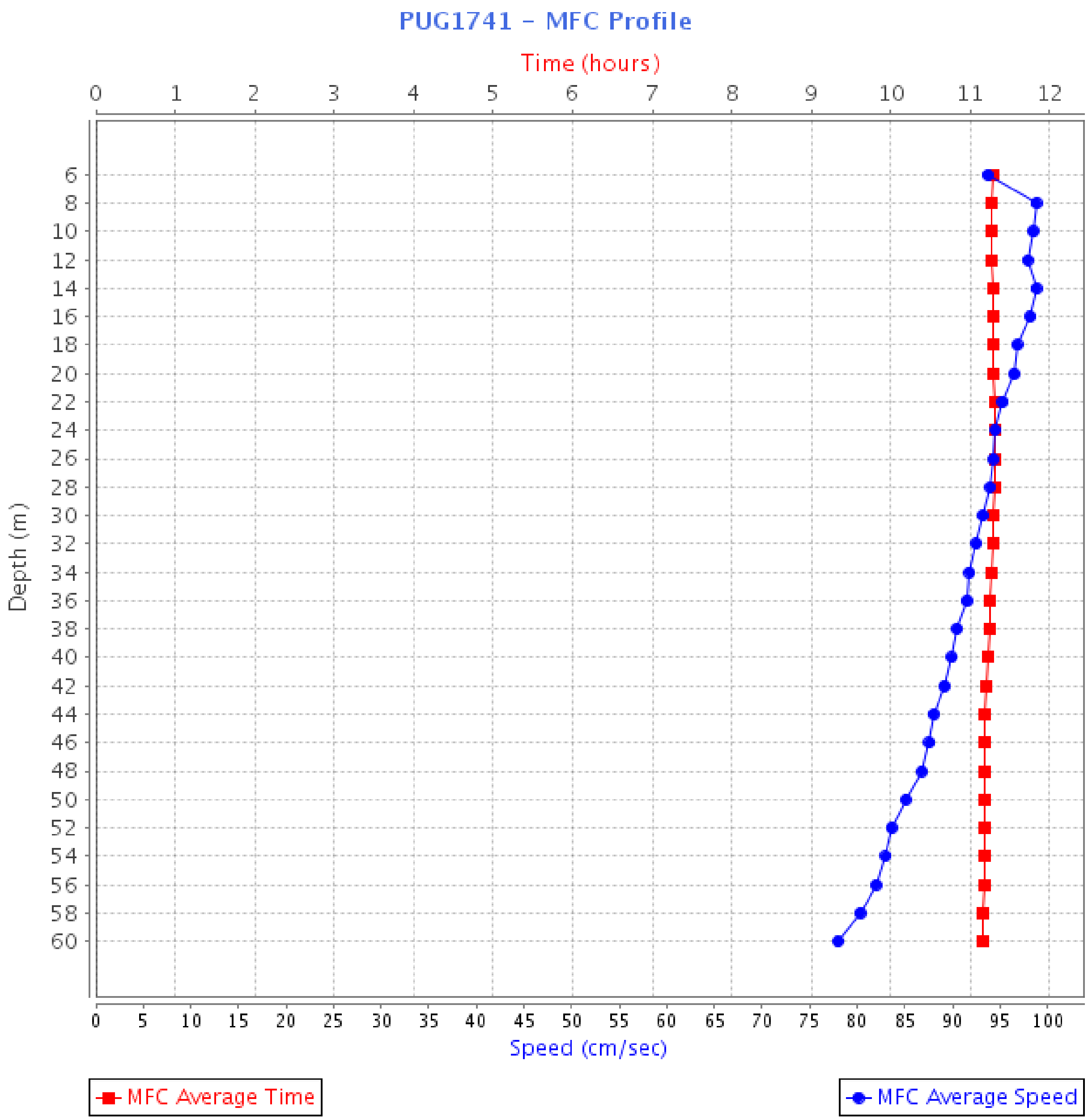

Figure 6-70. PUG1741 MFC timing (GI - red squares) and speed (blue circles) by depth bin. Bin 1 is the deepest bin observed at approximately 60.2 m below MLLW, and the top-most good bin is bin 28 (6.2 m below MLLW).

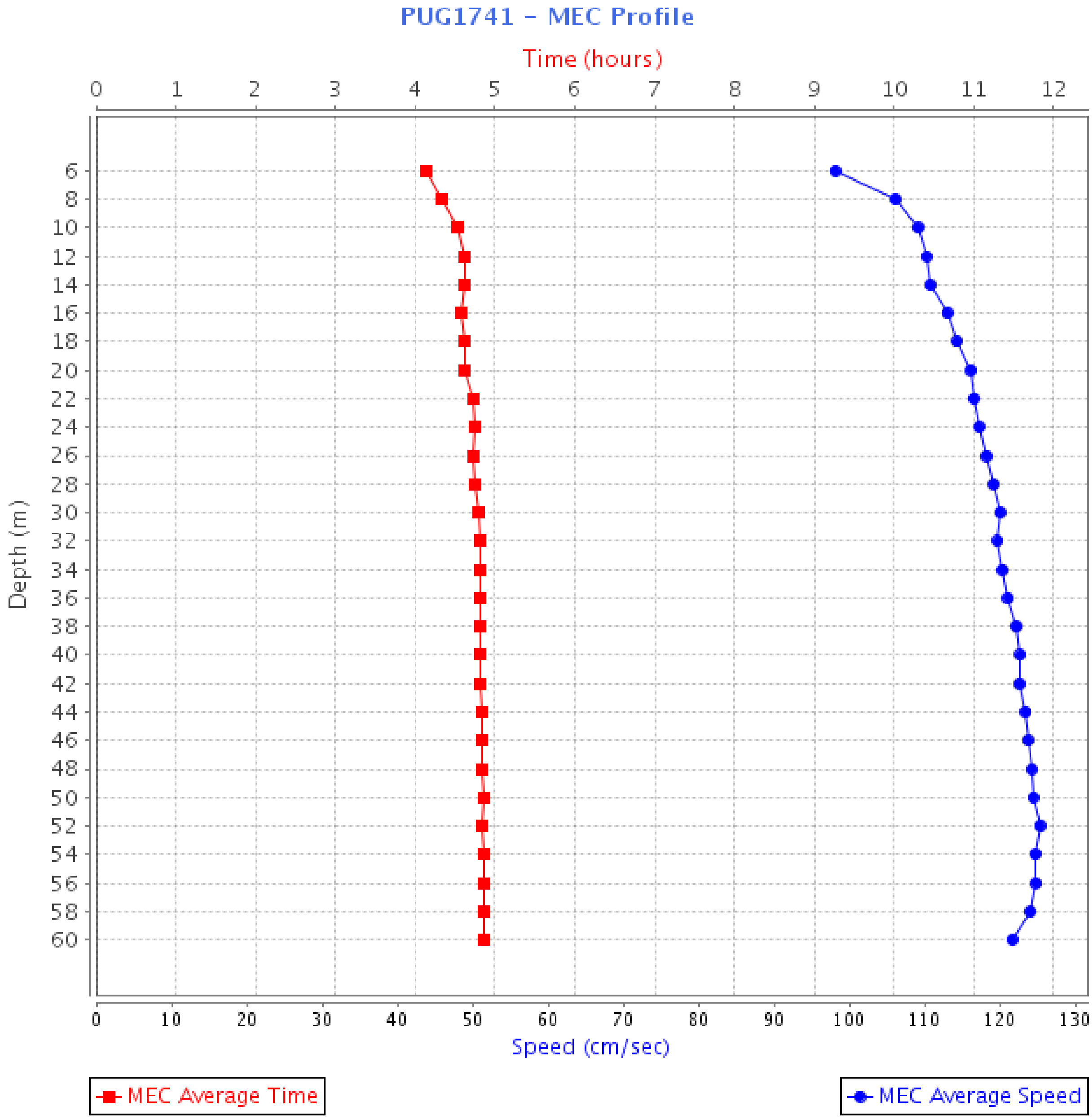

Figure 6-71. PUG1741 MEC timing (GI - red squares) and speed (blue circles) by depth bin. Bin 1 is the deepest bin observed at approximately 60.2 m below MLLW, and the top-most good bin is bin 28 (6.2 m below MLLW).

7. SPATIAL VARIATION

7.1. Harmonic constituents

Harmonic constituents were generated for all stations in this study using the methods described in section 3.6. For most stations, tidal harmonic constituents show that in general the M_2 tidal constituent (the principal lunar semidiurnal constituent) is the dominant constituent. This means that tidal characteristics for most stations in the Puget Sound and Salish Sea are primarily semidiurnal or mixed semidiurnal. Most stations are also rectilinear; they have a back and forth tidal motion between flood and ebb and do not exhibit rotary characteristics. Of the 135 stations analyzed, three stations (PUG1504 [Entrance to Ballard Locks], PUG1506 [Harbor Island East], and PUG1613 [Everett]) were weak and variable, and three stations (PUG1525 [The Narrows, North End, east side], PUG1633 [Point Partridge, 2.4 mi NW of], and PUG1716 [Waldron Island, 1.7 nmi west of]) showed other non-tidal influences that were larger than the astronomical tidal forces. These last three stations did not have stable harmonic constituents that were within error parameters and therefore do not have official published predictions. For all six of these stations, additional rotary analyses were calculated, and only GI values are published in the TCTs as subordinate stations, but the data is available on the CO-OPS Tides and Currents website (NOAA, 2019a). For the 128 harmonic stations whose constituents are included in the tidal current tables, variations in the amplitude of the constituents were strongly influenced by the bathymetry and topography near each station. Figure 7-1 shows the Defant ratio, the ratio of the principal diurnal constituents to the principal semidiurnal component (M_2, S_2, O_1, and K_1) of the tides for the major axis. The Defant ratio is defined as: $(K_1 + O_1) / (M_2 + S_2)$. This ratio is used to define the nature of the tide as it changes from strict semidiurnal to strict diurnal: for a Defant ratio less than 0.25, the tides are semidiurnal; for a Defant ratio between 0.25 and 1.5, the tides are mixed, primarily semidiurnal; for a ratio between 1.5 and 3, the tides are mixed but mostly diurnal; and for a ratio greater than 3, the tides are diurnal (Defant, 1958). The study area consists of mostly mixed, semidiurnal tides, with many of the stations in narrow channels or straits (such as Deception Pass) exhibiting the strongest semidiurnal tidal characteristics, and the stations in Haro Strait exhibiting the most diurnal tidal characteristics.

The spatial distribution of the tidal ellipses of the principal semidiurnal and diurnal constituents are shown in Figures 7-2 to 7-5, and enlarged, regional views of the M_2 ellipses are shown in Figures 7-6 to 7-8. Where possible, Table B-1 in Appendix B lists the major and minor ellipse amplitudes of all stations and the corresponding Defant ratios. The figures clearly show that M_2 is the dominant constituent, and that bathymetry (particularly the locations of channels) is the driving force behind the relative strength and orientation of the M_2 and other constituents, as well as the degree of rectilinearity of the ellipses. For example, station PUG1701, Deception Pass—a very narrow hydraulic strait that connects Skagit Bay with the San Juan Islands—is extremely rectilinear, M_2-dominated, and has the fastest tidal velocities measured in the survey.

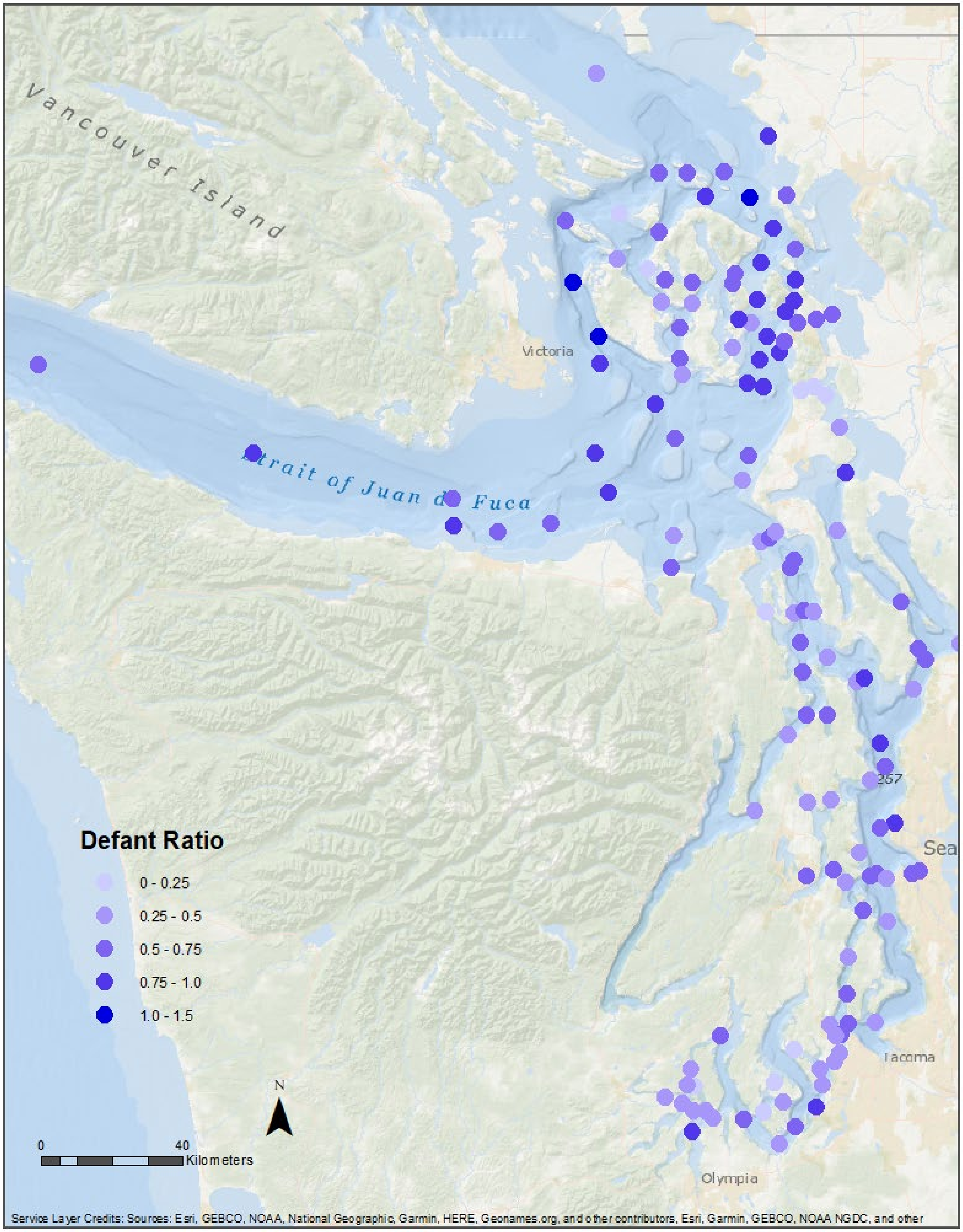

Figure 7-1. Defant ratios for survey stations. Strict semidiurnal tides (Defant ration <0.25, depicted in light purple) are observed at only a few stations, with mixed semidiurnal (0.25 to 1.5) to mixed diurnal tides (>1.5) dominating in most regions with darker purple representing the mixed semidiurnal stations and blue representing the mixed semidiurnal tending to diurnal stations. There are no diurnal stations (Defant ratio >3.0).

Figure 7-2. M_2 Tidal ellipses for the entire study region, showing the topographic steering of the ellipses.

Figure 7-3. S_2 tidal ellipses for the entire study region. Note that these are on a different scale than M_2 in order to see the ellipses. These data are at ¼ the scale of the M_2 data.

•

Figure 7-4. O_1 tidal ellipses for the entire study region. Note that these are on a different scale than M_2 in order to see the ellipses. These data are at ¼ the scale of the M_2 data.

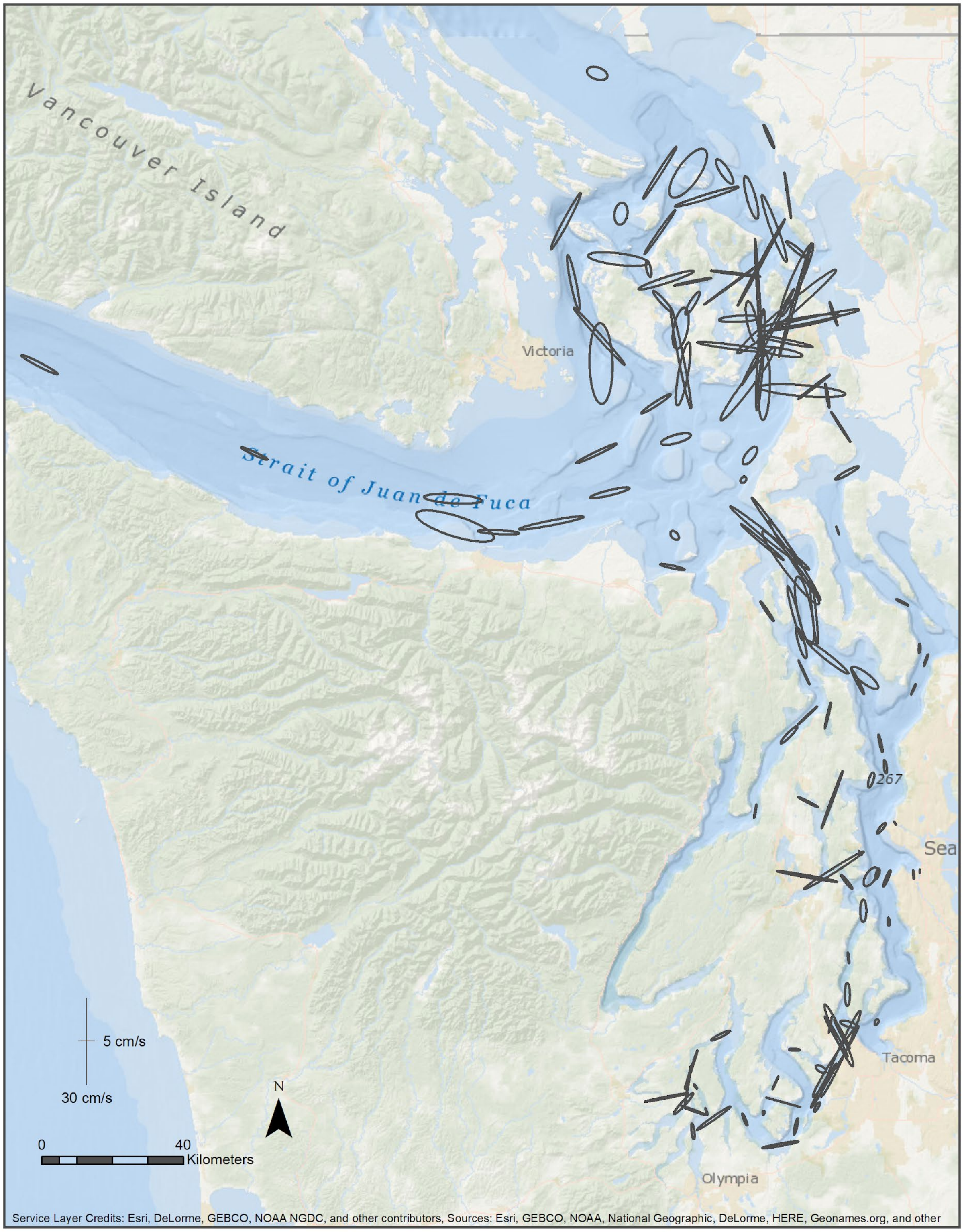

Figure 7-5. K_1 tidal ellipses for the entire study region. Note that these are on a different scale than M_2 in order to see the ellipses. These data are at ¼ the scale of the M_2 data.

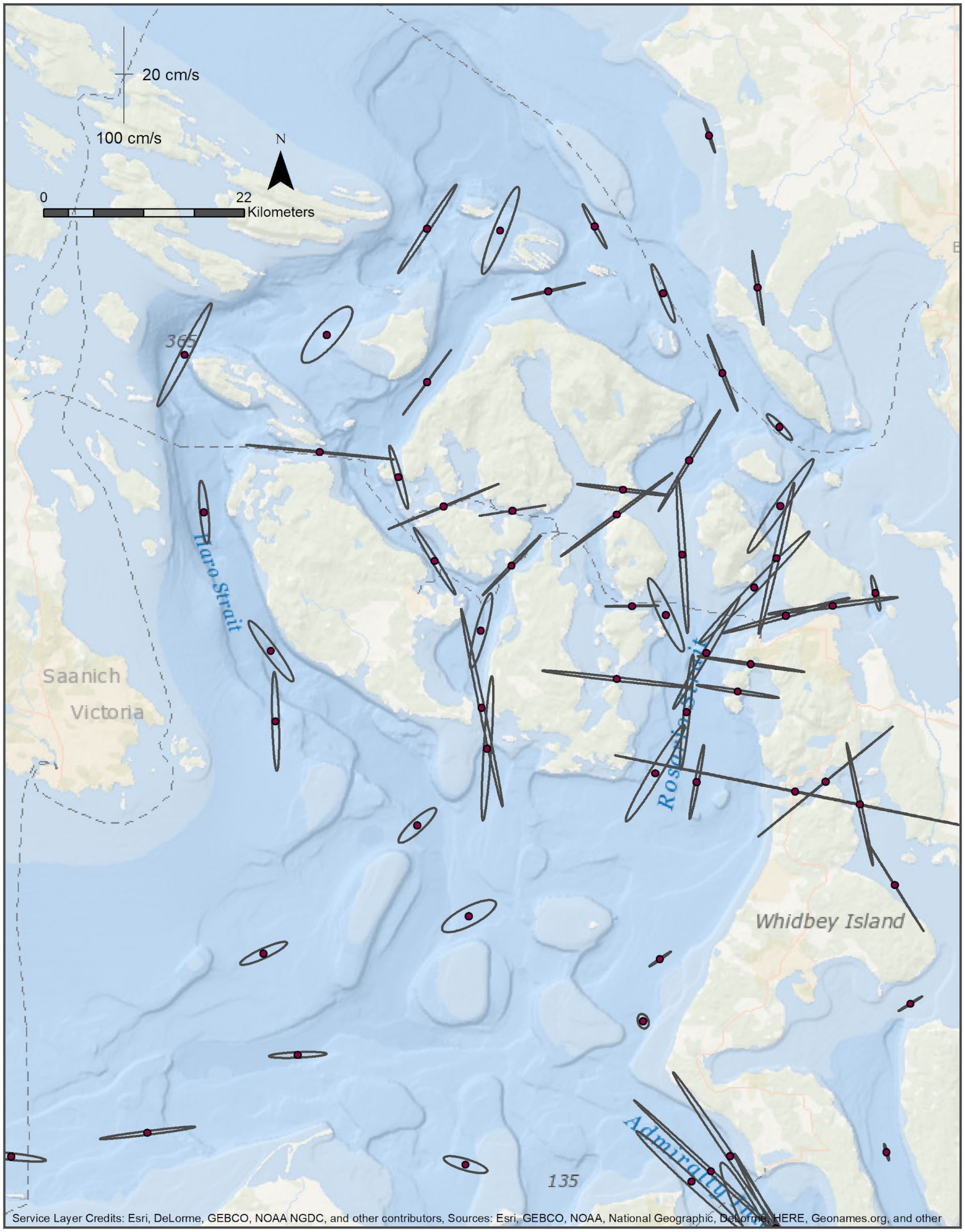

Figure 7-6. M_2 tidal ellipses for the San Juan Islands region. Deception Pass is notable as the extremely large east-west rectilinear ellipse in the channel north of Whidbey Island.

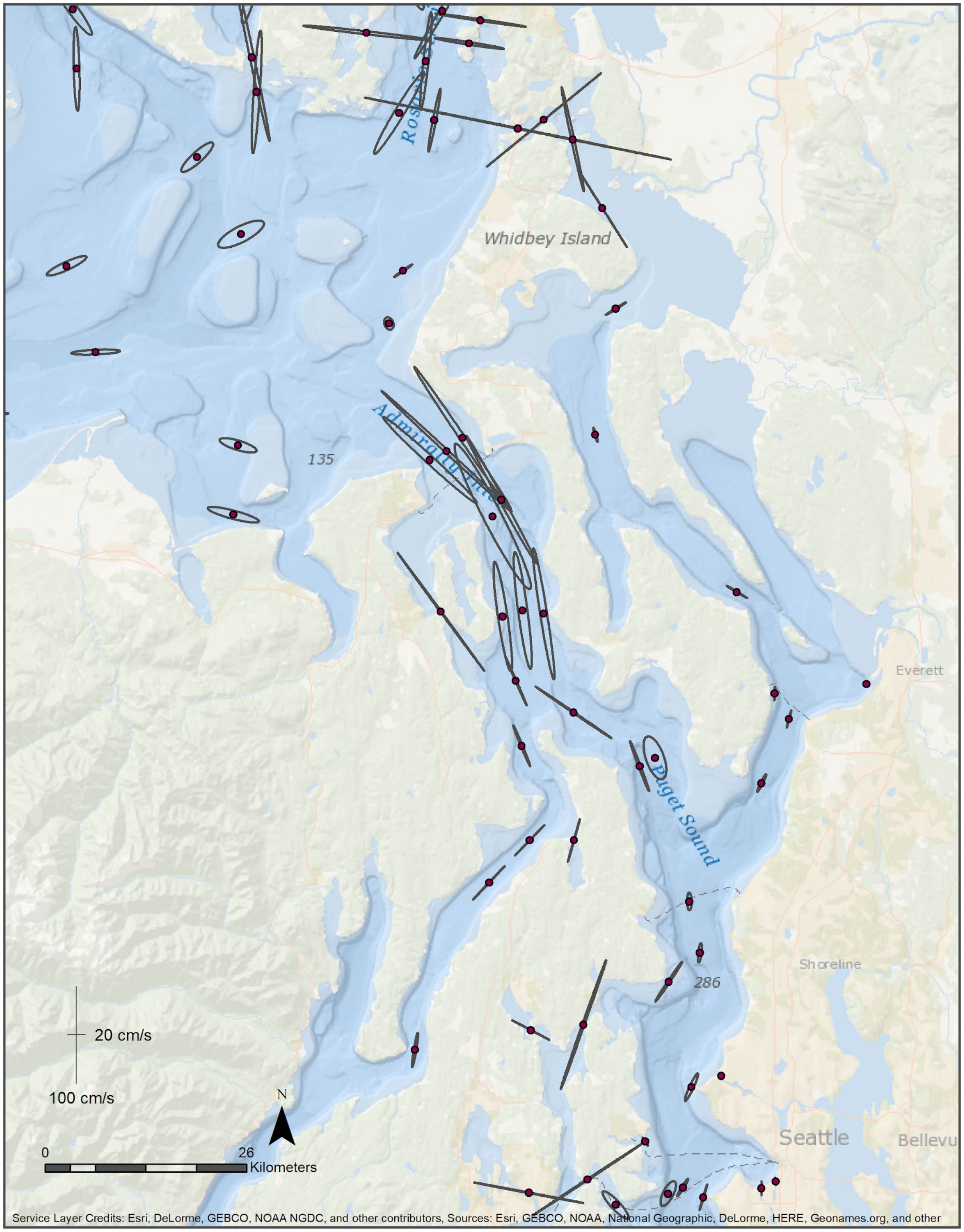

Figure 7-7. M_2 tidal ellipses for Admiralty Inlet and Skagit Bay region. Note the large M_2 magnitudes through Admiralty Inlet in the center of the figure.

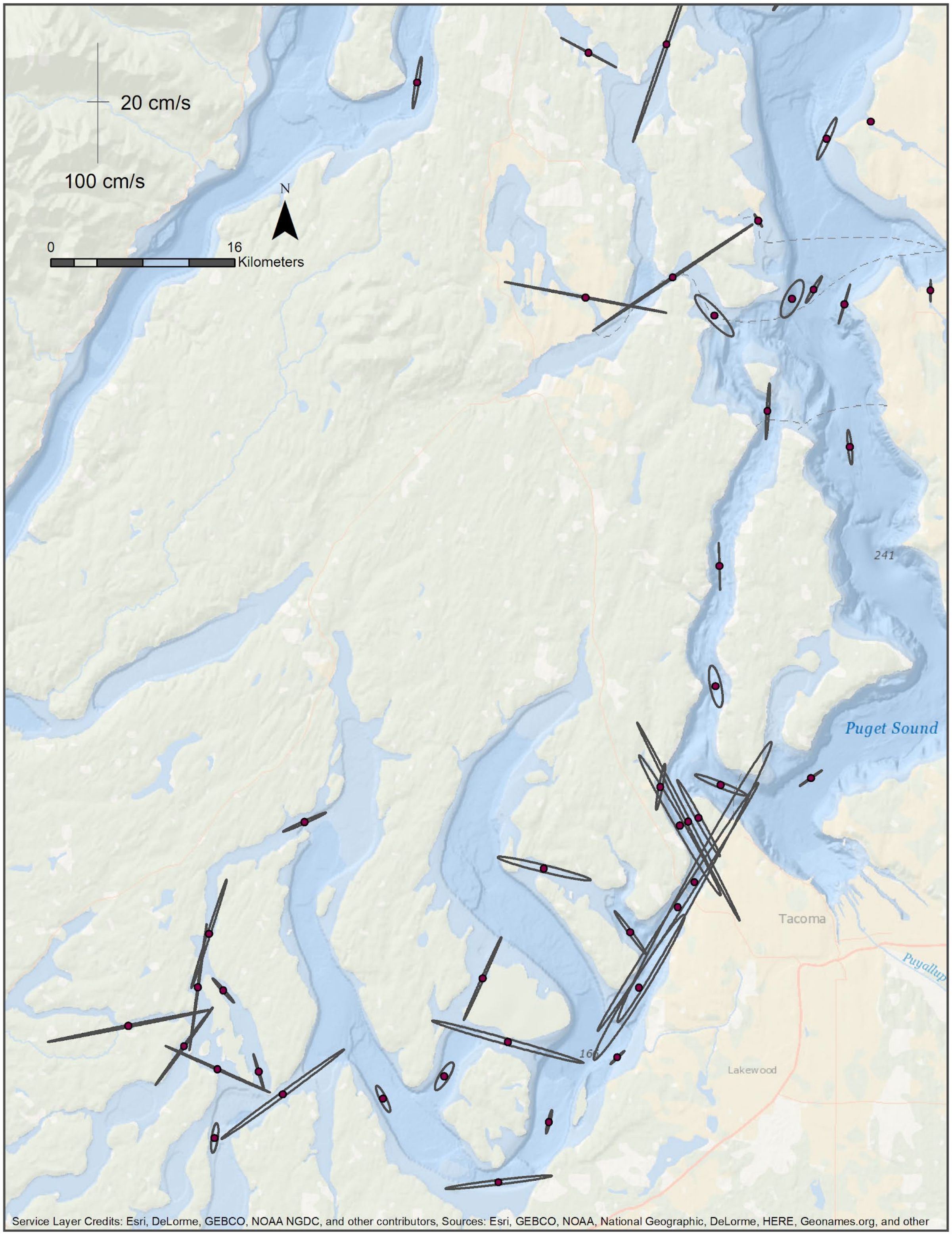

Figure 7-8. M_2 tidal ellipses for Puget Sound in the vicinity of Tacoma and Seattle.

7.2. Near-surface phases of the tide (timing and speed)

Spatial representation of the magnitude and timing of mean ebb and flood currents show the progression of the tides within the estuary and the changes in amplitude due to bathymetry. The following maps (Figures 7-9 to 7-12) show the spatial distribution of the mean current magnitude and direction at each station during the maximum flood and ebb currents, and Figures 7-13 to 7-16 show the corresponding GI timing of ebb and flood. These data are from the bin nearest to the 5 m depth that contains good data; these bins are also used for tidal current predictions published by CO-OPS. All current velocity maps show the current vectors on the same scale so that they can be compared with one another. All current velocity maps show the current vectors on the same scale so that they can be compared with one another, which immediately shows how the bathymetry influences the maximum flood and ebb speed and direction. Stations located in areas of significant topographic and bathymetric changes show distinct direction differences between flood and ebb based on bathymetry. Care must be used in interpreting the observed currents at these stations, which may not reflect the actual currents in the channel due to these bathymetric features. These analyses help to determine the correct direction for flood and ebb currents in locations where the topography is complex. For example, in Skagit Bay, the flood direction was reversed from the historical convention based on consideration of the overall GI timing and comparisons of tidal currents to nearby tidal water levels. Figures 7-11 and 7-15 show the magnitudes and timing, respectively, of the Admiralty Inlet region, including Deception Pass and Skagit Bay.

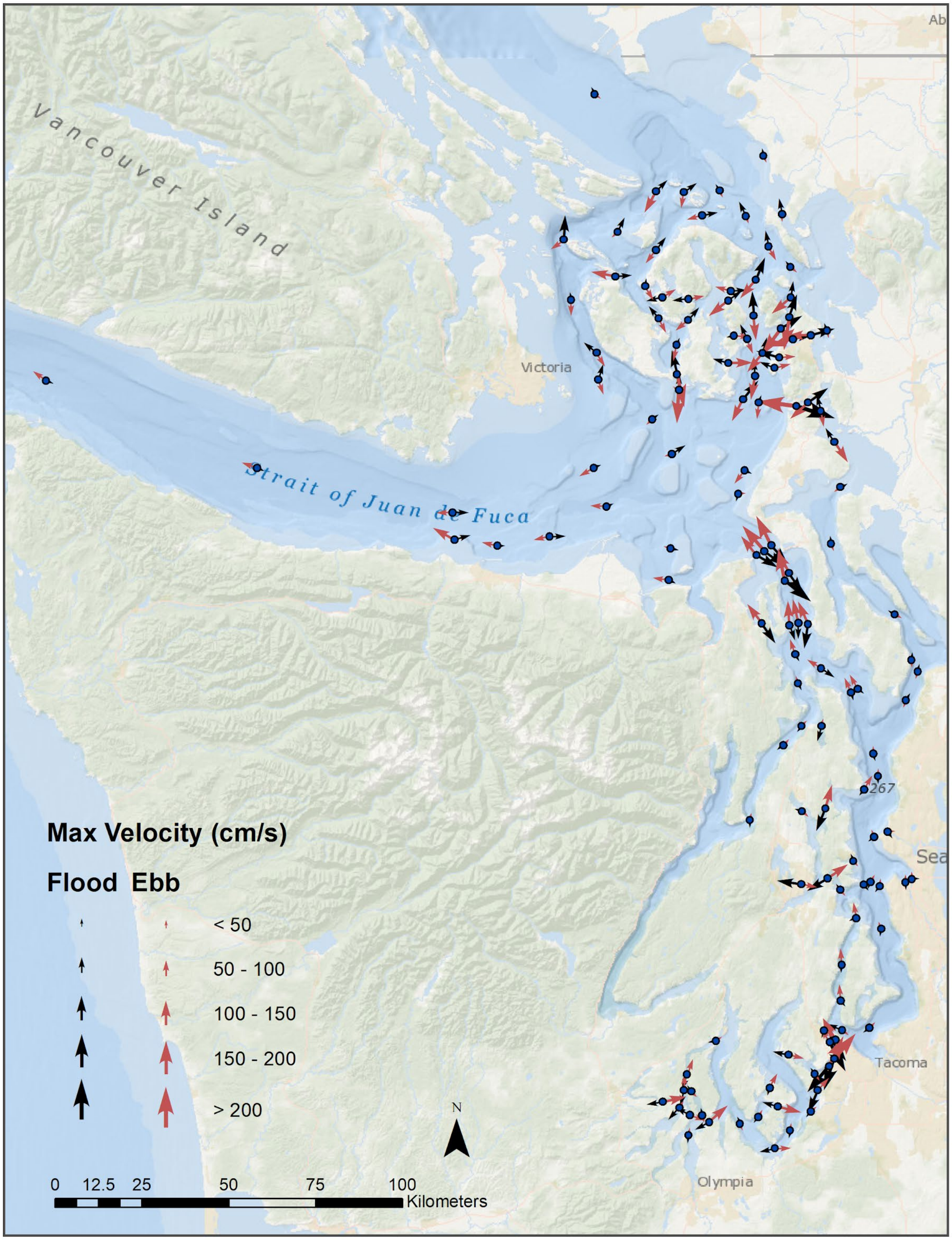

Figure 7-9. Mean values for the tidal currents during maximum flood and ebb at all stations in the survey.

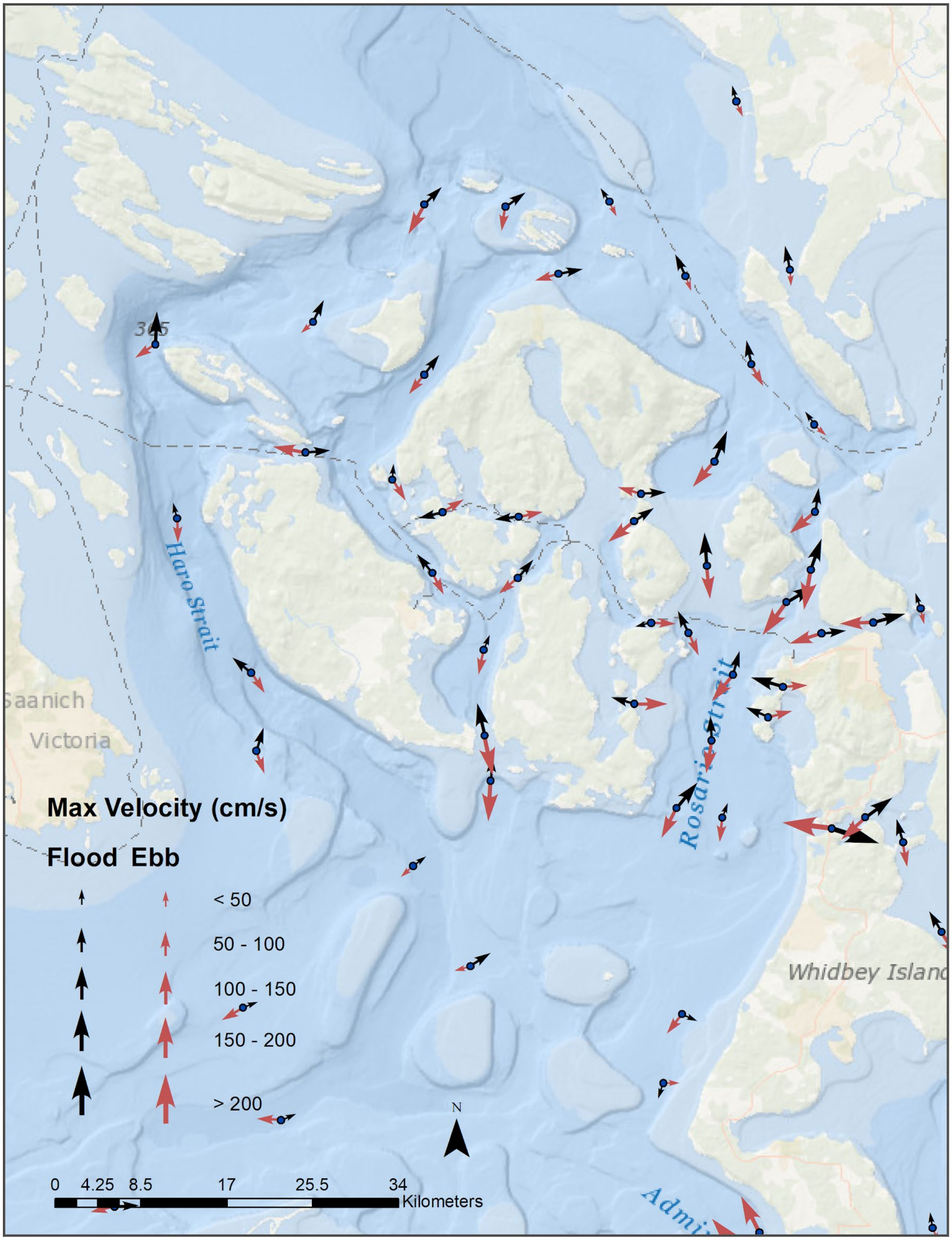

Figure 7-10. Mean values for the tidal currents during maximum flood and ebb at station in the San Juan Islands region of the survey. Deception Pass is shown in the very large arrows north of Whidbey Island.

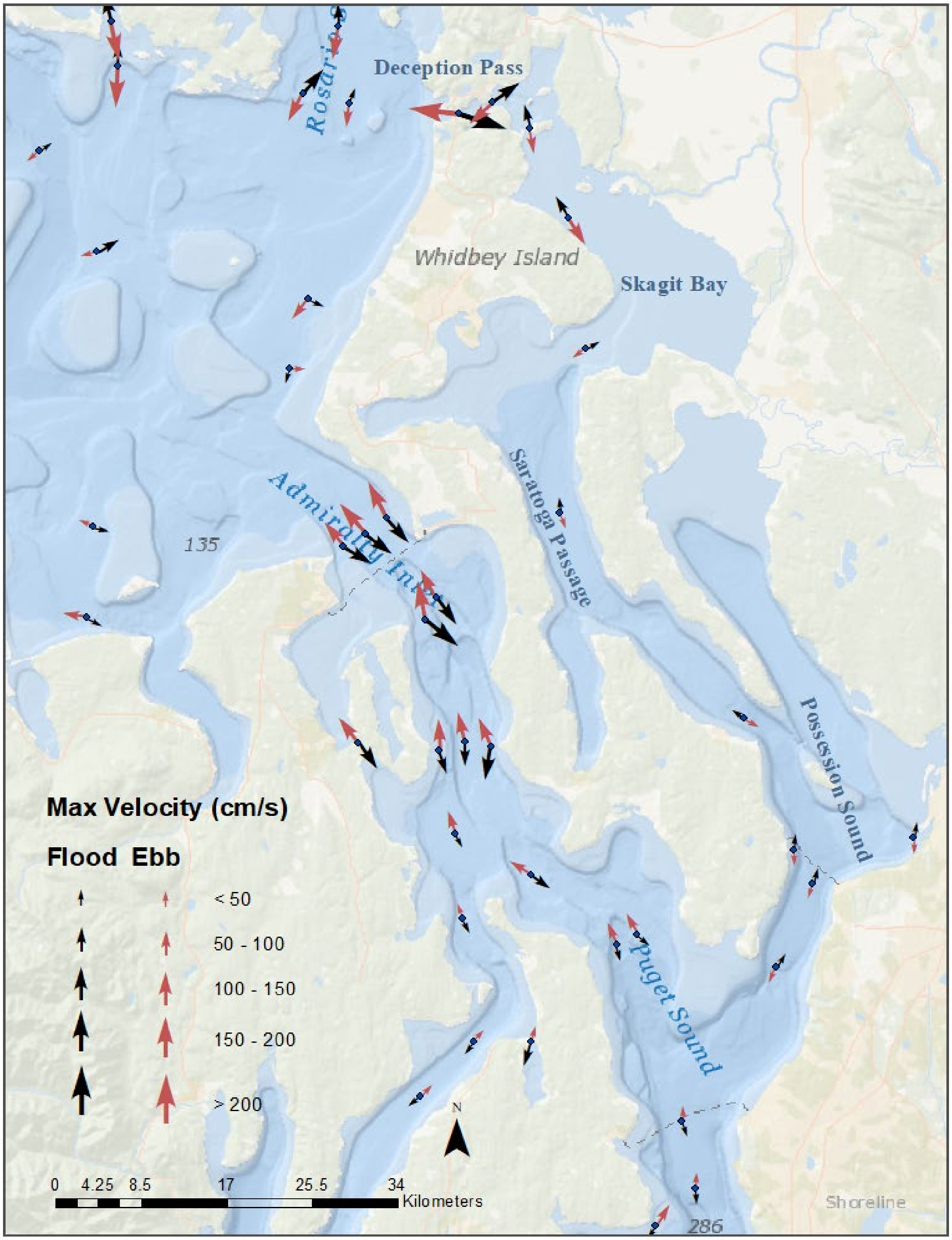

Figure 7-11. Mean values for the tidal currents during maximum flood and ebb at station in the Admiralty Inlet region of the survey. As described in the text, on the eastern side of Whidbey Island, Skagit Bay flood directions are now consistent with the flood directions in Saratoga Passage and Possession Sound.

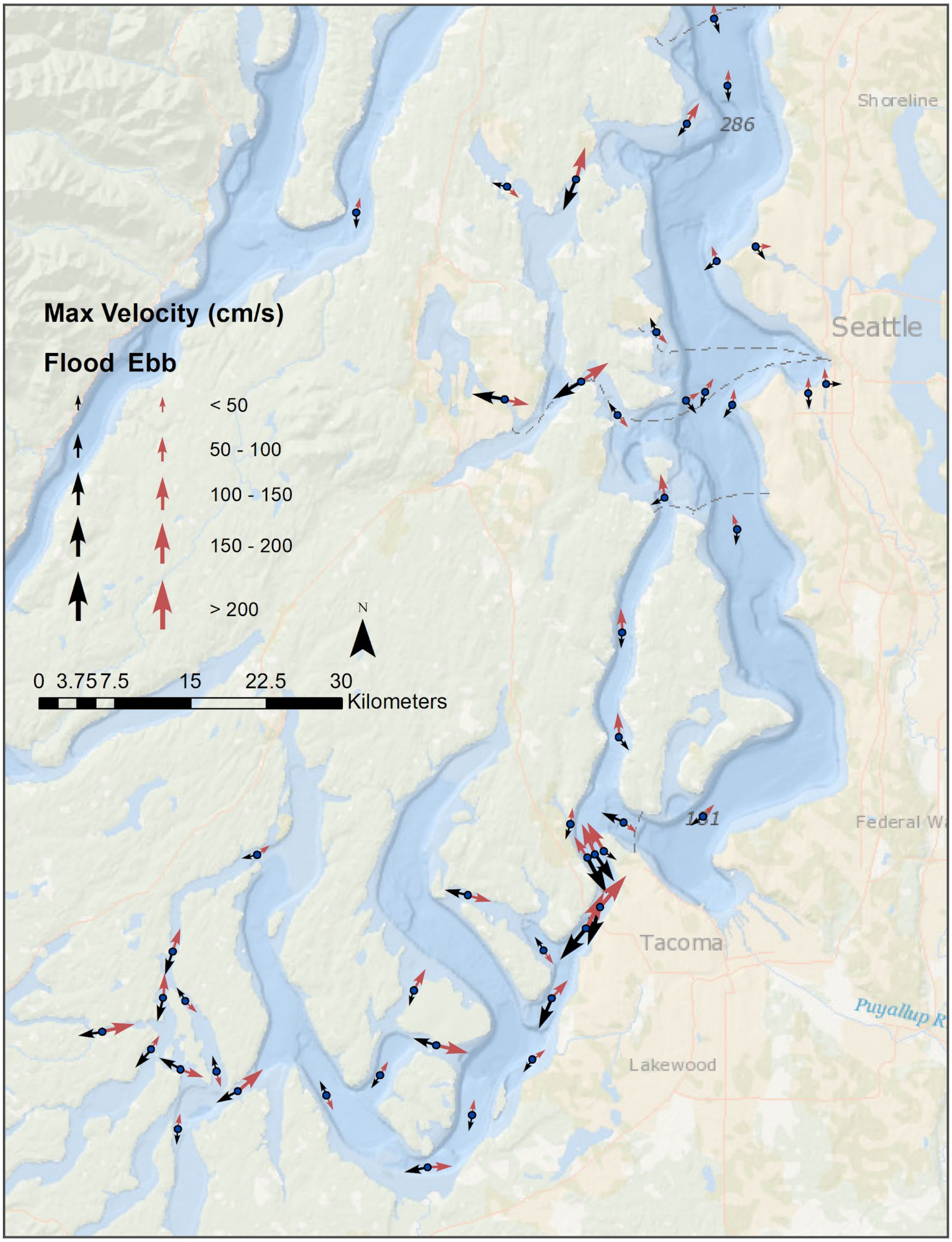

Figure 7-12. Mean values for the tidal currents during maximum flood and ebb at station in the Puget Sound.

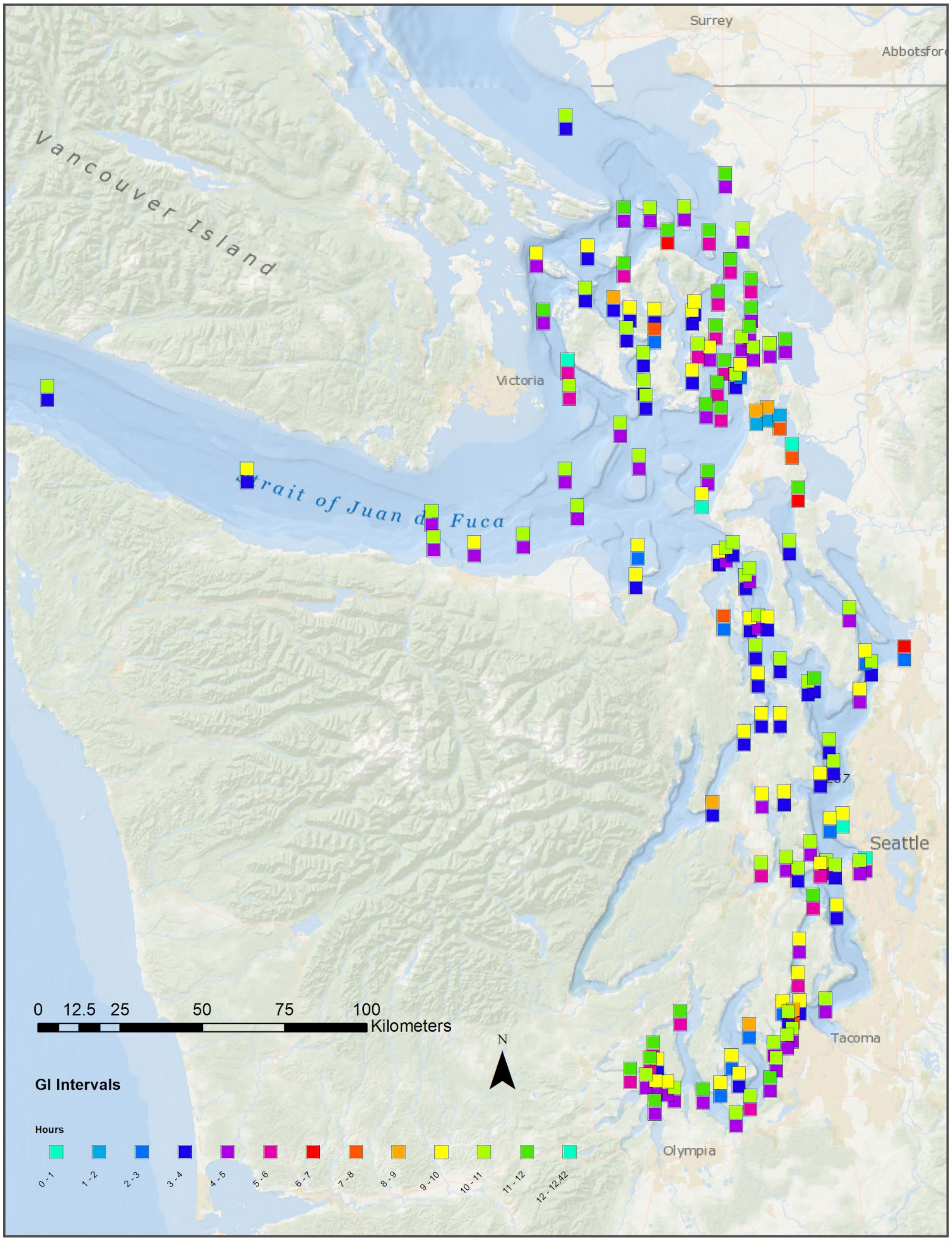

Figure 7-13. GI timing of maximum flood (top) and ebb (bottom) at all stations in the survey. Note that the colors represent hours from 0 to 12.42 with the end interval limits having the same colors to represent the cyclical tides.

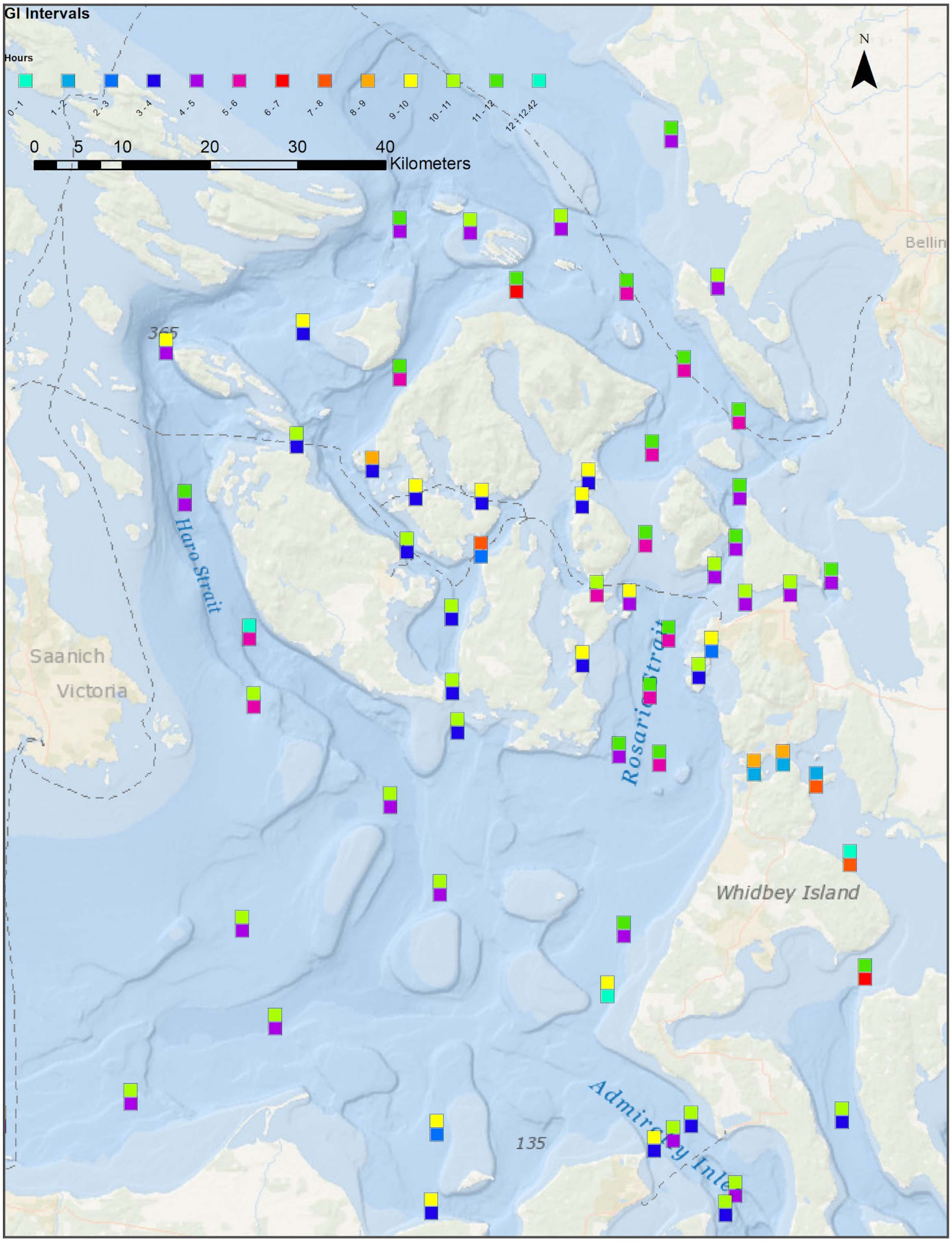

Figure 7-14. GI timing of maximum flood and ebb at stations in the San Juan Islands region of the survey.

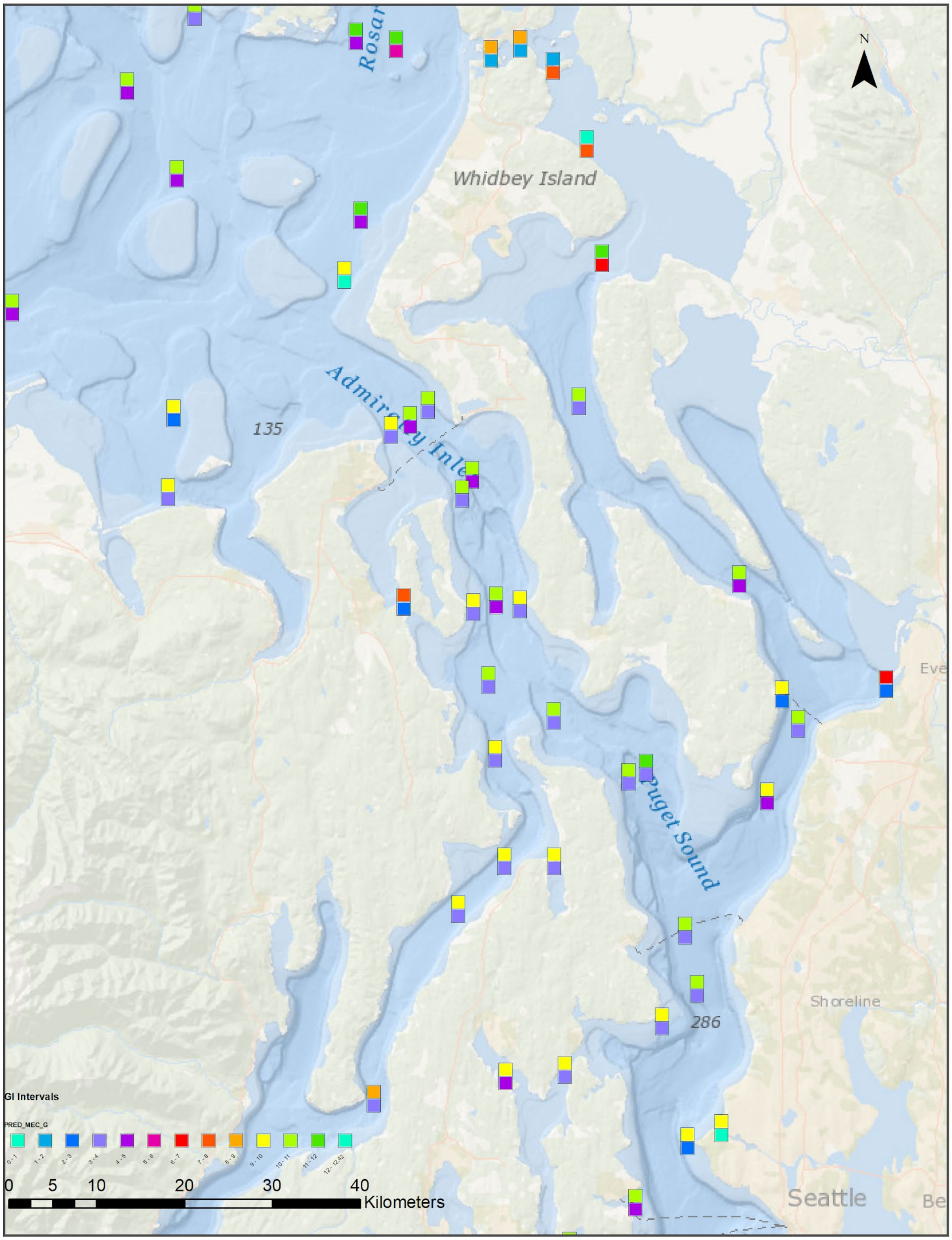

Figure 7-15. GI timing of maximum flood and ebb at stations in the Admiralty Inlet region of the survey. Hood Canal and Puget Sound are to the south.

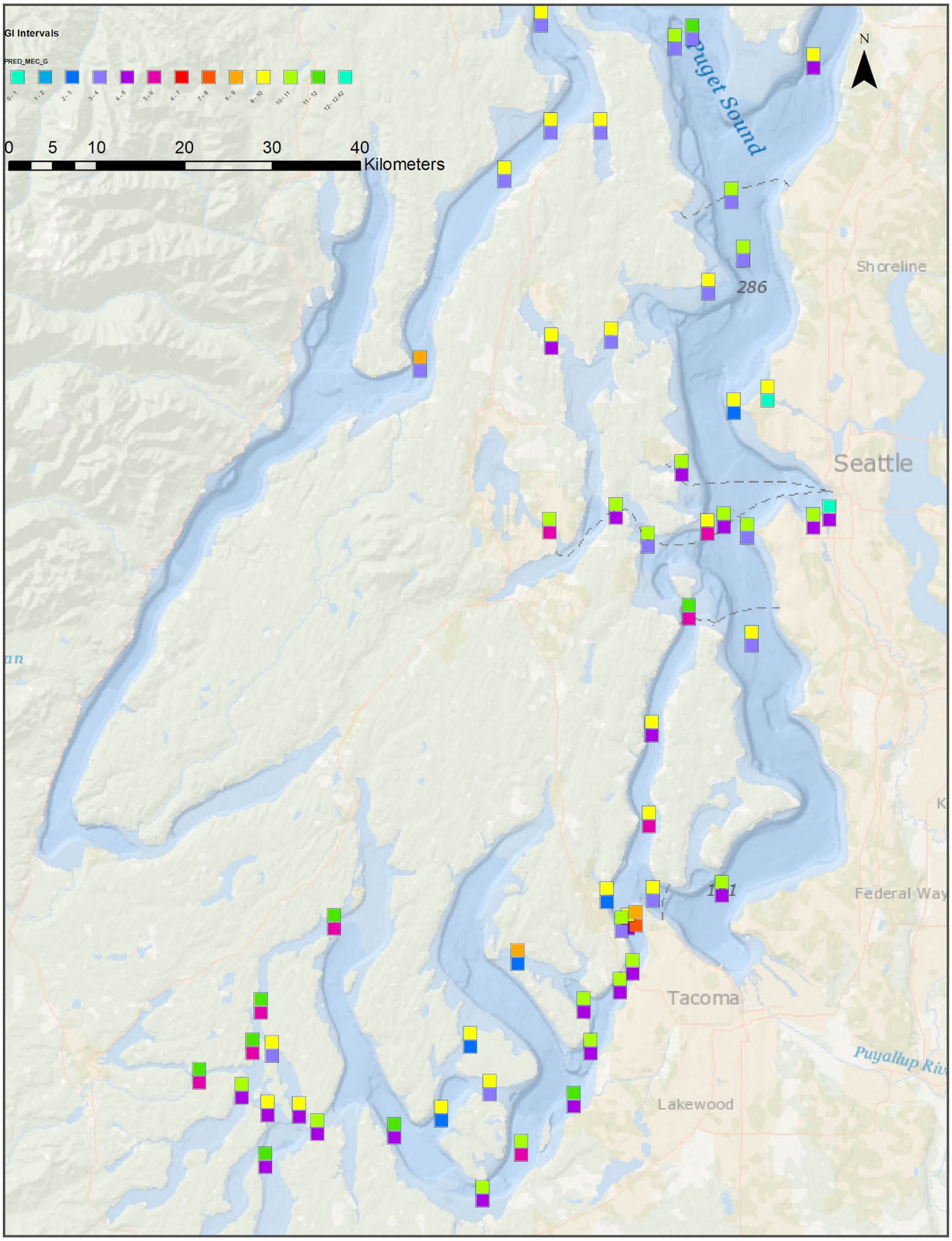

Figure 7-16. GI timing of maximum flood and ebb at stations in the Puget Sound and Hood Canal.

8. SUMMARY

CO-OPS occupied 136 stations from 2015–2017 throughout the Puget Sound and the greater Salish Sea within the state of Washington. In addition to the current data obtained by the ADCPs, CTD profiles were collected during deployment and recovery of the ADCP at each station. Additionally, CTD time series were collected at several stations by mounting a CTD sensor on the mooring chain below the ADCP. Partner-provided hydrophones were attached at two stations.

This current survey resulted in a comprehensive multi-year data set of currents, water temperature, salinity, and pressure observations. The tidal currents data were used to update NOAA tidal current predictions, as well as inform the development of the Salish Sea hydrodynamic model, which help to ensure safe and efficient navigation by improving the accuracy of observations and providing a higher density of predictions in the region.

All analyses and plots for the entire time series at all depths are available in detailed station reports (NOAA, 2019b). Updated tidal current predictions for each station are also available online via the CO-OPS Tides and Currents website. This data set is available to the public and research community by contacting CO-OPS' User Services, at co-ops.userservices@noaa.gov, to further investigate the circulation of this region, and support safe and efficient navigation operations.

9. ACKNOWLEDGMENTS

We would like to thank CO-OPS colleagues Patrick Burke and Greg Dusek for initially leading this project, the Pacific Operations Branch field leads Steve Bassett and Drew Maczko, all the engineers, physical scientists, analysts, and oceanographers who assisted in station planning, the preparation of equipment, in field operations, and in the processing and dissemination of the data. We would especially like to thank Captain John Gannon and the crew of the R/V Harmony for their efforts to make this project successful. Special thanks to Katerina Glebushko for her oversight in the processing of data, Helen Worthington for manuscript editing and Virginia Dentler for final publishing.

10. REFERENCES

Barnes, C.A. and C.C. Ebbesmeyer. (1978), Some aspects of Puget Sound's circulation and water properties. Estuarine Transport Processes. B. Kjerfve (ed). University of South Carolina Press, Columbia, SC. 209-228.

Cannon, G. A., ed. (1978), Circulation in the Strait of Juan de Fuca: Some recent oceanographic observations. NOAA Technical Report. ERL 399-PMEL 29.

Cannon, G.A. (1983), An overview of circulation in the Puget Sound Estuarine System. NOAA Technical Memorandum ERL PMEL-48.

Cannon, G.A., J.R. Holbrook, and D.J. Pahinski (1990), Variations in the onset of bottom-water intrusions over the entrance sill of a fjord. *Estuaries*, 13(1), 31-42.

Cothran, J. (2006), QARTOD: Quality Assurance of Real-Time Oceanographic Data. National Ocean Service.

Cox, J.M., C.C. Ebbesmeyer, C.A. Coomes, J.M. Helseth, L.R. Hinchey, G.A. Cannon, and C.A. Barnes (1984), Sythesis of current measurements in Puget Sound, Washington – Volume 1: Index to current measurements made in Puget Sound from 1908-1980, with daily and record averages for selected measurements. NOAA Technical Memorandum NOS OMS 5.

Defant, Albert (1958), Ebb and Flow The Tides of Earth, Air and Water. University of Michigan Press. Ann Arbor.

Dyer, K.R. (1997), Estuaries: A Physical Introduction. Second Edition. John Wiley and Sons Ltd. West Sussex, England. 195 pp.

Ebbesmeyer, C., and C. Barnes (1980), Control of a Fjord Basins Dynamics by Tidal Mixing in Embracing Sill Zones. Estuarine and Coastal Marine Science, 11, 311-330.

Ebbesmeyer, C.C., Coomes, C.A., Cox, J.M., Helseth, J.M., Hinchey, L.R., Cannon, G.A., and Barnes, C.A. (1984), Sythesis of current measurements in Puget Sound, Washington – Volume 3: Circulation in Puget Sound: An interpretation based on historical records of currents. NOAA Technical Memorandum NOS OMS 5.

Fanelli, P, C Paternostro, G. Dusek, C. Kammerer, J. Park, and A. Carisio (2014), Potential Location Assessment of Coastal and Estuarine Surveys (PLACES). NOAA CO-OPS-NCOP.

Foreman, M.G.G., R.A. Walters, R.F. Henery, C.P. Keller, and A.G Dooling (1995), A tidal model for eastern Juan de Fuca Strait and the southern Strait of Georgia. Journal of Geophysical Research, 100: 721-740.

Holbrook, J.R., R.D. Muench, D.G., Kachel, and C Wright, C. (1980), Circulation in the Strait of Juan de Fuca: Recent oceanographic observations in the eastern basin. NOAA Technical Report. ERL 412-PMEL 33.

Holbrook, J.R., G.A. Cannon, and D. Kachel. (1983), Two-year observations of coastal-estuarine interaction in the Strait of Juan de Fuca. In: Coastal Oceanography, H. Gade, H. Svendsen and A. Edwards (Eds). Plenum Press. New York. 411-426.

Khangaonkar, T., Z. Yang, T. Kim, and Roberts, M. (2011), Tidally averaged circulation in Puget Sound sub-basins: Comparison of historical data, analytical model, and numerical model. Estuarine, Coastal and Shelf Science, 93, 305-319.

Lanerolle, L.W., R. C. Patchen, and F. Aikman (2011), The second generation Chesapeake Bay Operational Forecast System ($CBOFS_2$) Model Development and Skill Assessment: Technical Report, NOAA Technical Report, NOS CS 29.

Lavelle, J.W., H.O. Mofjeld, E. Lempriere-Dogget, G.A. Cannon, D.J. Pahinski, E.D. Cokelet, L. Lyrtle, and S. Gill (1988), A multiply-connected channel model of tides and tidal currents in Puget Sound, Washington and a comparison with updated observations. NOAA Technical Memorandum. ERL PMEL-84.

LeBlond, P.H., K. Dyck, K. Perry, and D. Cumming (1983), Runoff and precipitation time series for the coast of British Columbia and Washington State. DOUBC Man. Rep. 31. University of British Columbia. 133 pp.

Masson, D. (2002), Deep water renewal in the Strait of Georgia. Estuarine, Coastal and Shelf Science, 54, 115-126.

Masson, D. (2006), Seasonal water mass analysis for the straits of Juan de Fuca and Georgia. Atmosphere-Ocean, 44:1, 1-15.

NOAA NOS Center for Operational Oceanographic Products and Services. (2019a). Retrieved from: http://www.tidesandcurrents.noaa.gov

NOAA NOS Center for Operational Oceanographic Products and Services, User Services. (2019b). Retrieved from: https://tidesandcurrents.noaa.gov/contact.html

NOAA (2019c). Tidal Current Tables, Atlantic Coast of North America. Silver Spring, MD: U.S. Department of Commerce.

NOAA (2019d), U.S. Coast Pilot 7, Pacific Coast: California, Oregon, Washington, Hawaii and Pacific Islands, 51st Edition. U.S. Department of Commerce, National Oceanic and Atmospheric Administration, National Ocean Service.

NOAA (2018), NOAA's Contribution to the Economy; Powering America's Economy and Protecting Americans. http://performance.noaa.gov/economics

Parker, B. B. (1977), Tidal hydrodynamics in the Strait of Juan de Fuca - Strait of Georgia. NOAA Technical Report. NOS 69. Rockville, MD: NOAA U.S. Department of Commerce

Parker, B. B. (2007). Tidal Analysis and Prediction Manual. Silver Spring, MD: Center for Operational Oceanographic Products and Services, National Ocean Service, NOAA.

Paternostro, C. L., A. Pruessner, and R Semkiw (2005), Designing a Quality Oceanographic Data Processing Environment. MTS/IEEE Oceans Conference. Washington, D.C.

Pawlowicz, R. (2002) Observations and linear analysis of sill-generated internal tides and estuarine flow in Haro Strait. Journal of Geophysical Research, 107, C6, 3056.

Sutherland, D.A., P. MacCready, N.S. Banas, and L.F Smedstad (2011), A model study of the Salish Sea estuarine circulation. Journal of Physical Oceanography. Vol 41, 1125-1143.

Swanson, R.L. (1974) Variability of Tidal Datums and Accuracy in Determining Datums from Short Series of Observations, NOAA Technical Report 64. Rockville, MD: NOAA U.S. Department of Commerce

Thomson, R.E. (1994), Physical oceanography of the Strait of Georgia-Puget Sound-Juan de Fuca Strait system. In: Review of the Marine Environment and the Biota of the Strait of Georgia, Puget Sound and Juan de Fuca Strait: Proceedings of the BC/Washington Symposium on the Marine Environment, Jan 13-14, 1994. Edited by R.H. Wilson et al.

Thomson, R.E., S.F. Mihaly and E.A Kulikov (2007), Estuarine versus transient flow regimes in Juan de Fuca Strait. Journal of Geophysical Research. Vol 112, C09022.

U.S. Integrated Ocean Observing System, 2019. Manual for Real-Time Quality Control of In-Situ Current Observations Version 2.1: A Guide to Quality Control and Quality Assurance of Acoustic Doppler Current Profiler Observations. 52 pp. https://doi.org/10.25923/sqe9-e310

U.S. Coast Guard (2016), Use of Electronic Charts and Publications in Lieu of Paper Charts, Maps and Publications. COMDTPUB P16700.4 Navigation and Vessel Inspection Circular 01-16, Washington D.C., U.S. Department of Homeland Security

Zervas, C. (1999), Tidal Current Analysis Procedures and Associated Computer Programs. NOAA Technical Memorandum NOS CO-OPS 0021, Silver Spring, MD: NOAA, U.S. Department of Commerce.

APPENDIX A. STATION LISTING

Table A-1. Station location and deployment information. Reference stations are indicated in bold.

Station ID	Station Name	Latitude	Longitude	Depth (m)	Deployment	Recovery
PUG1501	Agate Passage, south end	47.71102	-122.56715	7	7/27/2015	9/9/2015
PUG1502	Alki Point, 1 mile West of	47.58368	-122.45175	233	5/29/2015	9/14/2015
PUG1503	Edmonds, 2.5 miles West of	47.80712	-122.44413	184	5/28/2015	9/11/2015
PUG1504	Entrance to Ballard Locks	47.67098	-122.40700	10	7/28/2015	9/10/2015
PUG1505	Entrance to Eagle Harbor	47.61957	-122.49530	11	7/28/2015	9/10/2015
PUG1506	Harbor Island East	47.58845	-122.34397	15	7/25/2015	9/10/2015
PUG1507	Harbor Island West	47.58313	-122.36022	16	7/25/2015	9/10/2015
PUG1508	Liberty Bay (entrance), Port Orchard	47.70682	-122.62825	13	7/27/2015	9/15/2015
PUG1509	Point Jefferson, East of	47.74447	-122.46802	30	7/27/2015	9/11/2015
PUG1510	Port Washington Narrows, Warren Ave. Bridge	47.57957	-122.63065	7	7/26/2015	9/9/2015
PUG1511	President Point, 1.5 miles east of	47.76712	-122.43190	200	5/29/2015	9/11/2015
PUG1512	Restoration Point	47.57885	-122.46872	53	7/26/2015	9/10/2015
PUG1513	Rich Passage, East end	47.57002	-122.52980	31	7/26/2015	9/9/2015

PUG1514	Rich Passage, West end	47.58993	-122.56233	26	7/26/2015	9/9/2015
PUG1515	West Point, West of	47.66207	-122.44168	44	7/27/2015	9/10/2015
PUG1516	Alki Point, West of	47.57607	-122.42783	91	7/25/2015	9/14/2015
PUG1517	Blake Island, S of	47.52028	-122.48792	82	7/26/2015	9/10/2015
PUG1518	Anderson Point, East of, Colvos Passage	47.43943	-122.52578	115	7/23/2015	9/12/2015
PUG1519	Point Richmond, East of, Colvos Passage	47.37662	-122.52867	106	7/23/2015	9/12/2015
PUG1520	Dolphin Point, 1.3 miles East of	47.50155	-122.42358	183	7/24/2015	9/14/2015
PUG1521	Browns Point, 1.6 miles North of	47.32870	-122.45405	177	5/29/2015	7/23/2015
PUG1522	Dalco Passage	47.32512	-122.52468	71	7/23/2015	9/13/2015
PUG1523	Gig Harbor Entrance	47.32415	-122.57187	19	7/24/2015	9/14/2015
PUG1524	**The Narrows, North end - midstream**	**47.30600**	**-122.55003**	**46**	**5/29/2015**	**9/12/2015**
PUG1525	The Narrows, North End (east side)	47.30778	-122.54213	25	7/24/2015	9/12/2015
PUG1526	The Narrows, North End (west side)	47.30400	-122.55675	77	7/24/2015	9/14/2015
PUG1527	The Narrows, 0.3 miles North of Bridge	47.27432	-122.54532	52	5/29/2015	9/13/2015
PUG1528	The Narrows, South end (midstream)	47.26130	-122.55828	48	7/20/2015	9/13/2015

PUG1529	Hale Passage, East end	47.24790	-122.59560	34	7/20/2015	9/12/2015
PUG1530	Hale Passage, West end	47.28138	-122.66312	21	7/20/2015	9/12/2015
PUG1531	Gibson Point, 0.8 miles East of	47.21913	-122.58867	72	5/29/2015	7/17/2015
PUG1532	Steilacoom, 0.8 miles North of	47.18238	-122.60560	106	5/29/2015	7/17/2015
PUG1533	Ketron Island, West of	47.14860	-122.65940	124	5/30/2015	7/17/2015
PUG1534	Nisqually Reach, 0.5 miles South of Lyle Point	47.11693	-122.69885	62	5/30/2015	7/17/2015
PUG1535	Balch Passage, NE of Eagle Island	47.19062	-122.69155	20	5/30/2015	7/19/2015
PUG1536	Pitt Passage, NE of Pitt Island	47.22383	-122.71137	9	6/3/2015	7/17/2015
PUG1537	Drayton Passage	47.17258	-122.74148	51	5/30/2015	7/17/2015
PUG1538	Devils Head, West of	47.16067	-122.78937	80	5/30/2015	7/17/2015
PUG1539	**Dana Passage**	**47.16310**	**-122.86810**	**37**	**5/31/2015**	**9/13/2015**
PUG1540	Budd Inlet Entrance	47.14016	-122.92145	33	5/31/2015	7/16/2015
PUG1541	Peale Passage, South end	47.17495	-122.88697	14	6/1/2015	7/16/2015
PUG1542	Peale Passage, North end	47.21752	-122.91465	8	6/1/2015	7/15/2015
PUG1543	Squaxin Passage, North of Hunter Point	47.17627	-122.91900	14	6/1/2015	7/15/2015
PUG1544	Totten Inlet Entrance	47.18825	-122.94537	28	6/2/2015	7/15/2015

PUG1545	Libby Point, Hammersley Inlet	47.19892	-122.98900	7	6/2/2015	7/21/2015
PUG1546	Pickering Passage, West of Squaxin Island	47.21928	-122.93452	18	6/2/2015	7/18/2015
PUG1547	Pickering Passage, off Graham Point	47.24725	-122.92592	17	5/31/2015	7/16/2015
PUG1548	Pickering Passage, North end	47.30572	-122.85092	33	5/30/2015	7/16/2015
PUG1601	Hazel Point	47.69124	-122.76279	102	6/16/2016	8/25/2016
PUG1602	South Point	47.82166	-122.67672	65	6/16/2016	8/25/2016
PUG1603	Hood Canal Bridge	47.85474	-122.62942	98	6/17/2016	8/26/2016
PUG1604	Port Gamble Bay Entrance	47.85472	-122.57818	14	6/17/2016	8/26/2016
PUG1605	Possession Sound Entrance	47.89928	-122.36008	206	6/15/2016	8/28/2016
PUG1606	Point No Point, 1.2 miles E of	47.91249	-122.50197	207	6/17/2016	8/28/2016
PUG1607	Point No Point, 2.1 miles E of	47.91888	-122.48413	121	6/17/2016	8/27/2016
PUG1608	**Hood Canal Entrance**	**47.92838**	**-122.63882**	**96**	**4/20/2016**	**8/26/2016**
PUG1609	West of Mukilteo	47.94895	-122.32846	187	6/15/2016	8/27/2016
PUG1610	Foulweather Bluff, 1.9 miles NE of	47.95430	-122.57860	111	4/20/2016	8/26/2016
PUG1611	Olele Point, 1.8 miles ENE of	47.97881	-122.64549	64	6/21/2016	8/25/2016
PUG1612	Clinton Ferry Terminal	47.96899	-122.34507	35	6/15/2016	8/27/2016

PUG1613	Everett	47.97624	-122.23822	92	6/15/2016	8/27/2016
PUG1614	Port Townsend Canal	48.03247	-122.73261	7	6/18/2016	8/23/2016
PUG1615	Nodule Point, 0.5 miles SE of	48.02871	-122.66089	23	6/17/2016	8/20/2016
PUG1616	Admiralty Inlet (off Bush Point)	48.03348	-122.63765	113	4/20/2016	8/20/2016
PUG1617	Bush Point Light, 0.5 mile NW of	48.03084	-122.61334	101	6/18/2016	8/20/2016
PUG1618	Camano Head-Sandy Point, passage	48.04785	-122.38897	150	6/16/2016	8/27/2016
PUG1619	Marrowstone Point, 0.8 miles NE of	48.10633	-122.67247	64	6/18/2016	8/21/2016
PUG1620	Marrowstone Point, 1.65 miles NE of	48.11930	-122.66227	101	6/19/2016	8/20/2016
PUG1622	West of Camano Island	48.16968	-122.55320	88	4/27/2016	6/8/2016
PUG1623	Point Wilson, 0.6 miles NE of	48.15011	-122.74536	62	6/19/2016	8/21/2016
PUG1624	**Point Wilson, 1.6 miles NE of**	**48.15687**	**-122.72603**	**67**	**4/26/2016**	**8/21/2016**
PUG1625	Point Wilson, 2.7 miles NE of	48.16707	-122.70739	63	6/19/2016	8/21/2016
PUG1626	Skagit Bay, 1 mile north of Rocky Point	48.26712	-122.52957	32	4/27/2016	6/8/2016
PUG1627	Skagit Bay, 1 mile south of Goat Island	48.34478	-122.54505	23	4/27/2016	6/8/2016
PUG1628	Skagit Bay channel, SW of Hope Island	48.39783	-122.57955	19	4/27/2016	6/9/2016

PUG1629	Yokeko Point, Deception Pass	48.41272	-122.61317	23	4/27/2016	6/8/2016
PUG1630	Kanem Point, 1.5 miles SW of Protection Island	48.10765	-122.97365	69	4/25/2016	6/20/2016
PUG1631	Violet Point, 3.7 miles NW of Protection Island	48.16140	-122.96810	46	4/25/2016	6/12/2016
PUG1632	Smith Island, 5.5 miles WNW of	48.32455	-122.96475	129	4/26/2016	6/12/2016
PUG1633	Point Partridge, 2.4 miles NW of	48.25562	-122.79303	78	4/26/2016	6/9/2016
PUG1634	Smith Island, 3.4 miles ESE of	48.29638	-122.77632	51	4/26/2016	6/9/2016
PUG1635	New Dungeness Light, 2.8 miles NNW of	48.23348	-123.13343	157	4/25/2016	6/11/2016
PUG1636	Discovery Island, 7.6 miles SSE of	48.30015	-123.16716	115	4/25/2016	6/11/2016
PUG1637	Ediz Hook Light, 5.3 miles ENE of	48.18227	-123.28150	73	4/23/2016	6/9/2016
PUG1638	Ediz Hook Light, 1.2 miles N of	48.16669	-123.41582	92	4/23/2016	6/11/2016
PUG1639	Angeles Pt., 2 miles NNE of	48.17700	-123.52695	29	4/23/2016	6/11/2016
PUG1640	**Race Rocks, 4.5 miles S of**	**48.22320**	**-123.53230**	**150**	**4/23/2016**	**8/24/2016**
PUG1641	Pillar Point, 6 miles NNE of	48.30000	-124.03740	191	4/22/2016	6/10/2016
PUG1642	**Strait of Juan de Fuca Entrance**	**48.44998**	**-124.58380**	**251**	**4/22/2016**	**8/24/2016**

PUG1701	**Deception Pass (Narrows)**	**48.40619**	**-122.64312**	**40**	**4/20/2017**	**9/7/2017**
PUG1702	**Rosario Strait**	**48.45809**	**-122.75007**	**72**	**4/20/2017**	**8/23/2017**
PUG1703	**San Juan Channel, south entrance**	**48.46101**	**-122.95203**	**133**	**4/22/2017**	**8/27/2017**
PUG1704	Peavine Pass, west entrance	48.58708	-122.81926	18	4/19/2017	6/15/2017
PUG1705	Obstruction Pass, north of Obstruction Island	48.60327	-122.81273	20	4/19/2017	6/14/2017
PUG1706	Peapod Rocks Light, 1.2 nmi south of	48.62239	-122.74762	66	4/19/2017	8/25/2017
PUG1707	Sinclair Island, 1.0 nmi NE of	48.64420	-122.65872	74	4/24/2017	6/14/2017
PUG1708	**Lawrence Point, Orcas Island, 1.3 nmi NE of**	**48.67941**	**-122.71467**	**88**	**4/24/2017**	**8/25/2017**
PUG1709	Clark Island, 1.6 nmi north of	48.73126	-122.77338	103	4/24/2017	6/18/2017
PUG1710	Hale Passage, east of Lummi Point	48.73485	-122.68017	20	4/24/2017	6/14/2017
PUG1711	Matia Island, west of	48.77488	-122.84097	131	4/23/2017	6/18/2017
PUG1712	Parker Reef Light, north of	48.73264	-122.88638	70	4/23/2017	6/17/2017
PUG1713	Patos Island, south of Toe Point	48.77206	-122.93370	37	4/23/2017	6/16/2017
PUG1714	Patos Island Light, 1.4 nmi west of	48.77313	-123.00579	137	4/21/2017	6/16/2017
PUG1715	President Channel, East of Point Disney	48.67335	-123.00599	200	4/23/2017	6/16/2017

PUG1716	Waldron Island, 1.7 nmi west of	48.70422	-123.10477	64	4/21/2017	6/16/2017
PUG1717	Turn Point, Boundary Pass	48.69121	-123.24501	143	4/21/2017	6/17/2017
PUG1718	Haro Strait, 1.2 nmiwest of Kellett Bluff	48.58872	-123.22583	267	4/20/2017	6/16/2017
PUG1719	Spieden Channel, north of Limestone Point	48.62783	-123.11165	118	4/23/2017	6/16/2017
PUG1720	Spring Passage, south entrance	48.61154	-123.03410	38	4/22/2017	6/15/2017
PUG1721	Wasp Passage narrows	48.59247	-122.98957	28	4/22/2017	6/15/2017
PUG1722	Harney Channel, north of Point Hudson	48.58972	-122.92173	34	4/22/2017	6/19/2017
PUG1723	Upright Channel narrows	48.55384	-122.92262	52	4/22/2017	6/15/2017
PUG1724	South Haro Strait, south of Lime Kiln Light	48.49797	-123.15990	308	4/20/2017	8/28/2017
PUG1725	Cherry Point, 1.8 nmi southeast of	48.83379	-122.72793	20	6/21/2017	8/25/2017
PUG1726	Strait of Georgia, 4.5 nmi SW of Point Roberts	48.93889	-123.16513	120	4/21/2017	6/17/2017
PUG1727	Point Colville, 3.0 nmi east of (Lawson Reef, 1 nmi NW of)	48.41249	-122.74026	83	6/24/2017	8/23/2017
PUG1728	Point Colville, 1.4 nmi east of	48.41810	-122.78120	68	6/24/2017	8/23/2017
PUG1729	Belle Rock Light, east of	48.49679	-122.73080	57	6/23/2017	8/26/2017

PUG1730	Lopez Pass	48.47974	-122.81891	22	6/24/2017	8/29/2017
PUG1731	Fauntleroy Point Light, east of	48.52158	-122.77066	49	6/23/2017	8/26/2017
PUG1732	Strawberry Island, west of	48.56096	-122.75430	66	6/23/2017	8/25/2017
PUG1733	Thatcher Pass	48.52743	-122.80397	61	6/23/2017	8/26/2017
PUG1734	Guemes Channel, West Entrance	48.52124	-122.65218	18	6/22/2017	8/26/2017
PUG1735	Guemes Channel, East Entrance	48.52769	-122.60601	20	6/24/2017	8/26/2017
PUG1736	Saddle Bag Island Passage	48.53592	-122.56391	85	6/22/2017	8/27/2017
PUG1737	Allan Pass	48.47159	-122.69982	37	6/23/2017	8/29/2017
PUG1738	Burrows Pass	48.48952	-122.68672	31	6/24/2017	8/29/2017
PUG1739	Bellingham Channel South	48.53963	-122.68343	42	6/23/2017	8/25/2017
PUG1740	Bellingham Channel, off Cypress Head Light	48.55854	-122.66176	82	6/23/2017	8/24/2017
PUG1741	Bellingham Channel North	48.59281	-122.65768	70	6/22/2017	8/24/2017
PUG1742	Cattle Point, 1.2 nmi SE of	48.43437	-122.94661	117	6/21/2017	8/27/2017
PUG1743	Cattle Point, 4.6 nmi SW of	48.38401	-123.01567	155	6/20/2017	8/28/2017
PUG1744	Discovery Island, 3.0 nmi NE of	48.45207	-123.15544	143	6/20/2017	8/28/2017
PUG1745	Point George, west of	48.55671	-122.99848	162	6/21/2017	8/27/2017

PUG1746	Pear Point, east of	48.51140	-122.95290	72	6/20/2017	8/27/2017

APPENDIX B. STATION PLATFORM TYPES

Table B-1. Platform and sensor information, including deepest and shallowest measurements and total percent of the water column measured by the ADCP. Stations with unusable pressure sensors are denoted with a dagger (†) symbol.

Station ID	Platform Class	Mount Type	ADCP Freq (kHz)	Platform height (m)	Deep Bin (m)	Shallow bin (m)	MLLW depth (m)	% Water Column
PUG1501	Bottom	TRBM	1200	1	7.7	0.7	10	72%
PUG1502	Deep	DW 49	75	19	195.2	15.2	226	72%
PUG1503	Deep	DW 49	75	19	152.5	16.5	183	57%
PUG1504	SUBS	ES2	600	1	8.8	1.8	12	53%
PUG1505	SUBS	ES2	600	1	9.6	1.6	13	65%
PUG1506	SUBS	ES2	600	1	12.9	1.9	16	71%
PUG1507	SUBS	ES2	600	1	14.5	2.6	18	75%
PUG1508	Bottom	mTRBM	600	1	11.2	2.2	14	62%
PUG1509	SUBS	SUBS A2	300	6	21.6	5.6	32	67%
PUG1510	Bottom	TRBM	1200	1	6.2	1.2	8	75%
PUG1511†	Deep	DW 40	75	18	169.8	21.8	200	77%
PUG1512†	SUBS	SUBS A2 + CTD	300	6	42.7	4.7	53	76%
PUG1513	SUBS	SUBS A2	300	6	21.4	3.4	32	74%
PUG1514	SUBS	SUBS A2	600	6	17.5	3.5	26	57%

PUG1515	SUBS	SUBS A2	300	6	32.8	4.8	43	57%
PUG1516	SUBS	SUBS A2 + B3	300	14	75.5	7.5	96	80%
PUG1517	SUBS	SUBS A2	300	6	73.3	10.3	84	77%
PUG1518	SUBS	SUBS A2 + B3 + CTD	300	27	82.8	10.8	116	72%
PUG1519	SUBS	SUBS A2 + B3	300	19	81.5	9.5	107	67%
PUG1520	Deep	DW 40	75	18	150.5	14.5	181	65%
PUG1521	Deep	DW 40	75	18	140.5	8.5	171	74%
PUG1522	SUBS	SUBS A2	300	6	61.1	7.0	71	76%
PUG1523	Bottom	TRBM	600	1	16.3	2.3	19	71%
PUG1524	SUBS	SUBS A2	300	6	42.4	12.4	53	59%
PUG1525	SUBS	SUBS A2	600	6	17.7	2.7	26	63%
PUG1526	SUBS	SUBS A2	300	6	66.9	6.9	77	54%
PUG1527	SUBS	SUBS A2+CTD	300	6	42.9	4.9	53	70%
PUG1528	SUBS	SUBS A2	300	6	40.0	6.0	51	77%
PUG1529†	SUBS	SUBS A2	300	6	23.5	1.5	34	66%
PUG1530	Bottom	TRBM	600	1	21.2	3.2	24	71%
PUG1531	SUBS	SUBS A2 + Hydrophone	300	6	60.5	9.5	71	78%
PUG1532	SUBS	SUBS A2 + B3 + CTD	300	21	73.9	9.9	101	67%

PUG1533	SUBS	SUBS A2 + B3	300	39	79.5	11.5	125	59%
PUG1534	SUBS	SUBS A2 + CTD	300	6	53.8	8.8	65	65%
PUG1535	Bottom	mTRBM	600	1	18.2	2.2	21	69%
PUG1536	Bottom	mTRBM	1200	1	7.0	1.0	9	74%
PUG1537	SUBS	SUBS A2	300	6	43.8	5.8	54	79%
PUG1538	SUBS	SUBS A2	300	6	70.2	7.2	81	60%
PUG1539	SUBS	SUBS A2 + CTD	600	6	26.9	3.0	36	76%
PUG1540	SUBS	SUBS A2 + Hydrophone	600	6	21.7	3.7	30	78%
PUG1541	SUBS	ES2	600	1	10.8	1.8	14	61%
PUG1542	Bottom	TRBM	1200	1	5.2	0.2	7	44%
PUG1543	Bottom	mTRBM	600	1	9.6	0.6	12	76%
PUG1544	Bottom	TRBM	600	1	24.4	2.4	28	62%
PUG1545	Bottom	mTRBM	1200	1	5.9	1.4	7	64%
PUG1546	Bottom	TRBM	600	1	15.9	1.9	18	75%
PUG1547	Bottom	TRBM	600	1	18.0	2.0	21	76%
PUG1548	SUBS	SUBS A2	600	6	23.7	3.7	33	55%
PUG1601	SUBS	SUBS A2 + B3	300	44	46.8	4.8	95	63%
PUG1602	SUBS	SUBS A2	300	6	54.2	6.2	63	75%

PUG1603	SUBS	SUBS A2	300	24	63.7	6.7	92	69%
PUG1604	Bottom	mTRBM + CTD	600	1	9.9	1.9	13	73%
PUG1605	Deep	DW 40	75	21	174.0	18.0	207	60%
PUG1606	Deep	DW 49	75	21	172.9	16.9	206	78%
PUG1607†	SUBS	SUBS A2	300	44	73.3	7.3	121	55%
PUG1608	SUBS	SUBS A2	300	12	77.7	7.7	93	65%
PUG1609	Deep	DW 40	75	18	158.7	18.7	192	63%
PUG1610	SUBS	SUBS A2 + B3	300	34	70.1	6.1	107	81%
PUG1611	SUBS	SUBS A2	300	6	54.2	6.2	61	58%
PUG1612	SUBS	SUBS A2	600	6	24.3	6.2	33	77%
PUG1613	SUBS	SUBS A2	300	22	63.5	5.5	90	57%
PUG1614	SUBS	ES2	1200	1	4.6	0.5	6	76%
PUG1615	Bottom	TRBM	600	1	19.8	1.7	22	56%
PUG1616	SUBS	SUBS A2 + B3	300	34	68.9	6.9	106	68%
PUG1617	SUBS	SUBS A2	300	8	89.4	11.4	102	60%
PUG1618	SUBS	SUBS A2 + B3	300	53	91.7	7.7	149	74%
PUG1619	SUBS	SUBS A2	300	6	53.9	5.9	63	74%
PUG1620	SUBS	SUBS A2 + B3	300	34	61.9	5.9	100	72%
PUG1622	SUBS	SUBS A2	300	24	58.9	6.9	87	60%

PUG1623†	SUBS	SUBS A2	300	10	49.1	3.1	62	81%
PUG1624	SUBS	SUBS A2 + CTD	300	9	52.4	4.4	64	74%
PUG1625	SUBS	SUBS A2 + CTD & DO	300	10	50.0	5.0	63	39%
PUG1626	SUBS	SUBS A2	300	6	22.6	3.6	32	77%
PUG1627	Bottom	mTRBM	600	1	19.8	1.7	22	72%
PUG1628	Bottom	TRBM	600	1	14.9	1.9	18	62%
PUG1629	SUBS	SUBS A2	600	8	10.1	2.1	21	77%
PUG1630	SUBS	SUBS A2	300	6	58.7	6.7	68	74%
PUG1631†	SUBS	SUBS A2	300	6	37.1	4.1	46	74%
PUG1632†	SUBS	SUBS A2	300	32	93.1	13.0	129	60%
PUG1633	SUBS	SUBS A2	300	6	67.6	7.6	77	77%
PUG1634	SUBS	SUBS A2	300	6	41.0	4.0	50	73%
PUG1635	Deep	DW 49	75	18	129.8	13.7	158	57%
PUG1636	SUBS	SUBS A2	300	35	74.5	6.5	113	68%
PUG1637	SUBS	SUBS A2	300	6	62.6	6.6	72	79%
PUG1638	SUBS	SUBS A2	300	12	73.9	8.0	91	78%
PUG1639	SUBS	SUBS A2 + CTD	600	8	18.6	2.6	28	83%
PUG1640	Deep	DW 40 + CTD	300	21	120.2	18.2	149	69%

PUG1641	Deep	DW 40	75	18	160.4	12.4	188	63%
PUG1642†	Deep	DW 49	75	21	223.0	27.0	251	75%
PUG1701	Bottom	TRBM	600	1	37.4	4.4	40	73%
PUG1702	SUBS	SUBS A2	300	6	59.3	11.3	70	63%
PUG1703	Deep	DW 49	75	19	103.0	18.0	134	78%
PUG1704	Bottom	TRBM	600	1	14.7	1.6	17	69%
PUG1705	SUBS	ES2	600	1	16.4	2.4	19	65%
PUG1706	SUBS	SUBS A2	300	6	51.8	11.8	64	73%
PUG1707	SUBS	SUBS A2	300	6	62.0	6.0	72	82%
PUG1708	SUBS	SUBS A2	300	9	71.2	11.2	87	74%
PUG1709	SUBS	SUBS A2 + B3	300	24	72.7	6.7	101	70%
PUG1710	Bottom	TRBM	600	1	15.3	2.3	18	80%
PUG1711	SUBS	SUBS A2	300	6	114.4	10.4	126	76%
PUG1712	SUBS	SUBS A2	300	6	57.5	7.6	67	69%
PUG1713	SUBS	SUBS A2	600	6	28.1	3.1	36	61%
PUG1714	SUBS	SUBS A2	300	6	118.1	14.1	130	65%
PUG1715	Deep	DW 40	75	18	169.0	17.0	199	80%
PUG1716†	SUBS	SUBS A2 + CTD	300	7	52.3	8.3	64	61%
PUG1717	SUBS	SUBS A2 + B3	300	46	171.2	35.2	223	50%

PUG1718	Deep	DW 40	75	18	230.2	20.2	262	71%
PUG1719[†]	SUBS	SUBS A2 + B3 + B3	300	25	86.4	14.4	118	59%
PUG1720	SUBS	SUBS A2	600	6	29.0	3.0	37	83%
PUG1721	SUBS	SUBS A2	600	6	19.4	3.4	27	66%
PUG1722	Bottom	mTRBM	600	1	30.0	3.0	33	78%
PUG1723	SUBS	SUBS A2	300	6	41.5	7.4	51	76%
PUG1724[†]	Deep	DW 49 + CTD	75	20	272.6	32.6	308	60%
PUG1725	Bottom	mTRBM	600	1	16.9	2.4	19	74%
PUG1726	SUBS	SUBS A2 + B3 + CTD	300	36	77.4	7.5	117	76%
PUG1727	SUBS	SUBS A2 + B3 + CTD	300	9	68.3	8.3	81	74%
PUG1728	SUBS	SUBS A2	300	6	58.9	6.9	69	76%
PUG1729[†]	SUBS	SUBS A2	300	6	47.0	5.0	57	68%
PUG1730	SUBS	ES2	600	1	20.7	2.7	24	74%
PUG1731	SUBS	SUBS A2	300	6	40.3	6.3	50	73%
PUG1732	SUBS	SUBS A2	300	6	58.1	8.1	68	69%
PUG1733	SUBS	SUBS A2	300	6	50.5	6.5	60	71%
PUG1734	Bottom	TRBM	600	1	16.3	3.3	19	80%
PUG1735	Bottom	TRBM	600	1	15.7	2.7	18	69%

PUG1736	SUBS	SUBS A2	300	6	72.5	6.6	82	84%
PUG1737	SUBS	SUBS A2	600	6	28.3	3.3	36	73%
PUG1738	Bottom	TRBM	600	1	30.6	2.6	33	77%
PUG1739	SUBS	SUBS A2	600	6	35.9	3.9	44	77%
PUG1740	SUBS	SUBS A2	300	6	63.3	6.3	74	59%
PUG1741†	SUBS	SUBS A2	300	6	60.2	6.2	70	70%
PUG1742	SUBS	SUBS A2 + B3	300	23	91.8	7.8	121	33%
PUG1743	Deep	DW 40	75	15	61.9	11.9	150	74%
PUG1744	Deep	DW 40	300	39	96.6	12.6	142	59%
PUG1745	Deep	DW 40	75	15	131.1	16.1	159	72%
PUG1746	SUBS	SUBS A2 + B3 + CTD	300	20	46.0	6.0	73	55%

APPENDIX C. STATION HARMONICS

Table C-1. Amplitudes for the four major harmonic constituents (M_2, S_2, K_1, and O_1) for both major and minor axes. Amplitudes are in cm/s. The Defant ratio ($K_1 + O_1 / M_2 + S_2$) is shown for the major axes in the last column. Stations that do not appear in this table were not harmonic, i.e., the error or uncertainty values for the least squares harmonic analysis were too large. These stations are discussed in the text.

Station ID	Depth (m)	M_2 major	M_2 minor	S_2 Major	S_2 Minor	K_1 Major	K_1 Minor	O_1 Major	O_1 Minor	Defant Ratio
PUG1501	2.7	118.99	1.95	24.74	0.57	38.79	1.03	20.99	1.49	0.42
PUG1502	23.2	17.90	1.95	3.96	0.62	7.00	1.95	4.68	0.67	0.53
PUG1503	20.5	15.43	3.91	5.61	0.82	11.42	1.23	7.10	0.51	0.88
PUG1504	2.8	2.62	0.15	0.98	0.10	2.57	0.15	0.93	0.15	0.97
PUG1505	2.6	8.49	0.72	1.95	0.10	3.40	0.31	1.59	0.46	0.48
PUG1506	1.9	6.69	0.31	1.23	0.10	2.16	0.21	2.16	0.10	0.55
PUG1507	2.6	12.50	0.31	4.06	0.51	5.66	0.62	4.63	0.21	0.62
PUG1508	2.2	36.78	0.36	8.39	0.15	14.15	1.03	7.67	1.95	0.48
PUG1509	5.6	41.93	1.95	6.74	0.57	9.88	2.93	6.22	0.62	0.33
PUG1510	6.2	96.82	0.62	20.58	1.13	39.20	1.44	23.20	0.62	0.53
PUG1511	21.8	16.77	2.98	4.48	0.36	8.49	1.85	3.76	1.18	0.58
PUG1512	6.7	24.02	8.90	5.76	2.21	13.58	6.33	6.74	7.00	0.68
PUG1513	3.4	32.10	7.72	7.67	1.59	11.27	1.59	7.51	1.03	0.47
PUG1514	3.5	112.46	1.03	23.82	1.03	44.91	2.78	26.18	2.68	0.52

PUG1515	4.8	26.60	3.50	4.99	2.57	8.49	2.06	7.46	0.46	0.50
PUG1516	11.5	23.56	0.57	7.51	0.62	11.27	1.54	3.45	3.29	0.47
PUG1517	13.3	32.31	1.54	8.18	1.90	14.15	3.91	7.61	4.89	0.54
PUG1518	10.8	27.21	0.15	5.25	1.34	6.94	0.57	4.73	1.13	0.36
PUG1519	13.5	24.59	6.58	6.69	1.34	14.71	3.24	7.36	2.78	0.71
PUG1520	14.5	19.96	2.26	5.09	1.23	4.99	1.29	1.85	1.44	0.27
PUG1521	8.5	15.84	0.62	4.89	0.82	3.96	2.26	2.93	2.16	0.33
PUG1522	39.0	32.72	3.40	4.73	1.49	11.57	3.34	10.75	2.88	0.60
PUG1523	3.3	27.06	2.16	7.15	0.26	10.34	0.05	6.38	0.72	0.49
PUG1524	12.4	130.00	2.52	30.81	2.26	43.47	4.73	18.42	3.60	0.38
PUG1525	3.7	50.83	3.04	9.62	0.72	20.89	1.54	21.40	0.77	0.70
PUG1526	12.9	94.45	5.20	22.94	1.70	29.48	1.95	22.48	2.68	0.44
PUG1527	6.9	186.69	9.57	43.21	2.37	60.09	4.68	30.61	9.57	0.39
PUG1528	8.0	172.95	5.09	40.28	2.21	53.91	4.42	28.91	5.14	0.39
PUG1529	3.5	31.02	2.16	5.25	1.59	7.41	3.60	2.01	4.06	0.26
PUG1530	4.2	56.69	4.12	11.99	1.08	6.89	1.44	5.04	0.93	0.17
PUG1531	9.5	99.90	8.49	22.69	3.19	32.62	1.85	13.84	6.53	0.38
PUG1532	13.9	11.37	0.72	3.09	1.08	6.84	1.90	4.48	1.18	0.78
PUG1533	11.5	14.10	1.44	5.56	0.67	10.75	1.54	3.76	1.34	0.74

PUG1534	8.8	63.74	2.62	13.48	3.04	23.66	1.59	10.80	0.82	0.45
PUG1535	3.2	93.06	3.45	20.47	0.31	22.74	0.15	8.95	0.72	0.28
PUG1536	2.0	53.24	1.44	10.39	0.26	8.95	0.26	3.14	0.67	0.19
PUG1537	5.8	18.83	5.61	4.84	1.03	2.57	1.18	0.62	2.26	0.13
PUG1538	7.2	17.08	3.81	4.48	0.57	8.08	1.29	3.40	1.39	0.53
PUG1539	4.9	89.62	2.73	19.55	0.98	26.13	2.06	13.79	3.09	0.37
PUG1540	3.7	17.34	3.60	4.17	0.87	10.13	1.85	7.00	2.68	0.80
PUG1541	2.8	21.50	0.87	4.48	0.51	4.42	0.41	2.57	0.67	0.27
PUG1542	5.2	19.09	1.44	3.65	0.31	3.40	0.72	1.39	0.36	0.21
PUG1543	5.6	67.85	0.87	12.66	0.31	17.34	1.03	9.93	1.08	0.34
PUG1544	4.4	56.59	1.23	12.30	0.36	18.06	2.73	9.93	3.04	0.41
PUG1545	5.9	97.43	1.29	21.19	0.21	28.29	1.03	17.18	0.72	0.38
PUG1546	2.9	74.13	0.67	18.01	1.29	25.62	0.57	12.14	4.01	0.41
PUG1547	3.0	66.57	1.80	16.87	0.77	25.98	0.67	13.22	1.23	0.47
PUG1548	5.7	27.63	1.49	7.20	1.08	13.32	1.95	6.22	3.70	0.56
PUG1601	6.9	30.09	2.16	5.40	1.08	8.44	0.51	6.58	1.85	0.42
PUG1602	7.2	39.97	0.46	8.23	1.03	15.07	2.68	7.36	2.52	0.47
PUG1603	6.7	36.53	0.36	9.05	0.41	16.77	0.62	10.85	1.18	0.61
PUG1604	2.9	38.63	0.41	8.54	0.36	16.93	0.82	10.49	0.26	0.58

PUG1605	22.0	17.03	1.85	5.04	0.62	7.25	0.46	3.34	0.72	0.48
PUG1606	20.9	46.09	1.95	10.19	1.03	17.70	1.59	7.20	2.26	0.44
PUG1607	9.3	39.05	15.59	8.54	7.87	21.30	6.38	19.60	6.94	0.86
PUG1608	9.7	38.38	1.59	7.61	0.82	16.77	0.67	10.70	1.85	0.60
PUG1609	18.7	15.38	0.57	3.86	0.41	7.92	0.72	5.71	0.36	0.71
PUG1610	6.1	79.33	1.08	20.63	1.54	33.23	3.70	15.12	3.24	0.48
PUG1611	6.2	46.51	1.03	9.72	4.78	20.27	3.70	9.52	8.18	0.53
PUG1612	6.2	11.57	0.93	3.24	0.67	5.50	1.08	2.98	0.36	0.57
PUG1613	7.5	3.96	1.34	0.57	0.41	1.18	1.23	0.57	0.98	0.39
PUG1614	4.6	126.71	0.93	26.91	1.08	15.12	1.34	7.61	1.08	0.15
PUG1615	2.7	95.38	8.13	21.86	1.59	35.44	3.34	19.50	3.91	0.47
PUG1616	8.8	101.55	8.08	27.06	4.84	43.68	8.85	21.40	7.56	0.51
PUG1617	13.4	114.51	5.92	25.31	3.81	40.43	2.52	26.34	11.06	0.48
PUG1618	9.7	20.94	0.72	4.27	0.57	8.59	0.93	4.12	1.18	0.50
PUG1619	9.0	140.75	15.69	30.56	6.02	57.87	8.03	33.95	14.61	0.54
PUG1620	7.9	125.32	3.86	33.39	4.48	59.52	3.81	35.19	2.31	0.60
PUG1622	6.9	12.60	1.34	3.96	1.29	5.25	0.31	1.54	1.13	0.41
PUG1623	5.1	109.63	6.89	28.40	0.31	35.03	1.80	16.05	6.94	0.37
PUG1624	6.4	153.41	2.83	37.09	2.52	63.69	3.76	34.11	3.50	0.51

PUG1625	6.0	148.11	4.68	31.84	3.34	53.45	2.57	34.31	6.38	0.49
PUG1626	3.6	20.53	0.82	4.78	1.54	16.82	2.42	5.14	0.93	0.87
PUG1627	3.7	78.86	0.36	12.35	0.36	22.48	0.77	11.16	0.36	0.37
PUG1628	2.9	91.21	2.47	12.40	1.13	15.28	1.13	9.52	1.39	0.24
PUG1629	4.1	126.76	0.36	21.45	1.03	24.95	1.03	11.11	1.49	0.24
PUG1630	6.7	45.79	7.15	9.36	3.09	15.90	1.80	14.61	6.58	0.55
PUG1631	5.1	33.23	8.18	2.26	5.76	6.69	4.01	8.08	5.09	0.42
PUG1632	13.0	43.83	13.53	7.61	3.04	19.45	5.25	12.40	3.24	0.62
PUG1633	7.6	10.96	7.67	1.95	1.85	4.48	3.14	1.80	2.93	0.49
PUG1634	6.0	19.14	1.08	4.58	4.17	13.27	5.50	3.86	4.94	0.72
PUG1635	15.8	42.08	4.06	11.11	1.44	25.62	3.29	15.79	4.42	0.78
PUG1636	8.4	37.45	7.00	10.91	1.54	28.29	2.16	13.22	1.13	0.86
PUG1637	6.6	70.22	2.73	17.59	2.42	41.46	3.04	16.31	2.06	0.66
PUG1638	10.9	51.03	4.89	12.45	6.38	25.93	2.42	13.48	5.14	0.62
PUG1639	3.6	81.13	3.14	15.64	7.67	51.29	12.81	38.94	16.41	0.93
PUG1640	18.2	64.15	5.50	14.15	3.40	36.32	5.71	19.09	8.90	0.71
PUG1641	12.4	33.80	5.61	6.48	1.13	18.26	1.85	16.26	2.16	0.86
PUG1642	31.0	44.60	4.58	9.93	1.44	25.62	2.57	10.60	1.03	0.66
PUG1701	5.4	268.02	0.62	49.59	3.24	54.02	6.89	16.15	4.84	0.22

PUG1702	14.3	84.01	4.48	22.89	2.42	63.43	3.50	32.56	4.89	0.90
PUG1703	23.0	146.46	3.60	27.37	0.98	64.00	3.14	40.28	0.15	0.60
PUG1704	5.6	100.88	1.80	20.58	0.67	44.86	0.67	16.41	1.39	0.50
PUG1705	4.4	67.49	2.01	12.40	1.34	31.28	1.03	13.22	2.52	0.56
PUG1706	11.8	85.91	2.21	24.08	1.65	61.53	1.54	33.75	7.36	0.87
PUG1707	8.0	25.77	4.99	8.64	2.01	15.59	2.62	5.09	5.04	0.60
PUG1708	11.2	59.11	2.16	16.46	1.29	44.09	4.42	28.40	7.25	0.96
PUG1709	8.7	44.81	5.61	9.26	1.23	27.27	5.40	27.52	6.64	1.01
PUG1710	2.3	53.96	2.26	15.64	0.31	28.45	0.67	21.30	1.70	0.71
PUG1711	14.4	36.22	3.04	11.32	0.93	17.95	5.25	11.42	3.60	0.62
PUG1712	9.6	54.38	0.93	13.02	1.70	41.52	2.83	24.23	0.98	0.98
PUG1713	4.1	67.75	9.93	11.16	7.05	35.96	13.58	17.34	18.01	0.68
PUG1714	14.1	76.75	3.86	20.53	3.76	38.38	2.26	19.86	5.81	0.60
PUG1715	21.0	58.34	0.31	14.97	1.70	33.49	1.85	19.03	2.42	0.72
PUG1716	8.3	52.37	16.51	18.57	3.60	8.03	13.74	7.25	7.82	0.22
PUG1717	35.2	83.85	7.20	22.17	3.14	39.66	3.14	36.83	8.75	0.72
PUG1718	20.2	45.53	6.07	9.93	0.77	34.72	3.50	28.35	2.31	1.14
PUG1719	14.4	107.93	0.87	29.48	5.25	38.07	7.25	21.56	8.08	0.43
PUG1720	4.0	47.48	4.53	9.67	1.49	10.44	2.73	2.31	1.23	0.22

PUG1721	3.4	86.53	0.62	17.75	2.52	36.32	3.76	21.09	2.31	0.55
PUG1722	4.0	48.77	0.10	9.98	0.72	23.61	0.98	12.96	0.05	0.62
PUG1723	7.4	60.45	1.75	19.60	1.54	16.41	3.50	14.30	2.01	0.38
PUG1724	32.6	54.22	8.49	10.70	2.98	47.59	2.57	18.42	4.17	1.02
PUG1725	2.4	25.88	1.29	4.78	1.23	15.54	1.54	13.43	1.65	0.94
PUG1726	9.4	37.61	4.73	7.46	1.29	13.22	7.36	7.51	3.24	0.46
PUG1727	10.3	54.84	2.78	15.33	1.34	41.31	7.20	23.72	7.51	0.93
PUG1728	8.9	81.85	8.18	22.74	0.46	56.85	6.28	34.88	4.17	0.88
PUG1729	6.9	94.55	4.68	24.18	2.16	68.16	2.06	38.43	10.29	0.90
PUG1730	4.7	109.37	2.62	25.10	1.03	45.63	2.73	21.56	5.56	0.50
PUG1731	6.3	58.59	9.52	10.44	2.37	26.65	6.22	3.24	4.99	0.43
PUG1732	10.1	113.74	4.32	30.20	3.29	74.90	1.54	41.41	4.78	0.81
PUG1733	8.5	38.69	0.51	10.44	1.85	25.31	3.91	14.61	4.94	0.81
PUG1734	3.3	95.99	2.73	21.76	2.47	51.34	5.25	24.90	7.46	0.65
PUG1735	2.7	95.22	2.88	23.46	1.08	54.12	3.19	28.45	3.40	0.70
PUG1736	6.6	25.82	3.34	6.94	1.59	15.69	0.98	7.61	2.11	0.71
PUG1737	3.3	60.40	2.26	14.61	0.72	28.50	4.48	32.51	6.53	0.81
PUG1738	4.6	78.45	1.49	20.42	2.88	35.03	2.26	35.19	0.51	0.71
PUG1739	5.9	114.05	6.22	26.80	0.87	80.87	6.48	49.64	10.49	0.93

PUG1740	9.3	112.56	4.12	31.02	1.29	73.82	1.65	44.65	6.28	0.83
PUG1741	8.2	82.72	8.08	21.50	3.76	49.33	6.74	30.30	14.82	0.76
PUG1742	11.8	105.00	5.40	18.88	0.67	40.07	6.02	19.70	8.18	0.48
PUG1743	16.9	36.27	9.05	8.54	0.93	21.92	2.52	12.55	4.53	0.77
PUG1744	12.6	71.76	4.94	19.91	0.93	50.52	14.46	32.10	26.75	0.90
PUG1745	16.1	56.85	4.01	11.16	0.77	17.65	2.83	14.10	2.62	0.47
PUG1746	10.0	55.97	8.03	13.12	1.23	25.93	8.95	13.99	5.81	0.58

APPENDIX D. SAMPLE MOORING DIAGRAMS

Mooring diagrams and checklists for all mooring types are used in the field to assure the moorings are built correctly and to record the necessary metadata, including serial numbers for instruments, pingers, platforms, and releases. Additional metadata recorded on these checklists include lengths of all lines used and parts lists of components.

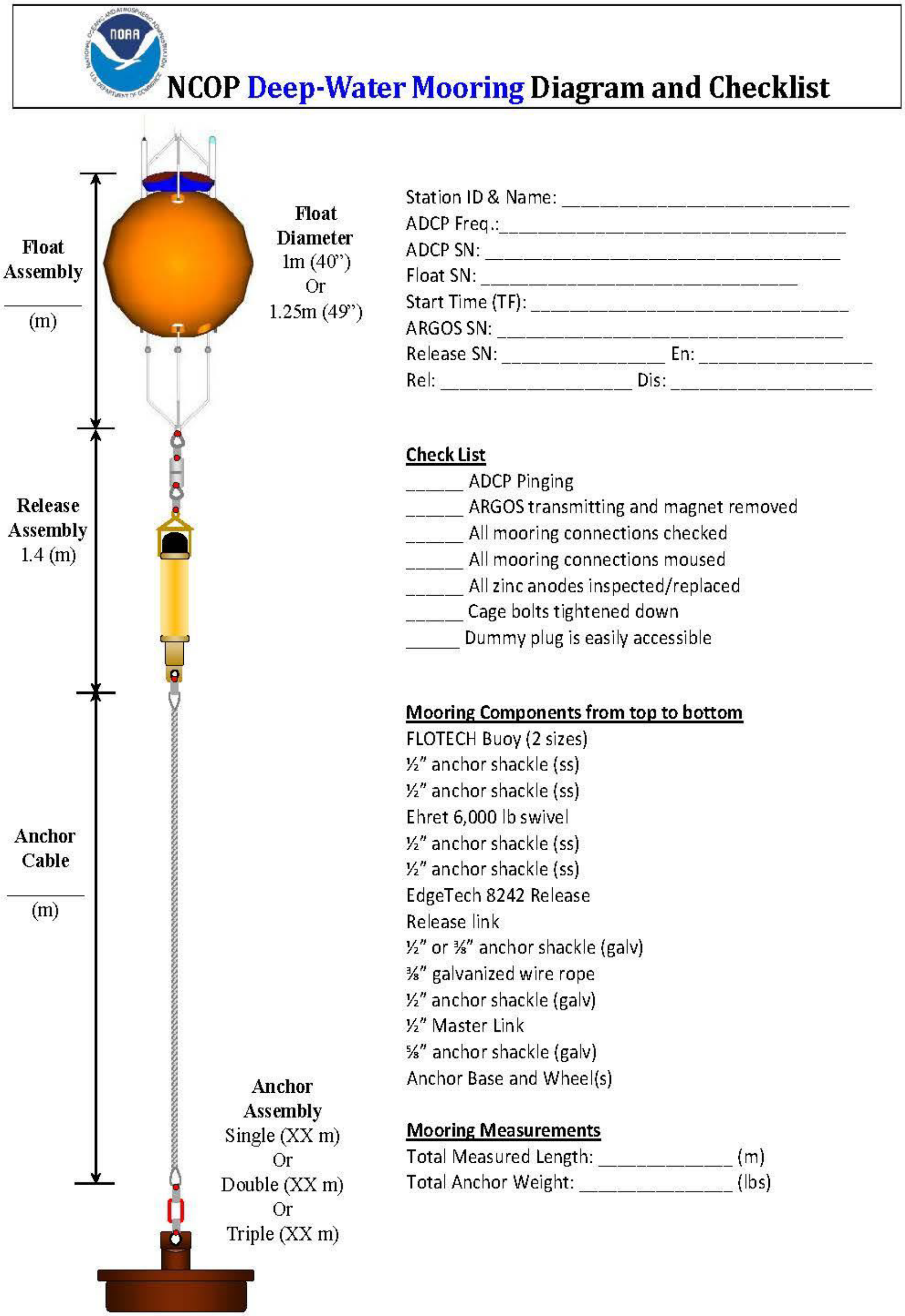

Figure D-1. Mooring diagram and checklist for a deep water mooring.

NCOP Single SUBS Mooring Diagram and Checklist

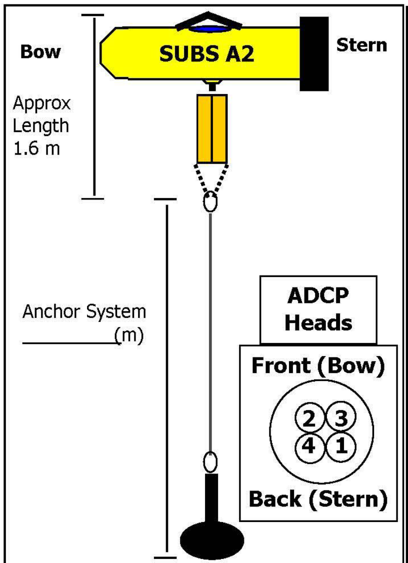

Total Measured Length ________(m)
Anchor Weight _______________(lbs)

Approx Total Length = 5.5 m
Approx Total Weight = 170 lbs
Approx Total Buoyancy = 140 lbs

Station ID & Name:_______________________________
ADCP Freq. & S/N: _______________________________
Start time (TF):_______________________________
ARGOS S/N:_______________________________
SUBS A2:_______________________________
CART1: S/N:__________ **En:**_______**Dis:**_________ **Rel:**__________
CART2: S/N:__________ **En:**_______**Dis:**_________ **Rel:**__________

Check List

- _____ADCP Pinging
- _____ADCP heads match diagram (left)
- _____Argos transmitting & magnet removed
- _____All mooring connections checked
- _____All zinc anodes inspected/replaced

Mooring Components from top to bottom—Single SUBS

SUBS A2 (Modified with Foam: Y/N)	1
Small Pin SS Bow Shackle (more info needed)	1
3/8″ SS HD Swivel shackle	1
CARTs in Tandem (set of 2)	1
CART Release link	2
5/16″ Galvanized bolt pin shackles	2
5/16″ Galvanized chain	1
1/2″ x 6″ Master Link	1
5/16″ Galvanized Cable with thimble end	1
7/16″ bolt pin anchor shackle	1
1/2″ x >3″ Galvanized Master Link (for crane hook)	1
5/8″ bolt pin anchor shackle	1
Anchor base/spindle	1
Railroad wheel/anchor	1

Figure D-2. Mooring diagram and checklist for a single SUBS mooring.

NCOP Double SUBS Mooring Diagram and Checklist

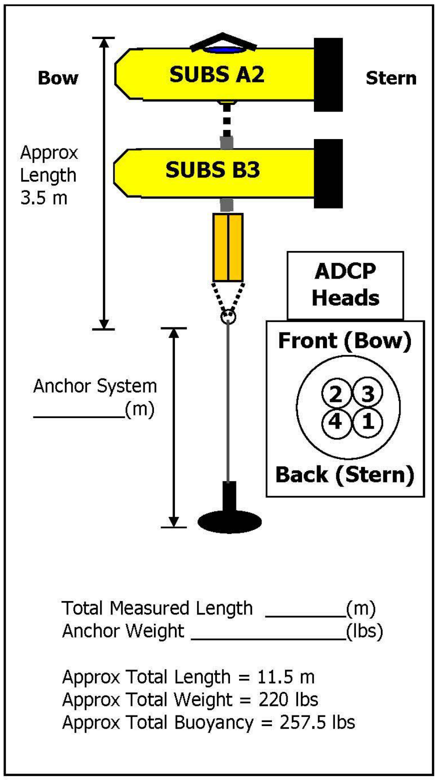

Station ID & Name:______________________________
ADCP Freq. & S/N: ______________________________
Start time (TF):______________________________
ARGOS S/N:______________________________
SUBS A2:________________**SUBS B3:**________________
CART1: S/N:__________ **En:**_______**Dis:**_________ **Rel:**__________
CART2: S/N:__________ **En:**_______**Dis:**_________ **Rel:**__________

Check List

_____ADCP Pinging
_____ADCP heads match diagram (left)
_____Argos transmitting & magnet removed
_____All mooring connections checked
_____All zinc anodes inspected/replaced

Mooring components from top to bottom– Double SUBS

SUBS A2	1
3/8″ SS HD Swivel	1
3/8″ SS 316 chain (1.5m)	1
5/16″ SS Bow Shackle	1
SUBS B3	1
5/16″ SS Bow Shackle	1
3/8″ SS HD Swivel shackle	1
CARTs in Tandem (set of 2)	1
CART Release link	2
5/16″ Galvanized bolt pin shackles	2
5/16″ Galvanized chain	1
1/2″ x 6″ Master Link	1
5/16″ Galvanized Cable with thimble end	1
7/16″ bolt pin anchor shackle	1
1/2″ x >3″ Galvanized Master Link (for crane hook)	1
5/8″ bolt pin anchor shackle	1
Anchor base/spindle	1
Railroad wheel/anchor	1

Figure D-3. Mooring diagram and checklist for a double SUBS mooring.

NCOP Triple SUBS Mooring Diagram and Checklist

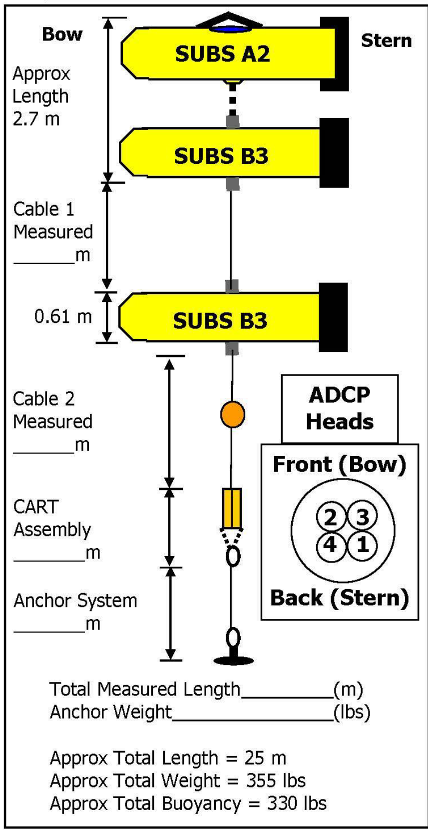

Station ID & Name:______________________________
ADCP Freq. & S/N: ______________________________
Start time (TF):______________________________
ARGOS S/N:______________________________
SUBS A2:__________**SUBS B3:**__________**SUBS B3:**__________
CART1: S/N:__________ **En:**________**Dis:**_________ **Rel:**__________
CART2: S/N:__________ **En:**________**Dis:**_________ **Rel:**__________

Check List

_____ADCP Pinging
_____ADCP heads match diagram (left)
_____Argos transmitting & magnet removed
_____All mooring connections checked
_____All zinc anodes inspected/replaced

Mooring Components from top to bottom—Triple SUBS

SUBS A2	1
3/8″ SS HD Swivel	1
3/8″ SS 316 chain (1.5m)	1
5/16″ SS Bow Shackle	1
SUBS B3	1
5/16″ SS Bow Shackle	1
1/4″ galv wire (Cable 1) approx m	1
5/16″ SS Bow Shackle	2
SUBS B3	1
5/16″ SS Bow Shackle	1
1/4″ galv wire (Cable 2) approx m	1
14″ Trawl Float—crimped in wire	1
3/8″ SS HD Swivel shackle	1
CARTs in Tandem (set of 2)	1
CART Release link	2
5/16″ Galvanized bolt pin shackles	2
5/16″ Galvanized chain	1
1/2″ x 6″ Master Link	1
5/16″ Galvanized Cable with thimble end	1
7/16″ bolt pin anchor shackle	1
1/2″ x >3″ Galvanized Master Link (for crane hook)	1
5/8″ bolt pin anchor shackle	1
Anchor base/spindle	1
Railroad wheel/anchor	1

Figure D-4. Mooring diagram and checklist for a Triple SUBS mooring.

NCOP TRBM Mooring Diagram and Checklist

Station ID & Name:____________________________
ADCP Freq.:__________________________________
ADCP SN:____________________________________
Start Time (TF):_______________________________
Bottom Mount Name:__________________________
Dive Locator SN:_________________Ch:___________
Release SN:_____________________ En: __________________
Rel:_____________________ Dis:__________________

Check List

______ ADCP Pinging
______ Dummy Plug is present
______ Float line bundled and under bungee cords
______ Float line attached to base and cage
______ Release secured to strongback
______ Release armed
______Dive Locator attached to base
______Float Fibrebolts tightened
______Gimbal properly oriented and secured to float
______ ADCP secured in Gimbal and has free movement
______ All mooring connections checked
______ All mooring connections moused
______ All zinc anodes inspected/replaced
______ Anchor line attached to base

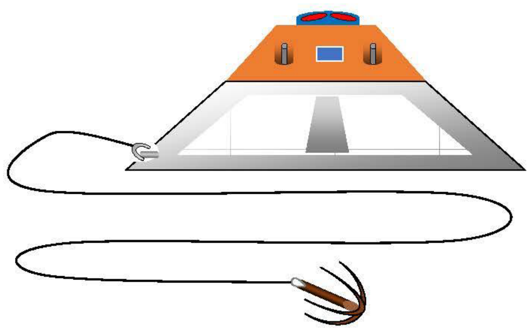

Mooring Components from top to bottom

Mooring Measurements

Float Line Length (3X water depth): ______________ (m)
Anchor Line Length: ________________ (m)

Figure D-5. Mooring diagram and checklist for a TRBM bottom mount

NCOP mTRBM Mooring Diagram and Checklist

Station ID & Name:____________________________
ADCP Freq.:__________________________________
ADCP SN:____________________________________
Start Time (TF):_______________________________
Bottom Mount Name:__________________________
Dive Locator SN:_________________Ch: ___________
Release SN:_____________________ Rcv: __________
Trans:__________ En:________ Rel: __________

Check List

______ ADCP Pinging
______ Dummy Plug is present
______ Float line coiled and secured in bucket
______ Float attached to float line
______ Release pin properly aligned with ring
______Release secured to strongback
______ Release armed and float line secured
______Dive Locator attached to shell
______Gimbal properly oriented and secured
______ ADCP secured in Gimbal and has free movement
______ All mooring connections moused and checked
______ All zinc anodes inspected/replaced
______ Anchor line attached to base

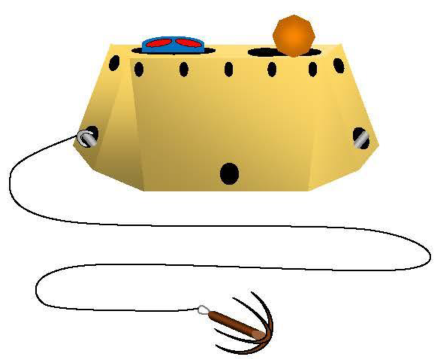

Mooring Measurements

Float Line Length (3X water depth): ______________ (m)
Anchor Line Length: ________________ (m)

Figure D-6. Mooring diagram and checklist for an mTRBM bottom mount

NCOP ES2 Mooring Diagram and Checklist

Station ID & Name:___________________________
ADCP Freq.:________________________________
ADCP SN:__________________________________
Start Time (TF):_____________________________
Bottom Mount Name:_________________________
Dive Locator SN:_________________Ch: ___________
Release SN:_____________________ Rcv: __________
Trans:__________ En:________ Rel: __________

Check List

______ ADCP Pinging
______ Dummy Plug is present
______ Float line coiled and secured in bucket
______ Float attached to float line
______ Release properly aligned
______ Release armed and float line secured
______Dive Locator attached to shell
______Gimbal properly oriented and secured
______ ADCP secured in Gimbal and has free movement
______ All mooring connections moused and checked
______ All zinc anodes inspected/replaced
______ Anchor line attached to base

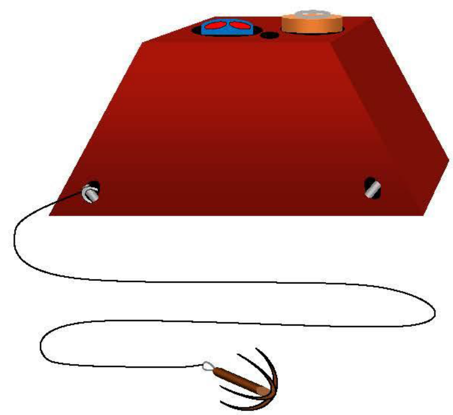

Mooring Measurements

Float Line Length (3X water depth): ______________ (m)
Anchor Line Length: ________________ (m)
Additional weight: _________________(lbs)

Figure D-7. **Mooring diagram and checklist for a ES2 type bottom mount**

ACRONYMS

Table of Acronyms

ADCP	acoustic Doppler current profiler
AIS	Automatic identification system
ATON	Aids to Navigation
C	Celsius
cm/s	Centimeters per second
CO-OPS	Center for Operational Oceanographic Products and Services
CTD	conductivity, temperature, and depth
CFR	Code of Federal Regulations
DO	Dissolved Oxygen
ES2	Bottom mount design “Eddie Shih 2”
ft	feet
GI	Greenwich Interval
IHO	International Hydrographic Organization
kg	kilogram
kHz	kilohertz
km	kilometer
kn	knots
LSQHA	Least squares harmonic analysis
m	meter
MEC	maximum ebb current
MFC	maximum flood current
MHHW	mean higher high water
MLLW	mean lower low water
MSI	Mooring Systems, Inc.
MTRBM	miniature trawl-resistant bottom mount
NCOP	National Current Observation Program
nmi	nautical mile
NOAA	National Oceanic and Atmospheric Administration
NOS	National Ocean Service
QARTOD	Quality Assurance/Quality Control of Real-Time Oceanographic Data
R/V	Research Vessel
s	second
SBE	Slack before ebb
SBE 37	Seabird CTD sensor model SBE 37
SBF	slack before flood
SUBS	subsurface taut-line mooring manufactured by Open Seas Instrumentation, Inc.
TCTs	(published) Tidal Current Tables
TRBM	trawl-resistant bottom mount

TRDI	Teledyne RD Instruments